5-8-2015

Design and Synthesis of Electrochromic and Highly Conductive Polymers for Flexible and Stretchable Electronics

Michael Thomas Otley
University of Connecticut - Storrs, michael.otley@uconn.edu

Design and Synthesis of Electrochromic and Highly Conductive Polymers for Flexible and Stretchable Electronics

Michael Thomas Otley, Ph.D.

University of Connecticut, 2015

Abstract

This dissertation will focus on the design and synthesis of π-conjugated oligomers and polymers for potential use in electrochromic windows, sunglasses, displays, and fabric as well as for highly conductive applications to serve as metal replacement for wires, conductors, thermoelectrics, and optically transparent conductors. Herein, this dissertation will take the reader through an introduction of electrochromics, which are materials that change color due to charge injection and removal, and then a comprehensive story involving the optimization of electrochromic devices, the color tuning of electrochromic devices, and the ability to generate neutrality ("black"). Specifically, **Chapter 3** details some of the optimization studies of electrochromic devices we have done over the last four years focusing on my study of long-term stability in electrochromic devices. Where functionalizing the electroactive monomer, while maintaining the same color as our standard chromophore 2,2-dimethyl-3,4-propylenedioxythiophene (ProDOT-Me_2), allowed the ability to form a polymer blend of the unreacted electroactive monomer, electrochromic polymer, and gel electrolyte resulting in exceptional stability of our lab's one step lamination procedure for electrochromic devices. In **Chapter 4** the structure property relationship of 1,3 substituted ProDOTs is examined, specifically, the result of stereochemistry of the

monomer on the subsequent homopolymer. An exceptional result was achieved where a 90 nm blue shift occurred from the trans-stereoisomer to the cis-stereoisomer of 1,3-di-isopropyl-propylenedioxythiophene (1,3-ProDOT-iP_2). This is due to the increased steric effects of the cis-stereoisomer that resulted in the breaking the planarity of the polymer chain thus reducing orbital overlap leading to shorter conjugation length and an increase in band gap. In **Chapter 5**, my first PhD project is detailed which consists of a landmark study in the field of electrochromics where the fundamental diffusion of two monomers in a solid gel electrolyte, a specific color can be linked to an exact monomer feed ratio, allowing for high-throughput screening of electrochromic copolymers to color match for a specific application. **Chapter 6** details our quest for achieving neutrality or "black" within our lab's one step lamination procedure for electrochromic devices. First, we used a static yellow dye to achieve neutrality and then carried out a full study on creating electrochromic dyes with the use of π-conjugated oligomers. The final electrochromic study presented in this dissertation, **Chapter 7**, details another pioneering study in the field of electrochromics where computational modeling was used to accurately predict the contrast and the neutrality of the electrochromic device before fabricating a single device that saves time, cost, and results in low waste. The last chapter of this dissertation, **Chapter 8**, focuses on highly conductive polymers for the development of flexible and stretchable electronics. The demonstrations of this technology include lighting a light bulb, an antenna, a thermoelectric device, and a cardio respiratory sensor.

Design and Synthesis of Electrochromic and Highly Conductive Polymers for Flexible and Stretchable Electronics

Michael Thomas Otley

B.S., University of Hartford, 2009

A Dissertation

Submitted in Partial Fulfillment of the

Requirements for the Degree of

Doctor of Philosophy

at the

University of Connecticut 2015

APPROVAL PAGE

Doctor of Philosophy Dissertation

Design and Synthesis of Electrochromic and Highly Conductive Polymers for Flexible and Stretchable Electronics

Presented by Michael Thomas Otley, B.S.

Major Advisor _____
Gregory A. Sotzing

Associate Advisor _____
Christian Brückner

Associate Advisor _____
Douglas Adamson

Associate Advisor _____
Luyi Sun

Associate Advisor _____
Nicholas Leadbeater

University of Connecticut

2015

Acknowledgements

I would like to thank and give my gratitude to everyone that has helped me in my academic career especially my parents for always supporting me and encouraging me to further my education. I owe a debt of gratitude to my advisor Dr. Gregory Sotzing for all his help and guidance throughout my graduate studies.

I would like to thank my fellow graduate peers in Chemistry, IMS, and in the Sotzing group including Fahad Alhashmi Alamer, Yumin Zhu, Xiaozhang Zheng, Mengfang Li, and Yang Guo who not only helped me with my research but also worked late with me to meet deadlines.

I am also grateful for UCONN Chemistry and all the faculty and staff that have been helpful to me during my time at the University of Connecticut. In addition, I need to thank the faculty and staff in the Department of Material Sciences for all the help they have given me. I would also like to thank the faculty and staff at the University of Hartford including my academic advisor Dr. Craft, my organic research advisor Dr. Shattuck, my genetics research advisor Dr. Levesque, and my organic professor Dr. Mahan. Last but not least the faculty and staff at Trinity College, and Dr. Guillermo Muhlmann at Capital Community College for helping me during my undergraduate career.

List of Abbreviations

ACN	acetonitrile
br	broad
CH_2Cl_2	methylene chloride
$CHCl_3$	chloroform
$CDCl_3$	deuterated chloroform
cm	centimeters
CP	conjugated polymer
δ	delta
d	doublet
dd	doublet of doublets
ddd	doublet of doublet of doublets
dddd	doublet of doublet of doublet of doublets
DMHDiol	2,6-dimethylheptane-3,5-diol
EC	electrochromic
ECD	electrochromic device
Et_2O	diethyl ether
EtOAc	ethyl acetate
EtOH	ethanol
g	gram
h	hour
H	hydrogen
H_2	dihydrogen

H_2O	hydrogen oxide
HCl	hydrochloric acid
Hz	hertz
IR	infrared
ITO	indium tin oxide
J	J-coupling
KBr	potassium bromide
LITRIF	lithium trifluoromethanesulfonate
M	molecular or molarity
m	multiplet
me	methyl
MeOH	methanol
$MgSO_4$	magnesium sulfate
MHz	megahertz
min	minutes
mL	milliliter
mmol	millimole
NaH	sodium hydride
$NaHCO_3$	sodium bicarbonate
NaOH	sodium hydroxide
NH_4Cl	ammonium chloride
NMR	nuclear magnetic resonance
OLED	organic light emitting diode

Otley (2015)

OPV	organic photovoltaic
OTE	optically transparent electrode
PEDOT	polyethylenedioxythiophene
ppm	parts per million
ProDOT	propylenedioxythiophene
ProDOT-Ac	(3-methyl-3,4-dihydro-2*H*-thieno[3,4-*b*][1,4]dioxepin-3-yl)methyl acrylate
ProDOT-BPM	2,2- (biphenylmethylmethoxy, methyl)-propylenedioxythiopene
ProDOT-iP_2	1,3-di-isopropyl-propylenedioxythiophene
1,3-ProDOT-Me_2	1,3-dimethyl-propylenedioxythiophene
ProDOT-Me_2	2,2-dimethyl-propylenedioxythiophene
ProDOT-tB_2	1,3-di-*tert*-butyl propylenedioxythiophene
pTSA	p-toluenesulfonic acid
q	quartet
rt	room temperature
s	singlet
sec	seconds
TMHDiol	2,2,6,6-Tetramethyl-3,5-heptanediol
THF	tetrahydrofuran
TLC	thin layer chromatography

Table of Contents

List of Figures

Otley (2015)

Otley (2015)

Otley (2015)

1. Chapter 1: Introduction

1.1 Conjugated Polymers Background

Runge first reported a conducting polymer in 1834 with the synthesis of polyaniline ("aniline black"), however, Runge was unaware of his discovery due to the lack of technology to properly characterize what he had made.[1] Conducting polymers were not fully explored until the late 1960's into the 1970's with the synthesis of polypyrrole and polyacetylene. In 2000, Alan J. Heeger was awarded the Nobel Prize for his work on polyacetylene that demonstrated high conductivity was possible within all-organic systems. In 1987, Heeger and colleagues published a paper in Nature reporting polyacetylene doped with Iodine and stretched four-fold (referred to as Naarman Acetylene) achieved the highest conductivity of an organic polymer with 22,000 S/cm.[2]

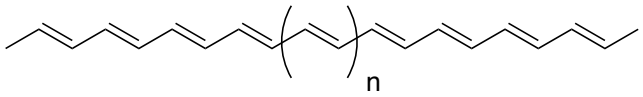

Figure 1.1 A chemical structure of polyacetylene.

However, polyacetylene is not air stable, so research continues to find a highly conductive organic material/polymer for the potential to replace metals. For further detail on highly conductive organic polymers and their applications, Chapter 8 of this dissertation focuses on the current organic polymers that have shown high conductivity but more importantly air stability.

Otley (2015)

1.1.1 Band Theory

In band theory, the electrons that move between discrete energy states known as bands determine the electrical properties of a material. The lowest unoccupied band is called the conduction band while the highest occupied band is known as the valence band, and the energy difference between these bands is what is the band gap. Figure 1.2 details the energy differences of band gaps of the three classes of materials metals, semiconductors, and insulators. Band theory is relevant to conducting polymers because upon oxidation of the polymer chain some conducting polymers can break conjugation thus increasing the band gap. Charges that are introduced in polymers and π-conjugated oligomers are stored in discrete states known as polarons, bipolarons, and solitons.[3] A polaron is formed when an electron is introduced or removed from the conjugated polymer chain. This results in chain deformation of the conjugated polymer thus changing the orbital overlap and electronic structure, and an electronic level is moved from the valence band into the band gap. When commencing an electron or "electron polaron" the electron polaron is retained in the newly formed level pulled from the conduction band. Removal of the electron or "hole polaron" results in an electron removed from the recently formed level. The energy potential between the band edge and the newly formed energy level will vary depending on band gap, conjugation, and chain length. Bipolarons are the result of combining two polarons with the same charge, and create two newly formed levels within the band gap. A negative bipolaron consists of two newly formed energy levels that are occupied while a positive bipolaron is unoccupied. Solitons are the third example of newly formed energy level that occurs only in

Otley (2015)

degenerate polymers, which are conjugated polymers that have alternating single and double bonds like polyacetylene (Figure 1.1).[3] Solitons can be filled with one electron, two electrons, or no electrons. The π-conjugated polymers in this thesis are all thiophene derivatives, which are not degenerate polymers due to the heteroatom, Sulfur, donating electrons to the conjugation within the thiophene ring.

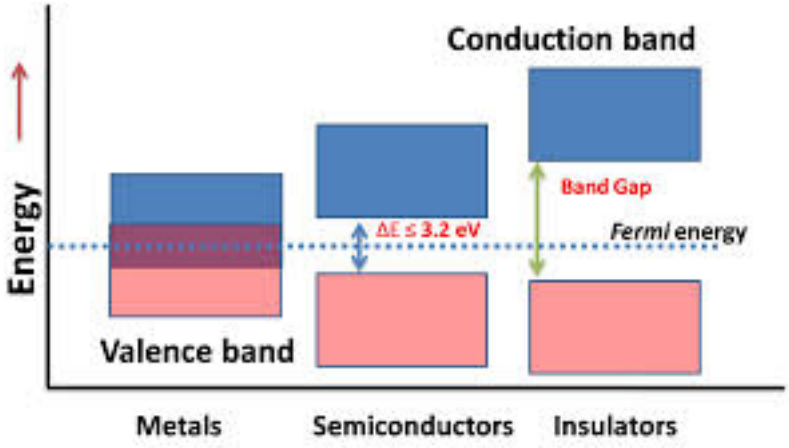

Figure 1.2. The band gap diagram of a metal, semiconductor, and insulator.

1.1.2 Color

In 1931 Commission Internationale de L'eclairage or better known as CIE (International Commission on Illumination) defined color in a more universal way than previously described. The idea of these systems is to represent color in a mathematical way allowing for an exact definition of each color to assist in accurate reproducibility of a certain hue. In 1976 the CIE updated their original system, and it is the most commonly used system for color characterization today as seen in Figure 1.3.[4] The sensitivity curves in the CIE 1931 and 1964 xyY color spaces are scaled to have equal areas under the curves. The chromaticity diagram illustrates a number of interesting properties of the CIE

xyY color space including representing all of the colors visible to the human eye. These chromaticities are shown in color and this visible region is called the gamut of human vision. The gamut of all visible chromaticities on the CIE plot is the tongue-shaped or horseshoe-shaped figure shown in color, and the curved edge of the gamut corresponds to a pure hue of a single wavelength with wavelengths listed in nanometers. The straight edge on the bottom part of the gamut is called the "line of purples". These colors, although they are on the border of the gamut are not monochromatic light. Less saturated colors appear in the interior of the diagram with white/black at the center. If any two points of color on the chromaticity diagram were chosen, then mixing of these two colors would result in a straight line between the two points with the resulting colors lying in between the two dyes. Therefore, mixing three colors result in a triangle formed by the source points on the chromaticity diagram with the mixed hues lying within the triangle. In this dissertation, Chapters 4-7 will go into further detail of color as it pertains to electrochromic polymers, which change color due to changes in band gap between the two-redox states. In the oxidized state a break in conjugation will result in an increase in band gap that results in a blue shift of the absorption. While reduction of the electrochromic oligomer/polymer to the neutral state results in a decrease of band gap and a red shift of the absorption from the reintroduction of conjugation to the polymer.

Otley (2015)

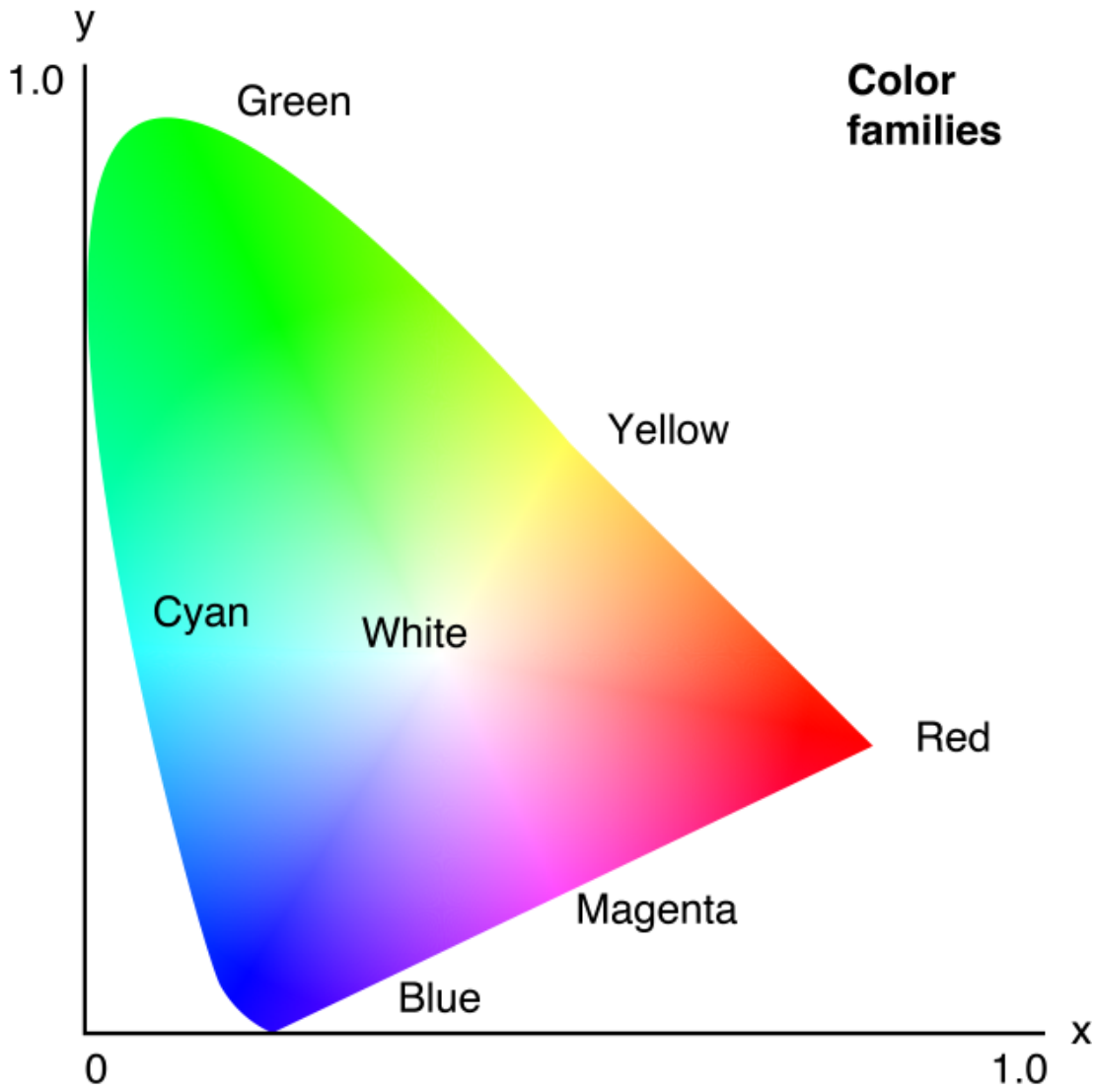

Figure 1.3 The 1976 CIE xyY Chromaticity diagram.

1.2 Electrochromics Background

Electrochromism is defined as the ability to change colors through charge injection and removal from a supplied current. S.K. Deb and J.A. Chopoorian originally discovered the field of electrochromics in 1968.[5] There are three types of electrochromic materials metal oxide films, molecular dyes, and conjugated polymers. This thesis

focuses on electrochromic materials made from conjugated polymers (CPs) that have an almost clear bleached state to a dark state color depending on the composition of the oligomer, homopolymer, and/or copolymer. The important factors when determining a good electrochromic material are switch times (from the light state to 75% of the dark state), the contrast ratio between the two states, long term stability, and coloration efficiency. Conjugated polymers were first discovered in the late 1970's with applications in areas such as organic transistors,[6,7] OLEDs,[8-11] organic photovoltaics (OPVs)[12-14] and displays.[15] Conjugated polymers have several advantages over the other two types of electrochromic materials, inorganic oxides and molecular dyes, in their flexibility, lower cost, and high coloration efficiency.[16] The extended π conjugation along the conjugated polymer backbone gives an optical absorption typically in the visible region. The energy gap between the HOMO and LUMO changes with the external bias, resulting in a color change. For example, one of the most successfully commercialized conjugated polymer's, poly (3,4-ethylenedioxythiophene) (PEDOT) shows a blue dark state and a very light and translucent sky blue color in the bleached state.

By functionalizing the chemical structure of propylenedioxythiophene (ProDOT), the electronic characteristics of the π system can be tweaked to yield different colors. Polymerization of two separate monomers into a copolymer is one route to obtain new colors due to the change of molecular composition of the conjugated polymers without having to synthesize a new monomer to match a particular color for an application.[17] Many copolymers of EDOT and pyrene or pyrrole, as well as other derivatives have been studied.[18-22] In some cases, copolymers were synthesized chemically in order to achieve

the desired color.[17] In other studies, copolymerization was performed by electrochemistry and the resulting copolymers did not have the same composition as the monomer feed ratio.[22] Trying to color match a particular color using these current methods is an onerous process, and also a large amount of electrolyte solvent, salt, and leftover monomers generated from each batch can raise both cost and environmental concerns.

Electrochromic devices employing conjugated polymers have been traditionally fabricated by depositing electrochromic films onto ITO substrates from a monomer solution. Then the device is assembled by sandwiching a UV-curable polymer electrolyte between the ITO with EC film and another piece of bare ITO electrode.[16,23] The polymer electrolyte then crosslinks upon UV exposure and changes from a liquid to a solid-state transparent gel which holds the two ITO pieces together. This method is inefficient since the film quality is greatly affected by the purity of the substrates and of the monomer solution. However, our group recently developed an *in situ* electrochromic device (ECD) assembly approach.[24] In this novel method, a monomer was mixed with the electrolyte before crosslinking, and polymerization occurs after the device has been assembled and hermetically sealed. This method not only significantly increases the success rate of the device fabrication, but also renders a solid gel matrix inside the device before polymerization. By taking advantage of this unique structure, various studies which are not possible using the traditional method can be achieved. This thesis demonstrates a novel platform employing *in situ* assembly, and using this for a high throughput color screening approach for conjugated copolymers. The method includes diffusing two separate monomers through each other in an *in situ* device which generates a gradient of

colors. This is the first demonstration of a rapid selection of copolymers from various feed ratios of two monomers in the same device.[25]

1.3 Electrochromic Devices, Fabric, and the Future

Chromatism is the ability to change color through some type of stimulus, and a variety of chromatic examples exist, such as electrochromism, thermochromism, and photochromism. Electrochromism is the ability to change color in response to an electrical charge, and the term electrochromism was originally used in 1932 to describe the phenomena of Franz-Keldish and Stark's effects.[26,27] Since the 1970's, electrochromic materials have become popular due to the development of conjugated conducting polymers. Inorganic electrochromism,[28-30] viologens,[31-34] and small-molecule organics have transformed the field.[35-37] Electrochromic applications that are currently commercialized include rear-view auto-dimming mirrors, smart windows, automotive sunroofs, and airplane windows.[38] Gentex and Donnelly make use of small molecules, viologens, to create the auto-dimming feature for a reflective mirror device.[39] Smart windows and sunroof applications make use of a variety of technologies; Sage makes windows and skylights based on an inorganic electrochromic material, tungsten trioxide, whereas a variety of other companies use LCDs (Liquid Crystal Displays) or SPDs (Suspended Particle Displays).[40] These systems all have a variety of advantages and disadvantages, but when it comes to making a smart fabric/device, the major issue is that their architectures cannot be translated without the use of an optically transparent conductor. Practically, this means that another technology must be sought if wearable and flexible color-changing devices are ever to become a commercial reality.

Otley (2015)

The attractiveness of ECDs (Electrochromic Devices) is the possibility of making flexible devices and displays with more potential applications than non-flexible displays. This is currently accomplished by using tin-doped indium oxide (ITO) coated onto poly(ethylene terephthalate) PET substrates. These flexible ECDs segue into the next generation of ECDs: electrochromic fabric devices (EFDs). EFDs are not only flexible, but stretchable as well. They are fully integrated fabrics that possess the ability to change color, through using all-organic materials, without the limitation of a rigid substrate.

Adaptive camouflage has been around for thousands of years in nature. For example, the cuttlefish and the chameleon each have the ability to adaptively change their color to camouflage into their surroundings for protection from predators, Figure 1.4. Also, their skin can change color due to emotion, when frightened, during fraternization, and more.

Figure 1.4 On the left a chameleon and on the right a cuttlefish showing their ability to use adaptive camouflage to conceal themselves from predators. "Bradypodion pumilum Cape chameleon female IMG 1767 (cropped)" by Chiswick Chap - Own work. Licensed under Creative Commons Attribution-Share Alike 3.0 via Wikimedia Commons.

Otley (2015)

Ideally, ECDs and EFDs would provide high contrast, sharpness of colors, and also a variety of colors in order to provide functions such as adaptive camouflage, fashion, wearable displays (advertising), etc. The military would benefit from adaptive camouflage not only for soldier protection but also for stealth vehicles, airplanes, ships, drones, and the like. However, ECDs and EFDs could change fashion forever. The designs could be infinite and forever changing, and some companies may even trend toward human advertising.

Otley (2015)

Figure 1.5 A conceptualized image of how adaptive camouflage technology could conceal a soldier.

Otley (2015)

1.3.1 Color-Changing Technologies Background

There are two major classes of electrochromic materials: organic and inorganic. The organic class is subdivided into small molecules and polymeric systems. Other color-changing technologies, like LCDs, Light Emitting Diodes (LEDs), and SPDs, are not strictly "electrochromic" as the voltage applied to effect a color change does not induce redox changes. Beyond these, there are two passive color-changing technologies: photochromic and thermochromic, using light and heat, respectively, to modulate color. Less common systems that also involve color have stimuli such as pressure or changes in pH, as well as those that employ structural color, mainly found in nature. The focus of this thesis is on organic polymeric electrochromic materials, as this class represents the best technical approach to developing ECDs/EFDs. Several examples of the other technologies, particularly those which have seen some measure of commercialization, will also be briefly discussed.

ECDs are electrochemical cells consisting of two electrodes separated by an ion-containing electrolyte. The electrolyte can be either a liquid, gel, or solid that is sandwiched between two substrates. The most commonly used substrates are ITO-coated on glass or PET.[41] Organic polymer electrochromics are conjugated polymers whose defining characteristic is an alternating single-double bond backbone. This backbone is amenable to either oxidation or reduction and thus a delocalization of charge resulting in electrical conductivity. Accompanying the oxidation and reduction processes is a change in the absorption characteristics of the material. Normally, conjugated conducting polymers are electrochemically deposited from a monomer/electrolyte bath onto the

desired substrate. However, a variety of processing improvements have made this process more versatile, including the use of spray-castable precursors.[42] Figure 1.6 shows a schematic representation of how an ECD can be assembled using such a precursor.

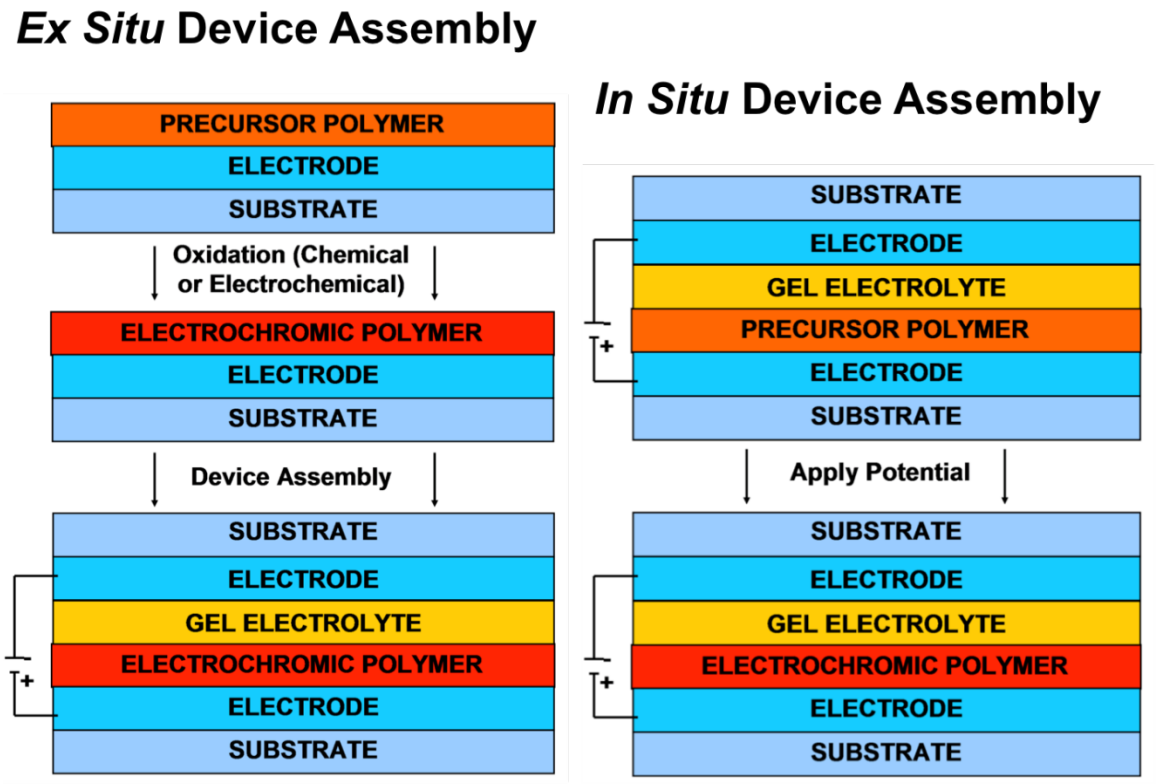

Figure 1.6 Schematic of the ECD assembly steps utilizing spray-castable precursor polymers and an external oxidative conversion (left) or an internal electrochemical oxidative conversion (right).

1.4 Previous Work on ECDs

The first published work on the subject of stretchable ECDs was an EFD in 2010 with the invention of "All-Organic Electrochromic Spandex" (Invernale *et al.*, *ACS Applied Materials & Interfaces*, 2(1), 296, 2010).[43] There had not been a fully functional

electrochromic fabric previously, though attempts at color-changing clothing had been made. These other types of color-changing clothing include thermochromic, photochromic, and LED/LCD technologies, and these will be discussed briefly at the end of this chapter. The seminal work on EFDs, by Invernale *et al.*, described an ECD based on spandex (a polyester-polyurethane co-polymer, alternatively known as Lycra or Elastane) electrodes and using a device architecture that has never before existed in the field. The fundamental advantages of this color-changing fabric system are numerous, though there are three key elements that make it the most promising technology for the true commercial realization of color-changing garments, adaptive camouflage, and wearable displays. The key benefits are the ability to use all-organic components, the architecture itself, and the processability of the system. Figure 1.6 shows a schematic of the device stack (bottom) as well as a representative electrochromic polymeric material (top). The conducting material was PEDOT-PSS, which is an aqueous dispersion of the conjugated conducting polymer poly(3,4-ethylenedioxythiophene) and the polymeric anionic dopant poly(styrene sulfonate). This material was soaked into the chosen substrate, in this case spandex, though we will discuss other fabric substrates following this section, as the follow-up paper on the seminal work closely examined this subject. The combination of substrate and conductor was then allowed to dry. The resulting fabric was now conductive, on the order of 0.1 S cm^{-1}, and it retained all of the characteristics of the base fabric, namely flexibility, stretchability, nap, and feel.

The formerly white spandex was then a light-blue color, due to the slight coloration of the PEDOT conductor. The impacts of color on the EFDs will be discussed

based in the third publication, which considers a variety of factors affecting perceived colors. It is important to note that the conductor is not a thin film coating of any kind, but is rather an intercalated, imbedded system of polymeric components of sufficient proximity to achieve percolation. The entirety of the spandex is an electrode; it cannot be damaged or conduction broken by rubbing, bending, or stretching the fabric. This is a unique advantage over other conjugated conducting polymer works performed on fabrics.[44-54] Two spandex electrodes were then cut to size, approximately 1 inch by 0.5 inches, and were assembled into an ECD. The working electrode was spray-coated with a processable conjugated conducting polymer precursor.[55,56] Once a sufficient thickness of this precursor was cast onto one of the spandex electrodes, it can be converted to a functional electrochromic polymer via chemical or electrochemical oxidation. Then, each electrode is coated with a UV-curable gel electrolyte composed of a crosslinkable polymer matrix, a lithium salt, and a photoinitiator. Once coated, the electrolyte is cured using a UV chamber with a 365 nm light source. The electrodes are then stacked such that the counter electrode is *beneath* the working electrode. One of the key elements of this system is that it creates an ECD using this never-before utilized architecture. The gel electrolyte provides a separation between electrodes, preventing electrical shorting, and its encasement of both electrodes also allows for an applied bias to accomplish electrochromic switching. The ion movement which accompanies the reversible oxidation/reduction reaction being experienced by the conjugated conducting polymer is able to be achieved using the "reflective device" architecture developed by Invernale *et al*. This proof-of-concept laminar stack easily expands to the conception of inter-woven

devices using individual electrochromic threads, as well as printable, flat electrochromic fabric devices (EFDs) that achieve the necessary chemistry using coplanar electrodes. It is a powerful and versatile device conception that forms a very promising foundation for the development of an EFD garment.

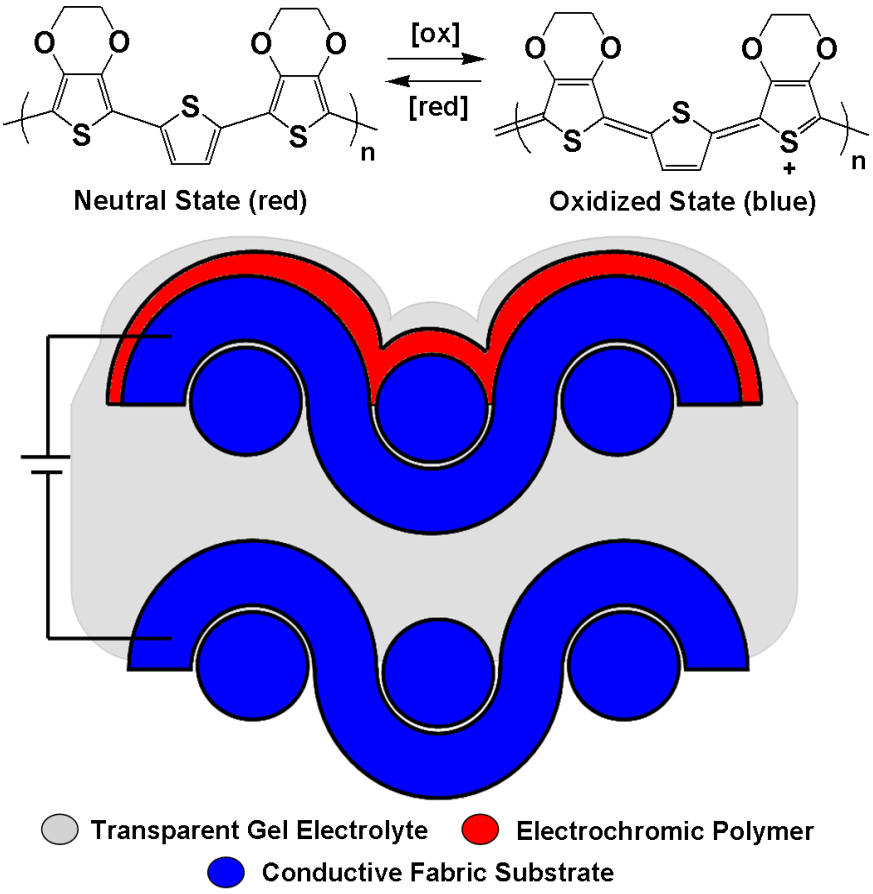

Figure 1.7 Schematic of the All-Organic Electrochromic Spandex Device developed by Invernale *et al*. Top: Chemical structure of the color-changing material in its two extreme states. Bottom: Device architecture showing the unique stack for an EFD. Adapted with permission from M. A. Invernale, Y. Ding, and G. A. Sotzing, *ACS Applied Materials & Interfaces* 2, 1 (2010) 296-300. Copyright 2010 American Chemical Society

Otley (2015)

Secondly, the electrode material, the fabric, the electrolyte, and the color-changing components are all composed of organic materials. No optically transparent conductor is needed to complete the device. Since this system does not require ITO (Tin-doped Indium Oxide, an optically transparent conductor that is ubiquitous to the display industry, as well as touch screen electronic devices), these devices have numerous properties concomitant with the desired specifications for a wearable ECD. The ability to avoid ITO, which is brittle and difficult to process, allows for a fabric material with the potential to bend, flex, stretch, and conform the way a garment should. As mentioned previously, the spandex electrodes retain the properties of the base fabric after impregnation with PEDOT-PSS. The formation of this percolated network of conducting material is accomplished at very low loading and is thus not restricting to the material. Figure 1.7 shows an electrode coated with conjugated conducting polymer that has been stretched and switched. You can clearly see a black background through the holes in the threading. The system is still completely functional. With the appropriate development of complementary electrolytes, this use of all-organic materials for the EFD's construction points towards the potential for the creation of a fully flexible, stretchable, breathable, and wearable EFD.

Otley (2015)

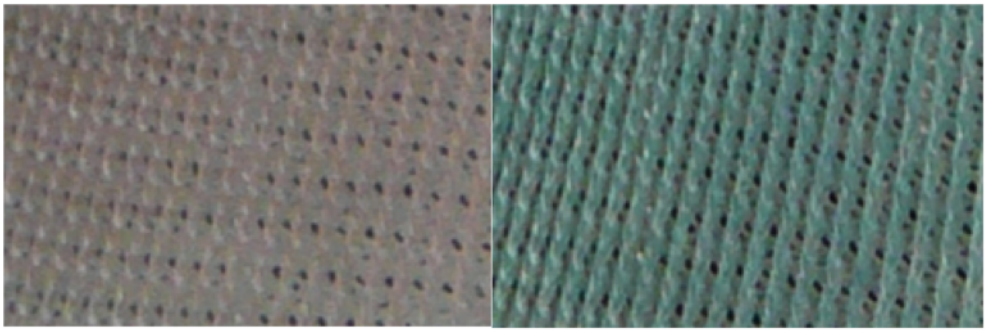

Figure 1.8 Images of a spandex electrode coated with an electrochromic polymer. The electrode was stretched to its maximum recommended elongation of 20% and was then cycled between its colored states. This system is fully functional in this manner due to the lack of ITO and the use of all-organic materials. Adapted with permission from M. A. Invernale, Y. Ding, and G. A. Sotzing, *ACS Applied Materials & Interfaces* 2, 1 (2010) 296-300. Copyright 2010 American Chemical Society

The third key advantage is the processability of these devices. For any technology, it is critical that the system must be amenable to a cost-effective product from both a materials cost perspective as well as the mechanical realities of assembly and manufacturing. Otherwise, its benefits will never outweigh its price. The use of an all-organic system allows for low raw material costs. The simplicity of the electrode design, coupled with the low loading percentage of conductor and the breadth of ways it could be impregnated (dip, soak, spray, inkjet, etc.), make the fabric electrode components readily suited to fit into many current manufacturing processes. The processable conjugated conducting polymers utilizing the precursor method also share these advantages. Figure 1.9 shows an image of an easily patterned simple word on a spandex EFD. This type of versatility allows any unforeseen obstacles in the assembly process to be overcome via compromises and alternative choices in processing. It also allows for creative designs and applications of the technology. For example, double-sided fabric ECDs are also possible

using this architecture. They can be alternating-color or same-color, depending on the choice of stack. Figure 1.10 shows an example of an alternating-color device with a mirror behind it. The only step that is not currently a common piece of equipment for a garment manufacturer would be the UV curing process. However, there are also thermally curable gel electrolyte compositions, and so it is thus entirely feasible that current manufacturers have everything they would need to implement this system. This sort of advantage can often be overlooked, but it is important to keep in mind if researchers wish to translate their ideas to real world applications and have an impact on a global scale. Current projects in the Sotzing laboratory are focused on bringing newer and better electrolyte systems to this fabric device architecture, imparting durability, flexibility, and stretchability, among other characteristics.

Figure 1.9 A simple phrase, UCONN, patterned in conjugated conducting polymer on a spandex EFD. The tremendous versatility in manufacturing choices affords not only innumerable processing options, but also for creative applications of the technology. Adapted with permission from M. A. Invernale, Y. Ding, and G. A. Sotzing, *ACS Applied Materials & Interfaces* 2, 1 (2010) 296-300. Copyright 2010 American Chemical Society

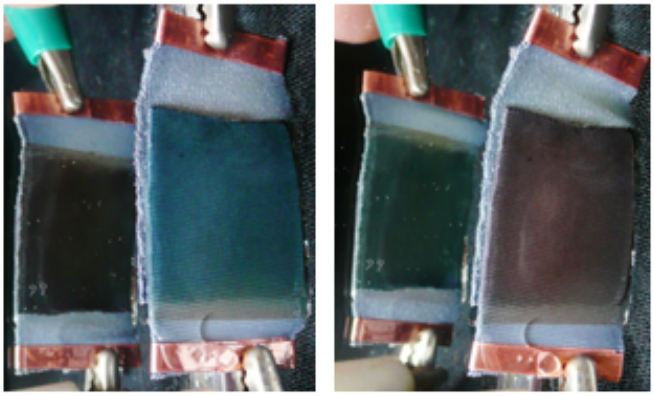

Figure 1.10 An example of a creative application of EFD technology: a double-sided fabric ECD. Both sides of the device have been coated with a conjugated conducting polymer in an alternating-color device stack. The mirror shows the color of the other side of the device. Adapted with permission from M. A. Invernale, Y. Ding, and G. A. Sotzing, *ACS Applied Materials & Interfaces* 2, 1 (2010) 296-300. Copyright 2010 American Chemical Society.

1.4.2 - Conductivity Trends of PEDOT-PSS Impregnated Fabric and the Effect of Conductivity on Electrochromic Textile

Following the invention of the EFD architecture, a variety of related and continuing studies were carried out. Ding *et al.* sought to more fully understand the nature of the conductor within a fabric matrix. "Conductivity Trends of PEDOT-PSS Impregnated Fabric and the Effect of Conductivity on Electrochromic Textile" (Ding *et al.*, *ACS Applied Materials & Interfaces*, 2, 1588, 2010) showed the differences between fabric types with respect to uptake and conductivity, the effect of processing conditions, conductor loading optimization, as well as an evaluation of the conductor's stability under mechanical stresses typically experienced by the fabric matrix.[57]

The spandex studied was composed of 5% spandex and 95% cotton. To better understand the differences between fabric type and their function as electrodes for EFDs,

other combinations and compositions were tested. 100% cotton, 100% polyester, 60% cotton/40% polyester, 58% polyester/40% rayon, 20% lycra/80% nylon, and 50% nylon/50% polyurethane fabrics were all examined during the study. Figure 1.11 represents the data for conductivity observed as well as a table of water uptake for the various materials. There is a correlation between the ability of a given fabric to absorb water, which is the carrier fluid for PEDOT-PSS, and the resultant conductivity of the electrode. However, this, alone, is not enough to explain the differences. Factors such as thread size or additives to the fabric can also interfere with or enhance the conductivity of the base fabric. Significant ongoing work in the Sotzing laboratory continues to investigate these effects in an effort to maximize the conductivity of fabric for a variety of applications, including use as a component in EFDs.

Otley (2015)

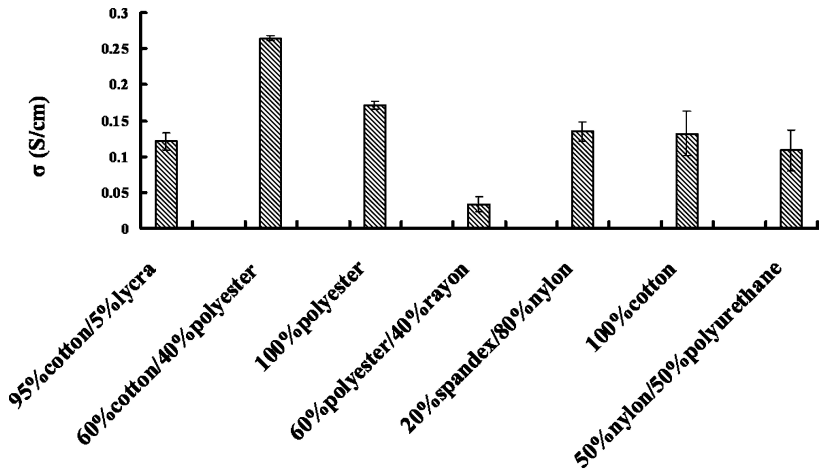

Textile type	Water absorbed (mg)
95%cotton/5%lycra	299.36
60%cotton/40%polyester	310.21
100%polyester	207.5
58%polyester/40%rayon	287.66
20%spandex/80%nylon	177.84
100%cotton	326.73
50%nylon/50%polyurethane	163.77

Figure 1.11 – Top: Conductivity of various textiles soaked with PEDOT-PSS. Bottom: Water absorbed by different fabrics. Reprinted with permission from Y. Ding, M. A. Invernale, G. A. Sotzing. *ACS applied materials & interfaces,* 2, 6 (2010): 1588-1593. Copyright 2010 American Chemical Society.

While water uptake was found to play a role, the variance between these fabrics with respect to their conductivities was relatively small. There were no order of magnitude increases, and the highest value obtained using the standard processing procedure was only 0.25 S cm^{-1}. Traditional ECDs use electrodes, such as ITO-coated substrates, with conductivities of 1,000 to 3,000 S cm^{-1}. It is well worth noting the observation that a 10,000-fold lower conductivity can sufficiently supply the necessary power to switch these fabric devices. However, low conductivities will also result in slower diffusion rates for the electrolyte, as ion movement is dependent upon the strength

of the applied bias that is driving their migration. Using the spandex fabric, it was found that by increasing the number of soaking cycles and soaking time, an optimum weight percent of PEDOT-PSS could be loaded into the fabric, resulting in a maximization of its conductivity. It was found that fabric was saturated with conductor after 60 seconds, but that multiple cycles in a refreshed solution resulted in increased loading. After 10 cycles, the fabric was as loaded with PEDOT-PSS as possible. This translated into a conductivity enhancement from 0.1 S cm^{-1} to 1.5 S cm^{-1}. This order-of-magnitude increase in conductivity resulted in a reduction in switching time from 16 seconds to 10 seconds. This result was not expected to be an order of magnitude change, however, because there are many other factors which effect ion diffusion in addition to conductivity.

Finally, hysteresis was studied for repeated stretching of the spandex electrode. This was done to ensure that the mechanical properties of the base fabric were not impeded by the addition of PEDOT-PSS and that conductivity does not suffer as a result. Figure 1.12 shows the hysteresis curves for the effect of conductivity under repeated stretching to different elongations. It was found that, under normal strain (for spandex, 20-25% elongation is the recommended maximum), the electrodes experienced slight losses in conductivity, changing by 12.5%, however when stretched to 80% elongation, the conductivity was halved. This is expected, as elongation of the fiber beyond a certain point will cause a loosening of the thread and fiber bundles that make up the material. This, then, causes a separation of conductive chains and a decrease in the substrate's ability to carry charges effectively.

Otley (2015)

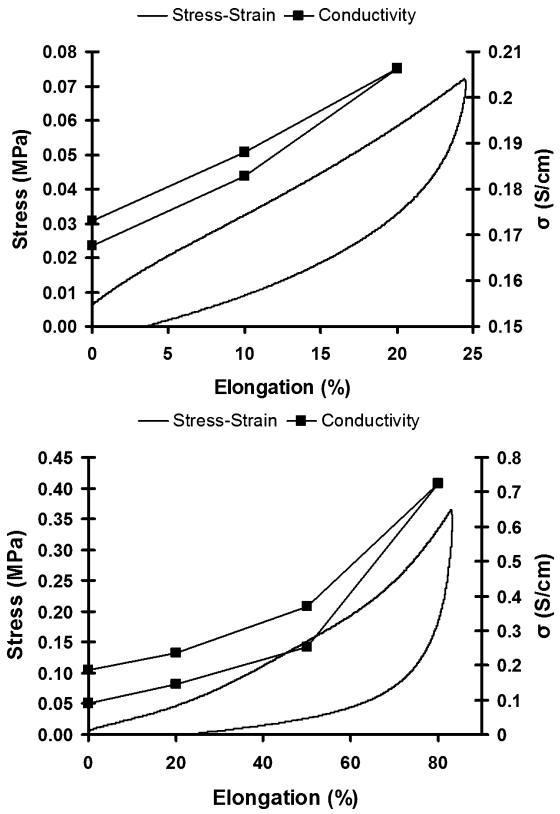

Figure 1.12 – Top: Hysteresis for conductivity and stress-strain for spandex electrodes at an elongation of 20%. Bottom: Hysteresis for conductivity and stress-strain for spandex electrodes at an elongation of 80%. Reprinted with permission from Y. Ding, M. A. Invernale, G. A. Sotzing. *ACS applied materials & interfaces,* 2, 6 (2010): 1588-1593. Copyright 2010 American Chemical Society.

1.4.3 - The Effects of Colored based Fabric on Electrochromic Textile

One of the most widely studied aspects of conjugated conducting polymers is the ability to tune their coloration to any desired hue and saturation. This work has been done towards the development of full-color displays, among other applications. For EFDs, color tuning is also a critical aspect and a crucial feature that must be understood and controlled if wearable displays, adaptive camouflage, or other products are to be developed. There is, however, a fundamental difference between a traditional ECD and

an EFD when it comes to the perceived color. Namely, EFDs are reflective devices and most ECDs and electrochromic polymers are evaluated via UV-Vis-NIR transmission spectra. Reflective devices must consider subtractive color mixing during their design, or else the resulting color of the material will not be as intended. For an electrochromic window, it is obvious that the spectrum of the color-changing polymer will tell you the color of the device very reliably, given the appropriate illuminant, however, using that same chromogenic polymer on a fabric device could have a drastically different result. "The effects of colored base fabric on electrochromic textile" was published in the *Journal of Coloration Technology* in 2011 by Invernale *et al*. and it addressed this particular dilemma.[58]

The architecture of these EFDs is such that the observed color is actually an agglomeration of the colors from the fabric, the conductor, and the color-changing polymer. These colors are then further affected by the electrolyte which surrounds them, as it changes the way light gets in to and out of the reflective device. The end result for the observer is simple, they only have to look at it and their eyes will calculate the perceived color for them, but for the researcher and the product development engineer, color description is very complex. There is still a significant amount of work to be done regarding color tuning for fabric electrochromics, but one of the pieces of the puzzle was explored and elucidated in this paper.[58]

The study focused on a single chromophore, a red to blue electrochromic polymer of bisEDOT-thiophene, which was used in the previous two studies. The aim was to explore how this material's color properties could be shifted without using a chemically distinct

electrochromic material. Fifteen different colored cotton fabrics were used in the production of EFDs, and the colors of each were monitored at each stage of the process. The thickness of the chromophore was kept constant, as were all other processing conditions. Figure 1.13 shows actual images of the fabric in each of its states from bare, electrode substrate, precursor coated, oxidized color state, and neutral color state. The CIE chromaticity coordinates for the transformations are also plotted as Figure 1.14. From this work, it is clear that the underlying substrate plays a critical role not only in its ability to perform the duties of an electrode but also as a chromatic component of the EFD.

Otley (2015)

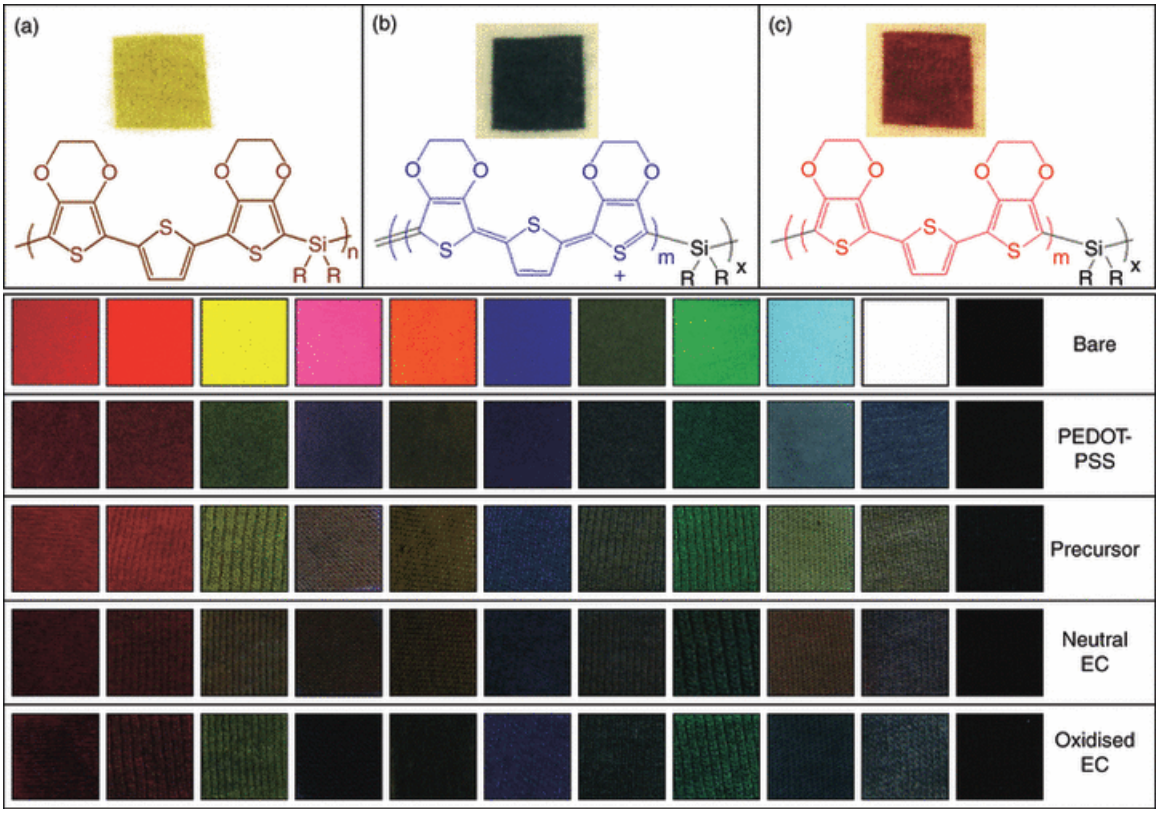

Figure 1.13 Top: images of white cotton fabric without PEDOT-PSS soaking that were spray-cast with a processable precursor polymer and converted chemically to the electrochromic. The chemical structures of the polymer in each colored stage are shown below. Bottom: Photographs of actual fabric showing the various colors obtained at each stage of EFD preparation procedure. Bare = base fabric; PEDOT-PSS = soaked fabric that is now an electrode; Precursor = spray-coated electrode with the precursor polymer; Neutral EC = converted electrochromic in the neutral state; Oxidized EC = converted electrochromic in the oxidized state. The fabrics are always in the same order, left to right: Red, Orange, Yellow, Hot Pink, Tangerine, Blue, Army Green, Irish Green, Light Blue, White and Black. © 2011 M. A. Invernale, Y. Ding, G. A. Sotzing. Coloration Technology © 2011 Society of Dyers and Colourists.

Otley (2015)

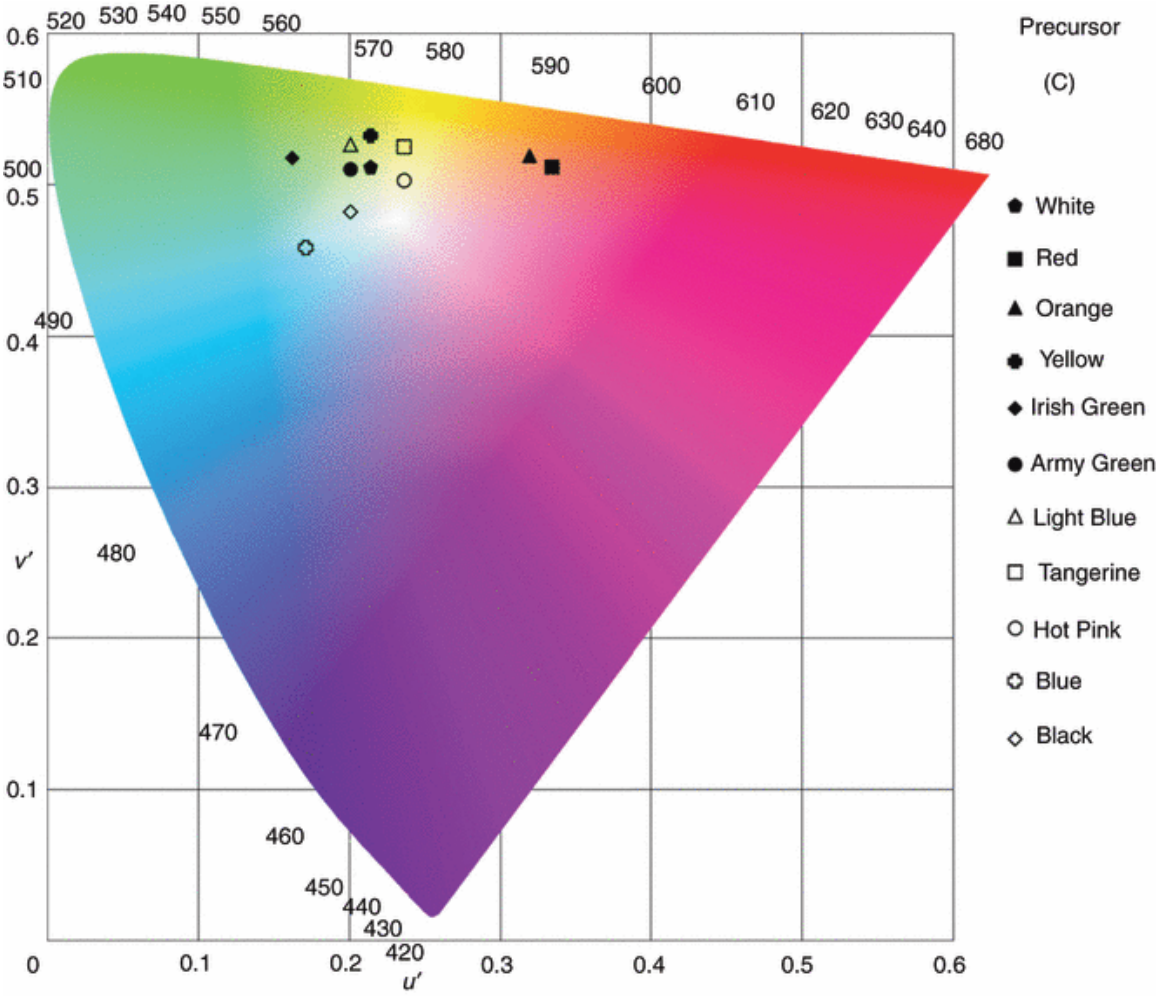

Figure 1.14 CIE Lu'v' chromaticity coordinates for PEDOT-PSS loaded fabric that has been coated with the precursor polymer. © 2011 M. A. Invernale, Y. Ding, G. A. Sotzing. Coloration Technology © 2011 Society of Dyers and Colourists.

1.4.4 Other Electrochromic Fabric

There have been other types of EFDs reported in the literature, and they each have significant architectural differences from the seminal EFDs discussed in the previous sections. One example, reported by Meunier *et al.*, illustrates the use of Prussian blue on a flexible substrate.[59] The device they fabricated exhibits the use of what they describe as

a four-layer system, consisting of a textile substrate, a flexible electrode (silver or carbon black), an electrochromic ink contained in a spacer, and a second electrode made of PET-ITO on top. The fabric used in the device consisted of PET coated with a layer of polyurethane. Then, atop of the PET and polyurethane, the first electrode, made of either carbon black or silver, was coated. A suspension of Prussian blue was sandwiched between the ITO-coated PET and the fabric electrode assembly, the edges sealed with neoprene glue for flexibility. However, as can be seen in Figure 1.15 the neoprene glue is highly visible, and the applications for EFDs will be limited due to the use of a rigid top layer of PET-ITO. The device architecture is essentially a reproduction of a standard reflective-type ECD, using a modified fabric as the opaque electrode instead of a metallic mirror or titanium dioxide-based white surface.

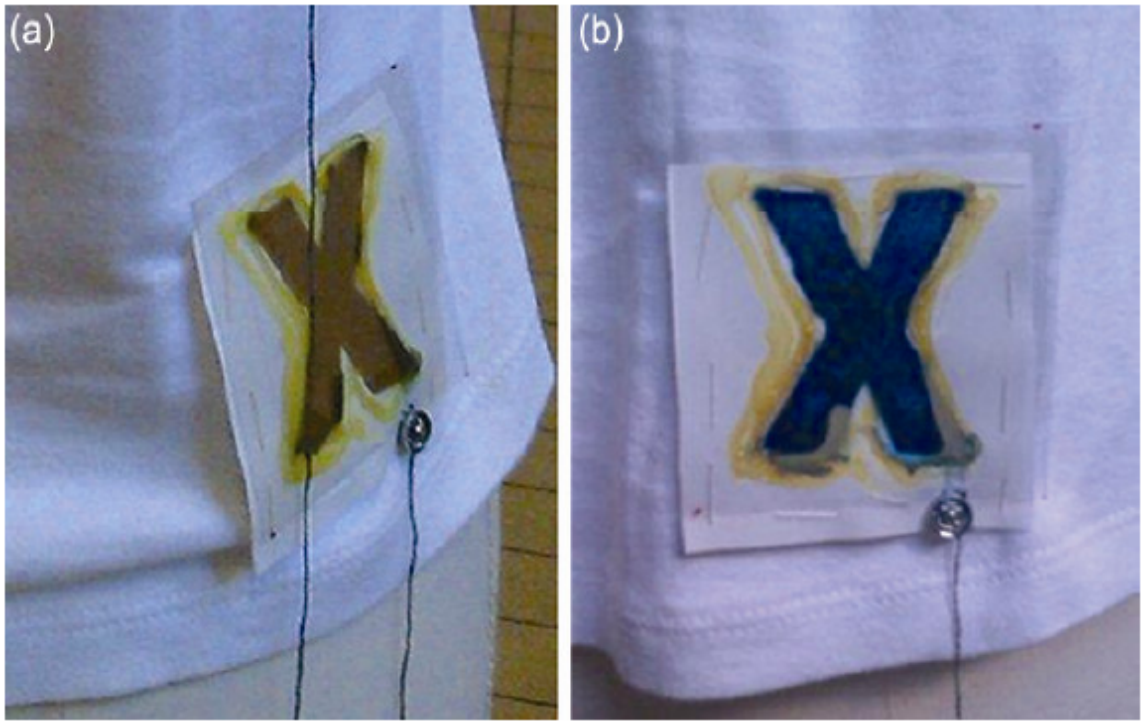

Figure 1.15 A flexible electrochromic fabric device using silver-coated fabric and PET-ITO as the electrodes and Prussian blue as the electrochromic material, shown in its a) oxidized and b) neutral states. Reprinted from Reference 59 with permission from NISCAIR Publications.

Another EFD construction exhibited an electrochromic effect but its operational mechanism relied on more than just the voltage of a traditional ECD. Laforgue used PEDOT nanofibers as a conducting matrix to resistively heat a fabric that had thermochromic microcapsules imbedded in the PEDOT regions, thus producing a color-changing effect.[60] Laforgue's work could be practically described as a thermoelectrochromic fabric system. This technology could be manufactured with nanofiber non-wovens and then employ the printing of logos with a thermochromic ink to produce color-changing fabric, as seen in Figure 1.16. This is a unique approach in that it does not require a second electrode or a sandwich, and it is entirely fabric-based, making

it amenable to flexibility and wearability. The downside of such a system is the heavy impact of ambient temperature on thermochromic systems, as well as the energy requirements for sustained resistive heating.

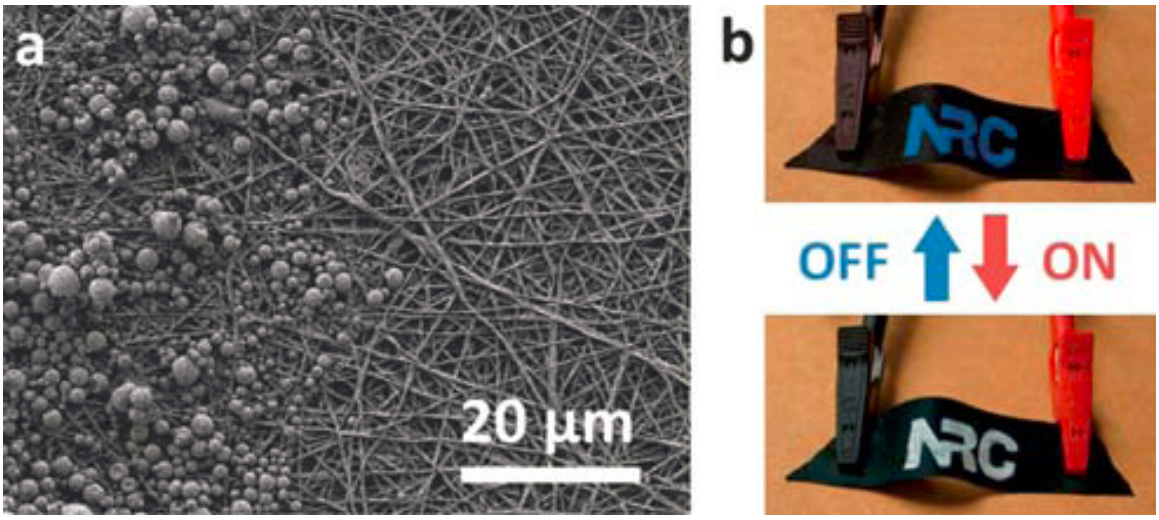

Fig 1.16 Laforgue *et al.* have produced a thermoelectrochromic system that uses resistive heating of a conductive, all-organic fabric to effect a color change in thermochromic microcapsules. (a) SEM image of thermochromic microcapsules painted on the PEDOT nanofibers. (b) Illustration of the electrochromic effect by applying 0.120 mA to the conductive fabric. Reproduced from Ref 35 with permission of The Royal Society of Chemistry.

1.5 Non-Electrochromic Color Changing Materials

Color-changing fabric is not limited to electrochromic materials. There have been several technologies besides electrochromism used for color-changing fabric, including thermochromic,[51,52] photochromic,[53-57] fiber optics,[58] LCDs,[59] and LEDs.[60,61] Some examples are described in detail in this section, ranging from shoes to shirts to intimate apparel. Some of the technologies have been commercialized, and could inform possible potential applications of ECDs.

Otley (2015)

1.5.1 Thermochromic Materials

Thermochromism is the ability to change color due to a change in temperature. Generally, thermochromic fabrics are manufactured with two separate dyes, where one dye stays constant despite a change in temperature and another, leuco dye (thermochromic), that is enclosed in microcapsules is attached to the fibers of the fabric.[62] The thermochromic dye is usually colorless in one state and colored in the other, which is caused by a chemical reaction that occurs when it reaches a certain temperature range (either a rise in temperature or a drop in temperature, depending on the dye). The color is dependent upon the dye of the fabric and the thermochromic dye in its colored and/or bleached state. There are several products currently commercialized exhibiting thermochromic fabrics. For example, in 2011, Puma released thermochromic shoes in conjunction with the Freezy Freakies brand, whose thermochromic dyes undergo a color change with a drop in temperature, as seen in Figure 1.17.[62-66]

Figure 1.17 – An example of a thermochromic fabric system, here in the form of a shoe marketed by Puma in 2011. *Photo: Puma.*

Otley (2015)

1.5.2 Photochromic Materials

Photochromism is the ability to reversibly change color when exposed to light, and the phenomenon was originally discovered in the 1880's. Photochromic dyes are typically made of organic molecules and are in their clear state until they are irradiated by ultraviolet light.[65,66] The λ_{max} (peak absorbance wavelength), which is 365 nm, is generally referred to as a "blacklight", and ultraviolet light is mostly in the 320 and 400 nm range. The photochromic dyes undergo a molecular excitation transition when exposed to ultraviolet light causing the dye to shift its energy into the visible range.[67] When not in the presence of heat and ultraviolet light the photochromic dye undergoes the reverse reaction and reverts to it's clear state.[67] Thus, photochromic fabric has significant limitations to adaptive camouflage, displays, and other applications because it is a passively-controlled system and cannot be made user-controlled. An example of a photochromic fabric can be seen in Figure 1.18. Del Sol has been manufacturing photochromic clothing since 1994, and uses its own proprietary Spectrachrome® photochromic dyes.[68]

Otley (2015)

Figure 1.18 An example of photochromic fabric from Del Sol. *Photo: DelSol.com*

1.5.3 LED and LCD Technology

Light-emitting diodes (LEDs) have been around since the early 1960's, originally only emitting red light. Since then, they have been developed to cover nearly the entire spectral range and have found utility in many display and lighting applications. The use of LEDs in shoes has been around since the early 1990's, with LA Gear's L.A. Lights,[68-71] which came out in 1992. However, the lights were only imbedded in the rubber portion sole of the shoe and not on the fabric itself. Philips, however, launched LumaLive in 2007, which uses LEDs sewn into clothing and fabrics, such as couches and pillows, to

display simple imagery as shown in Figure 1.19.[71] These devices require a lot of power, however, and the battery constraints make portability a concern.

Figure 1.19 An example of Phillips Lumalive clothing. *Photo: Philips.*

Liquid crystalline displays (LCDs) have been around even longer since liquid crystals were originally discovered in 1888, and have been used for simple monochromatic displays in everything from calculators to gas pumps. Their use in apparel seems limited, however, more recently, Studio Roosegaarde has been developing color-changing apparel that uses sensors to change the color of an LCD-garment according to mood.[75] The garment measures the person's heart rate, and an increase in pulse signals the LCD

clothing go from dark to light. As stated by the designer, it can be used on the red carpet or in sensual situations. Figure 1.20 shows a dress from the Intimacy Black clothing line released in 2010.

Figure 1.20 The left side shows the dark state and on the right is the clear state for Intimacy Black, an LCD-based apparel product line that links the color change to the wearer's heart rate. *Photo: Studio Roosegaarde.*

1.6 Conclusion

The realm of ECDs and EFDs are still in its infancy, with much research and development still needed in order to realize the full potential of this technology. Electrochromics could soon become reality for applications such as displays, sunglasses,

windows, color-changing clothing from fabric that is flexible with uses in adaptive camouflage, biomimicry, wearable displays, and fashion.

There remain several challenges for ECDs to become a mainstream technology, however. The need for full color displays requires the synthesis of a variety of electrochromic polymers that can cover the full visible range of colors. Enhancement of electrode conductivity and an understanding of substrate color are needed for the longevity, speed, and color tuning of the final devices. The design and durability of the electronic system must also be optimized. These challenges are not insurmountable, however, and will require simply time and effort on the part of talented engineers.

ECDs and EFDs also have the potential to serve as sensors, due to the fact that the fabric is already conductive. Under Armour is envisioning clothing that monitors heart rate, body temperature, and changes color.[76] The example is shown in Figure 1.21 where the woman's jogging suit changes from grey to blue. The conductive fabric can double as a sensor to monitor these parameters as well as serve as the display for the information.

Otley (2015)

Figure 1.21 – A concept of a future Under Armour product: a full-body running suit capable changing colour from grey to blue with an integrated arm-display and control mechanism. *Photo: Under Armour "I Will Innovation" ©2013.*

The fashion world can benefit from electrochromic fabric, as well. The designs can be endless and ever changing. A person could form their own design and download it to the clothing. Adaptive camouflage and military applications are logical extensions of this technology, as well. The future of this field may appear to be in the realm of science fiction, but it is rapidly becoming science fact. The basic technology exists to make it a

reality; it is only a matter of time before the challenges are met and EFDs become a part of our everyday lives.

1.7 Scope of Thesis

The goal of this Ph.D. was to design and synthesize a variety of small molecules, oligomers, and polymers for use in various electronic devices. Fortunately, several studies worked out, and has led to a very cohesive story for this dissertation. The story begins with the optimization of electrochromic devices to achieve well over 10,000 cycles with adding only one step to the synthetic procedure of the monomer. The next step was to deduce the structure property relationships of 1,3-substituted ProDOTs for a better understanding on how to color tune electrochromics. By understanding the polymer structure with various substituents and stereochemistry's we were able to use this knowledge to color tune by understanding how to cause a blue shift or red shift of a given electrochromic polymer. Now with the fundamental understanding of both the electrochromic polymer and the gel electrolyte of the electrochromic device, we were able to develop a system for high-throughput screening of electrochromic polymers. With the knowledge of the fundamental diffusion of small molecules in the gel electrolyte, we could calculate the exact feed ratio of a given copolymer to exactly color match for a specific application. Now that we had the ability to color tune electrochromics anywhere within the visible spectrum (and outside) we focused on systems that would completely absorb the visible region leading to a neutral or 'black' color. The importance of this work is the potential development of electrochromic displays, since all displays require neutral colors. This began with a static yellow dye mixed with PEDOT a blue polymer

that yielded a neutral color. However, the contrast was poor and left an undesirable yellow color in the clear state, so we development electrochromic dyes by using oligomers of ProDOT-Me_2. By increasing the size of the oligomer we were able to color tune from yellow to blue depending on the number of units of the oligomer. Then we made our highest contrasting neutral system that consisted of a dual copolymer system that we were able to accurately predict before building a single device through low level computational modeling. This work has the potential to impact industry and consumers and will hopefully be used to help develop electrochromic sunglasses, windows, displays, fabric, and fabric displays. The last chapter of this thesis reports the method to achieve the highest conductivities of conducting polymers to date. By fully characterizing and understanding the mechanism of this phenomenon we were able to replicate this in several systems with potential applications ranging from wires, to optically transparent conductors, to antennae, and cardio respiratory sensors.

Otley (2015)

1.8 References

1. A. Petr, A. Neudeck, L. Dunsch, *Chem. Phys. Lett.* **2005**, *401*, 130.
2. N. Basescu, Z.-X. Liu, D. Moses, A. J. Heeger, H. Naarmann, N. Theophilou, *Nature* **1987**, *327*, 403.
3. J. L. Bredas, G. B. Street, *Acc. Chem. Res.* **1985**, *18*, 309.
4. S.K. Deb, J.A. Chopoorian, *J. Appl. Phys.* **1968,** 37, 4818.
5. S. K. Deb, *Appl. Opt.* **1969**, *8*, 192.
6. M. Hamedi, R. Forchheimer, O. Inganas, *Nature Materials* **2007**, *6*, 357-362.
7. T.J. Ha, P. Sonar, A. Dodabalapur, *Applied Physics Letters* **2011**, *98*, 253305.
8. B. Hu, D. Li, O. Ala, P. Manandhar, Q. Fan, D. Kasilingam, P. D. Calvert, *Advanced Functional Materials* **2011**, *21*, 305-311.
9. W. H. Kim, a J. Mäkinen, N. Nikolov, R. Shashidhar, H. Kim, Z. H. Kafafi, *Applied Physics Letters* **2002**, *80*, 3844.
10. H. Youn, M. Yang, *Applied Physics Letters* **2010**, *97*, 243302.
11. C. Yumusak, N. S. Sariciftci, *Applied Physics Letters* **2010**, *97*, 033302.
12. F. Zhang, M. Johansson, M. R. Andersson, J. C. Hummelen, O. Inganäs, *Advanced Materials* **2002**, *14*, 662-665.
13. G. Li, V. Shrotriya, J. Huang, Y. Yao, T. Moriarty, K. Emery, Y. Yang, *Nature Materials* **2005**, *4*, 864-868.
14. S. Lee, S. Nam, H. Kim, Y. Kim, *Applied Physics Letters* **2010**, *97*, 103503.
15. P. Tehrani, L.-O. Hennerdal, A. L. Dyer, J. R. Reynolds, M. Berggren, *Journal of Materials Chemistry* **2009**, *19*, 1799.

16. A. A. Argun, P.-H. Aubert, B. C. Thompson, I. Schwendeman, C. L. Gaupp, J. Hwang, N. J. Pinto, D. B. Tanner, A. G. MacDiarmid, J. R. Reynolds, *Chem. Mater.* **2004**, *16*, 4401-4412.
17. P. M. Beaujuge, S. Ellinger, J. R. Reynolds, *Nat. Mater.* **2008**, *7*, 795-799.
18. A. T. Taskin, A. Balan, Y. A. Udum, L. Toppare, *Smart Materials and Structures* **2010**, *19*, 065005.
19. C. Zhang, Y. Xu, N. Wang, Y. Xu, W. Xiang, M. Ouyang, C. Ma, *Electrochimica Acta* **2009**, *55*, 13-18.
20. H. Seol, H. Jeong, S. Jeon, *Journal of Electroanalytical Chemistry* **2009**, *636*, 107-112.
21. M. Ak, E. Şahmetlioğlu, L. Toppare, *Journal of Electroanalytical Chemistry* **2008**, *621*, 55-61.
22. A. S. Sarac, G. Sonmez, F. C. Cebeci, *Journal of Applied Electrochemistry* **2003**, *33*, 295-301.
23. M. A. Invernale, V. Seshadri, D. M. D. Mamangun, Y. Ding, J. Filloramo, G. A. Sotzing, *Chemistry of Materials* **2009**, *21*, 3332-3336.
24. Y. Ding, M. A. Invernale, D. M. D. Mamangun, A. Kumar, G. A. Sotzing, *Journal of Materials Chemistry* **2011**, *21*, 11873-11878.
25. *http://ocw.mit.edu/courses/materials-science-and-engineering/3-091-introduction-to-solid-state-chemistry-fall-2004/readings/notes_10.pdf* **n.d.**, Accessed 6-5-2011.
26. W. Liptay, *Angewandte Chemie International Edition,* **1969**, *8*, 177-188.

27. R. J. Mortimer, *American Scientist*, **2013**, *101*, 38.

28. C. G. Granqvist, *Solar Energy Materials and Solar Cells,* **2000***, 60*, 201-262.

29. S. K. Deb, *Solar Energy Materials and Solar Cells,* **92,** 2 (2008) 245-258.

30. E. Avendaño, L. Berggren, G. A. Niklasson, C. G. Granqvist, A. Azens, *Thin Solid Films*, **2006,** *496*, 30-36.

31. P. M. S. Monk, *The Viologens: Physicochemical Properties, Synthesis and Applications of the Salts of 4,4'-Bipyridine*, J. Wiley & Sons, Chichester, (**1998**).

32. R. Cinnsealach, G. Boschloo, S. N. Rao, D. Fitzmaurice, *Solar Energy Materials and Solar Cells,* **1998,** *55*, 215-223.

33. X. W. Sun, J. X. Wang, *Nano Letters,* **2008***, 8*, 1884-1889.

34. D. G. Kurth, J. P. López, W. Dong, *Chemical Communications,* **2005**, *16*, 2119-2121.

35. C. G. Granqvist, *Handbook of Inorganic Electrochromic Materials*, Elsevier, p. 663 (**1995**).

36. Y. Ohsedo, I. Imae, Y. Shirota, *J. Poly. Sci. Part B: Polym. Phys.* **2003**, *41*, 2471-2484.

37. I. Imae, K. Nawa, Y. Ohsedo, N. Noma, Y. Shirota, *Macromolecules*, **1997**, *30*, 380-386.

38. A. Pawlicka, *Development of Electrochromic Devices*. *Recent Patents on Nanotechnology,* **2009**, *3*, 177.

39. J. P. Desmond, P. J. Lawlor. "Rearview mirror." U.S. Patent No. D351,370. 11 Oct. **1994**.

40. C. M. Lampert, *Solar Energy Materials and Solar Cells,* **2003**, *76*, 489-499.

41. C. G. Granqvist, A. Hultåker, *Thin Solid Films*, **2002**, *411*, 1-5.

42. P. M. Beaujuge, J. R. Reynolds. *Chemical Reviews* **2010,** *110*, 268-320.

43. M. A. Invernale, Y. Ding, G. A. Sotzing. *All-organic electrochromic spandex, ACS Applied Materials & Interfaces* **2010**, *2,* 296-300.

44. R. V. Gregory, W. C. Kimbrell, H. H. Kuhn, *Journal of Coated Fabrics,* **1991**, *20*, 167-175.

45. S. Beaupré, J, Dumas, M. Leclerc, *Chemistry of Materials,* **2006**, *18*, 4011-4018.

46. X. Li, G. Zhao, J. Qian, Z. Fu, *Gaodeng Xuexiao Huaxue Xuebao/Chemical Journal of Chinese Universities,* **2009,** *30*, 1052-1054.

47. X. Li, J. Qian, Z. Fu, *Preparation and electrochromic properties of polyaniline based on conducting textile. Journal of Beijing Institute of Clothing Technology (Natural Science Edition),* **2009**, *29*, 12-17.

48. S. Takamatsu, K. Matsumoto, I. Shimoyama, *Stretchable yarn of display elements.* Paper presented at the *Proceedings of the IEEE International Conference on Micro Electro Mechanical Systems (MEMS),* **2009**. 1023-1026.

49. Q. Zhang, B. Xin, L. Lin, *Advanced Materials Research,* **2013***, 651,* 77-82.

50. J. Molina, M. F. Esteves, J. Fernández, J. Bonastre, F. Cases, *European Polymer Journal,* **2011**, *47*, 2003-2015.

51. J. Mokhtari, M. Nouri, *Fibers and Polymers,* **2012,** *13*, 139-144.

52. F. M. Kelly, L. Meunier, C. Cochrane, V. Koncar, *Displays,* **2013**, 34, 1-7.

53. F. M. Kelly, L. Meunier, C. Cochrane, V. Koncar, *IEEE/OSA Journal of Display Technology,* **2013**, *9*, 626-631.
54. F. M. Kelly, J. H. Johnston, T. Borrmann, M. J. Richardson, *Eur. J. Inorg. Chem.* **2007**, 5571-5577.
55. M. A. Invernale, Y. Ding, D. M. D. Mamangun, M. S. Yavuz, G. A. Sotzing. *Advanced Materials* **2010**, *22*, 1379-1382.
56. G. A. Sotzing, J. R. Reynolds, P. J. Steel, *Advanced Materials* **1997**, *9*, 795-798.
57. Y. Ding, M. A. Invernale, G. A. Sotzing. *ACS applied materials & interfaces,* **2010**, *2*, 1588-1593.
58. M. A. Invernale, Y. Ding, G. A. Sotzing. *Coloration Technology* **2011**, *127*, 167-172.
59. L. Meunier, F. M. Kelly, C. Cochrane, V. Koncar, *Indian Journal of Fibre and Textile Research,* **2011**, *36*, 429-435.
60. A. Laforgue, *J. Mater. Chem.* **2010**, 20, 8233-8235.
61. K. Fujita, H. Inagaki, N. Ishimura, T. Kataoka, T. Kito, N. Matunami, N. Nakasuji, M. Ozaki, Y. Shibahashi. *Thermochromic textile material*. U.S. Patent 4,681,791, issued July 21, **1987**.
62. R. M. Christie, I. D. Bryant. *Coloration technology* **2005**, *121*, 187-192.
63. T. Cheng, T. Lin, J. Fang, R. Brady. *Textile research journal* **2007**, *77*, 923-928.
64. T. Cheng, T. Lin, R. Brady, and X. Wang. *Fibers and Polymers* **2008**, *9*, 521-526.
65. S. Billah, M. Reduwan, R. M. Christie, R. Shamey. *Coloration Technology* **2008**, *124*, 223-228.

66. S. Billah, M. Reduwan, R. M. Christie, K. M. Morgan. *Coloration Technology* **2008**, *124*, 229-233.

67. M. Aldib, R. M. Christie. *Coloration Technology* **2011**, *127*, 282-287.

68. J. K. Guy, *Fiber optic fabric*. U.S. Patent No. 20,040,037,091. 26 Feb. **2004**.

69. D. Swain, *Display system in article of clothing*. U.S. Patent No. 7,787,240. 31 Aug. **2010**.

70. J. Cheung, *Clothing or footwear illumination system having electro-luminescent and LED light sources*. U.S. Patent No. 7,329,019. 12 Feb. **2008**.

71. D. Graham-Rowe, *Photonic fabrics take shape*. *Nature Photonics* **2007**, *1*, 6-7.

72. W. Freeman, *Puma x freezy freakies(color change.) www.kicksonfire.com,* Feb. 14, **2011**.

73. https://www.delsol.com

74. Bemis, Jon L., Mariamia Godinez, and Mark R. Goldston. "Footwear with flashing lights." U.S. Patent 5,303,485, issued April 19, **1994**.

75. http://www.studioroosegaarde.net/project/intimacy-black/

76. T. Riggs. *Under armour thinks touchscreen clothing is the next big thing*. *Zaggs,* March 25, **2013**.

Otley (2015)

2. Chapter 2: Experimental Procedures, Materials, and Instrumentation

This chapter provides an overview of the procedures, materials, instrumentation, and general synthesis in this dissertation. More in depth synthesis and procedures for each particular system are contained in each corresponding chapter.

2.1.1 Materials

All materials were used as purchased unless indicated within the procedure that the solvent or reagent was additionally purified. All reagents and solvents were purchased from Sigma Aldrich and Fisher Scientific unless specified.

2.1.2 General Synthesis

All general organic lab techniques were followed including techniques for extremely water sensitive reactions. For example, all glassware was flame-dried under vacuum (0.9 torr), all solvents were transferred via cannulation, and all reactions described in this thesis were only performed under ultra high purity argon. The molecules were characterized with ^{1}H NMR and ^{13}C NMR on a 500 MHz Bruker Avance. Gas Chromotography Mass Spectrometry (GC/MS) was performed on a Hewlett Packard 6890, and infrared spectrometry was performed on a Nicolet Magna-IR 560 Spectrometer.

2.2 Monomer Synthesis

All chemicals were purchased and used as is if there is no purification mentioned in the experimental. All solvents were distilled other than tetrahydrofuran (THF) and toluene which were cannulated from the dry solvent system under argon. The chemicals purchased for synthesis were: neopentyl glycol, 3-methylbutan-2-one, isobutyraldehyde, lithium diisopropylamide (LDA), diisobutyl aluminum hydride (DiBAL),

dodecylbenzene sulfonic acid (DBSA), p-toluene sulfonic acid (pTSA), pinacolone, pivaldehyde, 4Å molecular sieves were purchased from Sigma Aldrich, the silica gel and TLC plates used for column chromatography were purchased from Sorbent, and 3,4-dimethoxythiophene (DMOT) was purchased from a chemical supplier in China. The general synthesic procedures of the common monomers used in this dissertation are listed here for quick reference, and certain chapters contain more specific details of mechanisms and synthesis.

Otley (2015)

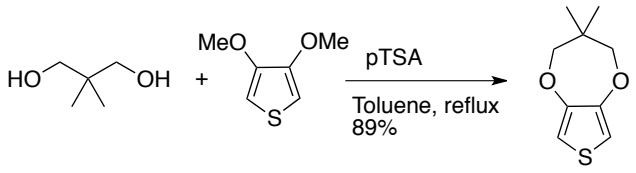

2,2-dimethyl-propylenedioxythiophene (ProDOT-Me_2)

The procedure was modified from the literature.[1] 3,4-Dimethoxythiophene (DMOT) (20 g, 138 mmol), neopentyl glycol (28 g, 270 mmol), p-toluene sulfonic acid (pTSA) (7.2 g, 20 mmol) and 1500 mL of dry toluene were combined in a 2000 mL 3-neck round bottom flask equipped with a Soxhlet extractor with type 4 A molecular sieves in the thimble as seen in the synthetic scheme above. The oil bath was heated to 180°C to reflux, and allowed to reflux overnight. The reaction mixture was cooled, and the toluene was evaporated under vacuum. Then the reaction mixture was dissolved in ethyl acetate, and washed with plenty of water. Due to the presence of pTSA, while washing with water, an emulsifier results if left in toluene, but with ethyl acetate an emulsion does not form. The ethyl acetate was removed under vacuum, and the crude product was purified by column chromatography on silica gel with 4:1 hexanes/ethyl acetate as the eluent to yield Pro-DOT-Me2 as a white solid. Then recrystallization was performed to ensure ultra high purity for use in devices with hexanes as the solvent (22.60 g, 89%). ^{1}H-NMR (500 MHz; $CDCl_3$): δ 6.45 (s, 1H), 3.71 (s, 2H), 1.01 (s, 3H). ^{13}C-NMR ($CDCl_3$) δ 150.1, 105.6, 80.2, 39.0, 21.8. MP: 45-46.5˚C. GC/MS (m/z): 184

Otley (2015)

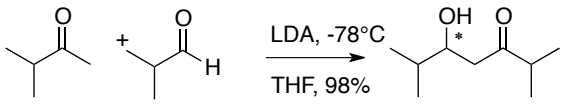

5-hydroxy-2,6-dimethylheptan-3-one (HDMH-One)

The procedure was modified from the literature.[2] To a solution of 3-methylbutan-2-one (15 g, 174 mmol), in anhydrous THF (500 mL), at -78°C was added a 2.0 M solution of LDA in hexane (105 mL, 210 mmol) over a period of 30 min. The reaction was stirred at -78°C for another 30 min. To the resulting white suspension isobutyraldehyde (12.6 mL, 174 mmol) was added drop-wise via syringe and the reaction continued for another 30 minutes at -78°C. Adding 10 mL of water quenched the reaction. Approximately 80% of the THF was removed and the mixture was then poured into a saturated aqueous solution of NH_4Cl. The aqueous layer was extracted twice with diethyl ether (200 mL) and the organic layer was washed with water. The organic layer was then dried over $MgSO_4$ and concentrated to give a crude white oil of β-hydroxy ketone (27 g, 98%). The crude product was recrystallized from petroleum ether to give pure white solid with a yield of 90%. ^{1}H NMR ($CDCl_3$, 500 MHz, δ): 3.61 (lH, ddd), 3.12 (lH, d), 2.68 (lH, dd), 2.40 (lH, dd), 1.12 (6H, s) 0.89 (6H, s); ^{13}C-NMR: 209.45, 75.11, 38.03, 34.41, 26.35; FTIR (KBr): 3475, 2800, 1700, 1460, 1380, 1360, 1320, 1280, 1060, 1000 cm^{-1}. GC/MS (m/z): 158

Otley (2015)

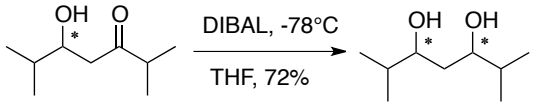

2,6-dimethylheptane-3,5-diol (DMH-Diol)

The procedure was modified from the literature.[3,4] To a solution of β-hydroxy ketone (10 g, 63 mmol) in THF (250 mL) was added 1 M DIBAL in hexane, (126 mL, 126 mmol) at -78°C, and the solution was stirred for 2 hrs at this temperature. The reaction mixture was allowed to warm to room temperature and continued overnight at room temperature. The reaction mixture was then quenched with 2 N aqueous HCl solution. The mixture was then extracted twice with ether (200 mL), and the combined organic layer was washed with saturated aqueous $NaHCO_3$ solution and with brine. Drying with anhydrous $MgSO_4$ and concentration gave the crude DMHDiol (8.5 g, 84 % yield) as a white solid. The crude diol was further purified by column chromatography using petroleum ether and ethyl acetate mixture (80:20) to give purified product with a yield of 72%. ^{1}H NMR ($CDCl_3$, 500 MHz, δ): 3.51 (2H, bs), 3.43 (2H, dd), 1.72 (lH, ddd), 1.29 (lH, ddd), 0.89 (12H, s); ^{13}C-NMR: 80.23, 35.45, 31.42, 26.09, 25.89; FTIR (KBr): 3400 (b), 2910, 1480, 1130, 880 cm^{-1}. GC/MS (m/z): 160

Otley (2015)

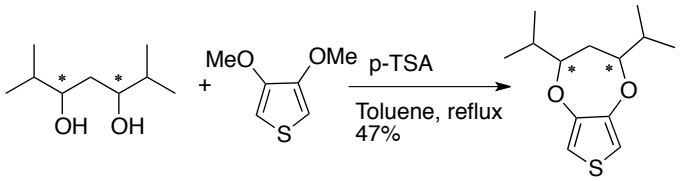

1,3-di-isopropyl-propylenedioxythiophene (1,3-ProDOT-iP_2)

A similar procedure was followed for the synthesis of the 1,3-ProDOT-iP_2 monomer as reported previously for ProDOT-Me_2. However, the temperature of the reaction was monitored closely and held at 140°C for the oil bath. The reaction was deemed completed when the DMOT was consumed according to GC/MS. The molar proportion between the reactants is modified to DMOT: 2,6-dimethylheptane-3,5-diol: pTSA = 1.00 : 2.00 : 0.30. 3,4-Dimethoxythiophene (DMOT) (2 g, 14 mmol), 2,6-dimethylheptane-3,5-diol (4.48 g, 28 mmol) and pTSA (0.8 g, 4.2 mmol), were reacted to yield 2.3 g of crude 1,3-ProDOT-iP_2. The crude product was purified by column chromatography on a silica gel with toluene and hexane mixture (25:75) as eluent to obtain a light yellow solid. Then recrystallization with isopropyl alcohol ensured high purity for use in devices (47%, 1.56 g). ^{1}H NMR ($CDCl_3$, 500 MHz, δ): 6.50 (2H, s), 3.96 (2H, m), 2.10 (1H, m), 1.90 (1H, m), 1.55 (3H, s), 1.25 (3H,s); ^{13}C NMR: 150.63, 106.26, 90.45, 35.32, 23.63; GC-MS (m/z): 240

Otley (2015)

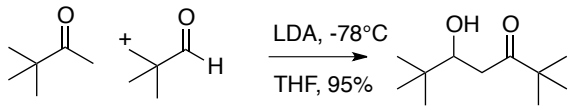

5-Hydroxy-2,2,6,6,-tetramethyheptan-3-one (HTMH-One)

2,2,6,6-Tetramethyl-3,5-heptanediol (TMHDiol) was synthesized by a similar procedure reported earlier. To a solution of pinacolone (10 g, 100 mmol), in anhydrous THF (500 mL), at -78°C was added a 2.0 M solution of LDA in hexane (60 mL, 120 mmol) over a period of 30 min. The reaction was stirred at -78°C for another 30 min. To the resulting white suspension pivaldehyde (10.9 mL, 100 mmol) was added drop-wise via syringe and the reaction continued for another 30 minutes at -78°C. The reaction was then quenched by adding 10 mL of water. Approximately 80% THF was removed and the mixture was then poured into saturated aqueous solution of NH_4Cl. The aqueous layer was extracted twice with diethyl ether (200 mL) and the organic layer was washed with plenty of water. The organic layer was then dried over $MgSO_4$ and concentrated to give a crude yellow solid of β-hydroxy ketone (17.2 g, 95%). The crude product was recrystallized from hexane to give pure white solid with a yield of 81%. ^{1}H NMR ($CDCl_3$, 500 MHz, δ): 3.64 (lH, ddd), 3.16 (lH, d), 2.74 (lH, dd), 2.46 (lH, dd), 1.14 (9H, s) 0.91 (9H, s); ^{13}C-NMR: 209.23, 75.26, 38.11, 34.45, 26.50, 25.93; FTIR (KBr): 3475, 2800, 1700, 1460, 1380, 1360, 1320, 1280, 1060, 1000 cm^{-1}. GC-MS (m/z): 186

Otley (2015)

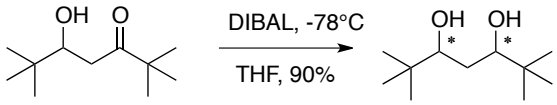

2,2,6,6-Tetramethyl-3,5-heptanediol (TMHDiol)

To a solution of β-hydroxy ketone (10 g, 53 mmol) in THF (250 mL) was added 1 M DIBAL in hexane, (118 mL, 118 mmol) at -78°C, and the solution was stirred for 2 hrs at this temperature. The reaction mixture was allowed to warm to room temperature and continued for another 8 hrs at room temperature. After 8 hrs the reaction mixture was quenched with 2 N aqueous HCl solution. The mixture was then extracted twice with ether (200 mL), and the combined organic layer was washed with saturated aqueous $NaHCO_3$ solution and with brine. Drying with anhydrous $MgSO_4$ and concentration gave the TMHDiol (9 g, 90% yield) as a white solid. ^{1}H NMR ($CDCl_3$, 500 MHz, δ): 3.54 (2H, bs), 3.45 (2H, dd), 1.74 (1H, ddd), 1.31 (1H, ddd), 0.91 (18H, s); ^{13}C-NMR: 81.82, 35.23, 31.29, 25.99, 25.80; FTIR (KBr): 3400 (b), 2910, 1480, 1130, 880 cm^{-1}. GC/MS (m/z) 188

Otley (2015)

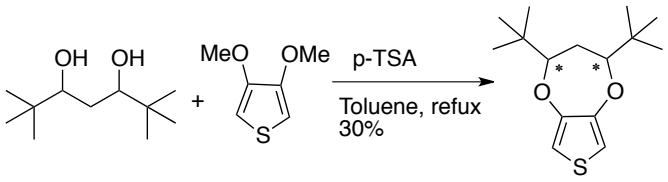

1,3-di-*tert*-butyl-propylenedioxythiophene (ProDOT-tB_2)

The synthesis of ProDOT-tB_2 is similar to the transetherifications reported earlier. The amounts used were: 3,4-Dimethoxythiophene (DMOT) (2 g, 14 mmol), 2,2,6,6-tetramethylheptane-3,5-diol (28 mmol) and p-toluene sulfonic acid (0.67 g, 2.08 mmol) (DBSA). The molar proportion between the reactants is thus maintained to DMOT : 2,2,6,6-tetramethylheptane-3,5- diol : DBSA = 1.00 : 2.00 : 0.30. The oil bath was heated to 140°C and allowed to reflux until the reaction was completed according to GC/MS. The reaction mixture was cooled and the toluene was removed under vacuum. A viscous, oily substance was obtained, which was then dissolved into ethyl acetate and extracted with water three times to remove any water soluble component from the crude reaction mixture. The organic layer was collected and the solvent was evaporated to obtain a light brown oily liquid. The crude product was purified by column chromatography on a silica gel with Ethyl acetate and Hexanes (Ethyl acetate: Hexanes = 05:95) as eluent to obtain a white solid. The solid was then recrystallized from isopropyl alcohol to ensure high purity (30%, 1.12 g). ^{1}H NMR ($CDCl_3$, 500 MHz, δ): 6.50 (2H, s), 3.28 (2H, dd), 2.15 (1H, dd), 1.81 (1H, d), 1.03 (18 H, s); ^{13}C NMR: 150.93, 106.40, 90.65, 35.49, 33.30, 29.91, 26.38; GC-MS (m/z): 268

Otley (2015)

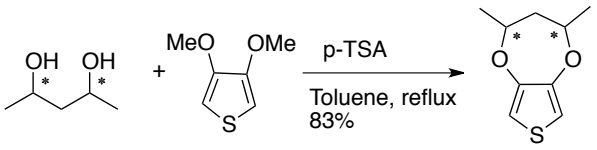

1,3-dimethyl-propylenedioxythiophene (1,3-ProDOT-Me_2)

The synthesis of 1,3-ProDOT-Me_2 was carried out by transetherification of 3,4-dimethoxythiophene with 2,4-Pentane-diol (a mixture of isomers). The reaction procedure was similar as described for 1,3-ProDOT-tB_2. The molar proportion between the reactants is maintained to DMOT : 2,4-Pantane-diol : DBSA = 1.00 : 2.00 : 0.30. 3, 4-dimethoxythiophene (DMOT) (2 g, 14 mmol), 2,4-Pentane-diol (28 mmol) and dodecylbenzene sulfonic acid (0.67 g, 2.08 mmol) (DBSA), were reacted to yield 1.6 g of crude 1,3-ProDOT-Me_2. The crude product was purified by column chromatography on a silica gel with a 1:4 ethyl acetate: hexanes solvent system to obtain a white solid (83%, 2.13 g). ^{1}H NMR ($CDCl_3$, 500 MHz, δ): 6.50 (2H, s), 3.96 (2H, m), 2.10 (1H, m), 1.90 (1H, m), 1.55 (3H, s), 1.25 (3H,s); ^{13}C NMR: 150.63, 106.26, 90.45, 35.32, 23.63; GC-MS (m/z): 184

Otley (2015)

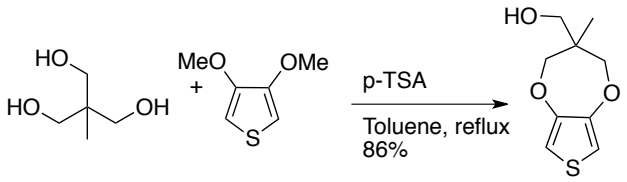

(3-Methyl-3,4-dihydro-2H -thieno[3,4-b][1,4]dioxepin-3-yl)- methanol (ProDOT-OH)

3,4-Dimethoxythiophene (4 g, 27.8 mmol) was taken with 1500 mL of toluene and to this 1,1,1-tri(hydroxy-methyl)ethane (4.32 g, 36.10 mmol) was added followed by p-TSA (0.52 g, 2.78 mmol). The oil bath was heated to 180°C and the mixture was under a continuous flow of argon for 48 h. Excess toluene was evaporated and the greenish black residue was extracted with ethyl acetate, washed repeatedly with water, dried over sodium sulfate and ethyl acetate was removed under vacuum. The crude product was purified by silica gel column chromatography eluting with pet. ether/ethyl acetate (80 : 20) to give a colourless viscous oil which solidified over a period of two days to a white solid. Yield: 4.6 g (86%), ^{1}H NMR (500 MHz, $CDCl_3$) d: 0.95 (s, 3H), 1.70 (s, 1H), 3.73 (d, J ~ 12 Hz, 2H), 3.74 (s, 2H), 4.08 (d, J ~ 12 Hz, 2H), 6.48 (s, 2H); ^{13}C NMR ($CDCl_3$) d: 17.18, 43.93, 65.62, 76.60, 105.77, 149.56; GC/MS (m/z): 200

Otley (2015)

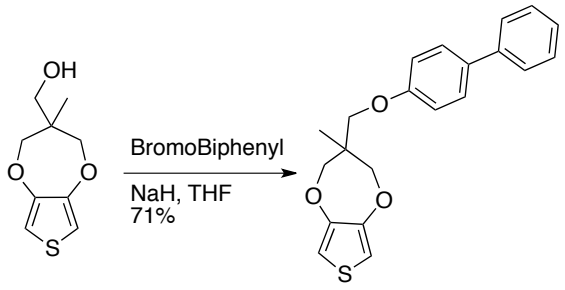

BPMOM-ProDOT

The procedure was modified from the literature.[5] In a flame-dried flask, NaH (60% in mineral oil) (0.3 g, 7.5 mmol) was taken and washed three times with dry pet. ether (2 mL). The pet. ether was removed and dry THF (5 mL) was added followed by ProDOT-OH (1 g, 5 mmol) dissolved in THF (5 mL). The mixture was allowed to stir for ten minutes and finally the halide (7 mmol) was added. After 24 h, the reaction mixture was quenched by adding water, and the product was extracted with ethyl acetate. The organic layer was washed with brine, water, dried over anhydrous $MgSO_4$ and evaporated to give a viscous liquid. Purification was by column chromatography on silica gel using pet. ether–ethyl acetate (95 : 5) a white solid was obtained. Yield ~ 1 g (71.4%); ^{1}H NMR (500 MHz, $CDCl_3$) d: 1.02 (s, 3H), 3.55 (s, 2H), 3.73 (d, J ~ 12 Hz, 2H), 4.05 (d, J ~ 12 Hz, 2H), 4.57 (s, 2H), 6.47 (s, 2H), 7.31–7.47 (m, 5H), 7.55–7.63 (m, 4H); ^{13}C NMR ($CDCl_3$) d: 17.63, 43.60, 73.16, 73.42, 76.85, 105.70, 127.25, 127.28, 127.41, 128.04, 128.92, 137.57, 140.68, 141.04, 150.01; GCMS (m/z): 366

Otley (2015)

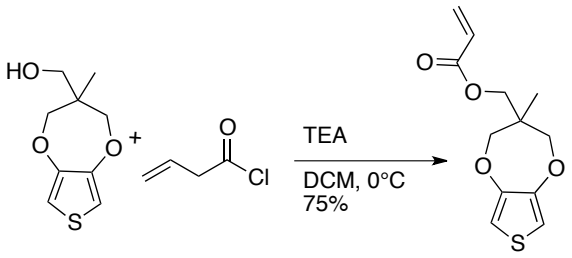

ProDOT-Ac

Under Argon in a three-necked flask, ProDOT-OH (0.26 g, 1.3 mmol) was added to 30 mL of freshly distilled dichloromethane (DCM), and .36 mL of triethylamine (TEA) (0.26 g, 2.6 mmol) was then added to the solution. The solution was then cooled to 0°C and 0.16 mL of acrolyl chloride (0.18 g, 2 mmol) was added dropwise. After two hours the reaction was extracted with 30 mL of water, and 3 x 30 mL of DCM. The organic layer was dried over $MgSO_4$, filtered, and concentrated under vacuum. The crude product was purified using column chromatography with a 1:1 DET/hexanes solvent system. Then the pure fractions from the column were further purified by recrystallization using hexanes as the solvent (0.24 g, 75%). ^{1}H-NMR (500 MHz; $CDCl_3$): δ 6.52 (s, 2H), 6.45 (dd, *J* = 17.3, 1.3 Hz, 1H), 6.18 (dd, *J* = 17.3, 10.5 Hz, 1H), 5.89 (dd, *J* = 10.4, 1.3 Hz, 1H), 4.31 (s, 1H), 4.08 (d, *J* = 12.0 Hz, 1H), 3.79 (d, *J* = 12.0 Hz, 1H), 1.03-1.00 (s, 3H). GC/MS (m/z): 254

Otley (2015)

2.3 Device Material

Lithium trifluoromethanesulfonate (LITRIF), dimethoxyphenylacetophenone (DMPAP), propylene carbonate, poly (ethylene glycol) diacrylate (Mn = 700), pyrrole and bithiophene were purchased from Sigma-Aldrich. EDOT was purchased from Heraeus Clevious GmbH.

2.3.1 General Polymer Electrolyte

5 g of propylene carbonate, 5 g of poly (ethylene glycol) diacrylate (MW = 700), 1 g of LITRIF, and 17.5 mg of DMPAP were added together and sonicated for 15 minutes until dissolved. The electrolyte is observed from colorless to a light yellow liquid before UV exposure, and a transparent colorless gel afterward.

2.3.2 Device Assembly

A rubber gasket was glued between two pieces of ITO consisting of either glass or plastic. The gel electrolyte was filled into the gasket and cured by 365nm UV light. A potential of 3V was applied to the device for 30sec and a potential bias of ±2 V was used for switching. Electrochemistry was carried out using CHI 400 and 660A potentiostats. A PR-670 SpectroScan Spectroradiometer (Photo Research, Inc.) was used for color analysis.

2.4 Instrumentation

This section will provide a brief overview of instrumentation and techniques used in characterizing the electrochromic devices.

Otley (2015)

2.4.1 Ultraviolet-Visible-Near Infrared Spectrophotometry

All spectrophotometry was performed on a Carey UV-Vis-NIR 5000 Spectrophotometer for the electrochromic device studies and also PEDOT:PSS thin film studies. Color calculations were done using Varian's color software (1976 CIE standards, a 10 degree crossover angle, and a D65 illuminant).

Measurement of photopic contrast

Contrast is defined as the change in transmittance between the two extreme redox states of an electrochromic material. Often, contrast is reported at a single-wavelength (λ_{max}). However, for the best representation for reporting contrast is photopic contrast, which consists of a full-spectrum calculation because it's weighted to the sensitivity of the human eye.[26] For best accuracy, photopic contrast $\Delta T_{photopoic}$ is calculated using the transmittance values in the spectral range of 350-850 nm. For both bleached ($T_{photopic,b}$) and colored state($T_{photopic,c}$) in according to the following equation,

(2.1) $$T_{photopic} = \frac{\int_{380}^{780} T(\lambda).S(\lambda).P(\lambda).d\lambda}{\int_{380}^{780} S(\lambda).P(\lambda)\, d\lambda}$$

and photopic contrast,

(2.2) $$(\Delta T_{photopoic}) = \%T_{photopic,b} - \%T_{photopic,c}$$

where $P(\lambda)$ is the normalized spectral response of the human eye, $S(\lambda)$ is the normalized spectral emittance of a blackbody (at 6000°K), and $T(\lambda)$ is the spectral transmittance of the device.

Otley (2015)

Figure 2.1 A Carey UV-Vis-NIR 5000 Spectrophotometer

2.4.2 Colorimetry

To measure color in a precise location within the solid-state electrochromic devices a Spectrascan PR-670 was used to determine the (u', v') color coordinates. These coordinates were then plotted on the 1976 CIE chromaticity diagram described in Chapter 1. The procedure for using the Spectrascan PR-670 includes putting the device or desired substrate inside a black box with a hole on top for a pure white lamp to illuminate the substrate and a hole in the side for the colorimeter. Then point at the desired location and then use the supplied software to convert the coordinates to the chromaticity diagram.

Otley (2015)

Figure 2.2 A Spectrascan radiometer PR-670 used to measure color coordinates.

Otley (2015)

2.6 References

1. C. Gaupp, D. Welsh, J. R. Reynolds, *Macromol. Rapid Commun*. **2002**, *23*, 885–889.
2. *Organic Syntheses,* 1990, Vol. 69, p. 44.
3. A. E. G. Miller, J. W. Bliss, and L. H. Schwatzman, *J. Org. Chem.,* **1959,** *24*, 627.
4. K. Ziegler, K. Schneider, and J. Schneider, *Justus Liebig's Ann. Chem.,* **1959,** *623*, 9.
5. S. Mishra, S. Rabindra, A. Ambade, A. Contractor, A. Kumar. *J. Mater. Chem.* **2004**, *14*, 1896-2000.

Otley (2015)

3. Chapter 3: Optimization of Electrochromic Devices: Acrylated Poly(3,4-propylenedioxythiophene) For Enhancement of Lifetime and Optical Properties Electrochromic Devices

3.1 Overview

This chapter concentrates on the progress we have made over my graduate career on the optimization of electrochromic devices with a focus on acrylated ProDOTs for the enhancement of optoelectronic properties. Other electrochromic device optimization studies that I have worked on include ultra flexible devices, and several other studies that look at the different variables/parameters of an electrochromic device.

3.2 Introduction:

Utilizing our in situ method for the one step assembly of single-layer electrochromic devices (ECDs) with a 3,4-propylenedioxythiophene (ProDOT) acrylate derivative, long-term stability was achieved. By coupling the electroactive monomer to the cross-linkable polymer matrix, preparation of the electrochromic ProDOT polymer can occur followed by UV crosslinking. Thus, we achieve immobilization of the unreacted monomer, which prevents any degradative processes from occurring at the counter electrode. This approach eliminated spot formation in the device and increased stability to over 10,000 cycles when compared to 500 cycles with conventional ProDOT devices wherein the monomer is not immobilized. The acrylated electrochromic polymer exhibits similar electrochromic properties, such as photopic contrast (48% compared to 46%) and switch speed (both 2 seconds). This method can be applied to any one-layer electrochromic system where improved stability is desired.

Otley (2015)

Electrochromics alter light transmission through charge injection and removal.[1] Electrochromic materials are gaining popularity due to rapid response speed and high contrast.[2,3] Current commercial applications, such as electrochromic mirrors and smart windows, are primarily small molecule organic or inorganic in composition.[4] Recent high-profile commercial applications include Boeing's use of electrochromic windows in their 787 Dreamliner to eliminate window shades, and Mercedes Benz's use of an electrochromic roof panel in the SLK.[5] Organic ECDs are regarded as the next generation of eyewear, windows, displays, and even fabric.[6-15] These devices are possible due to the use of Conjugated Polymers (CPs) that were originally discovered in the 1970's. CPs rely on the extended π conjugation along the polymer backbone for its spectral absorption. The energy gap between the HOMO and LUMO for CPs changes with an applied voltage since the material changes from an insulator to a semiconductor. This results in absorption shifts and visible color changes, thereby offering a full visible spectral range of colors for these polymers. These properties make conjugated polymers of considerable interest for devices where the optical modulation of transmittance and/or reflectance is desired.

Poly(3,4-Ethylenedioxythiophene) (PEDOT) was first reported as an electrochromic material in 1994. When prepared, it yielded an electrochromic polymer that gave a transition from dark blue in its neutral state to a light, sky blue in its oxidized state.[16] Poly(3,4-propylenedioxythiophene) (PProDOT) and its derivatives have shown the ability to yield higher contrasts than PEDOT.[17] PEDOT has a six-membered planar ring, but ProDOT's seven-membered ring is non planar. This results in increased spacing

along the polymer backbone, reducing the stacking of the polymers, and thus reducing electron chain hopping. In doing so, the absorption in the near infrared (NIR) is reduced along with the tail into the visible region, making them more transmissive in their oxidized state. By modifying the R groups on P(ProDOT), the color transitions can be tuned across the visible spectrum. For example, 2,2-PProDOT-Me_2 transitions between purple and sky blue while 1,3-PProDOT-tBu_2 transitions between yellow and sky blue.[18] Further, Reynolds *et. al.* reported black using EDOT in a donor acceptor polymeric system.[19] Previously reported acrylated ProDOTs and PEDOTs include, for example, 3,4-propylenedioxythiophene-methacrylate (ProDOT-MA) was used as a means for photopatterning electrochromic devices.[20-22] The patterning was accomplished by polymerizing the conjugated polymer by heat, and then the device was photopatterned by UV irradiation. Also, Reynolds *et. al*. recently reported a methacrylate substituted ProDOT copolymer for photopatterning applications.[23]

Our group previously reported the *in situ* method for the fabrication of electrochromic devices (ECDs) that simplified the assembly of ECDs by allowing open-air fabrication, low waste, and shorter assembly steps and times.[24,25] With this *in situ* method, a single layer is prepared between two optically transparent electrode (OTE) substrates which reduces the practice of processing electrochromic devices to a simple lamination procedure. This new procedure can replace the need for the previously reported procedure of a dual layer ECD approach.[26,27] Recently reported in the literature was the demonstration of high-throughput screening of ProDOT monomers (using the *in situ* method), whose polymers are of a single absorption, within a single ECD resulted in

copolymers of different feed ratios exhibiting the full spectral range of the subtractive colors from yellow to blue.[28]

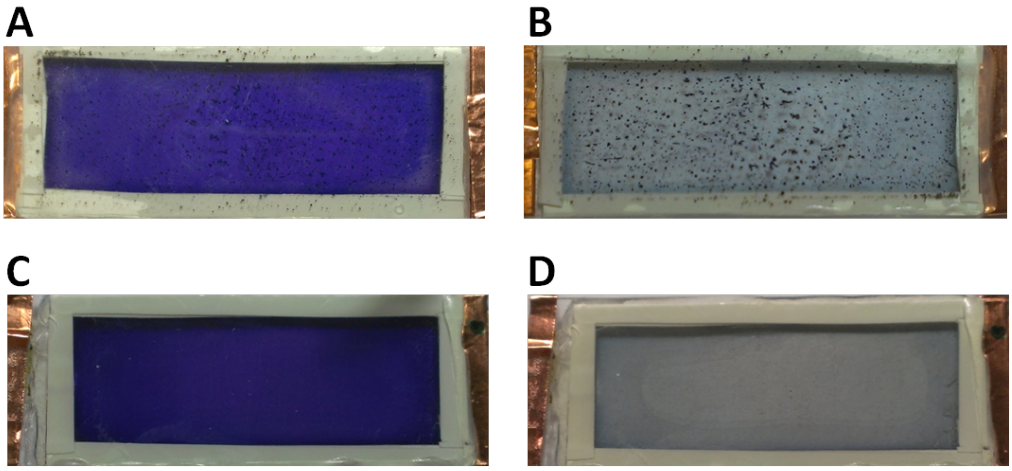

Figure 3.1. (A, B) is the control device (1.9 cm x 5.1 cm with an active area (polymer area) of 1.4 cm x 4.2 cm), PProDOT-Me_2, in the neutral and oxidized states, respectively, that shows spotting after 4,000 cycles. (C, D) is the neutral and oxidized states of PProDOT-Ac, respectively, after 10,000 cycles. Reprinted with permission from M. T. Otley, et al. *ACS Appl. Mater. Interfaces* **2014**, *6*, 1734. Copyright 2014 American Chemical Society.

Long-term stability of *in situ* ECDs is imperative to the commercialization of its many promising applications. Previously, the stability of the *in situ* ECDs heavily relied on the unpolymerized monomers not aggregating on the electrode. When a defect is present in the device, occasionally, spotting issues were seen within the ECDs after several hundred switching cycles that exacerbated over time on some of the devices. The hypothesis was that these spots were caused by unreacted monomers because, with the *in situ* method, polymerization occurs after device assembly by electrochemically polymerizing the monomer in the gel electrolyte. The leftover monomers (*ca.* 95.5%)[24] diffuse[28] towards these nucleation spots on the counter electrode causing the spots to

increase in size over time. The sites where these spots occur are a matter of debate, but most likely they are occurring at a defect site on the indium tin oxide (ITO) coating, since it is only occasionally seen considering the area of the substrate. However, by using a poly(3,4-propylenedioxythiophene) P(ProDOT) modified with an acrylate group (ProDOT-Ac), the conjugated polymer and unreacted monomers can be UV cross-linked at the same time as the gel matrix, integrating them into a tightly cross-linked network that prevents any migration of unreacted materials, thus increasing stability and overall optical quality.

3.3 Results and Discussion

The *in situ* procedure used in our lab has simplified the assembly of ECDs due to open-air fabrication, less waste, and the application of a single layer between OTEs in what could be envisioned as a standard lamination procedure. Most PProDOT-Me_2 devices perform flawlessly without spotting, but as seen in Figure 3.1A, B spotting does occur in some devices after cycling for a period of time. For optical consistency and long-term stability of ECDs, an alternative method was studied. The hypothesis was if an acrylate group was added to the monomer, the unreacted monomers could be locked into the gel matrix upon UV curing. This would, in turn, prevent migration of the monomers to the counter electrode thereby preventing nucleation and growth, provided the spots are due to unreacted monomer. The comparison between the devices prepared from the control, ProDOT-Me_2, and an acrylated ProDOT (ProDOT-Ac) can be seen in Figure 3.1. The PProDOT-Ac device in Figure 3.1C, D shows no evidence of spotting after 10,000

cycles. After 10,000 cycles the PProDOT-Ac devices were still operating exceptionally; 10,000 cycles was chosen as our upper bound because it is a sufficient lifetime for smart glass and eyewear applications. For example, if a window application was cycled once a day it would last 27 years, and for sunglass applications that were cycled 10 times per day it would last close to 3 years.[29] The PProDOT-Ac devices were optimized for film quality and contrast at 7.5% w/w compared to the control, PProDOT-Me_2, at 2.5% w/w. This highlights the low waste and low cost of the *in situ* procedure due to the small concentration of monomer needed for assembling devices.

Otley (2015)

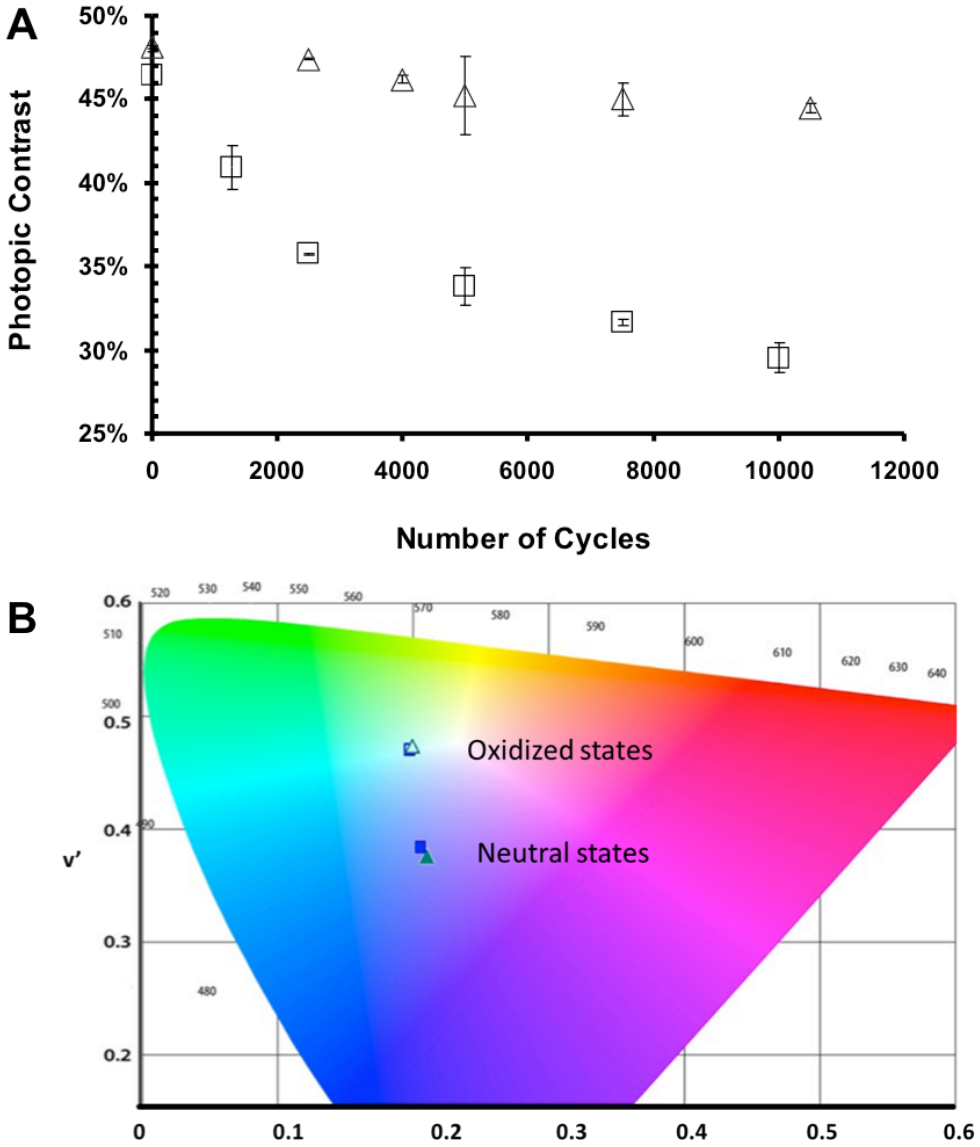

Figure 3.2 (A) The photopic contrast for PProDOT-AC (shown in triangles) with an initial photopic contrast (48%) higher than PProDOT-Me_2 (46% shown in squares), and a drop of only 3 % in the contrast over 10,000 cycles. (B) The color coordinates of PProDOT-Ac and PProDOT-Me_2 in the neutral and oxidized states. Reprinted with permission from M. T. Otley, et al. *ACS Appl. Mater. Interfaces* **2014**, *6*, 1734. Copyright 2014 American Chemical Society.

Otley (2015)

The photopic contrast is improved initially in the PProDOT-Ac devices as seen in Figure 3.2A with an initial photopic contrast of 48% as compared to the control's initial contrast of 46%. Though, the benefit of using the acrylated ProDOT is seen over the course of 10,000 cycles where only a 3% drop in photopic contrast is observed. The PProDOT-Me_2 devices averaged a 14% drop in contrast over 10,000 cycles, where contrast is affected due to deleterious side reactions on the counter electrode. Figure 3.3A, B shows the loss in contrast after 10,000 cycles. The cycling experiments were performed in the most extreme conditions with constant switching over a continuous period of 24 hours, only stopped in order to take contrast measurements. The color of the PProDOT-Me_2 and PProDOT-Ac devices are almost identical, as seen in Figure 3.2B. The color coordinates were determined using the CIE Lu'v' color coordinates (u', v') for each device. The color of the PProDOT-Ac devices were purple with the u', v' color coordinates of 0.2118 and 0.3737, respectively, in the neutral state. The oxidized state was clear as seen with other PProDOTs and similar to the PProDOT-Me_2 device where u´, v´ were 0.2008 and 0.4712 respectively.

Otley (2015)

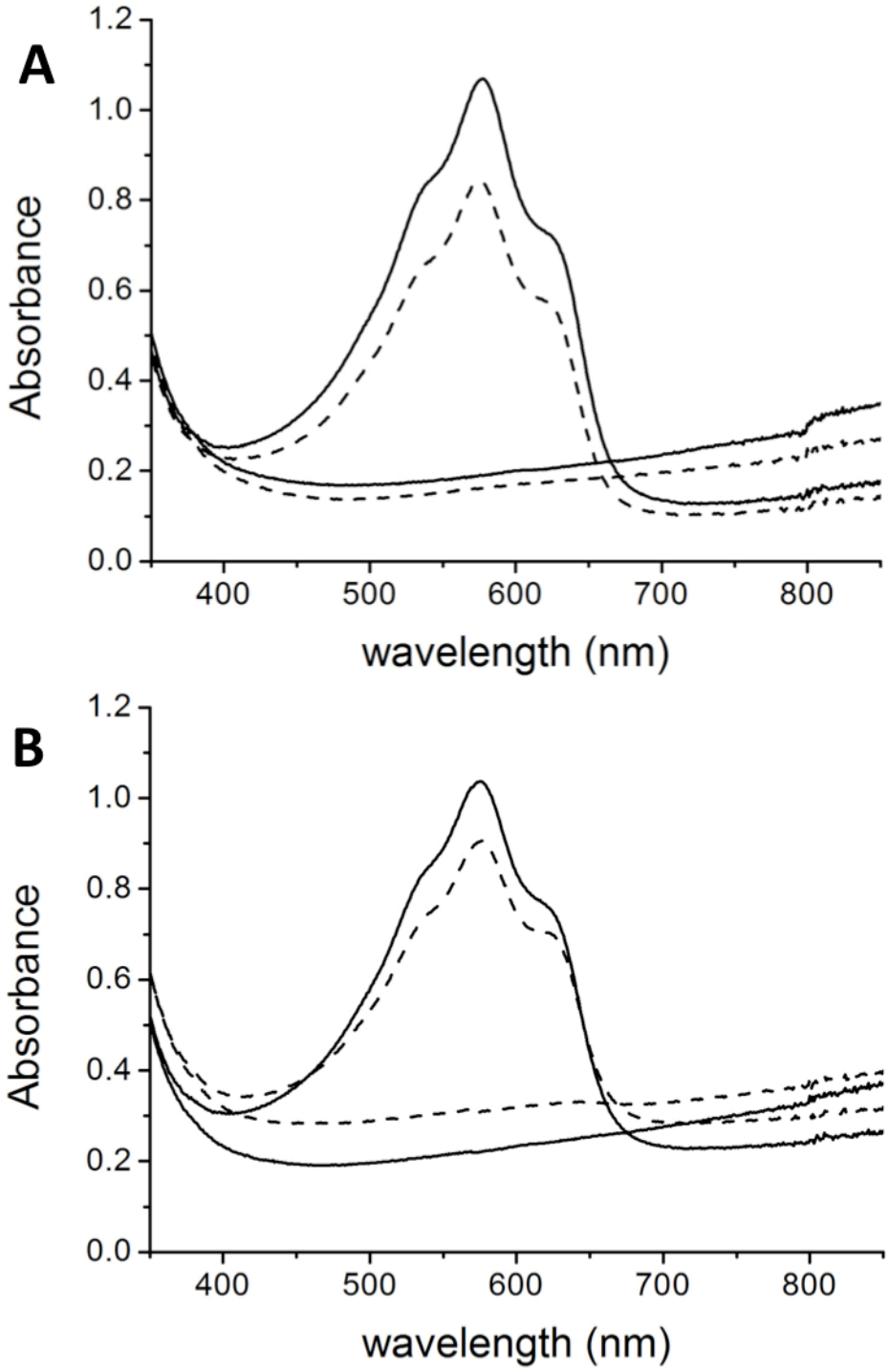

Figure 3.3. The UV-Vis spectra of PProDOT-Ac (solid) and PProDOT-Me_2 (dashed) at initial (A), and after 10,000 cycles (B). Reprinted with permission from M. T. Otley, et al. *ACS Appl. Mater. Interfaces* **2014**, *6*, 1734. Copyright 2014 American Chemical Society.

Otley (2015)

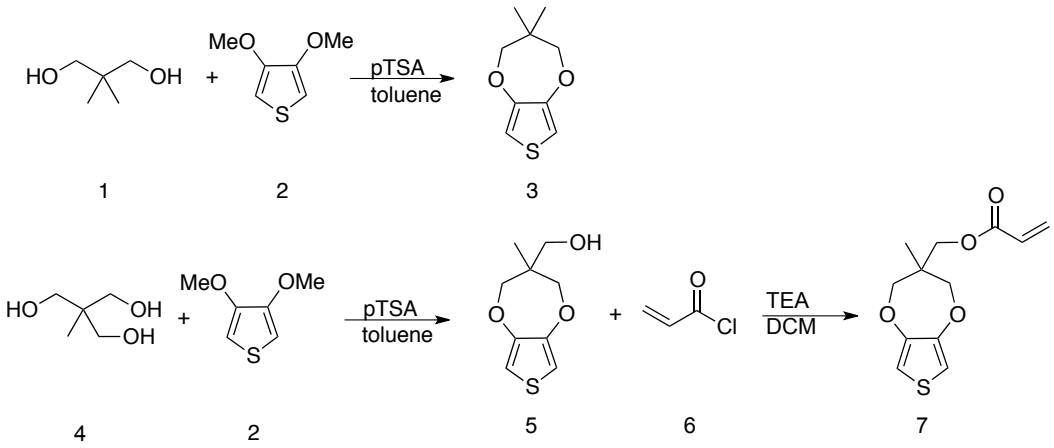

Scheme 3.1. Synthesis of the control compound 3, and the acrylated ProDOT compound 7. Reprinted with permission from M. T. Otley, et al. *ACS Appl. Mater. Interfaces* **2014**, *6*, 1734. Copyright 2014 American Chemical Society.

ProDOT-Me_2 was prepared according to Scheme 3.1, involving a transetherification between dimethoxythiophene (DMOT) and 2,2-dimethylpropane-1,3-diol catalyzed by p-toluenesulfonic acid. The synthesis of ProDOT-Ac is also a transetherification ring closure with DMOT and p-toluenesulfonic acid, but using 1,1,1-tri(hydroxy-methyl)ethane as the diol to produce (3-Methyl-3,4-dihydro-2H-thieno[3,4-b][1,4]dioxepin-3-yl)-methanol (ProDOT-OH). The synthesis of ProDOT-Ac includes one additional step of adding the acrylate group which is obtained by deprotonation of the hydroxyl group on the ProDOT-OH monomer, followed by an addition of acryloyl chloride. Overall, this synthesis adds one additional high yielding step with an average of 75% after recrystallization. The electropolymerization of the ProDOT-Ac electroactive monomer onto the electrode is seen in Scheme 3.2, followed by UV curing of the device. During the UV curing of the device, not only does the gel crosslink with itself, but also to

the electrochromic polymer on the electrode and monomers still in the gel matrix (Scheme 3.2).

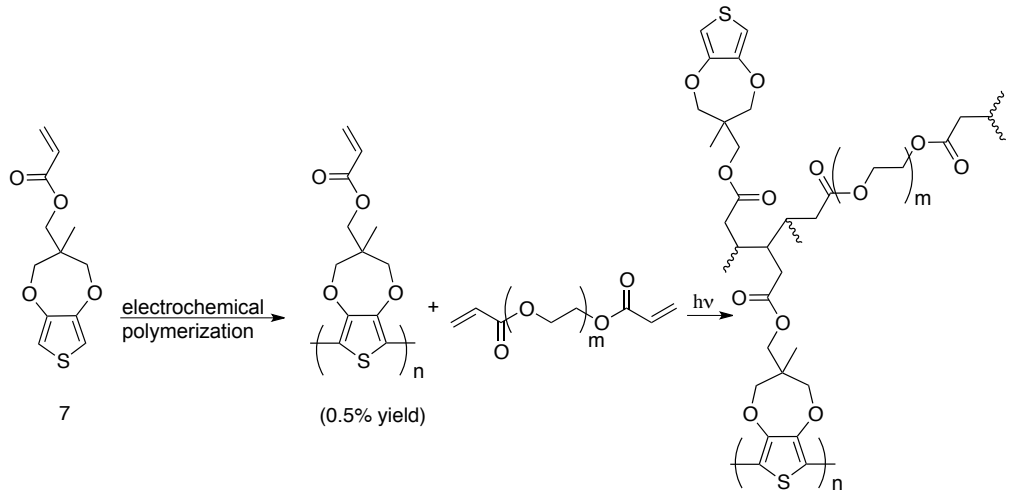

Scheme 3.2. The reactions occurring within the single layer of a device during *in situ* electrochemical polymerization and subsequent photochemical crosslinking. Reprinted with permission from M. T. Otley, et al. *ACS Appl. Mater. Interfaces* **2014**, *6*, 1734. Copyright 2014 American Chemical Society.

Response time for the ProDOT-AC devices were evaluated by optical spectroscopic measurements upon switching potential bias. Devices were switched between 2 V and +2 V with an 8 s pulse width. The transmittance (%T) value was measured at 555 nm, the most sensitive wavelength to human eye,[30] and was monitored as a function of time during the redox cycling process. Herein, the switching speed of the devices (~5.8 cm^2 active area) was defined as the time required to achieve 95% of the full transmittance swing. From the %T vs time curve, bleaching time is calculated to be 2 s and coloring time is 1 s.

Otley (2015)

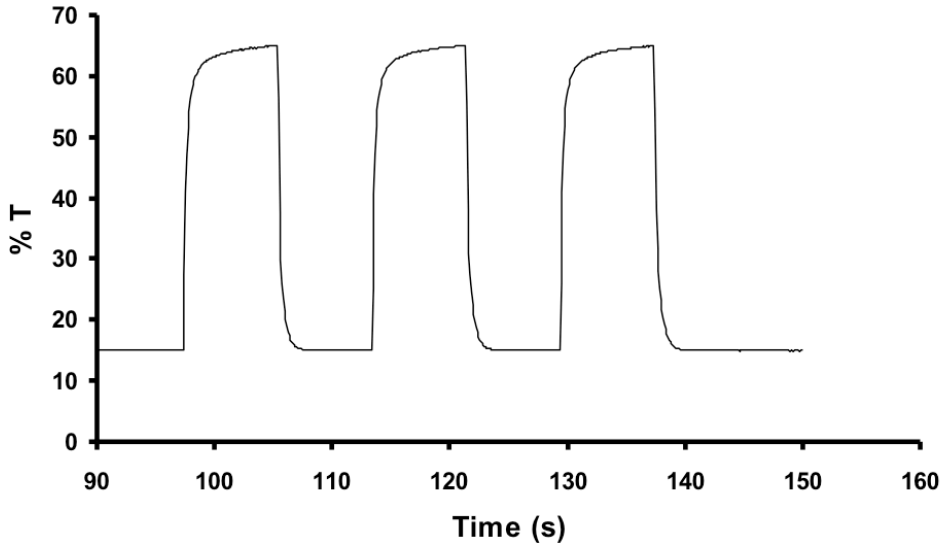

Figure 3.4. Switching speed for PProDOT-Ac. Reprinted with permission from M. T. Otley, et al. *ACS Appl. Mater. Interfaces* **2014**, *6*, 1734. Copyright 2014 American Chemical Society.

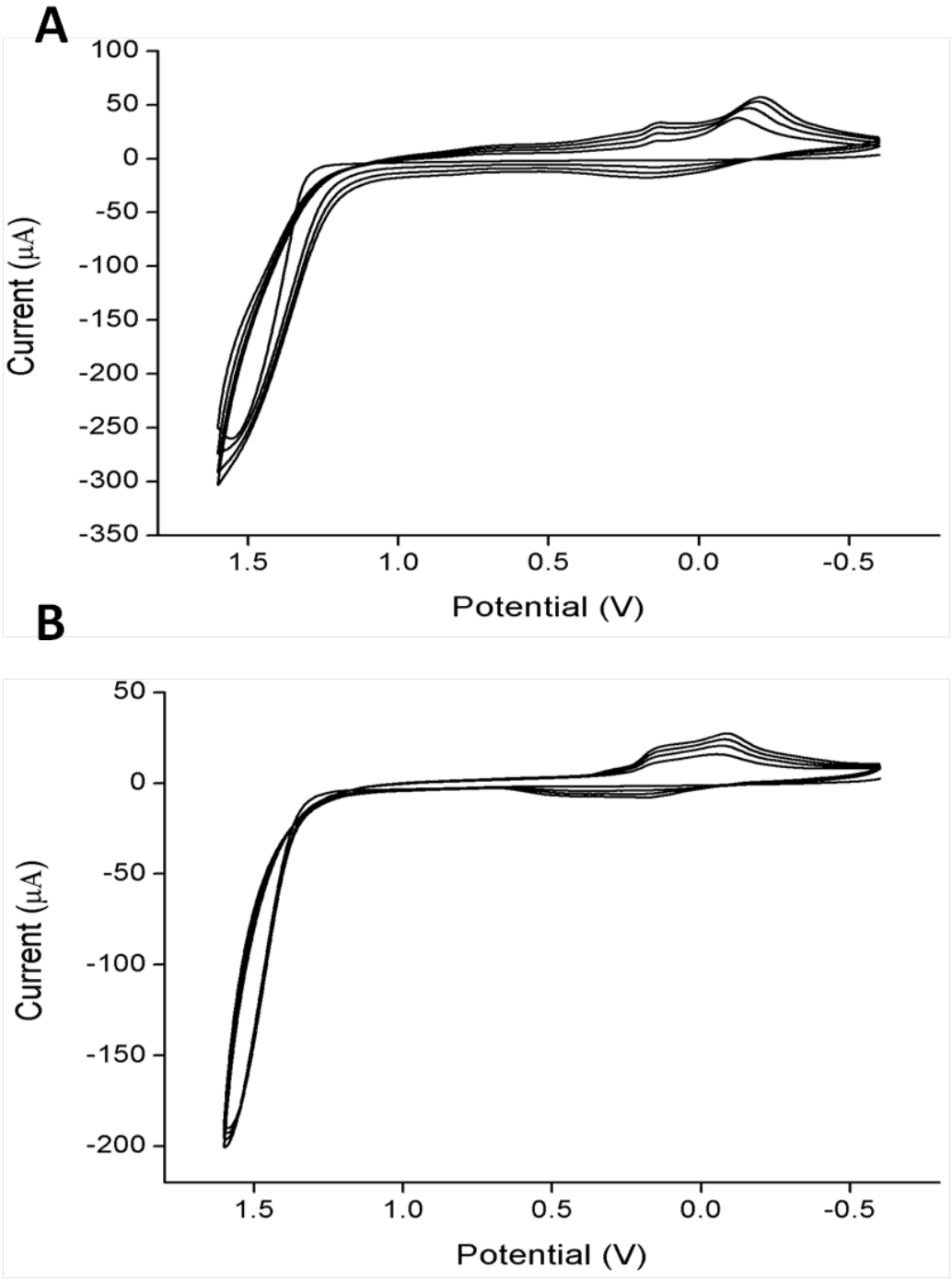

Figure 3.5 (A) Is the ProDOT-Me_2 cyclic voltammograms, and (B) is the ProDOT-Ac cyclic voltammogram. Performed at 100 mV/s with 10 mM of monomer in 0.1 M LITRIF/ACN solution. Reprinted with permission from M. T. Otley, et al. *ACS Appl. Mater. Interfaces* **2014**, *6*, 1734. Copyright 2014 American Chemical Society.

Cyclic voltammetry for ProDOT-Me_2 and ProDOT-Ac, as seen in Figure 3.5A, B respectively, was performed inside a 0.1 M LITRIF/ACN electrolyte solution containing a 10 mM monomer concentration. A platinum button electrode (2 mm diameter) was chosen as the working electrode. A platinum flag (0.5 cm^2) was used as the counter electrode, and a silver wire was used as a pseudo-reference electrode. The potential was scanned between -0.6 and +1.6 V for 4 cycles at a scan rate of 100 mV/s. Seen in the two CVs, the polymers exhibited well defined waves with chemical reversibility. Oxidation onset potential during the first scan of the two CVs indicate that the two monomers have the same oxidation potential, *ca.* +1.25 V with a peak at *ca.* +1.6 V. The deposited polymers then undergo reversible redox reactions, switching from its oxidized form to the neutral form. As the potential decreases from +1.6 V to -0.6 V, the oxidized polymers gradually became reduced. A reduction peak potential (E_{red} peak) is observed at -0.15 V for both PProDOT-Me_2 and PProDOT-Ac. Potential was then reversed at -0.6 V, during this reversed anodic scan both polymers are observed to have similar oxidation peak potentials *ca.* +0.2 V. In the following CV cycles, current intensity increases as more polymers become deposited onto the Pt button electrode. The higher current intensity observed in the CV of PProDOT-Me_2 indicates the greater redox activity of PProDOT-Me_2 than PProDOT-Ac.

3.4 Conclusions

In conclusion, we have achieved long-term stability of *in situ* electrochromic devices, preparing samples that switched for over 10,000 cycles without any spotting defects and with minimal losses (3%) in photopic contrast. By crosslinking the backbone of the polymer to the gel matrix, the migration of monomers was inhibited by locking them within the solid-state gel matrix. This new procedure added only one additional step to the synthesis of the monomer, and the only modification to the device fabrication procedure was to electrochemically polymerize the monomer in the solution state. The photopic contrast of these devices was comparable with the more commonly used ProDOTs such as 2,2-dimethyl-propylenedioxythiophene (ProDOT-Me_2) with the major difference being that the ProDOT-Ac devices lost 3% photopic contrast after 10,000 cycles while the ProDOT-Me_2 devices lost 4% contrast after just 500 cycles. The colored state of the ProDOT-Ac devices was similar to the ProDOT-Me_2 devices allowing them to be interchangeable from an electrochromic perspective. Most importantly, the oxidized states of the ProDOT-Ac devices were transparent, making these monomers capable of use in eyewear, windows, or any other application where a colorless bleached state is required. The one-step lamination procedure for making electrochromic devices allows open air fabrication, fast assembly times, and lower waste than traditional methods for manufacturing ECDs.

Otley (2015)

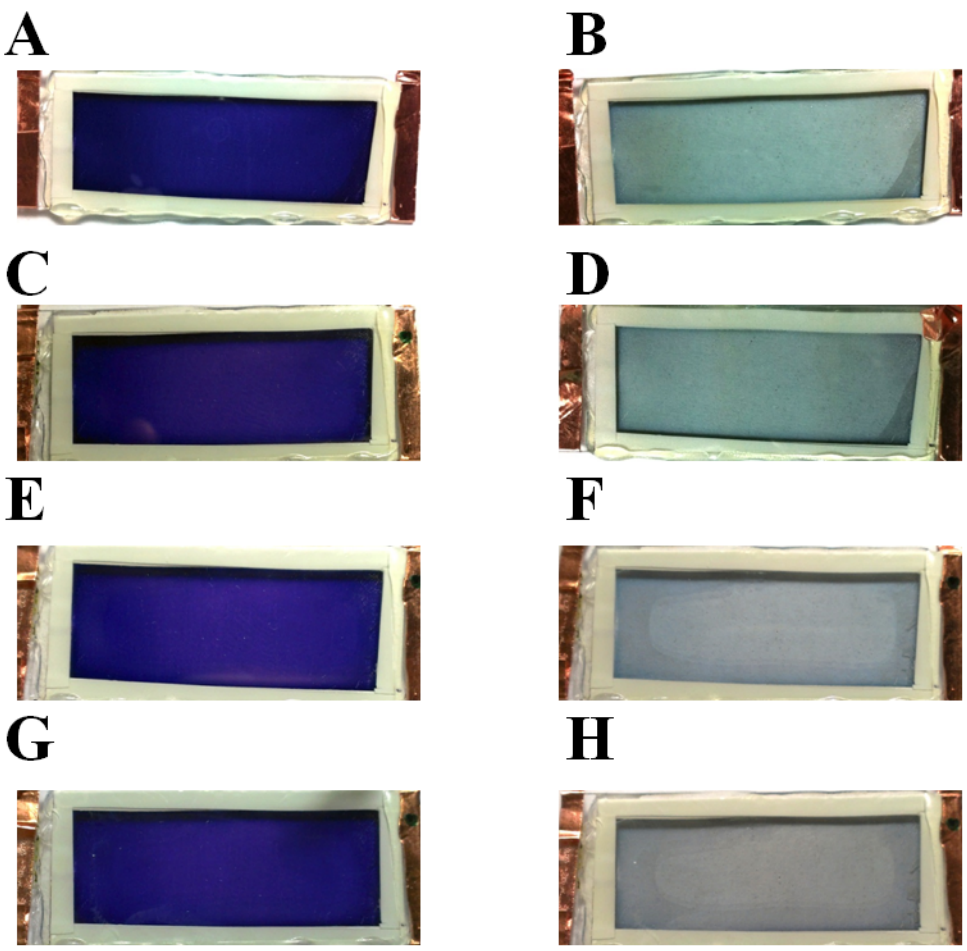

Figure 3.6 The first ProDOT-Ac device tested after 3 cycles (A, B), 7500 cycles (C, D), 9110 cycles (E, F), and 10,510 cycles (G, H). Reprinted with permission from M. T. Otley, et al. *ACS Appl. Mater. Interfaces* **2014**, *6*, 1734. Copyright 2014 American Chemical Society.

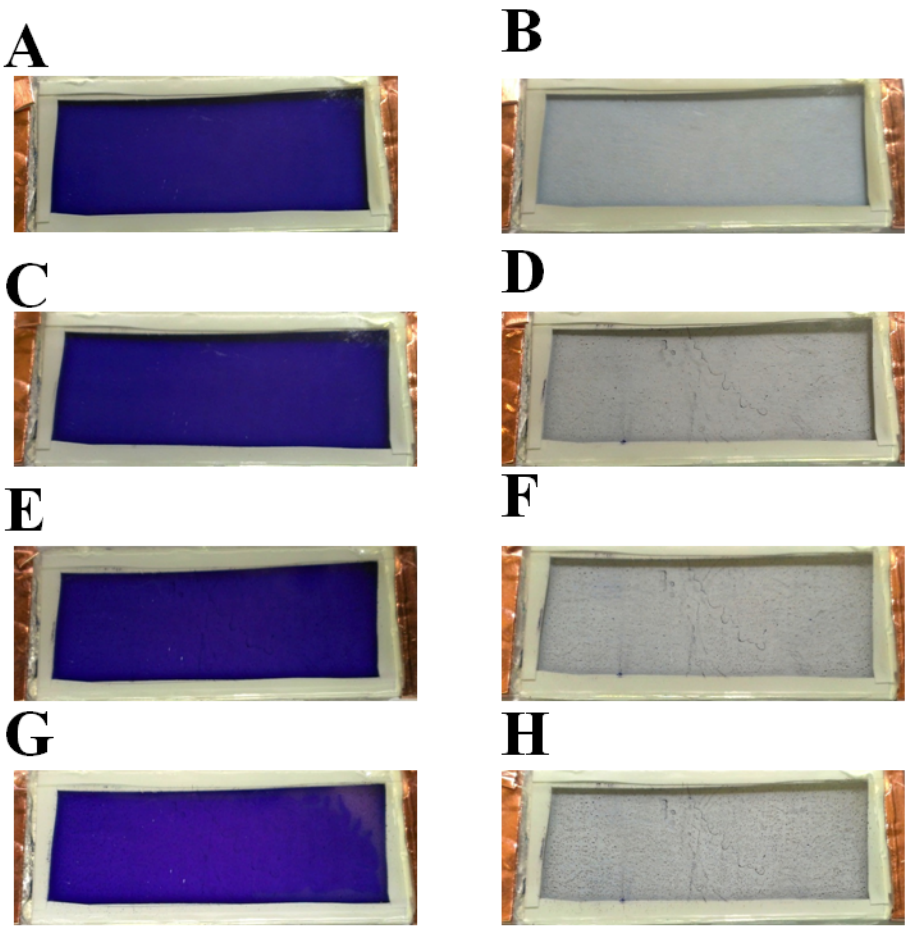

Figure 3.7. The first control, ProDOT-Me_2, device used for stability testing after 6 cycles (A, B), 200 cycles (C, D), 400 cycles (E, F), and 1000 cycles (G, H). Reprinted with permission from M. T. Otley, et al. *ACS Appl. Mater. Interfaces* **2014**, *6*, 1734. Copyright 2014 American Chemical Society.

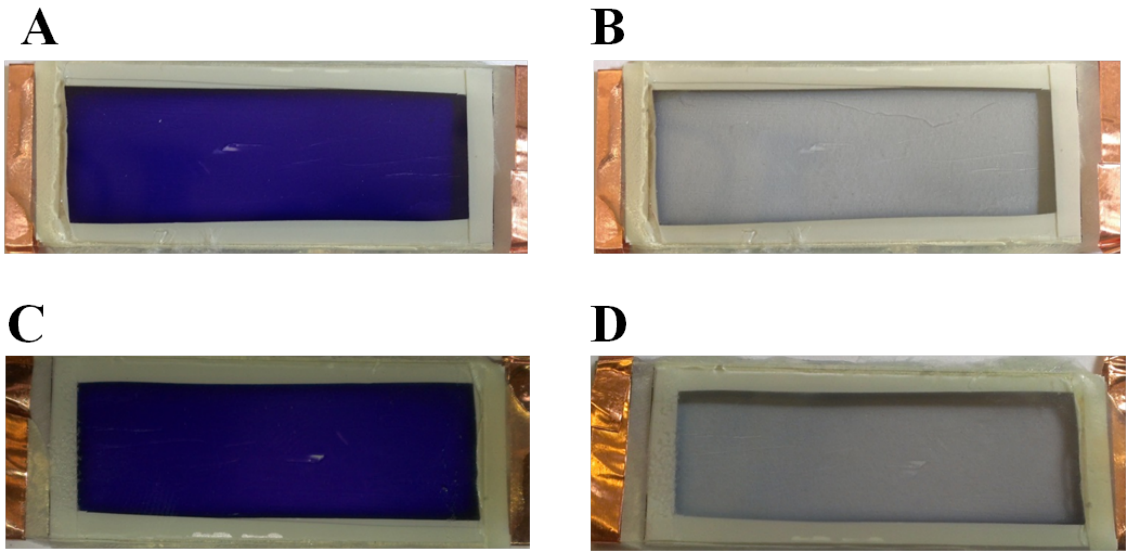

Figure 3.8 The second ProDOT-Ac device used in stability testing after 3 cycles (A, B), and 10,000 cycles (C, D). Reprinted with permission from M. T. Otley, et al. *ACS Appl. Mater. Interfaces* **2014**, *6*, 1734. Copyright 2014 American Chemical Society.

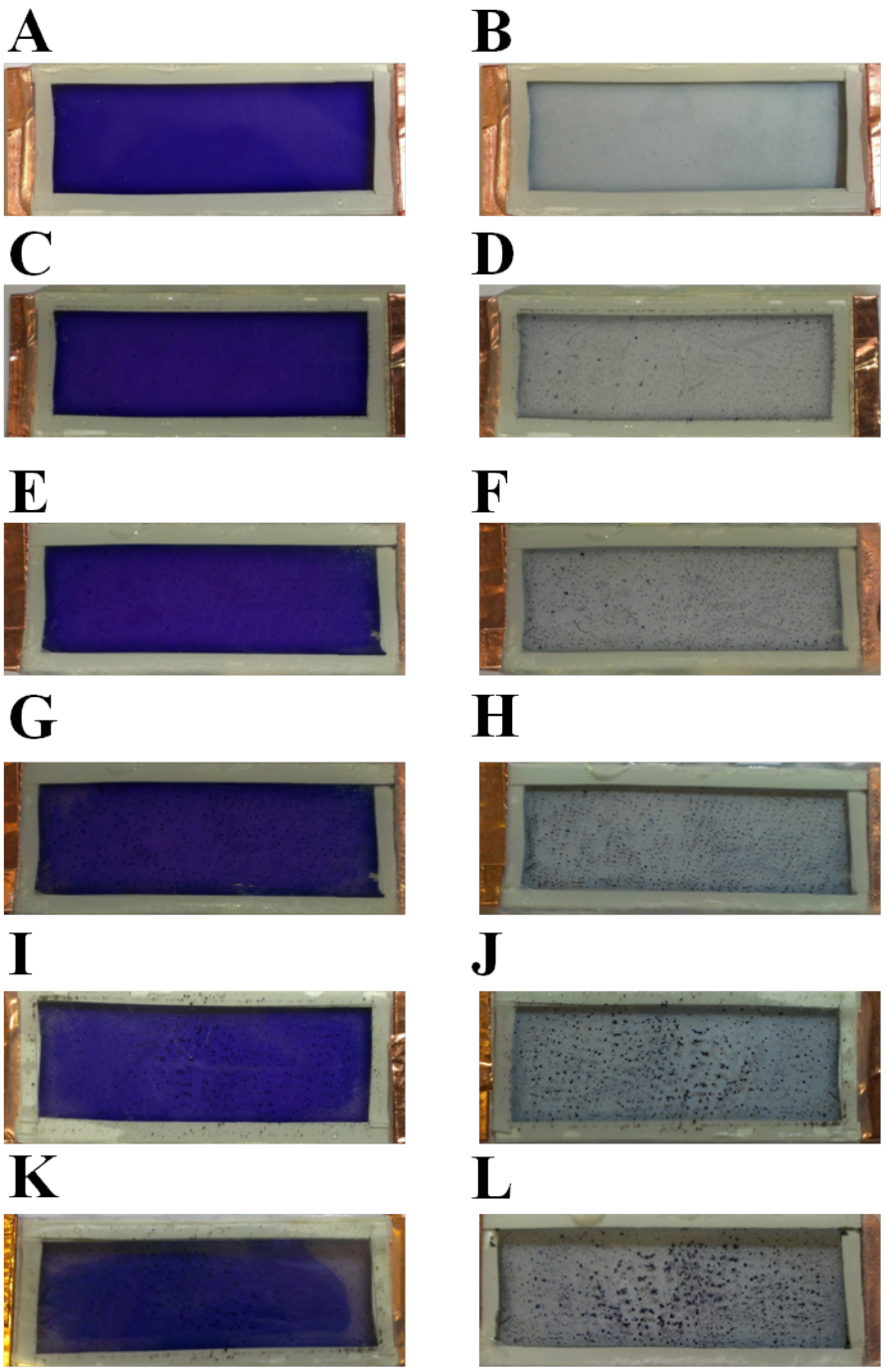

Figure 3.9 The second control (ProDOT-Me_2) device used in stability testing after 1 cycle (A, B), 620 cycles (C, D), 1280 cycles (E, F), 2560 cycles (G, H) 4000 cycles (I, J), and 10,000 cycles (K, L). Reprinted with permission from M. T. Otley, et al. *ACS Appl. Mater. Interfaces* **2014**, *6*, 1734. Copyright 2014 American Chemical Society.

Otley (2015)

3.5 Materials and Methods

Lithium trifluoromethanesulfonate (LITRIF), dimethoxyphenylacetophenone (DMPAP), propylene carbonate, poly (ethylene glycol) diacrylate (M_n = 700), and acetonitrile were purchased from Sigma-Aldrich and were used as received. Indium-doped tin oxide (ITO) glass was purchased from Delta Technologies and cleaned by sonication in acetone prior to use. The electroactive monomer, 2,2-dimethyl-3,4-propylenedioxythiophene (ProDOT-Me_2), was synthesized using a transetherification ring closure starting with commercially available 3,4-dimethoxythiophene and 2,2-dimethylpropane-1,3-diol (Sigma-Aldrich) according to the literature procedure.[17] Acryloyl chloride, 1,1,1-tri(hydroxy-methyl)ethane, and p-toulenesulfonic acid (pTSA) for preparation of ProDOT-Ac were used as purchased from Sigma Aldrich. Toluene (Sigma Aldrich) was cannulated from our dry solvent/degassing system (S. G. Waters). Dichloromethane and triethylamine were distilled before use and were purchased from Sigma Aldrich. Sealant (UVS 91) was purchased from Norland Optics and used as received. Conductive copper adhesive tape was purchased from Newark Electronics and used as received.

3.5.1 Gel polymer electrolyte

Traditional devices were prepared using 5 g of propylene carbonate, 5 g of poly (ethylene glycol) diacrylate (M_n = 700), 1 g of lithium trifluoromethanesulfonate (LITRIF), and 17.5 mg of 2,2-dimethoxy-2-phenyl-acetophenone (DMPAP) were added together and sonicated for 15 minutes until dissolved.

Otley (2015)

3.5.2 Electrochromic device assembly

Two electrochromic devices were fabricated using the *in situ* assembly approach. First, ProDOT-Ac monomer was added to the gel electrolyte in a 7.5 wt% ratio and drop-cast onto the ITO coated glass substrate, another piece of ITO coated glass substrate was put on top. A potential of +3 V was applied to the device for 30 s polymerizing the monomer in the *liquid state*. The device was then cured using UV light at 320 $\mu W/cm^2$ intensity for 5 minutes. The device was cycled between ±2 V for switching the electrochromic device between the oxidized and neutral states for stability testing. Second, the control device consisted of 2.5 wt% ProDOT-Me_2 added to the gel electrolyte, and then sandwiched between two ITO substrates using UV curable glue as an edge sealant and copper tape leads. Then the device cured for 5 minutes using UV light at 320 $\mu W/cm^2$, a potential of +3 V was applied to the device for 30 s to polymerize the monomer in the *solid state.* The device was then cycled between ±2 V for switching the electrochromic device between the oxidized and neutral states for stability testing.

3.5.3 Equipment

All electrochemistry was performed using CHI 400 or CHI 660A potentiostats. Spectroelectrochemical studies were carried out using a CARY 5000 UV-VIS-NIR spectrophotometer. Colorimetric measurements were obtained by a PR-670 SpectroScan Spectroradiometer (Photo Research, Inc.). Cyclic voltammetry for ProDOT-Me_2 and ProDOT-Ac was performed using 0.1 M LITRIF/ACN electrolyte solutions containing 10 mM monomers. A platinum button electrode (2 mm diameter) was chosen as working electrode. A platinum flag (0.5 cm^2) was used as counter electrode and a silver wire as

the pseudo-reference electrode. Potential was scanned between -0.6 and +1.6 V for 4 cycles at a scan rate of 100 mV/s. Both ^{1}H and ^{13}C NMR was performed on a Bruker DMX500 high resolution digital NMR spectrometer. Gas chromotography and mass spectrometry was carried out on a Hewlett Packard 6890 Series Gas Chromatography Mass Spectrometer. Infrared spectroscopy was performed on a Nicolet Magna 560 FTIR Spectrometer.

3.5.4 Synthesis

(3-Methyl-3,4-dihydro-2H -thieno[3,4-b][1,4]dioxepin-3-yl)- methanol (ProDOT-OH) (5) 3,4-Dimethoxythiophene (4 g, 27.8 mmol) was taken with 500 mL of toluene and to this 1,1,1-tri(hydroxy-methyl)ethane (4.32 g, 36.10 mmol) was added followed by p-TSA (0.52 g, 2.78 mmol). The reaction mixture was refluxed with a soxhlet over 4 Å molecular sieves under a continuous flow of argon for 12 h. Excess toluene was evaporated, and the greenish black residue was extracted with ethyl acetate, washed repeatedly with water, and dried over magnesium sulfate. The ethyl acetate was then removed under vacuum. The crude product was purified by silica gel column chromatography eluting with hexanes/ethyl acetate mixture (80 : 20) to give a colorless viscous oil which solidified to a white solid. Yield: 4.6 g (86%), ^{1}H NMR (500 MHz, $CDCl_3$) d: 0.95 (s, 3H), 1.70 (s, 1H), 3.73 (d, J ~ 12 Hz, 2H), 3.74 (s, 2H), 4.08 (d, J ~ 12 Hz, 2H), 6.48 (s, 2H); ^{13}C NMR ($CDCl_3$) d: 17.18, 43.93, 65.62, 76.60, 105.77, 149.56; GC/MS (m/z): 200

(3-methyl-3,4-dihydro-2H-thieno[3,4-b][1,4]dioxepin-3-yl)methyl acrylate (ProDOT-Ac) (7) Under Argon in a three-necked flask, ProDOT-OH (0.26 g, 1.3 mmol)

was added to 30 mL of freshly distilled dichloromethane (DCM), and 0.36 mL of freshly distilled triethylamine (TEA) (0.26 g, 2.6 mmol) was then added to the solution. The solution was then cooled to 0°C and 0.16 mL of acryloyl chloride (0.18 g, 2 mmol) was added dropwise. After two hours, the reaction was extracted with 30 mL of water and 3 x 30 mL of DCM. The organic layer was dried over $MgSO_4$, filtered, and concentrated under vacuum. The crude product was purified using column chromatography with a 1:1 DET/hexanes solvent system. Then the pure fractions from the column were further purified by recrystallization using ethanol as the solvent yielding dense white crystals. (0.24 g, 75%). Mp: 59.5-60°C. ^{1}H-NMR (500 MHz; $CDCl_3$): δ 6.52 (s, 2H), 6.45 (dd, J = 17.3, 1.3 Hz, 1H), 6.18 (dd, J = 17.3, 10.5 Hz, 1H), 5.89 (dd, J = 10.4, 1.3 Hz, 1H), 4.31 (s, 1H), 4.08 (d, J = 12.0 Hz, 1H), 3.79 (d, J = 12.0 Hz, 1H), 1.03-1.00 (s, 3H). ^{13}C NMR (126 MHz; $CDCl_3$): δ 165.9, 149.6, 131.1, 128.1, 105.8, 76.3, 66.4, 42.7, 17.2. GC/MS (m/z): 254. FT-IR (KBr, cm^{-1}): 3113, 2962, 2890, 1720, 1637, 1481, 1459, 1408, 1389, 1375, 1299, 1213, 1192, 1170, 1028, 1000, 981, 971, 873, 808, 782, 771, 667.

Otley (2015)

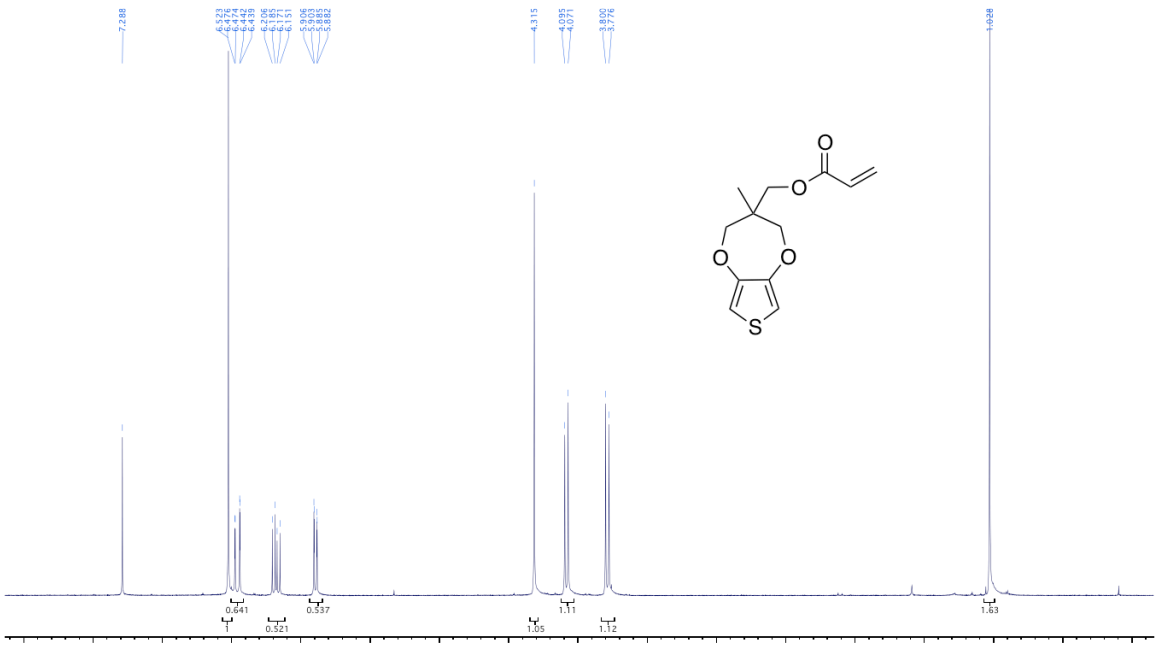

Figure 3.10 The ^{1}H NMR spectrum of ProDOT-Ac.

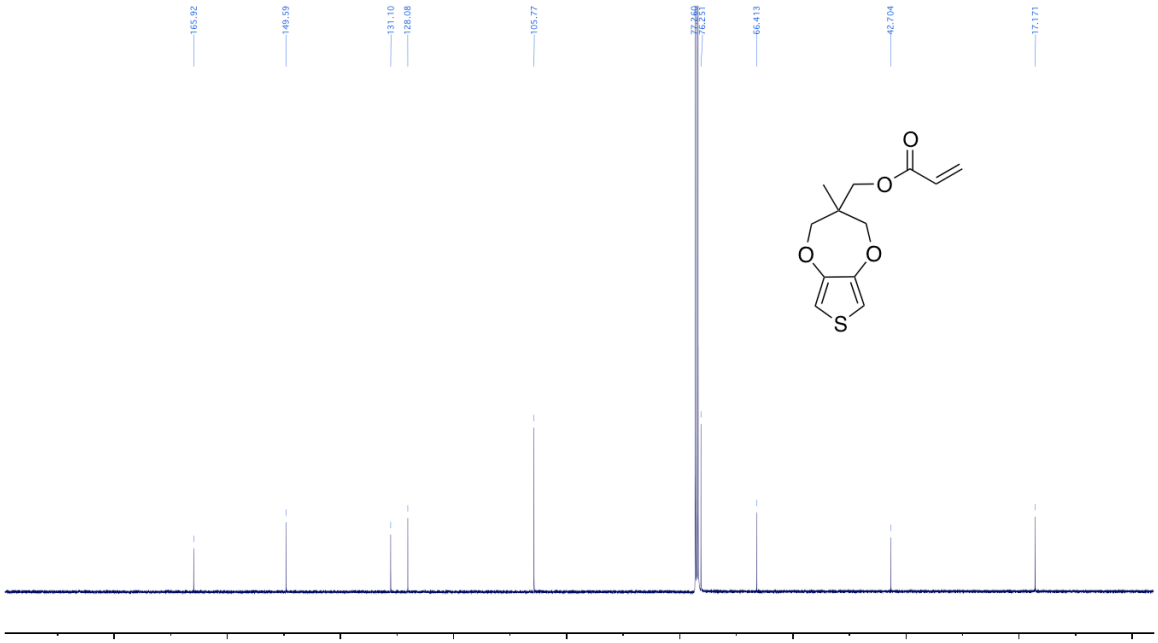

Figure 3.11 The ^{13}C NMR spectrum of ProDOT-Ac.

Otley (2015)

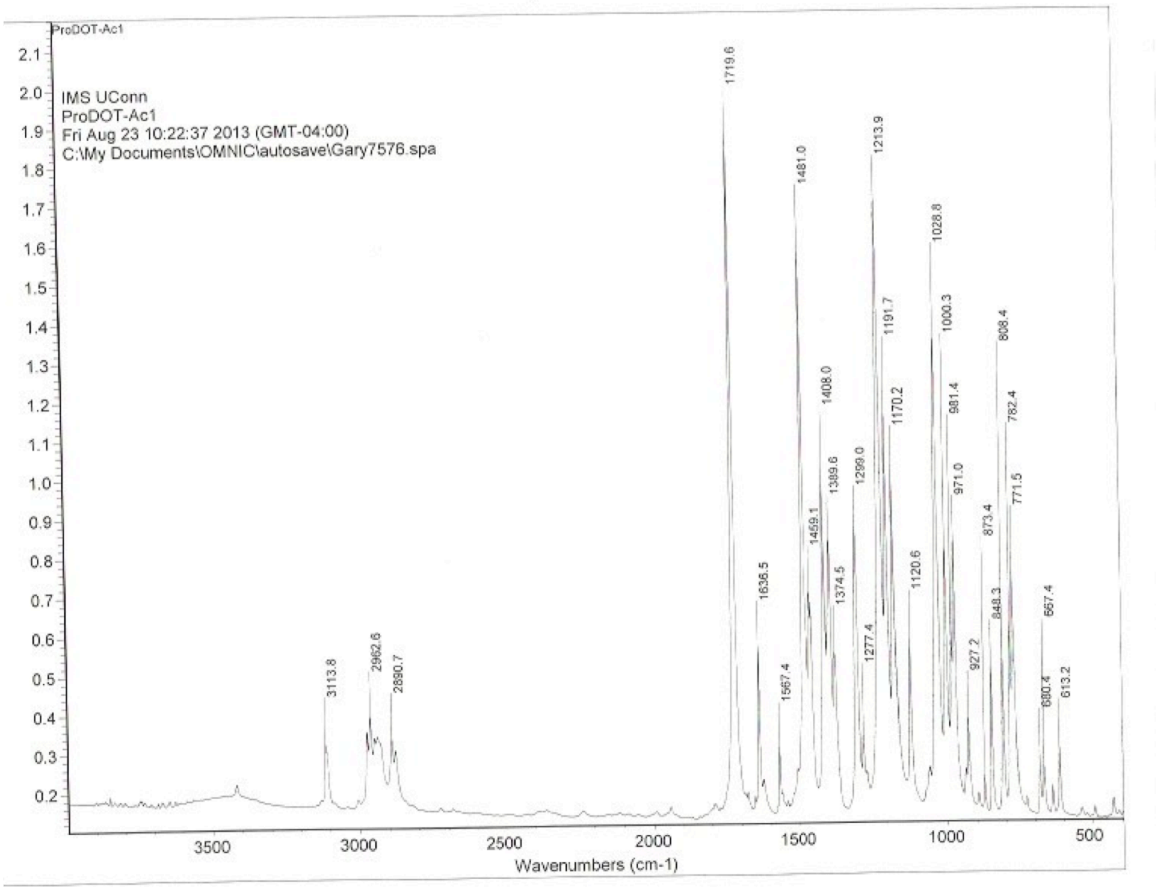

Figure 3.12 The FTIR spectrum of ProDOT-Ac.

Otley (2015)

3.6 References

1. R. J. Mortimer, *Am Sci*, **2013**, *101*, 38.
2. A. A. Argun, P. H. Aubert, B. C. Thompson, I. Schwendeman, C. L. Gaupp, J. Hwang, N. J. Pinto, D. B. Tanner, A. G. MacDiarmid, J. R. Reynolds, *Chem Mater,* **2004**, *16*, 4401-4412.
3. R. Mortimer, A. Dyer, J. Reynolds, *Displays,* **2006**, *27*, 2-18.
4. C. G. Granqvist, **1995**, *Handbook of Inorganic Electrochromic Materials*, Elsevier, p. 663.
5. A. Pawlicka, *Recent Patents on Nanotechnology,* **2009**, *3*, 177-181.
6. M. Hamedi, R. Forchheimer, O. Inganas, Towards Woven Logic from Organic Electronic Fibres. *Nat Mater,* **2007**, *6*, 357-362.
7. T. J. Ha, P. Sonar, A. Dodabalapur, *Appl Phys Lett,* **2011**, *98*, 253305.
8. B. Hu, D. Li, O. Ala, P. Manandhar, Q. Fan, D. Kasilingam, P. D. Calvert, *Adv Funct Mater,* **2011**, *21*, 305-311.
9. W. H. Kim, A. J. Mäkinen, N. Nikolov, R. Shashidhar, H. Kim, Z. H. Kafafi, *Appl Phys Lett,* **2002**, *80*, 3844.
10. H. Youn, M. Yang, *Appl Phys Lett,* **2010**, *97*, 243302.
11. C. Yumusak, N. S. Sariciftci, *Appl Phys Lett,* **2010,** *97*, 033302.
12. F. Zhang, M. Johansson, M. R. Andersson, J. C. Hummelen, O. Inganäs, *Adv Mater,* **2002**, *14*, 662-665.
13. G. Li, V. Shrotriya, J. Huang, Y. Yao, T. Moriarty, K. Emery, Y. Yang, *Nat Mater,* **2005**, *4*, 864-868.

14. S. Lee, S. Nam, H. Kim, Y. Kim, *Appl Phys Lett,* **2010**, *97*, 103503.

15. P. Tehrani, L. O. Hennerdal, A. L. Dyer, J. R. Reynolds, M. Berggren, *J Mater Chem,* **2009**, *19*, 1799.

16. Q. B. Pei, G. Zuccarello, M. Ahlskog, O. Inganas, *Polymer,* **1994**, *35*, 1347.

17. D. M. Welsh, A. Kumar, E. W. Meijer, J. R. Reynolds, *Adv Mater,* **1999**, *11*, 1379-1382.

18. T. Dey, M. A. Invernale, Y. Ding, Z. Buyukmumcu, G. A. Sotzing, *Macromolecules,* **2011**, *44*, 2415–2417.

19. P. M. Beaujuge, S. Ellinger, J. R. Reynolds, *Nat Mater,* **2008**, *7,* 795.

20. J. Kim, J. You, B. Kim, T. Park, and E. Kim, *Adv Mater*, **2011**, *23*, 4168–4173.

21. J. Kim, J. You and E. Kim, *Macromolecules*, **2010**, *43*, 2322–2327.

22. J. Kim, Y. Kim, E. Kim, *Macromol Res,* **2009**, *17*, 791– 796.

23. J. Jensen, A. L. Dyer, D. E. Shen, F. C. Krebs and J. R. Reynolds*, Adv Funct Mater,* **2013**, 23, 3728–3737.

24. Y. Ding, M. A. Invernale, D. M. D. Mamangun, A. Kumar, G. A. Sotzing, *J Mater Chem,* **2011**, *21*, 11873-11878.

25. M. A. Invernale, Y Ding, D. Mamangun, M. S. Yavuz, and G. A. Sotzing, *Adv Mater*, **2010**, *22*, 1379–1382.

26. S. A. Sapp, G. A. Sotzing, J. L. Reddinger, J. R. Reynolds, *Adv Mater*, 1996, *8*, 808-811.

27. S. A. Sapp, G. A. Sotzing, J. R. Reynolds, *Chem Mater,* **1998**, *10*, 2101-2108.

28. F. Alhashmi Alamer, M. T. Otley, Y. Ding, G. A. Sotzing, *Adv Mater*, **2013**, 25, 6256-6260.

29. A. W. Czanderna, D. K. Benson, G. J. Jorgensen, J. G. Zhang, C. E. Tracy, S.K. Deb, *Solar Energ Mat Sol C*, **1999**, *56*, 419-436.

30. V. Seshadri, J. Padilla, H. Bircan, B. Radmard, R. Draper, M. Wood, T. F. Otero, G. A. Sotzing, *Org Electron*, **2007**, *8*, 367–381.

4 Chapter 4: The Influence of Stereochemistry of 1,3-Substituted Poly(3,4-propylenedioxythiophene)s on Optoelectronic Properties

4.1 Overview

Pure cis and trans 1,3-substituted poly(propylenedioxythiophene)s PProDOTs have not been previously reported in the literature. Here, the pure stereoisomers are compared by varying the ratio of the two stereoisomers, systematically, to evaluate structure-property relationships as it pertains to visible absorption, color, and electrochemical redox potentials. A blue shift of approximately 90 nm in the visible lambda max is indicative that the cis-1,3-substituted PProDOT has disruption of conjugation based upon interactions with one of the substituents of the 7-membered ring. The results of this study yield invaluable information into the structure property relationships of 1,3-substituted ProDOTs allowing for better control of color tuning electrochromic polymers.

4.2 Introduction

Conjugated polythiophene, polypyrrole, polyaniline, and their derivatives have been implemented in electrochromic devices due to open atmosphere processing techniques and high electrochromic contrast.[1,2] Poly(3,4-ethylenedioxythiophene) (PEDOT), a polythiophene derivative, has gained considerable attention for electrochromic devices due to PEDOT's low oxidation potential, high optical contrast, and fast switching speed.[3,4] Another polythiophene derivative with even greater contrast, Poly(2,2-dimethyl-3,4-propylenedioxythiophene) (PProDOT-Me_2), continues to be an exciting electrochromic material for such devices switching between purple in the neutral state and colorless transparent in the oxidized state.[5] Reynolds *et al.* reported that PProDOT-

Otley (2015)

Me_2 has high contrast in the visible, NIR, and mid-IR regions,[6] and that PProDOT-Me_2 lacked the typical large NIR absorption exhibited by conductive polymers resulting in a more transparent oxidized state that translates to improved contrast as well as a significant improvement of the switching speed attributed to faster ion movement. The 2,2 substituted ProDOTs were further functionalized by Reynolds and Kumar improving contrast as well as exhibiting color variability.[7,8]

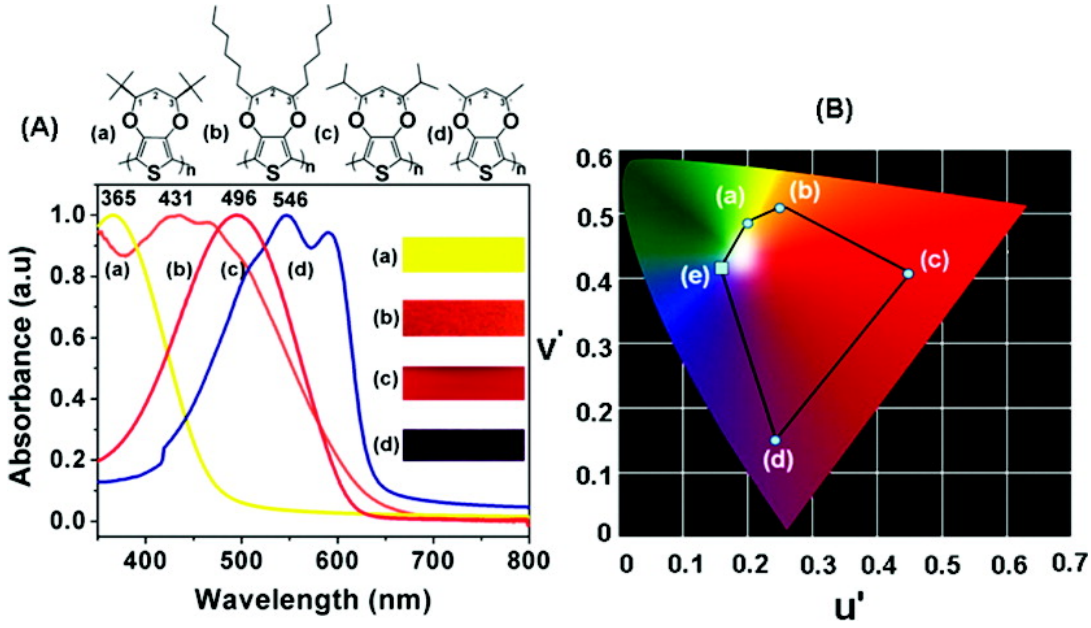

Figure 4.1 (A) Spectral comparison of neutral P13ProDOT-TB_2 (a), P13ProDOT-Hex2 (b), P13ProDOT-IP_2 (c), and P13ProDOT-Me_2 (d) electrochemically deposited on ITO-glass with the exception of P13ProDOT-Hex_2, which was spray-coated. (B) CIE u'–v' coordinate plot of the neutral states of the five chromophores (a), (b), (c), (d), and P22ProDOT-Bz_2 (e, square) reported by Reynolds et al.(3).
Published in: Tanmoy Dey; Michael A. Invernale; Yujie Ding; Zeki Buyukmumcu; Gregory A. Sotzing; *Macromolecules* **2011,** 44, 2415-2417. Copyright © 2011 American Chemical Society.

The 1,3-substituted ProDOTs were first reported in 2002 by Reynolds *et al.* using a Mitsunobu reaction to form the sterically hindered seven-membered ring.[9] The starting

material was a mixture of diastereomers thus resulting in a mixture of diastereomeric 1,3 substituted ProDOT monomers forming atactic electrochromic polymers. Sotzing *et al*. reported in 2011 by changing the substituents at the 1,3 position the full single-wavelength subtractive color spectrum could be obtained as seen in Figure 1.[10] The monomers were synthesized using non-stereospecific reactions resulting in polymers that were not stereochemically pure. This study demonstrates the importance of stereochemistry in the formation of the monomer and the subsequent electrochromic polymers and their optical properties.[11]

4.3 Results and Discussion

The synthesis begins with an Aldol reaction to form the β-hydroxy ketone, which is a near quantitative yield. The stereochemistry is then set in the reaction sequence using boranes for stereospecific reductions. After setting the stereochemistry, the diols are used in a transetherification reaction to close the sterically hindered seven-membered ring forming the desired stereospecific 1,3-diisopropyl-3,4-propylenedioxythiophene (ProDOT-iP_2). Due to the steric hindrance of the isopropyl groups the transetherification reaction is very sensitive to temperature. If the temperature is too high the diol will eliminate or react with itself forming a multitude of side products. If the temperature is too low there will not be enough energy in the system to close the seven-membered ring.

The β-hydroxy ketone can also be reduced with lithium aluminum hydride or diisobutyl aluminum hydride, and the subsequent transetherification to the 1,3-substituted ProDOT results in a racemic mixture. However, it was found that it is possible to separate the two stereoisomers via recrystallization. Performing a recrystallization in acetone at

cryogenic temperatures can separate the trans-stereoisomer, and then the cis-stereoisomer can be recovered from the mother liquor and recrystallized in ethanol. Of note, the trans-stereoisomer oils out in the acetone at cryogenic temperatures allowing for separation, but requires an additional recrystallization in ethanol to form crystals.

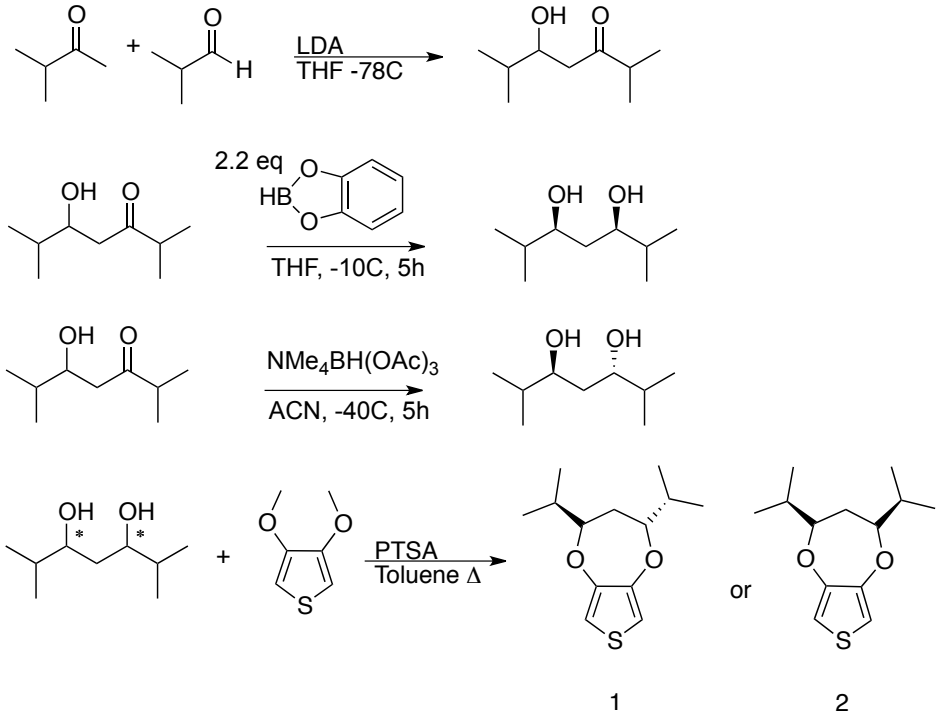

Scheme 4.1 An Aldol addition is used to form a β-hydroxy ketone is followed by a stereospecific reduction to set the stereochemistry. Then one of the diols is chosen for forming the desired cis or trans ProDOT-iP_2 monomer.

The two-stereochemically pure monomers and a racemic mixture were studied for their optical properties with a UV-Vis spectrophotometer. The resulting electrochromic polymers have vastly different colors from a monomer that only differs at one stereocenter. The UV-Vis spectra of pure cis and trans homopolymers and the racemic mixture can be seen in Figure 4.2. A 90 nm blue shift from pure trans to pure cis was

seen, and the racemic mixture (synthesized using a non-stereoselective reduction) is a broader peak with a lambda max between the two pure homopolymers.

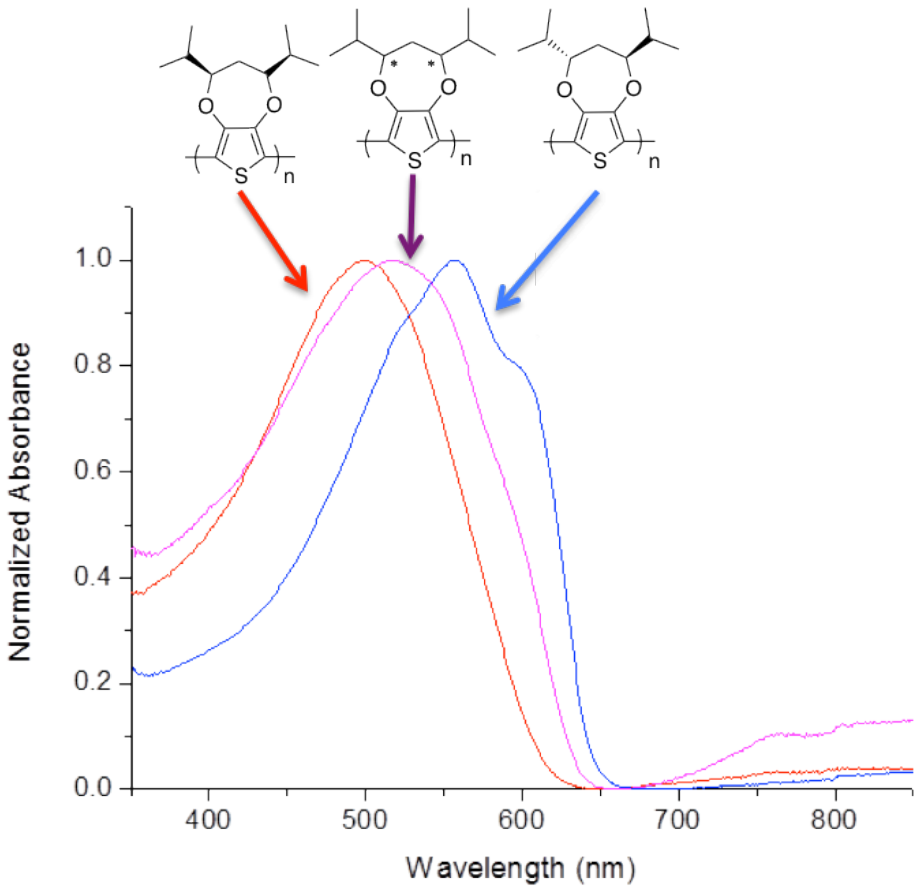

Figure 4.2 The UV-Vis spectrum of cis-ProDOT-iP$_2$, racemic ProDOT-iP$_2$, and trans-ProDOT-iP$_2$.

Computational modeling of both ProDOT-iP$_2$ stereoisomers was used to determine the cause for the 90 nm blue shift from the trans-ProDOT-iP$_2$ to the cis-ProDOT-iP$_2$. Gaussian computational modeling of the trimer of each stereoisomer is shown in Figure 4.3, and the trans-ProDOT-iP$_2$ shows planarity along the polymer backbone allowing for bond overlap. However, the cis-ProDOT-iP$_2$ has steric interactions

of the bulky 1,3-substutuents on the seven-membered ring causing an increase in bond angle along the polymer backbone, thus decreasing bond overlap and changing conjugation length.

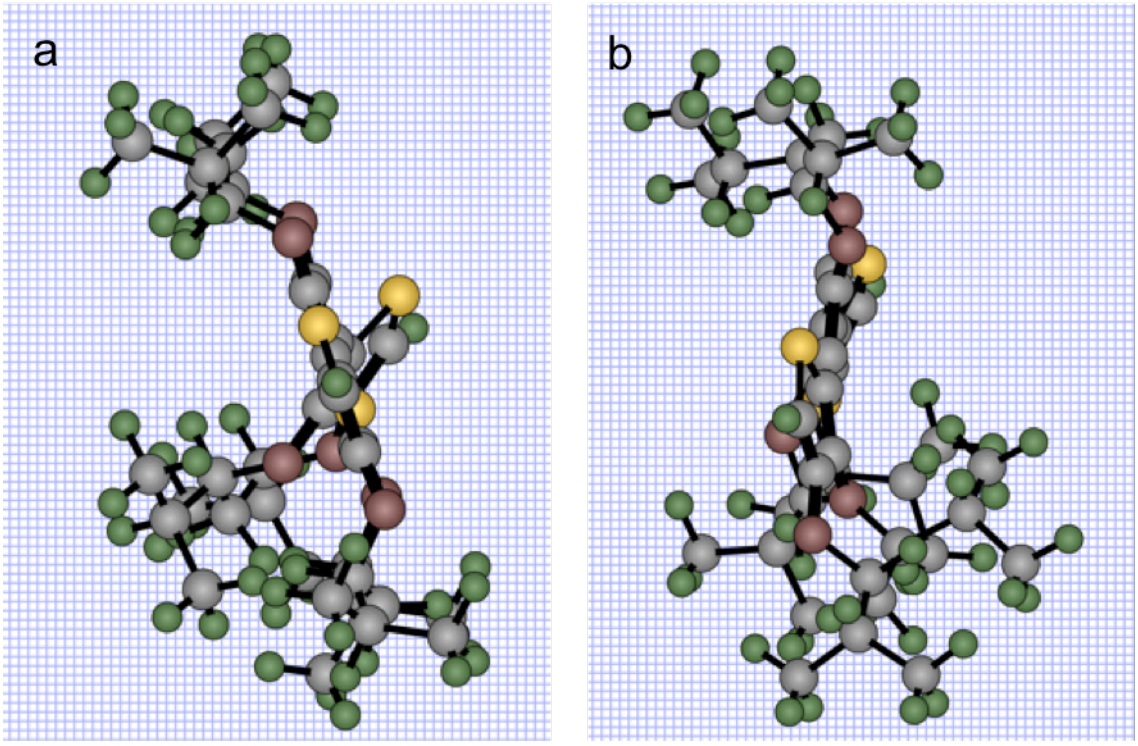

Figure 4.3 (a) The cis-stereoisomer of the ProDOT-iP$_2$ trimer (b) the trans-stereoisomer of ProDOT-iP$_2$ trimer.

Devices were made using the one-step lamination procedure to make electrochromic polymers.[12-16] The resulting electrochromic devices have vastly different colors from a monomer that only differs at one stereocenter. The homopolymer devices can be seen at the top of Figure 4.4. The monomers can then be used in different ratios to form copolymers with colors between the two pure cis and pure trans ProDOT-iP$_2$ with the resulting color dependent upon the feed ratio as seen in Figure 4.4.

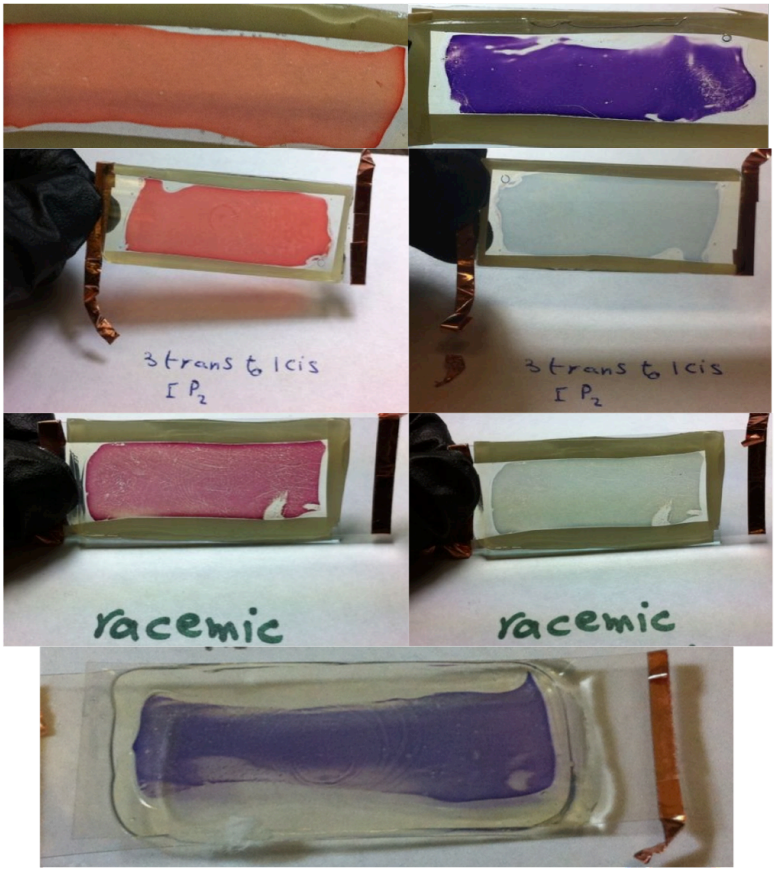

Figure 4.4. The electrochromic devices from top to bottom: with cis-ProDOT-iP_2 (top left) and trans-ProDOT-iP_2 (top right). 3 cis: 1 trans-ProDOT-iP_2 (2^{nd} row from top)*, racemic ProDOT-iP_2 (3^{rd} row from top), and 3 trans: 1 cis-ProDOT-iP_2 (bottom). *The label in the picture is incorrect, but the figure caption accurately describes the device as 3 cis: 1 trans.

4.4 Conclusion

The effect of stereochemistry in sterically substituted 1,3-ProDOTs has been proven to be substantial on the optoelectronic properties of the electrochromic polymers. A 90 nm shift of the homopolymers whose monomers only differ at one stereocenter has

not been reported in the literature before or even close. Computational modeling of the two homo-oligomeric stereoisomers revealed the key interactions of the substituents between the 1st and 3rd units creating a drastic change in bond angle, thus leading to such a large difference in band gap between the two homopolymers.

Otley (2015)

4.5 References

1. P. M. S. Monk, R. J. Mortimer, D. R. Rosseisnsky, Cambridge University Press, Cambridge, (**2007**).
2. D. L. Meeker, S. K. Dhurjati, J. M. Mudigonda, D. C. Osborn, J. P. Loveday, J.P. Ferraris. *Macromolecules* **1998**, *31*, 2943-2946.
3. S. A. Saap, G. A. Sotzing, J. L. Reddinger, J. R. Reynolds, *Adv. Mater*. **1996**, *8*, 808.
4. L. B. Groenendaal, F. Jonas, D. Freitag, H. Pielartzik, J. R. Reynolds, *Adv. Mater*. **2000**, *12*, 481.
5. D. M. Welsh, A. Kumar, E. W. Meijer, J. R. Reynolds, *Adv. Mater*. **1999**, *11*, 1379.
6. I. Schwendeman, J. Hwang, D. M. Welsh, D. B. Tanner, J. R. Reynolds, *Adv. Mater.* **2001**, *13*, 634-637.
7. K. Krishnamoorthy, A.V. Ambade, M. Kanungo, A.Q. Contractor, A. Kumar. *J. Mater. Chem.* **2001**, *11*, 2909-2911.
8. C. L. Gaupp, D. M. Welsh, J. R. Reynolds. *Macromolecular rapid communications* **2002**, *23*, 885-889.
9. K. Zong, L. Madrigal, J.R. Reynolds, *Chem Comm* **2002**, *21*, 2498-2499.
10. T. Dey, M. A. Invernale, Y. Ding, Z. Buyukmumcu, G. A. Sotzing, *Macromolecules* **2011**, *44*, 2415-2417.
11. M. T. Otley, F. A. Alamer, Y. Zhu, A. Kumar, G. A. Sotzing, *Angewandte Chemie Int (preparation)*.

12. Y. Ding, M. A. Invernale, D. M. D. Mamangun, G. A. Sotzing, *J. Mater. Chem*. **2011**, *21*, 11873.
13. M. A. Invernale, Y. Ding, D. Mamangun, M. S. Yavuz, G. A. Sotzing, *Adv. Mater*. **2010**, *22*, 1379.
14. F. Alhashmi Alamer, M. T. Otley, Y. Ding, G. A. Sotzing. *Adv. Mater.* **2013**, *25*, 6256.
15. M. T. Otley, F. Alhashmi Alamer, Y. Zhu, A. Singhaviranon, X. Zhang, M. Li, A. Kumar, G. A. Sotzing. *ACS Appl. Mater. Interfaces,* **2014**, *6*, 1734.
16. A. Kumar, M. T. Otley, F. A. Alamar, Y. Zhu, B. G. Arden, G. a. Sotzing, *J. Mater. Chem. C* **2014**, *2*, 2510.

5 Chapter 5: High Throughput Screening of Electrochromic Polymers

5.1 Background

Analogous to the paint industry, where two or three dyes can be combined to make any color, various feed ratios of only two or three different monomers in the synthesis of conjugated copolymers (CPs) could yield the same result for electrochromic applications. Utilizing the in situ method for preparing electrochromic devices (ECDs),[1, 2] developed by our lab, and the fundamental diffusion of small molecules in a solid state electrolyte, a specific color can be linked to an exact monomer feed ratio, allowing for a high-throughput evaluation of conjugated copolymer compositions for color-specific electrochromic applications. Specifically, monomers diffuse from their respective starting points inside a gel electrolyte matrix, generating a diffusion gradient as they eminate outwards. Monomers across this gradient are then oxidatively copolymerized, in situ, and a colorimetric analysis at all points along the diffusion path is obtained. The monomer feed ratio of a two-component system can then be linked to the optical properties of the resultant copolymer. If each of two homopolymers generated from each of the two respective monomers exhibits a single wavelength absorption, then the copolymer will exhibit a single wavelength absorption and any color associated with a single wavelength absorption can be obtained. Here, we evaluate several different monomers in which the conjugated homopolymers have a single wavelength absorption with a focus on 1,3-di-*tert*-butyl-3,4-propylenedioxythiophene (ProDOT-tBu_2) and 2,2-dimethyl-3,4-propylenedioxythiophene (ProDOT-Me_2), since their respective homopolymers are at the high and low energy extremes of the visible spectrum. From ProDOT-tBu_2 and ProDOT-

Me_2, copolymers generated from a gradient of monomer feed ratios were found to exhibit single wavelength spectra exhibiting all colors except green and black. A unique and important feature of these two homopolymers is that they both have the same highly transmissive sky blue color in their oxidized state, something that is essential for most eyewear and display applications. These findings could have a significant impact on electrochromic applications such as displays, eyewear, windows, and fabric wherein achieving a specific color or color set is critical to its functional use. Further, these colors could be obtained on a relatively short timescale, avoiding numerous synthetic procedures to obtain application specific colors. Our in situ approach allows for the use of a small subset of monomers, when copolymerized, generating an innumerable variety of colors.

Conjugated polymers have drawn attention since their discovery in the late 1970s, mainly due to promise in applications such as organic transistors,[3,4] OLEDs,[5-8] organic photovoltaics (OPVs),[9-11] and displays.[12] CPs exhibit electrochromism, the ability to reversibly switch colors with applied voltage.[13] Owing to their flexibility, low cost in manufacturing, color versatility and high coloration efficiency, CPs have great potential for transition to the industrial sector.[14,15] The extended π conjugation along the CP backbone renders its spectral absorption, typically, within the visible region and the energy gap between the HOMO and LUMO changes with the external bias, resulting in absorption shifts and visible color changes. These properties make conjugated polymers of considerable interest for devices where the optical modulation of transmittance and/or reflectance is desired. Poly(3,4-ethylenedioxythiophene) (PEDOT), as an electrochromic,

is dark blue in the neutral state and a lighter blue in the oxidized state.[16] By tuning the chemical structure of the polymer, the electronic character of the π system can be adjusted to yield different colors and color transitions. For example, PProDOT-Me_2 switches between purple and sky blue.[17] CPs are important in the field of electrochromics because they can encompass the entire visible spectral range, including black.[18]

Generally, electrochromic devices consisting of CPs can be prepared by two general methods. A first method involves designing a polymer structure that would be thought to have a specific color, while exhibiting solubility, and then to prepare this polymer via synthetic procedures, followed by its purification and characterization. The soluble conjugated polymer is then processed as a thin film onto indium doped tin oxide (ITO) coated substrate. In a recent study, Scherer et al. chemically polymerized a diblock copolymer poly(4-fluorostyrene-r-styrene)-b-poly(D,L-lactide) (P(F)S-b-PLA) as a network in V_2O_5.[19] In some cases, copolymers with precise compositions were made by oxidative chemical polymerization in order to achieve the desired color.[18] A second method involves electrochemical deposition[20-25] of CP from an electrolyte bath where the fabrication of an ECD involves depositing the CP film onto the ITO substrate from a monomer solution, and then sandwiching a polymer electrolyte between two pieces of ITO.[26-28] For example, Toppare et al. synthesized a copolymer of 1-(perfluorophenyl)-2, 5-di(thiophen-2yl)-1H-pyrrole and EDOT exhibiting multichromism with transitions of red-violet, amber, green, and blue.[29]

Recently, our group reported an approach for electrochromic device assembly[1,2] that involves the mixing of electroactive monomer with oligoethlyene glycol acrylate, salt

and plasticizer followed by a one layer sandwiching of this mixture between two ITO coated substrates. Sequentially, the electrolyte is UV crosslinked, and the CP is formed via electrochemical oxidation of the electroactive monomer. This method not only increases the success rate of device fabrication but also renders the CP within the crosslinked polyelectrolyte. This approach utilizes all of the chemicals used for the preparation of the CP and thereby reduces chemical waste. Here, this novel in situ electrochromic polymer fabrication technique is exploited for high-throughput screening of color for electrochromics. Diffusion of each monomer within the polymer electrolyte is established as well as a diffusion gradient of two monomers, and homopolymers from which represent the energy extremes of the visible spectrum are generated and converted to electrochromic copolymers having a single wavelength between the two extremes of each of the homopolymers representing all colors of the subtractive visible spectrum with the exception of green. Knowledge of the monomer diffusion allows for precise calculation of the monomer feed ratio to generate the color of interest for an electrochromic device. Our high-throughput screening method was verified by preparation of electrochromic devices by pinpointing a color coordinate obtained from the screening technique and using the calculated composition to generate the desired color of the electrochromic device.

5.2 Transetherification of ProDOT Derivatives

The general reaction our group uses to synthesize ProDOT monomers is the Williamson transetherification.[30,31] This synthetic route of ProDOT derivatives has been used for over the last ten years by several groups including the Reynolds group.[32] The

reasoning behind this is scalability for commercial applications because the starting material, 3,4-dimethoxythiophene (DMOT), is an inexpensive starting material making synthesis of these monomers for electrochromic applications cost-effective. Previous synthetic routes to make ProDOT derivatives included the Mitsunobu reaction, but this left carboxylic acid groups at the 2,5 position on the thiophene ring which had to be "burned" off after the ProDOT was synthesized.[33-35]

As discussed in the introduction, the importance of all the possible electrochromic commercial applications makes it necessary to modify and optimize conditions for each monomer, so it can be used commercially. However, forming a seven membered ring with bulky substituents has shown to be troublesome which is, most likely, the reason no one outside our group has synthesized any of the monomers reported in this thesis with bulky alkyl groups (groups larger than methyl) at the 1,3 position of the ProDOT.

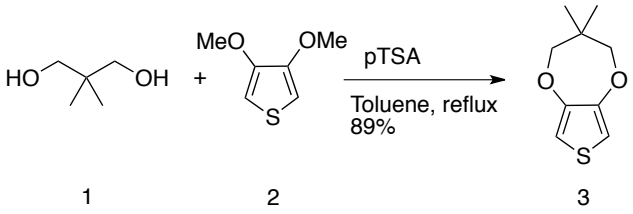

Scheme 5.1 General synthesis of ProDOT-Me_2

The first synthesis is of the most common ProDOT, 2,2-dimethyl-propylenedioxythiophene (ProDOT-Me_2) (**3**), and the synthesis of this monomer is shown in Scheme 5.1. The methyl groups at the 2,2 position on the propylene bridge help the transetherification mechanism because there are no alpha hydrogens available for elimination. This allows the procedure to be modified by raising the temperature to

shorten the reaction time. Original trials were performed following the literature[32] at 100°C (inside the reaction flask), but this led to side products such as double addition of the diol onto DMOT and slow completion times. Thus, the temperature was raised to 180°C in the oil bath to ensure a rapid reflux, and the reaction time is down to hours instead of days. Also, there were not any double addition side products seen in the GC/MS when the temperature is raised. The reaction mixture can now be concentrated and not run in dilute conditions because double addition of the diol is not a factor allowing for less solvent to be used. These modifications make scaling up the reaction more feasible. Scheme 5.2 shows the mechanism of this reaction, and the benefits of raising the temperature of the reaction can be seen.

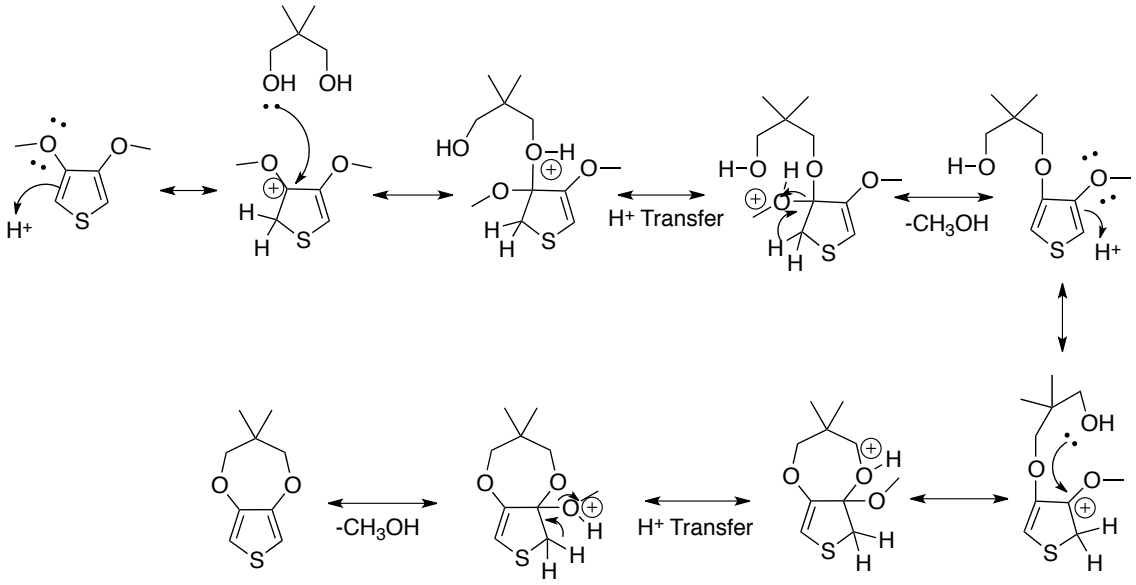

Scheme 5.2 General mechanism for the transetherification of ProDOTs.

There are several reasonable reaction mechanisms that can be drawn for the transetherification of ProDOT derivatives. There have not been any mechanisms reported in the literature specific to this system, so reported in this thesis is a reasonable route from the various diols and dimethoxythiophene to the ProDOT product. In Scheme 5.2 the mechanism starts off with protonating the alpha carbon of the methoxy group on the thiophene ring, since this system is basically an enol ether. This gives the already **δ** positive carbon a positive charge and allows for a nucleophillic attack by the diol. A proton transfer is now possible from the attached hydroxyl group of the diol to the geminal oxygen on the methoxy group. This makes the methoxy a good leaving group as methanol when the ring regains its aromaticity from the proton leaving the alpha carbon. The protonation and deprotonation of the alpha carbon happens on a short timescale.

As seen in the mechanism the side product of this reaction is methanol, and the diol is competing with the methanol in a reversible reaction. However, under high temperature conditions the solvent is refluxed at a rapid rate through a Soxhlet filled with 4**Å** molecular sieves that traps not only water but also methanol. The elimination of methanol from the reaction mixture drives the reaction towards the diol-addition allowing it to add onto the DMOT forming the ProDOT derivative.

Otley (2015)

5.3 1,3 Substituted ProDOT's and Steric Hindrance

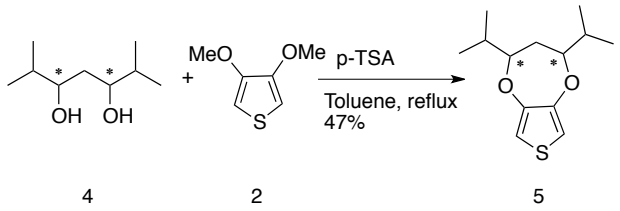

4 2 5

Scheme 5.3 General synthesis of ProDOT-iP_2.

The reactions become more complicated when alpha hydrogens are located next to the hydroxyl groups on the diol used in transetherification. As seen in Scheme 5.3 is the synthesis of 1,3-di-isopropyl-ProDOT (ProDOT-iP_2) (**5**). This reaction is much more sensitive to temperature for several reasons. First, due to the alpha hydrogens if the reaction temperature is too high the diol can undergo elimination, or the diol can react with itself (either intermolecular or intramolecular) forming a variety of side products but the most common seen in the GC/MS and ^{1}H NMR confirmed are substituted tetrahydrofurans (intramolecular) resulting from a 1,2 hydride shift from the tertiary carbon of the isopropyl group. Second, if the temperature is too low then the diol will not attach to the thiophene ring because there is not enough energy in the system to drive the formation of the seven membered ring due to steric hindrance of the bulky substituents at the 1,3 position of the propylene bridge. This results in longer reaction times, and not full consumption of the DMOT leading to a much more difficult purification compared to the

Otley (2015)

2,2 substituted ProDOTs.

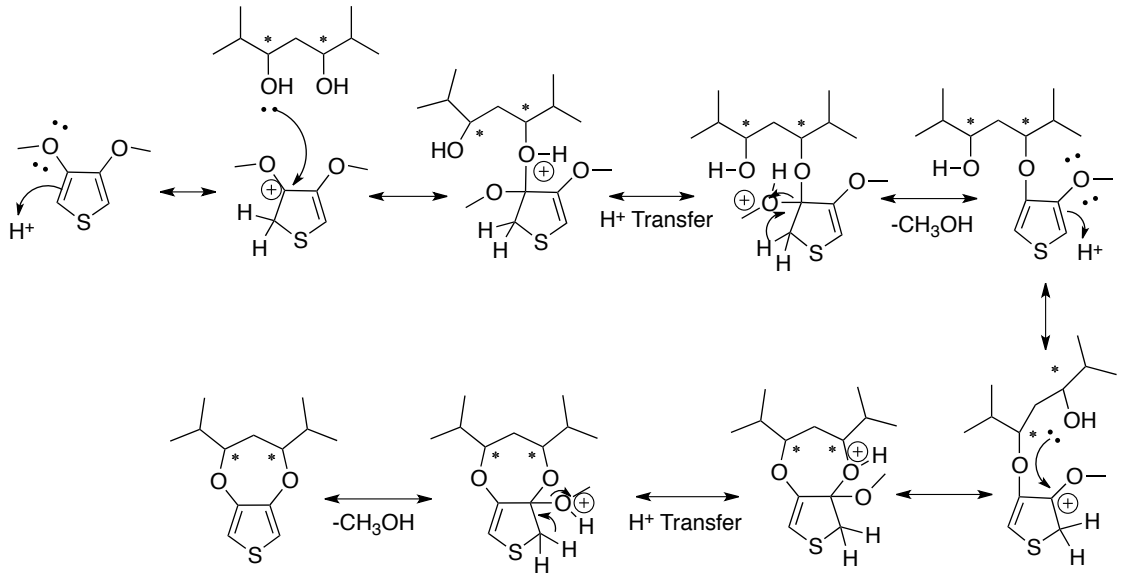

Scheme 5.4 General reaction mechanism for ProDOT-iP_2.

The mechanism of ProDOT-iP_2 shown in Scheme 5.4 shows that forming the 1,3 substituted ProDOTs are much more difficult with steric hindrance now being a factor. The mechanism follows the same path as the ProDOT-Me_2 shown in Scheme 5.2. However, the big isopropyl groups on the diol makes the second addition of the hydroxyl group onto the thiophene ring much more difficult. That intermediate, with the diol mono-attached and the remaining methoxy group still attached to the thiophene, is seen longer in the reaction than with ProDOT-Me_2 (**3**) while monitoring the reaction by GC/MS.

Otley (2015)

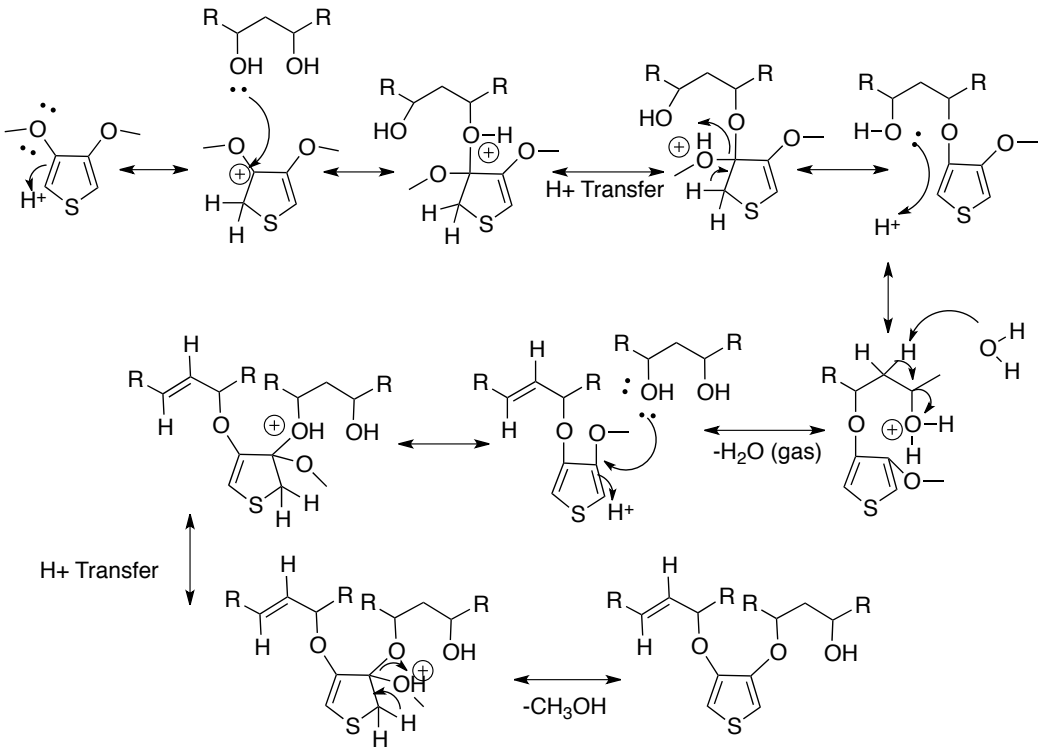

Scheme 5.5 A possible mechanism for the double addition of the diol.

The mechanism in Scheme 5.5 shows one of the possible side products of the transetherification reaction with a diol containing alpha hydrogens. The possibility of elimination exists in this system (as seen by GC/MS), and the more hydrogens alpha to the hydroxyl group on the diol increases the probability of elimination. Scheme 5 shows that if the diol that first attaches to the thiophene ring undergoes elimination, then the chances for double addition increases. This can lead to a variety of products in the reaction mixture, and can be seen by GC/MS. However, the diol does not need to undergo elimination for double addition to occur, and this intermediate is seen when the reaction is run at lower temperatures ~100°C according to the GC/MS. The reason for this is the diol is still relatively stable at 100°C so the diol doesn't eliminate, but with the lower

energy in the system the formation of the seven-membered ring is less likely allowing a second diol to attack the thiophene ring.

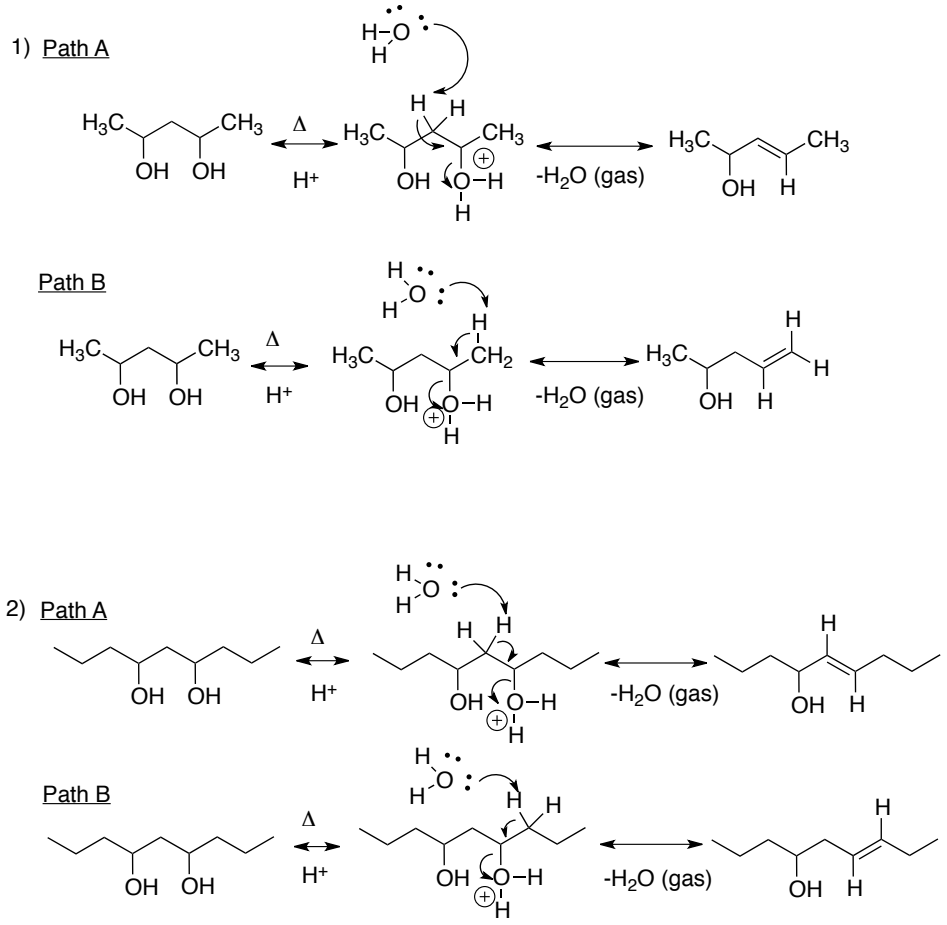

Scheme 5.6 Possible reaction pathways for the elimination of the diol.

The mechanisms in Scheme 5.6 show the possible paths of elimination the diol can undergo in the transetherification reaction. The reversible arrows are shown in the scheme because all the eliminations are reversible, but the reaction uses molecular sieves to drive the reaction to the right (elimination). The temperature in these reactions is at least 140°C in the oil bath, so water is driven off as a gas, condensed, and trapped in the molecular sieves contained in a thimble within the Soxhlet. Scheme 5.6 Path A shows the

most probable elimination route of a 2,4-Pentanediol, since the hydrogens between the two-hydroxyl groups are acidic. The deprotonation of the diol in Scheme 5.6 Path B is less likely (but possible), since the hydrogens are less acidic and primary (Zaitsev's Rule). The mechanism of Scheme 5.6.2 shows a diol with a longer carbon chain than Scheme 5.6.1. This increases the chances of elimination, since there are several more secondary carbons as compared to Scheme 5.6.1 with the diol only containing one secondary carbon alpha to the hydroxyls. A base has several more options in Scheme 5.6.2, and the amount of side products possible is much greater than Scheme 5.6.1 due to hydride shifts between alpha and beta carbons next to each hydroxyl group.

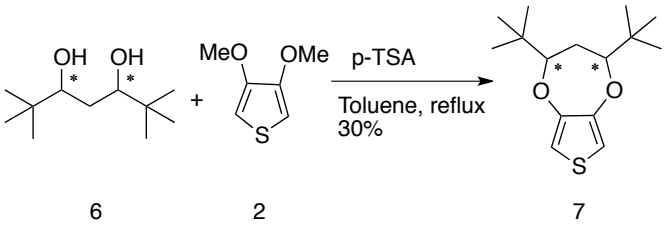

Scheme 5.7 General synthesis of ProDOT-tBu_2.

The synthesis of 1,3-di-*tert*-butyl-propylenedioxythiophene (ProDOT-tB_2) (**7**) is shown in Scheme 5.7. This monomer is the most difficult to synthesize and purify of all the ProDOT derivatives presented in this thesis. The reaction times are much longer than any other derivative, and so is the time to purify it. The DMOT is not fully consumed in this reaction even if 2 mole equivalents of the diol are added every few days. The extreme steric hindrance of the *tert*-butyl groups makes even mono-addition to the DMOT difficult. The reaction is run at a temperature where some elimination is possible,

but not enough to have all of the diol react with itself before it can add to the ring. However, if the temperature was any lower in the reaction the diol would simply not add onto the DMOT resulting in zero product formed. The diol in this reaction, like the diol in the ProDOT-iP_2 reaction, does form intermolecular and intramolecular side products. However, in this system the more prevalent side product is the intermolecular side product that has been both GC/MS and ^{1}H NMR confirmed. The intramolecular side product has also been ^{1}H NMR confirmed because it was necessary to confirm the GC/MS data since the GC/MS indicated the intramolecular product formed was a di-substituted oxetane.

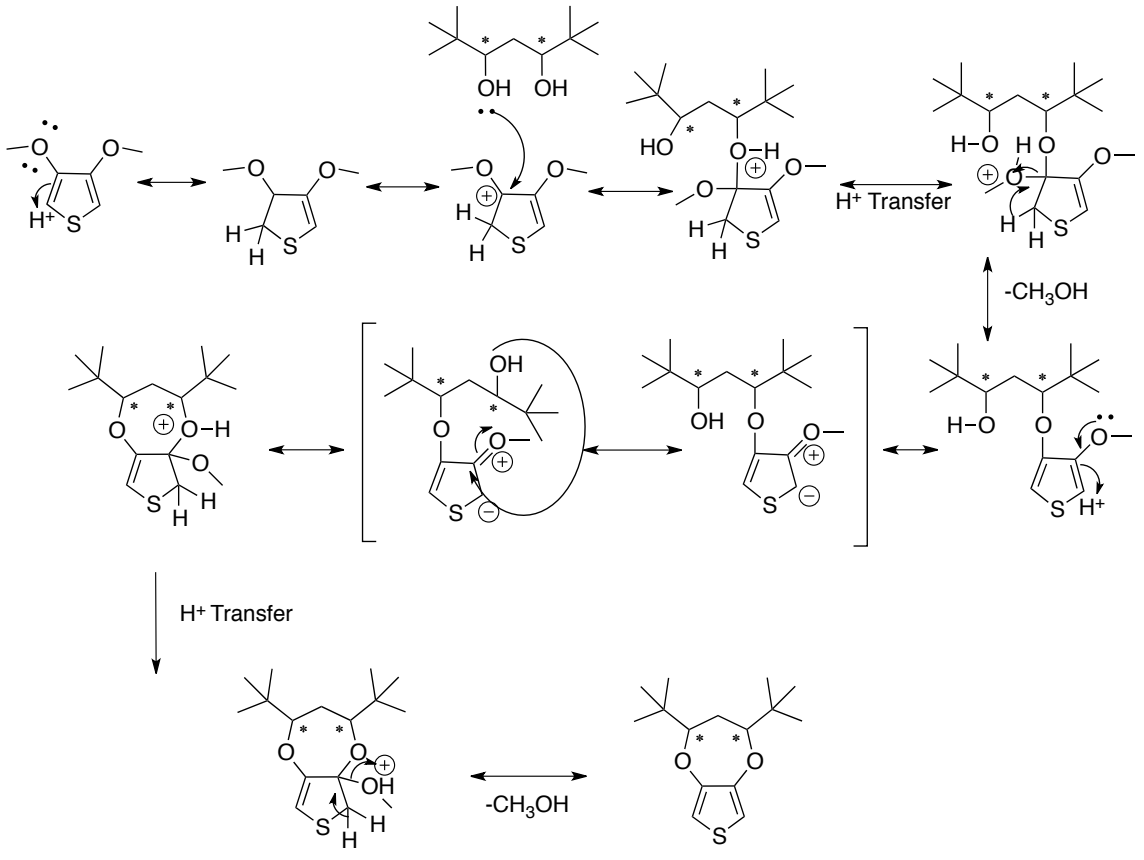

Scheme 5.8 General transetherification mechanism of ProDOT-tBu_2.

Otley (2015)

The mechanism of ProDOT-tBu_2 can be seen in Scheme 5.8. Again, this mechanism is similar to the other ProDOT mechanisms. However, the two-bracketed structures show the difficulty for the second hydroxyl group to add onto the thiophene ring. It's extremely difficult for the hydroxyl group to get close enough to attack the positive carbon on the thiophene ring with the three methyls of the *tert*-butyl group rotating around. The remaining methoxy group on the thiophene ring also makes attack due to steric hindrance even more difficult. This results in poor yield, slow reaction times, and difficult purifications.

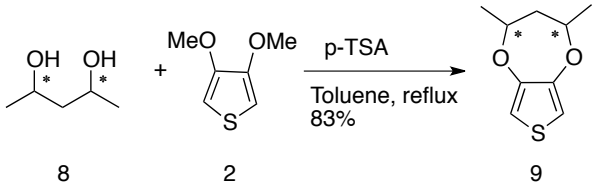

8 2 9

Scheme 5.9 Transetherification reaction of 1,3-ProDOT-Me_2.

The question became whether or not the problem was steric hindrance alone and/or the elimination of the diol resulting in poor conversion and yield of 1,3-ProDOT-iP_2 and 1,3-ProDOT-tB_2. To answer this question 1,3-ProDOT-Me_2 was synthesized and the reaction was run several times. The GC/MS showed that some of the diol did react with itself both intermolecularly and intramolecularly in a similar fashion to the previous 1,3 substituted ProDOT reactions. However, not as much of the diol reacted with itself as the previous two reactions because without the steric hindrance seen with the isopropyl and *tert*-butyl substituents the 2,4-pentanediol was able to add to the thiophene ring much faster before side reactions could consume much of the diol.

Otley (2015)

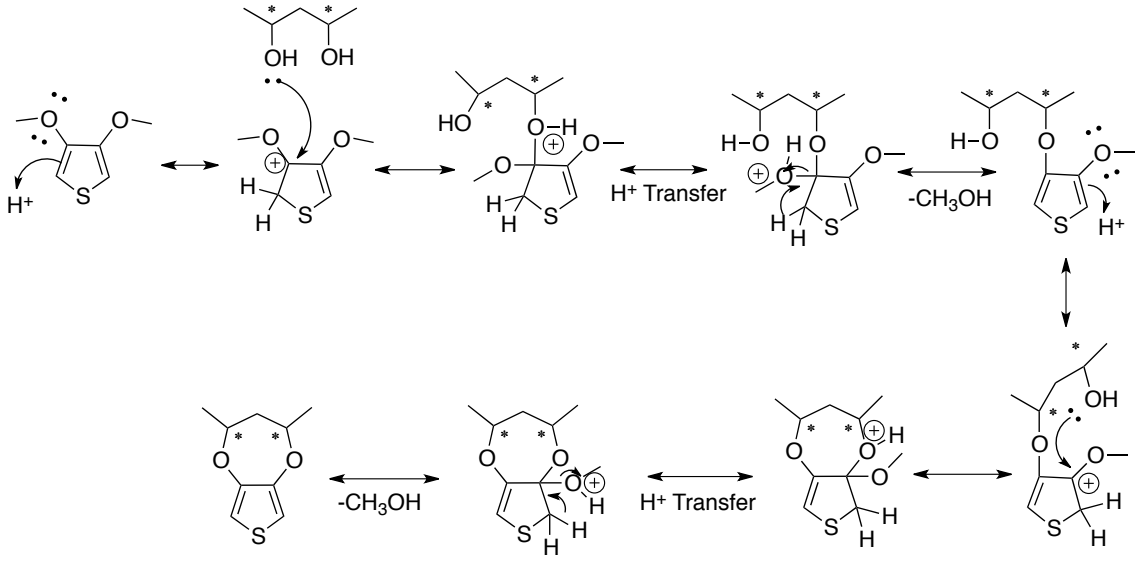

Scheme 5.10 General transetherification mechanism of 1,3-ProDOT-Me_2.

The mechanism depicted in Scheme 5.10 shows the diol with the much smaller alkyl group can attach to the ring easily proving that steric hindrance does not pose a problem in this system. The limiting factor in this reaction is temperature compared with the 2,2-ProDOT-Me_2 because as seen in Scheme 5.6.1 Path A and B elimination is a problem. However, only the two hydrogens alpha to both hydroxyls are likely to eliminate which reduces the amount of side products seen. Again, the ideal temperature for low decomposition of the diol to side products versus fast reaction times is at 140°C for the oil bath.

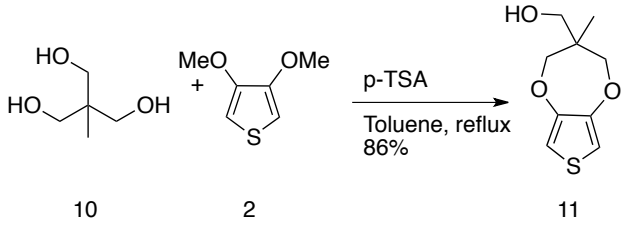

Scheme 5.11 General synthesis of ProDOT-OH.

Otley (2015)

Then the question became whether or not the ProDOT-Me_2 was the only ProDOT that could be synthesized at such a rapid reflux, or could all the procedures for making 2,2 substituted ProDOTs be modified by increasing the temperature. The (3-methyl-3,4-dihydro-2*H*-thieno[3,4-*b*][1,4]dioxepin-3-yl)methanol (ProDOT-OH) monomer is a common precursor for several ProDOT derivatives used by the group (see experimental Chapter 2), so it was a perfect candidate for the study. The results proved that it could be run at 190°C in an oil bath, which shortened the reaction time and led to fewer side products. This also meant that scaling up the reaction into more concentrated conditions was possible, so the large-scale synthesis of this ProDOT derivative would be feasible.

Compound	Reaction Time	Conversion of DMOT (GC/MS)	Pure Yield
ProDOT-Me_2	4-8h	100%	89%
ProDOT-OH	4-8h	100%	86%
1,3-ProDOT-Me_2	8-12h	100%	83%
1,3-ProDOT-iP_2	24-48h	95%	47%
1,3-ProDOT-tB_2	48-96h	60%	30%

Table 5.1 Reaction times, conversion of DMOT, and yields for ProDOT derivatives.

The data in Table 5.1 shows the time of reaction for each of the ProDOT derivatives reported in this thesis, and also the amount of the starting material, DMOT, that gets converted into the product or a side product according to GC/MS. The pure yields are also reported in the table and a trend becomes recognizable. The trend shows

that as steric hindrance increases the reaction time increases, and the addition to the starting material decreases. Using this information, future studies for synthesizing these sterically hindered ProDOT's is underway. First, metal catalyst reactions have been entertained. The Ullman reaction[36] is not practical because Ullman reactions are generally run under extremely high temperatures, which would lead to elimination. Then palladium-catalyzed reactions were looked at, including the Buchwald-Hartwig reaction.[37,38] In the literature there is only a thesis that contains failed reactions for the di-substituted, and very poor yields for the mono-substituted product between an alcohol/diol and a thiophene. The path currently being investigated in our group is a tetra-substituted diol that would not undergo elimination.

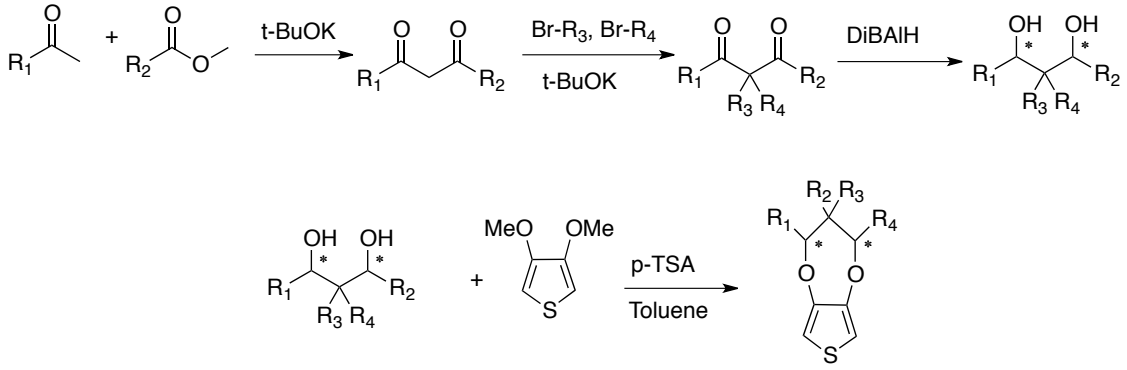

Scheme 5.12 Synthetic scheme for a tetrasubstituted ProDOT.

The reaction sequence in Scheme 5.12 shows a Claisen condensation,[39,40] followed by a double alkyl addition, reduction, and finally the transetherification. The reactions have been run successfully, and the full characterization of the monomers and optimization of the reactions are presently underway. The hypothesis is that the methyl

groups located at the 2,2 position on either the ProDOT-iP_2 and ProDOT-tB_2 won't affect the color of the homopolymers and allow for better yields and faster reaction times.

5.4 Diffusion Study of ProDOTs

The main goal of this research is the application of these monomers for potential use in windows, displays, clothing, and an unlimited amount of potential applications. Each monomer reported in this thesis has a specific purpose for the diffusion study. The monomer ProDOT-Me_2 is a dark blue homopolymer with a trasmissive light blue bleached state. ProDOT-iP_2 is a red homopolymer and ProDOT-tBu_2 is a yellow homopolymer, and both have a completely clear bleached state due to the large alkyl groups along the backbone, which increases the bond angle between repeating units on the polymer causing a change in band gap.

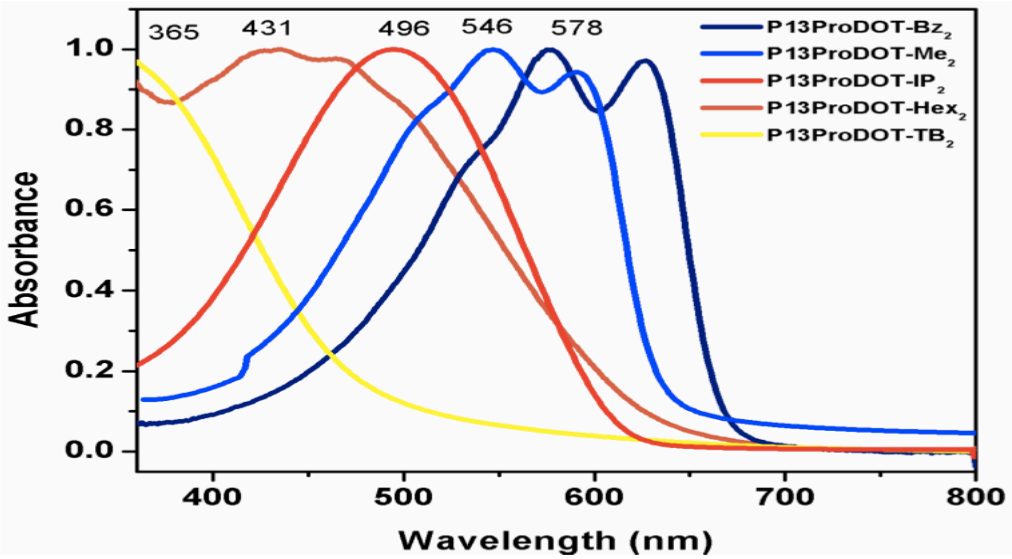

Figure 5.1 The UV-Visible spectrum of various 1,3 substituted ProDOTs.

In order to get any color between the three monomers ProDOT-tB_2, ProDOT-iP_2, and ProDOT-Me_2 seen in Figure 5.1 as the yellow, red, and blue homopolymers, respectively, it was hypothesized to diffuse the monomers through each other to obtain a way of high throughput screening in our *in situ* devices.[41] This method of making conjugated polymers takes advantage of small molecule diffusion through a cross linked gel. The diffusion of these monomers leads to a concentration gradient. When the two monomers are at separate points on the gel, then diffused together, they diffuse into each other resulting in a concentration gradient of different ratios between the two monomers. Then diffusion is terminated when an electrochemical potential is applied to the device electropolymerizing the monomers into copolymers with different compositions of the two monomers as repeat units as seen in Scheme 5.13.

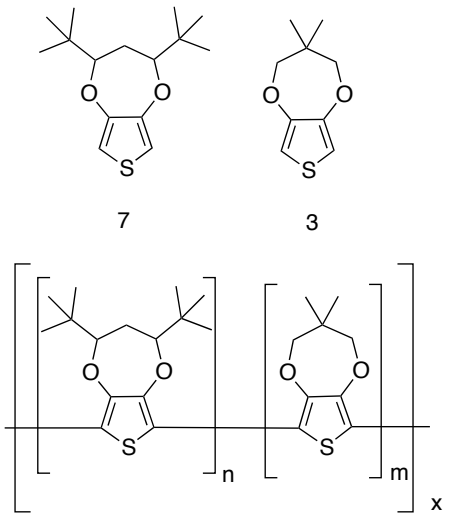

Scheme 5.13 The copolymers formed within the copolymer region of the high throughput screening device.

Compounds 7 and 3 in Scheme 5.13, ProDOT-tB_2 and ProDOT-Me_2 respectively, are shown both as monomers and a copolymer. Where n and m can be any integer

including 0, 1, 2, 3….in the copolymer region. This results in an assortment of different colors spanning the region between the color coordinates of each of the individual homopolymers from these monomers. Each monomer showed different diffusion behavior in a cross linked gel matrix, such as diffusion speed, concentration gradient, and the distance through which diffusion can occur. This is due to sterics and the size of the molecule because the data shows in Table 5.2 that as the size of the molecule increased, the speed of diffusion decreased. Due to each monomer diffusing at different rates in our solid-state system, the diffusion rate of each monomer was determined in order to know the exact feed ratio of each monomer. To determine the diffusion coefficient an experiment was designed with an open reservoir in the middle of a cured solid-state device (see experimental for details and Figure 5.2). The solution containing the monomer (see experimental for details) was inserted into the reservoir and allowed to diffuse over a period of time. In Figure 5.3 the diffusion study is shown at t = 0 and then when completed.

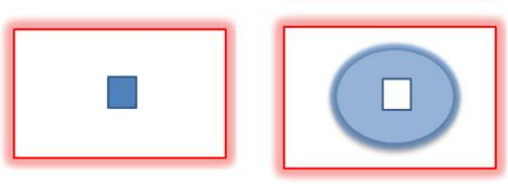

Figure 5.2 A schematic of the device fabricated to study single monomer diffusion.

The actual photos are of EDOT, seen in Figure 5.3, are in the colored and bleached state after diffusion and electropolymerization. The first monomer studied for diffusion was EDOT, and diffusion took place over a period of 2 hours to 24 hours. The lithium trifluoromethanesulfonate (LITRIF) salt was part of the solution to create

homogeneity between the bulk polymeric gel electrolyte and the monomer solution. This ensured that the monomer was the only diffusing species in the system. The diffusion was terminated by removing the solution from the reservoir, and electrochemically converting the diffused monomer to a polymer via application of an applied voltage. The distance EDOT traveled was measured after its conversion to PEDOT by tracing the deep blue color of PEDOT in its dark state.

Figure 5.3 The single monomer diffusion device after EDOT has diffused and electrochemically polymerized in the colored and bleached states.

As the monomer diffuses from the reservoir into the surrounding gel matrix, the concentration gradient decreases with increasing distance from the reservoir. This process is a non-steady-state diffusion that can be described by Fick's second law. According to Fick's law, the diffusion coefficient follows Equation 1 in a short time scale, and remains constant throughout the diffusion process. Therefore D can be calculated based on the distance the monomer traveled in time t using Equation 1. Table 5.2 summarizes the D values of several monomers that were studied. According to the Stokes-Einstein equation, the diffusion coefficient can be affected by temperature, viscosity, and is inversely proportional to the molecule size. The results agree well with the prediction, for example, the largest molecule used in this study ProDOT-tBu_2 (Table 5.2) only travelled 1.9 mm after 15 hours while EDOT can reach the same distance in 3 hours.

$$x = (2Dt)^{1/2} \quad (1)$$

Otley (2015)

Where x is the distance monomer travelled from the reservoir, D is the diffusion coefficient; t is the time of the diffusion.

Monomer	$D(m^2/s)$
Pyrrole	2.95E-9
Bithiophene	2.58E-10
EDOT	9.5E-10
ProDOT-Me_2	1.21E-11
ProDOT-tBu_2	4.63E-12

Table 5.2 Diffusion rates of the monomers studied for high throughput screening.

The results of the diffusion study can be seen in Table 5.2, and the trend follows the size of the molecule. Pyrrole is the fastest followed by bithiophene, EDOT, ProDOT-Me_2, and then ProDOT-tBu_2 is the slowest. With the diffusion study of each monomer completed it was now time to diffuse the monomers together to determine if the high throughput screening hypothesis was correct. The model for the high throughput screening study can be seen in Figure 5.4. Where A and B are different monomers that are allowed to diffuse over a period of time. Where the two circles overlap would be the copolymer containing varying concentrations of each monomer as seen in Scheme 5.13.

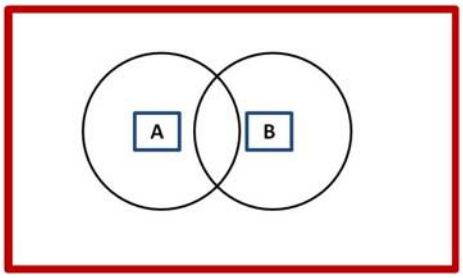

Figure 5.4 A schematic of the high throughput screening device for two monomers.

Otley (2015)

The actual study involved several systems, but reported in this thesis is just one example of high throughput screening. The system presented is that of ProDOT-Me_2 and ProDOT-tBu_2, a blue and yellow homopolymer respectively. This system was picked because each monomer is on opposite ends of the absorption spectrum seen in Figure 5.1, so hypothetically we could see all colors in between the blue and yellow color of the two homopolymers.

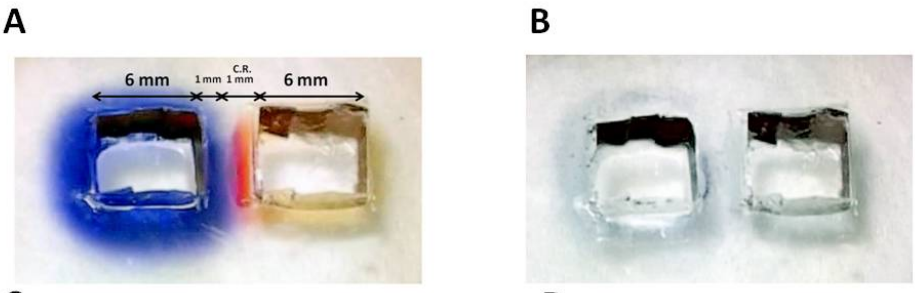

Figure 5.5 An electrochromic device used for high throughput screening (A) is the neutral state (B) is the oxidized state of ProDOT-Me_2 and ProDOT-tBu_2 homopolymers and copolymers (copolymer region is between the two wells).

The results of the high throughput diffusion device can be seen in Figure 5.5 where ProDOT-Me_2 is in the left reservoir and ProDOT-tBu_2 is in the right reservoir. The dark state can be seen in Figure 5.5.A which shows a novel way to make red. There isn't anything published in the literature where yellow and blue make red, but that's because the monomers are not dyes and the actual molecular structure of the polymer is changed. Also, the dark state is not the only important part of electrochromics but also the bleached state, and in Figure 5.5.B a completely clear bleached state is seen around the ProDOT-tBu_2 region making it a perfect candidate for use in displays.

Otley (2015)

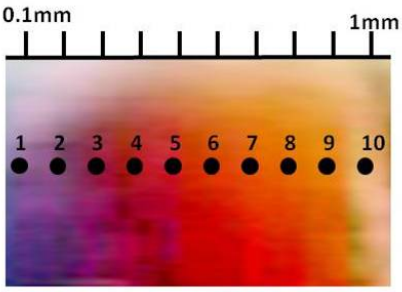

point	ProDOT-Me_2: ProDOT-tB_2
1	2.97: 0.02
2	2.5: 0.03
3	2.1: 0.05
4	1.8: 0.1
5	1.5: 0.19
6	1.35: 0.36
7	1.15: 0.69
8	098: 1.32
9	084: 2.51
10	0.72: 4.7

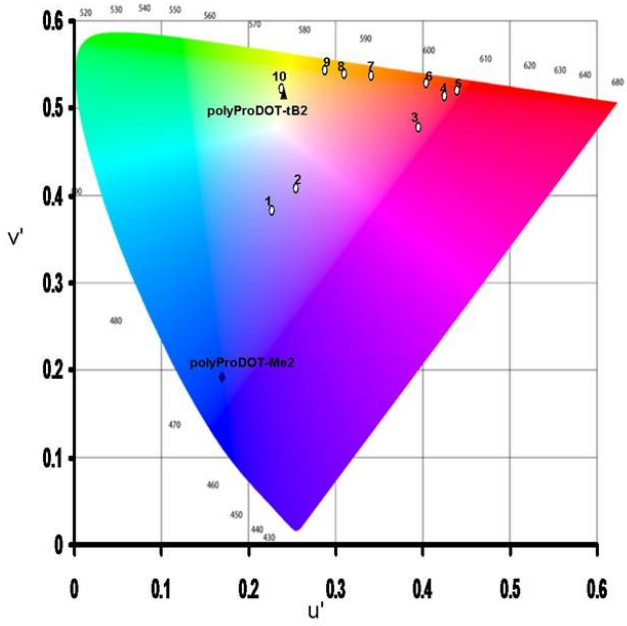

Figure 5.6 A zoomed in view of the copolymer region on the high throughput screening device of ProDOT-Me_2 and ProDOT-tBu_2, feed ratios, and the color coordinates of the ten points chosen within the copolymer region.

A closer look at the results shows almost all colors between blue and yellow on the color coordinate system. The close-up picture of the device clearly shows blue, purple, pink, red, orange, and yellow. The table in Figure 5.6 shows the feed ratio between the two monomers at a given point, and these feed ratios demonstrated to yield almost exactly the same color by mixing the two monomers together at that proportion. The color coordinate graph shows the color coordinates of the 10 points chosen in the copolymer region between the two reservoirs.

5.5 Conclusion

The hypothesis that steric hindrance leads to the reduced yield and longer reaction times proved true. However, continued optimization of the transetherification reaction by

changing other variables such as solvent could prove fruitful. In addition, synthesizing derivatives similar in color like the route shown in Scheme 5.12 can hopefully overcome both the steric hindrance issue and the elimination problem. Also, alternative synthetic routes are being studied for future use in our lab including metal catalyzed reactions.

The high throughput study proved that with only two monomers an entire spectrum of colors could be achieved. This will save time to match a specific color need within an electrochromic device. Currently, in order to match a specific color a monomer is synthesized based on it's hypothesized color, and if it were not an exact match several other derivatives would have to be synthesized. This can take months when the method shown in this thesis only takes 24 hours. Also, this not only saves time it reduces waste from synthesizing several monomer derivatives to try to match a specific color. These results prove electrochromic displays are possible in the future. By using only a few monomers any color can be achieved, and also having a bleached state that is completely clear are ideal for pixels.[42-44] Electrochromic displays would save energy, have a lower cost, be flexible, and have better thermal properties than current LCD technology.

5.6 Device Assembly

A rubber gasket was glued between two pieces of ITO consisting of either glass or plastic. Rectangular holes were carved on the top ITO piece and rubber was fitted into the holes to form two reservoirs. The gel electrolyte was filled into the gasket and cured by 365nm UV light. After curing, the small rubber parts were removed from the holes that formed two reservoirs in the solid-state device. Monomer solutions of different concentrations (wt : wt content of EDOT to total weight of solution placed in reservoir)

were put in these reservoirs and the chemicals were allowed to diffuse for time a period of time. At the end of this period, the leftover solution was removed and the monomer in the gel electrolyte was polymerized. A potential of 3V was applied to the device for 30sec and a potential bias of ±2 V was used for switching. Electrochemistry was carried out using CHI 400 and 660A potentiostats. A PR-670 SpectroScan Spectroradiometer (Photo Research, Inc.) was used for color analysis.

Otley (2015)

5.7 References

1. Y. Ding, M. A. Invernale, D. M. D. Mamangun, A. Kumar, G. A. Sotzing, *Journal of Materials Chemistry* **2011**, *21*, 11873-11878.
2. M. A. Invernale, Y Ding, D. Mamangun, M. S. Yavuz, and Gregory A. Sotzing, *Adv. Mater*. 2010, 22, 1379–1382
3. M. Hamedi, R. Forchheimer, O. Inganas, *Nat Mater* **2007**, *6*, 357-362.
4. T.-J. Ha, P. Sonar, A. Dodabalapur, *Applied Physics Letters* **2011**, *98*, 253305.
5. B. Hu, D. Li, O. Ala, P. Manandhar, Q. Fan, D. Kasilingam, P. D. Calvert, *Advanced Functional Materials* **2011**, *21*, 305-311.
6. W. H. Kim, a J. Mäkinen, N. Nikolov, R. Shashidhar, H. Kim, Z. H. Kafafi, *Applied Physics Letters* **2002**, *80*, 3844.
7. H. Youn, M. Yang, *Applied Physics Letters* **2010**, *97*, 243302.
8. C. Yumusak, N. S. Sariciftci, *Applied Physics Letters* **2010**, *97*, 033302.
9. F. Zhang, M. Johansson, M. R. Andersson, J. C. Hummelen, O. Inganäs, *Advanced Materials* **2002**, *14*, 662-665.
10. G. Li, V. Shrotriya, J. Huang, Y. Yao, T. Moriarty, K. Emery, Y. Yang, *Nature Materials* **2005**, *4*, 864-868.
11. S. Lee, S. Nam, H. Kim, Y. Kim, *Applied Physics Letters* **2010**, *97*, 103503.
12. P. Tehrani, L.-O. Hennerdal, A. L. Dyer, J. R. Reynolds, M. Berggren, *Journal of Materials Chemistry* **2009**, *19*, 1799.

13. A. A. Argun, P.-H. Aubert, B. C. Thompson, I. Schwendeman, C. L. Gaupp, J. Hwang, N. J. Pinto, D. B. Tanner, A. G. MacDiarmid, J. R. Reynolds, *Chem. Mater.* **2004**, *16*, 4401-4412.

14. R. Mortimer, a Dyer, J. Reynolds, *Displays* **2006**, *27*, 2-18.

15. Q.B. Pei, G. Zuccarello, M. Ahlskog, O. Inganas, Polymer 35, **1994**, 1347.

16. P. M. Beaujuge , S. Ellinger , J. R. Reynolds , *Nat. Mater.* **2008** , *7* , 795.

17. P. Camurlu, E. Sahmetlioglu, E. Sahin, I. Akhmedov, C. Tanyeli, L. Toppare, *Thin Solid Films* **2008**, *516*, 4139 – 4144.

18. M. R. J. Scherer, L. Li, P.M. S. Cunha, O. A. Scherman, and U. Steiner*, Adv. Mater.* **2012**, *24*, 1217–1221

19. M. R. a Alves, H. D. R. Calado, C. L. Donnici, T. Matencio, *Synthetic Metals* **2010**, *160*, 22-27.

20. A. T. Taskin, A. Balan, Y. A. Udum, L. Toppare, *Smart Materials and Structures* **2010**, *19*, 065005.

21. C. Zhang, Y. Xu, N. Wang, Y. Xu, W. Xiang, M. Ouyang, C. Ma, *Electrochimica Acta* **2009**, *55*, 13-18.

22. H. Seol, H. Jeong, S. Jeon, *Journal of Electroanalytical Chemistry* **2009**, *636*, 107-112.

23. M. Ak, E. Şahmetlioğlu, L. Toppare, *Journal of Electroanalytical Chemistry* **2008**, *621*, 55-61.

24. A. S. Sarac, G. Sonmez, F. C. Cebeci, *Journal of Applied Electrochemistry* **2003**, *33*, 295-301.

25. A. A. Argun, P.-H. Aubert, B. C. Thompson, I. Schwendeman, C. L. Gaupp, J. Hwang, N. J. Pinto, D. B. Tanner, A. G. MacDiarmid, J. R. Reynolds, *Chem. Mater.* **2004**, *16*, 4401-4412.

26. M. A. Invernale, V. Seshadri, D. M. D. Mamangun, Y. Ding, J. Filloramo, G. A. Sotzing, *Chemistry of Materials* **2009**, *21*, 3332-3336.

27. J. Kim, J. You, B. Kim, T. Park, and E. Kim, *Adv. Mater.* **2011**, *23*, 4168–4173.

28. V. K. Thakur , G. Ding , J. Ma , P. S. Lee , and X. Lu *, Adv. Mater.* **2012**, *24*, 4071–4096.

29. *http://ocw.mit.edu/courses/materials-science-and-engineering/3-091-introduction-to-solid-state-chemistry-fall-2004/readings/notes_10.pdf* **n.d.**, Accessed 6-5-2011

30. W. Williamson, *Liebigs Ann Chem.* **1851**, *77*, 37-49.

31. W. Williamson, *Chem. Soc.* **1852**, *106*, 229.

32. C. Gaupp, D. Weslh, J. R. Reynolds, *Macromol. Rapid Commun.* **2002**, *23*, 885–889.

33. O. Mitsunobu, M. Yamada, *Bull. Chem. Soc. Jpn.* **1967**, *40*, 2380-2382.

34. O. Mitsunobu, M. Yamada, T. Mukaiyama, *Bull. Chem. Soc. Jpn.* **1967**, *40*, 935-939.

35. K. Zong, L. Madrigal, L. Groenendaalb, J. R. Reynolds, J. *Chem. Commun.,* **2002**, 2498-2499.

36. F. Ullmann, J. Bielecki. *Chemische Berichte* **1901**, *34*, 2174–2185.

37. G. Mann, C. Incarvito, A. L. Rheingold, J. F. Hartwig, *J. Am. Chem. Soc.* **1999**, *121*, 3224–3225.

38. K. E. Torraca, X. Huang, C. A. Parrish, S. L. Buchwald, *J. Am. Chem. Soc.* **2001**, *123*, 10770–10771.

39. L. Claisen, A. Claparede, *Berichte der Deutschen Chemischen Gesellschaft* **1881**, *14*, 2460–2468.

40. Claisen, L., *Berichte der Deutschen Chemischen Gesellschaft* **1887**, *20*, 655–657.

41. Y. Ding, M. A. Invernale, D. M. D. Mamangun, A. Kumar, G. A. Sotzing, *Journal of Materials Chemistry* **2011**, *21*, 11873-11878.

42. A. A. Argun, P.-H. Aubert, B. C. Thompson, I. Schwendeman, C. L. Gaupp, J. Hwang, N. J. Pinto, D. B. Tanner, A. G. MacDiarmid, J. R. Reynolds, *Chem. Mater.* **2004**, *16*, 4401-4412.

43. P. M. Beaujuge, S. Ellinger, J. R. Reynolds, *Nat. Mater.* **2008**, *7*, 795-799.

44. G. Sonmez, C. K. F. Shen, Y. Rubin, F. Wudl, *Angewandte Chemie (International ed. in English)* **2004**, *43*, 1498-502.

6. Chapter 6: Design and Synthesis of Electrochromic Dyes

6.1 Rationale Behind Electrochromic Dyes

The subtractive color mixing of the electrochromic polymer PEDOT with an organic yellow solvent dye was our first neutral system that we achieved using the one-step lamination procedure during my graduate studies.[1] The goal was to use the "subtractive color mixing" theory to achieve neutrality with PEDOT, a broad absorbing blue homopolymer, with something that would fill in the higher energy portion of the visible spectrum. We then started to look at dyes, however, a dye would only work in our one step lamination procedure if it was UV stable and electrochemically stable. A series of dyes were tested and the one that proved to absorb at the correct wavelength, was UV stable, and electrochemically stable was Macrolax Yellow G. The UV-Vis spectra of the individual absorptions, the absorption of PEDOT and the yellow dye together un-optimized, and the optimized large area device with it's UV-Vis spectrum can be seen in Figure 6.1. The results of these experiments with using dyes went better than expected, however, the need for higher contrasts and more transmissive bleached states lead to the idea of developing a system of electrochromic dyes.

Otley (2015)

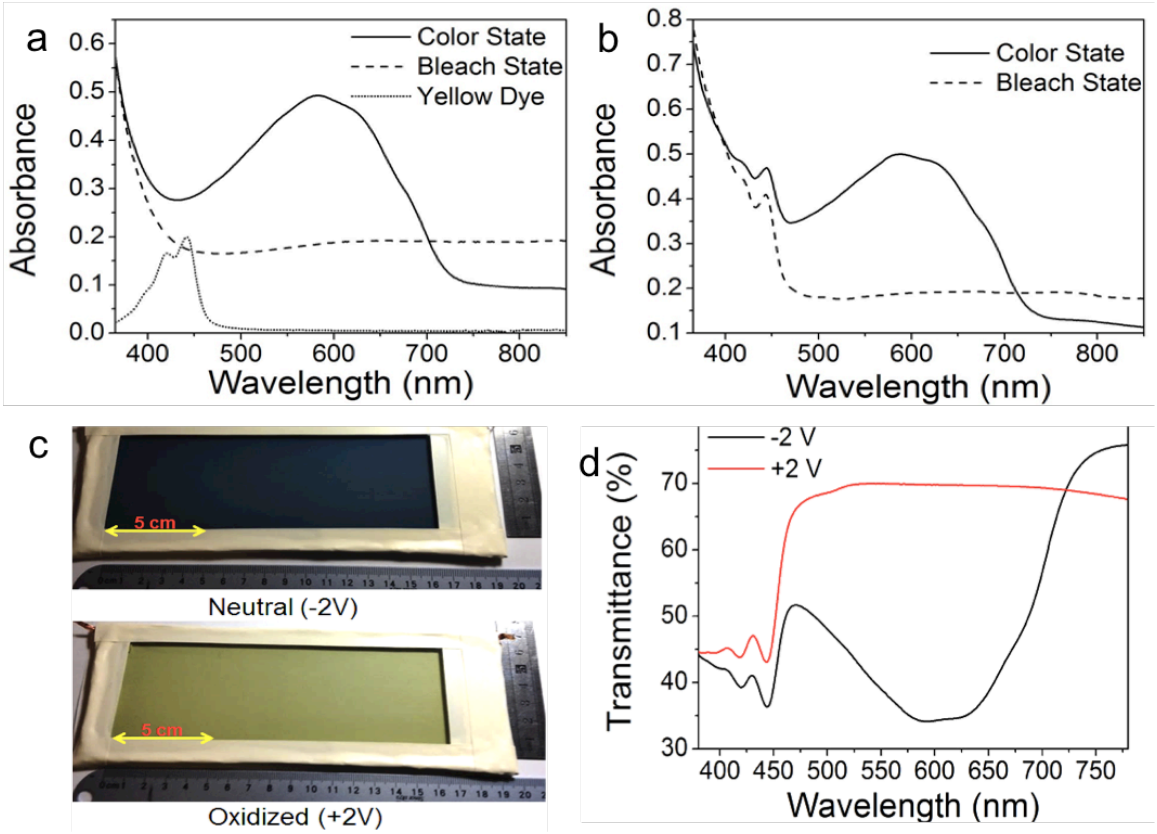

Figure 6.1 Achieving neutrality with the use of a yellow solvent dye. (a) The spectra of the yellow dye and PEDOT separately (b) is the spectrum of an un-optimized mixture of the two (c,d) is the image of a large area device and the UV-Vis spectrum for an optimized system. Adapted from © 2014 Y. Zhu, et al. Chemical Communications © 2014 RSC.

6.2 Overview of The Design and Synthesis of Electrochromic Dyes

A series of π-conjugated oligomers were synthesized with a common electroactive monomer, 2,2-dimethyl-3,4-propylenedioxythiophene (ProDOT-Me_2), to form homo-oligomers of increasing size exhibiting single-wavelength absorptions at rising intervals starting at 250 nm for the monomer up to 594 nm for the polymer. In addition to the experimental data, excited state calculations exhibited a decrease in transition energy with increasing conjugation length, which demonstrates that the optical properties are

similar to what is expected of constrained linear polyene systems. Electropolymerization of the oligomers shows much broader absorption spectra then that of the electroactive monomer. As a proof of concept, the π-conjugated oligomers were demonstrated for use as electrochromic dyes where the desired oligomer, according to predicted wavelength, is synthesized and end-capped to prevent any reactivity with other electroactive species present in the device or electrochemical cell.

6.2.1 Introduction

As technology becomes more inseparable from consumers, the ability to construct thinner/smaller and flexible displays for cell phones, tablets, and eyewear is of great importance to make technology less cumbersome. Electrochromic materials are envisioned to be the next iteration of displays due to the ability to work on flexible substrates and have low power consumption.[2] Electrochromic devices (ECDs) reported to date have been made from small organic molecules,[3] organic conjugated polymers,[4] and inorganics.[5] Organic π-conjugated materials exhibit fast switch speed, color variability, and high optical memory that result in low power consumption in an application.[4] Recently, electrochromics have been commercialized and used for windows in the new Boeing 787 Dreamliner.[6]

Since its first report in 1994, poly(3,4-ethylenedioxythiophene) (PEDOT) has been extensively studied for use in electrochromics, indium doped tin oxide (ITO) replacement, capacitors, organic light emitting diodes (OLEDs), and transistors.[7] A derivative of PEDOT is poly(3,4-propylenedioxythiophene) (ProDOT), which displays higher contrasts than PEDOT due to a more transmissive bleached state.[8] PEDOT has a

six-membered planar ring in comparison to ProDOT's non-planar seven-membered ring, which results in increased spacing along the polymer backbone, minimized stacking of the polymers, and decreased electron chain hopping between the polymers. This structure results in a more transmissive oxidized state due to the absorption in the near infrared (NIR) being reduced along with the tail into the visible region. Derivatives of ProDOT can have color transitions tuned across the visible spectrum by modifying the R groups on the seven membered ring.[9] Reynolds *et. al.* reported a black electrochromic using EDOT in a donor acceptor polymeric system,[10] and we have demonstrated the ability to use a dual copolymer system to achieve neutrality and the ability to computationally predict contrast and neutrality.[11] A recent report on electrochromics demonstrated high-throughput screening of ProDOT monomers that exhibited a continuum of single-wavelength colors spanning the entire subtractive visible spectrum. Moreover, neutrality was accomplished using commercially available organic solvent dyes with PEDOT, long-term stability of acrylated ProDOTs was achieved in high-contrasting ECDs, and ProDOT-Me_2 was used in several optimization studies for ECDs.[12]

π-conjugated oligomers have received considerable attention due to their light-harvesting abilities as photovoltaics, OLEDs, organic-field transistors, and electrochromic materials.[13] Some common oligomers based on the thiophene motif include sexithiophene, which has been studied as a photovoltaic, OLED, and as a transistor.[14] Oligomeric violigens are currently used commercially as the electrochromic material in automotive rearview auto-dimming mirrors.[15] Reynolds *et. al.* reported

electrochromic discrete oligomers that were photopatterned from EDOT and ProDOT monomers with an acrylate end group.[16]

Some downsides to discrete oligomers as electrochromics previously reported in the literature can be longer synthetic routes than that of some electrochromic polymers. Also, electrodimming mirrors, for example, consist of some molecule organic viologens that have to be in an electrolyte solution for reasonable switch speeds.

In this study, one electroactive monomer of ProDOT-Me_2 was used to synthesize homo-oligomers of increasing conjugation length to examine the structure and properties of the various oligomers. The absorption spectra measured demonstrated a dependence on chain length similar to what is expected of finite polyene systems, and excited state calculations were used to describe the origin of the observed transitions and trends within the group of oligomers. The diffusion of the oligomers in solution were studied and showed slower diffusion than the monomer. Then, oligomers were synthesized with endcapped groups to demonstrate their potential use as electrochromic dyes.

6.3 Results and Discussion

This study was designed to use a single monomer, ProDOT-Me_2, as a platform for color tuning electrochromic devices by modifying the conjugation length of the oligomer. First, a series of discrete oligomers were strategically synthesized to determine the optical properties of each chromophore. Ground state and excited state caculations were performed to explain the nature of the observed photophysical properties of ProDOT-Me_2 oligomers (from the monomer to the pentamer). Cyclic voltammetry was performed on each oligomer to obtain experimental energy values of the HOMO and LUMO, and

theoretical predictions were used to verify the measured values. Polymerization of the discrete oligomers were performed in solution and characterized. Then ProDOT-Me_2 with an alkylated end-capped ProDOT-Me_2 was polymerized with ferric chloride to produce the hexamer by controlling the stoichiometric amounts of the monomers for the fast generation of electrochromic dyes.

6.3.1 Synthesis

The initial step required to perform this oligomeric study was to synthesize the electroactive monomer, ProDOT-Me_2, by a Williamson transetherification from dimethoxythiophene and neopentyl glycol. The coupling of two ProDOT-Me_2 monomers to form the dimer was prepared via an Ullman reaction deprotonating with *n*-butyllithium and then adding copper iodide to facilitate the coupling. To synthesize the trimer, a dibromo-ProDOT-Me_2 derivative was synthesized from ProDOT-Me_2 with NBS in chloroform at room temperature, and this reaction goes to completion within minutes. The dibromo-ProDOT-Me_2 is then coupled with ProDOT-Me_2 via a Kumada reaction using dichloro[1,3-bis(diphenylphosphino)propane]nickel as the catalyst. This reaction is allowed to run for two days until completion, and to obtain high yields, the magnesium bromide etherate has to be recrystallized prior to use. The use of *n*-butyllithium as a base shows some dimer as a minor product, and the use of lithium diisopropylamide (LDA) results in the formation of only the desired product.[17] The tetramer is coupled together from Bis-ProDOT-Me_2 again using an Ullman coupling with copper iodide. The pentamer is synthesized in a similar manner to the trimer using the Kumuda reaction with dibromo-ProDOT-Me_2, but the dimer is used to form the pentamer. Similar to the trimer

reaction LDA minimizes the amount of tetramer seen as a minor side product in this reaction.

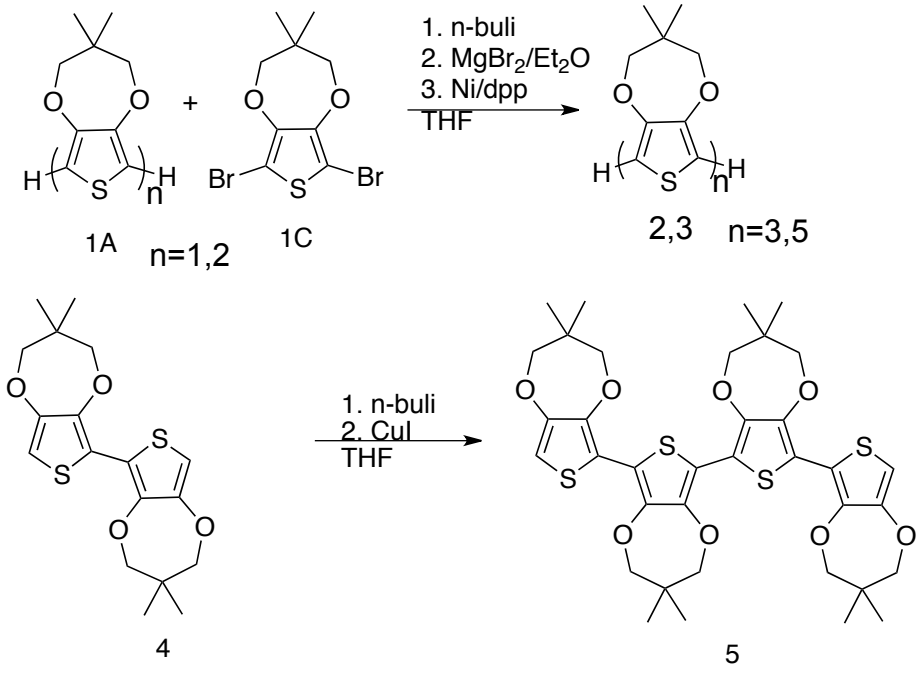

Scheme 6.1 Synthesis of the discrete oligomers.

6.3.2 Absorption Spectra and Theoretical Analysis

The absorption spectrum shown in Figure 6.1 illustrates the dependence of the optical properties of ProDOT-Me_2 on chain length and its subsequent effect on band gap. The monomer and discrete oligomers exhibited increasing absorption maxima from 251 nm to 444 nm as the conjugation length increases, and the polymer, ProDOT-Me_2, displays an absorption maximum at 575 nm.

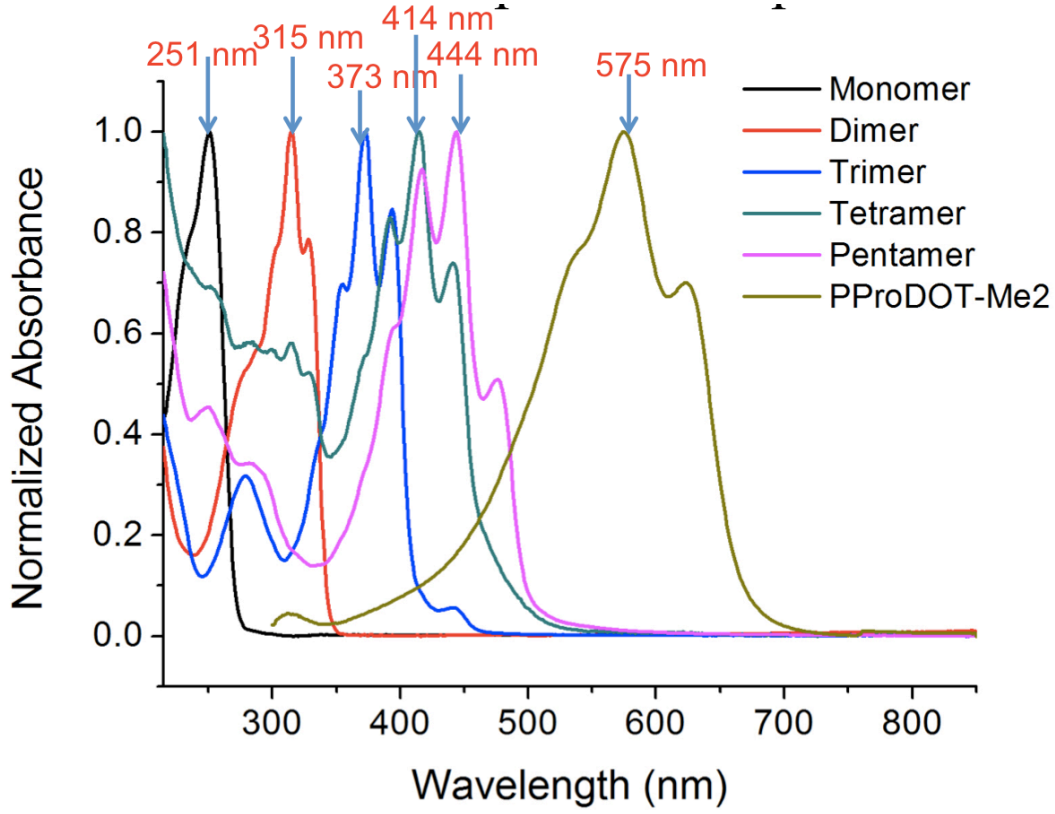

Figure 6.2 Absorption spectra of the discrete oligomers and polymer of ProDOT-Me_2.

The spectra are similar to the common spectral motifs that are observed with an linear polyene chain, which is the structural foundation of the ProDOT-Me_2 polymer. While the linear polyene parent compound is a simplification of the macrocyclic structure of the repeating unit, informative parallels can be drawn to explain the observed and calculated trends. Each absorption spectrum is characterized by a strongly absorbing band ($S_0 \rightarrow S_1$) that increases in excitation wavelength along with the chain length. Analysis of the calculated ground state geometries of the oligomers in DMSO suggests that the structures are mostly planar and constrained, which allows for well-resolved absorption spectra at room temperature. Consequently, the vibronic progression of the strongly-

allowed transition is visible. The vibronic intervals are on the order of ~1300 – 1400 cm^{-1} and can be attributed to the symmetric stretching of C-C and C=C observed for both linear and constrained polyenes.[18] There are greater vibrational degrees of freedom as the oligomer chain length increases, thus leading to the observed broadening of the absorption bands.

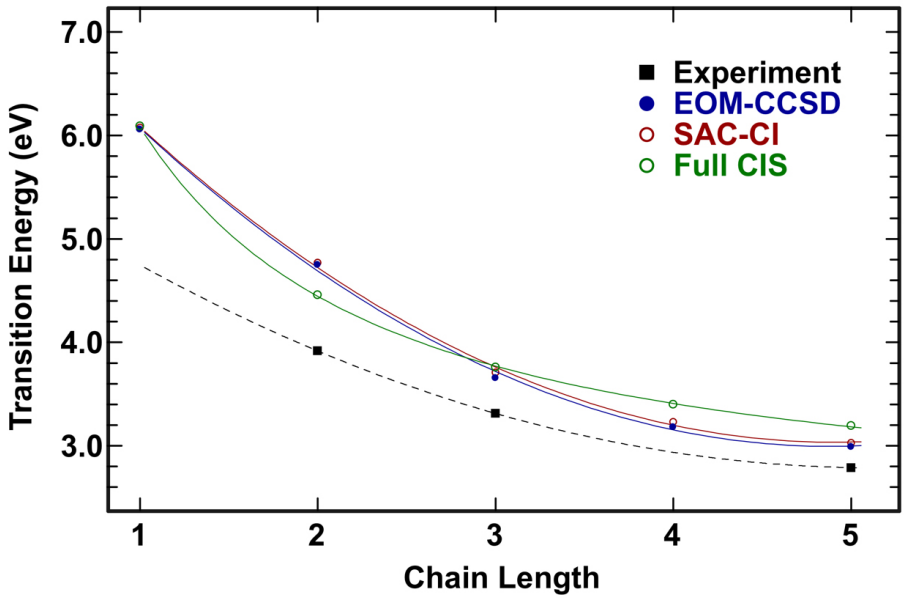

Figure 6.3 Comparison of the experimental and theoretical electronic transitions of the oligomers of **ProDOT-Me$_2$**. The experimental transition energies were obtained from the measured absorption maxima of the S_1 transition for each oligomer in dimethylsulfoxide. Each excited state calculation was performed with a dimethylsulfoxide solvent environment, as implemented in Gaussian 09 using the PCM model.

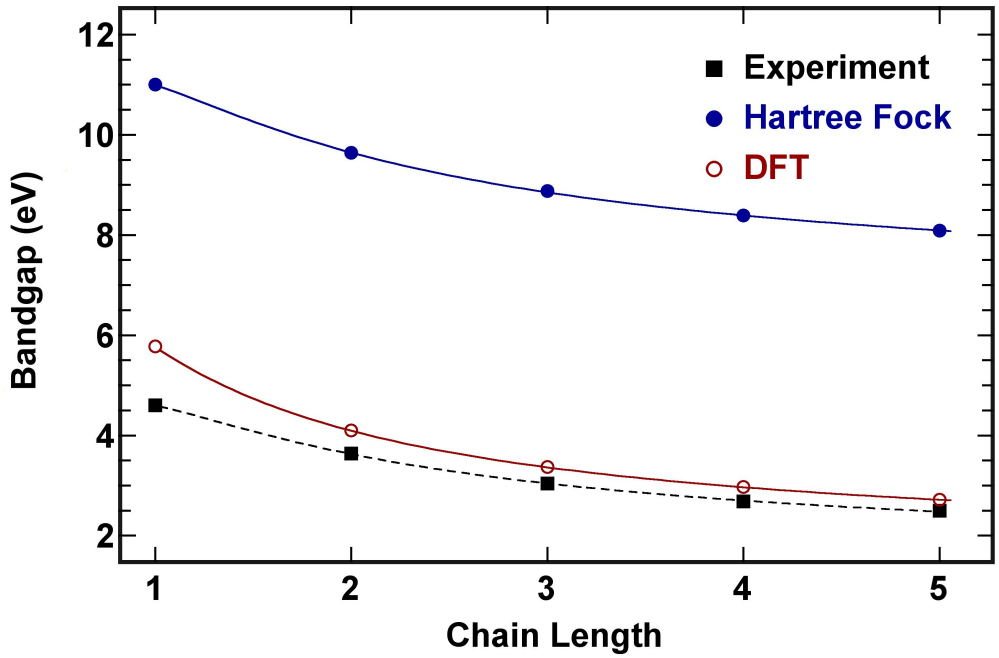

Figure 6.4 Comparison of the experimental and theoretical bandgap measurements.

The theoretical methods used here, including EOM-CCSD, SAC-CI, and CISF, are in good agreement with respect to the magnitude and trend of the observed S_1 transition energies of the ProDOT-Me_2 oligomers (**Figure 6.3**). The EOM-CCSD methodology has proven to be a reliable method for calculating transition energies and oscillator strengths of functionalized polyene chains and macrocycles,[19-26] while the SAC-CI methods are primarily of value because they provide reliable excited state electron densities and transition dipole moments.[27-31] The level-ordering results depicted in **Figure 5** demonstrates the general bathochromic shift of the optical transitions as the oligomer chain length increases, and that the spectra are dominated by the strongly allowed $S_0 \rightarrow S_1$ transition. The S_1 excited state is similar to the strongly-allowed $^1B_u^+$

state of linear polyenes in terms of ionic character and oscillator strength. As the chain length increases, the oscillator strength of the S_1 transition is also shown to increase. Moreover, the calculations illustrate a more subtle affect, in which the nature of bond alternation of a polyene leads to convergence to a constant excitation energy and band gap as the chain is elongated towards an infinite polyene (i.e., the ProDOT-Me_2 polymer).[32-35] Higher-energy transitions shown in Figure 6.2 correlate with the peaks that are blue-shifted relative to the S_1 transitions, and while these bands are largely indiscrete in the observed spectra, they are likely due to higher symmetry-allowed $^1B_u^+$–like transitions.

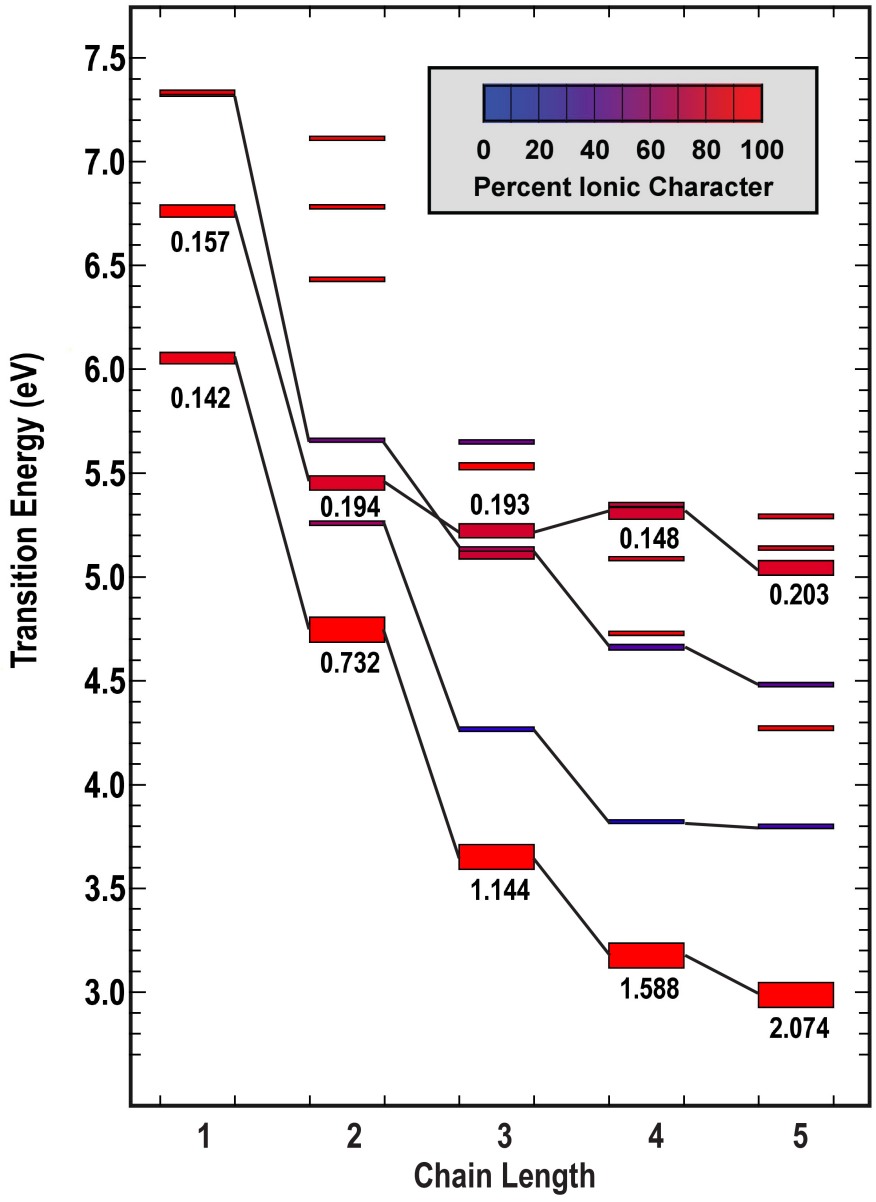

Figure 6.5 Excited singlet state level ordering of the first six excited states of various oligomers of ProDOT-Me_2, as calculated using EOM-CCSD methods. The excited states are each represented by a rectangle, the height of which is proportional to the oscillator strength. The calculated oscillator strengths are presented directly above or below the state rectangle for selected transitions. The ionic versus covalent character of the states are indicated by color based on the scheme shown in the upper right.

Figure 6.5 was generated using ground state equilibrium geometries, which indicates that the results represent Franck-Condon vertical excitations. The transition energies and oscillator strengths of the SAC-CI results are not quantitatively identical to the results in Figure 6.2, but predict the same trends. The ground states of each of the oligomers are characterized by electron density largely surrounding the polyene chain and oxygen atoms of the polymer. Upon excitation into S_1, the electron density shifts to surround the sulfur atoms and creates a high degree of charge separation along the polyene chain, which exemplifies the $^1B_u^+$–like transition described above.

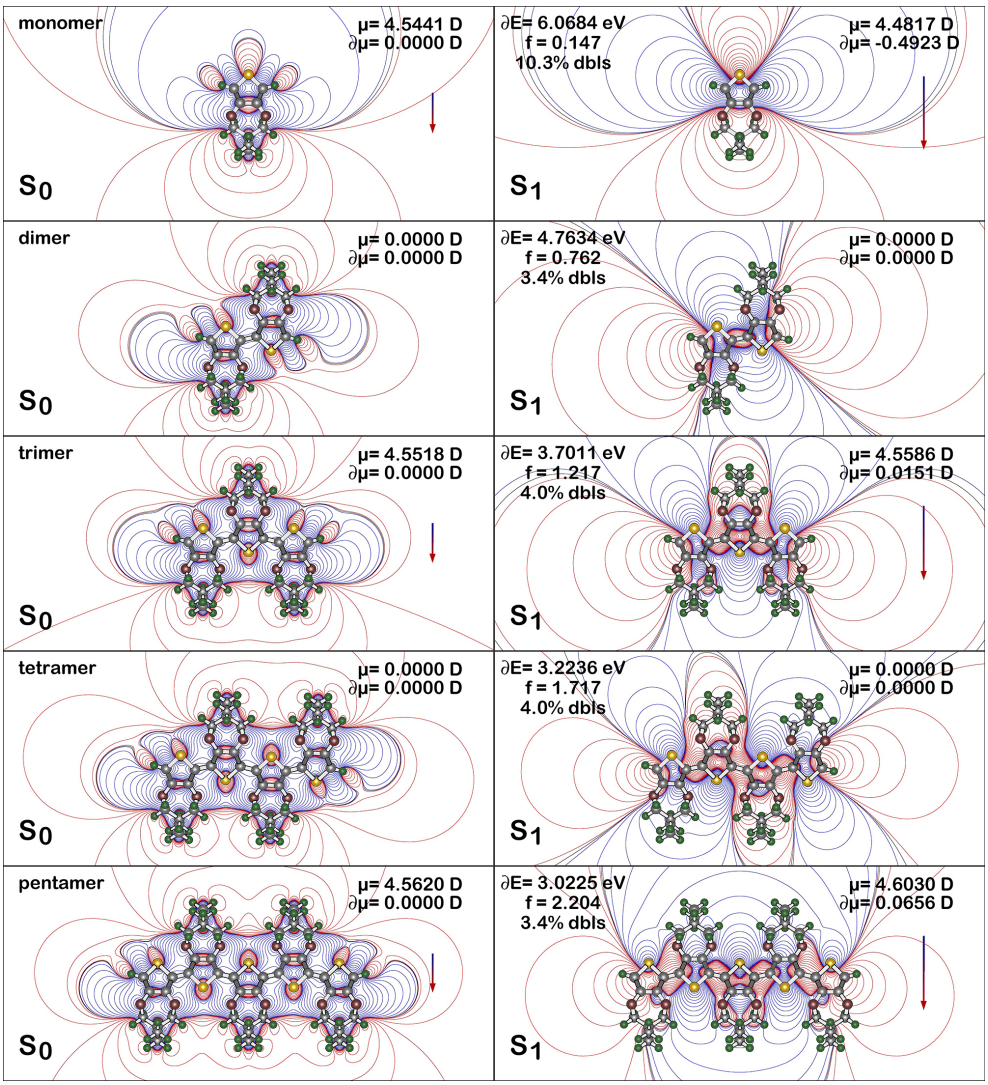

Figure 6.6 Electrostatic properties of the ground state (S_0) and the charge shifts induced by excitation into the first excited singlet state (S_1) for various polymeric chains of **ProDOT-Me$_2$**, which is based on SAC-CI methods. The ground state contours display the approximate electrostatic field surrounding the molecule, where red contours indicate regions of excess positive charge and blue contours indicate regions of excess negative charge. The contours associated with the excited state (S_1) represent the shift in charge induced by excitation into these states, where red contours indicate increased positive charge and blue contours indicate increased negative charge following excitation. The arrows display the dipole moment direction, and the transition energies (δE in electron volts relative to uncorrelated ground state), oscillator strengths (f) and dipole moments (μ in Debye) are shown at the top of each panel. The contribution of doubly excited configurations (dbls) is shown as a percentage at upper left of each excited state.

Otley (2015)

6.3.3 Cyclic Voltammetry

Cyclic voltammetry was performed using 0.1 M LITRIF/ACN electrolyte solutions containing 10 mM concentrations of the monomers or oligomers with a platinum button electrode as the working electrode, a platinum flag was used as counter electrode, and a silver wire as the pseudo-reference electrode as seen in Figure 6.7. Potential was scanned between -0.6 and +1.6 V for 4 cycles at a scan rate of 100 mV/s. The experimental HOMO was calculated from the oxidation onset of the cyclic voltammograms of each respective oligomer as shown in **Figure 6.8** as normalized current vs potential. The cyclic voltammograms of each respective molecule is shown in the supplemental information as Figure 6.7. The experimental bandgaps of the oligomers were calculated from the UV-Vis spectra shown in Figure 6.2, and plotted in Figure 6.6 to give the experimental LUMO. The trend exhibited in the experimental bandgaps shown in Figure 6.8 coincides with the theoretical data detailed in Table 6.1 and Figure 6.5.

Otley (2015)

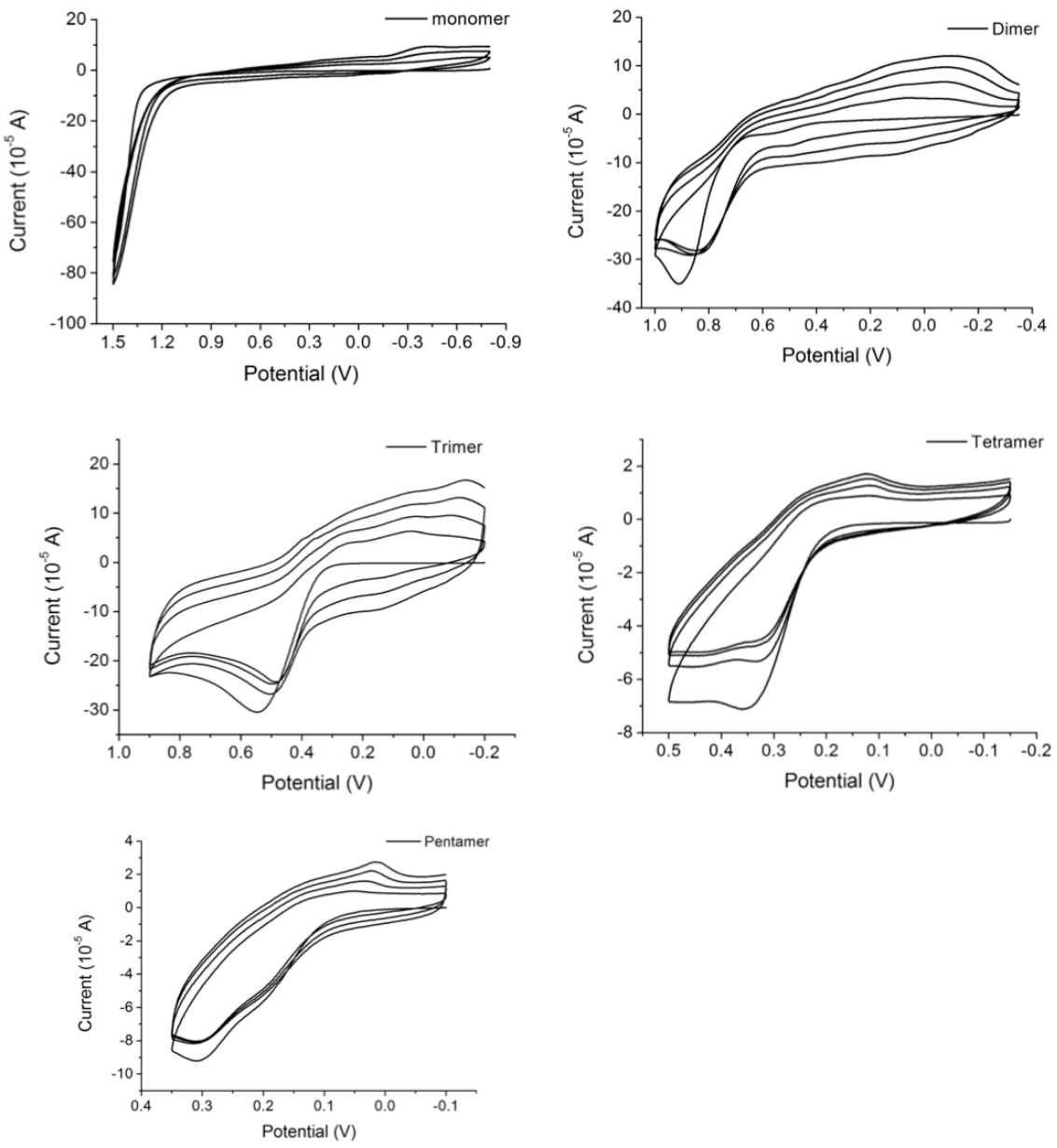

Figure 6.7 Cyclic voltammetry for ProDOT-Me_2 and it's oligomers were performed using 0.1 M LITRIF/ACN electrolyte solutions containing 10 mM monomers/oligomers.

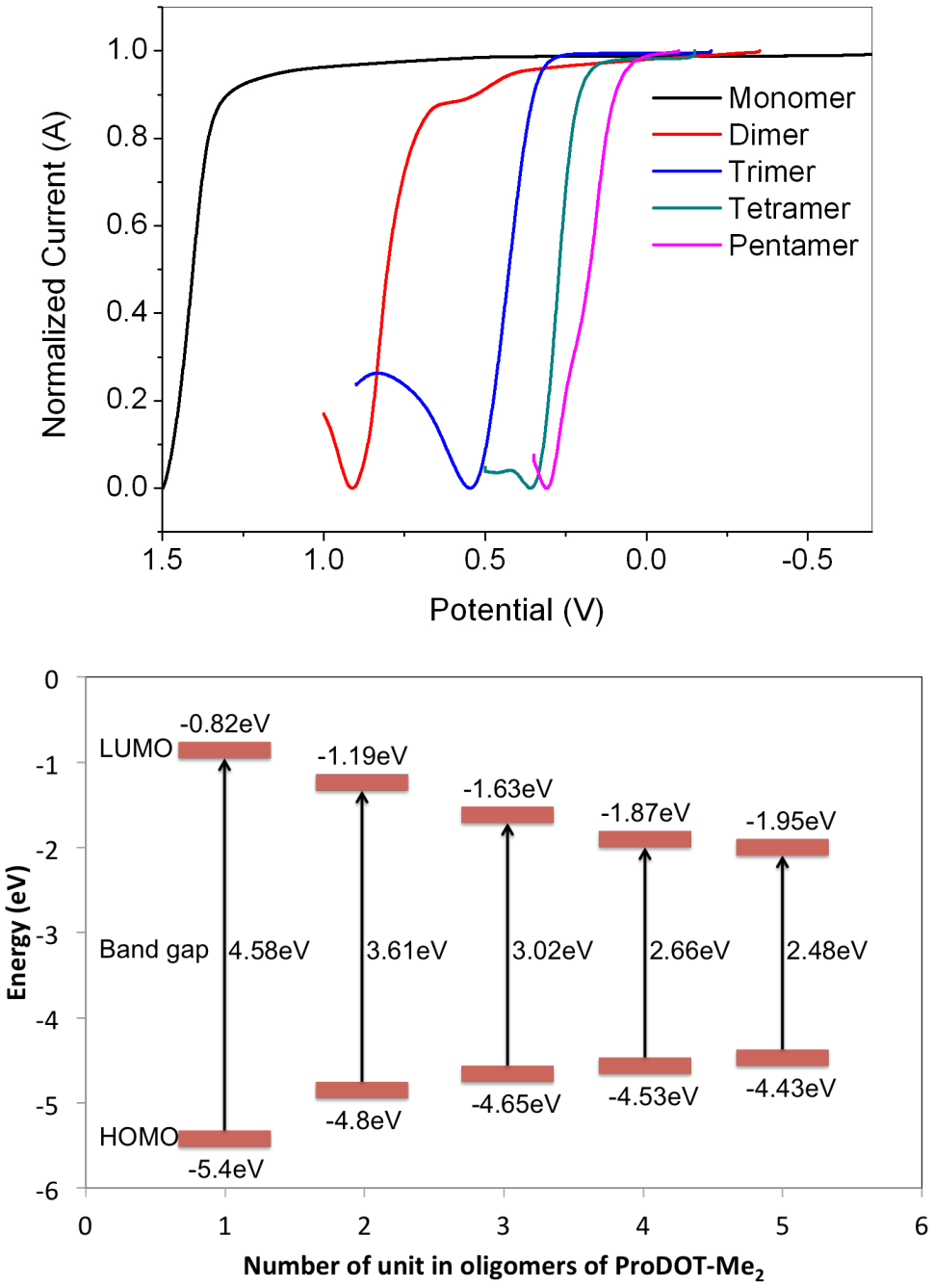

Figure 6.8 Normalized cyclic voltammogram of the oligomers, and the experimental HOMO, LUMO, and bandgaps.

Otley (2015)

Table 6.1 Experimental and calculated bandgap energies (eV) of **ProDOT-Me$_2$** in dimethylsulfoxide.

Oligomer	Experiment	DFT	Hartree-Fock
monomer	4.58	5.76	10.99
dimer	3.61	4.08	9.62
trimer	3.02	3.35	8.86
tetramer	2.66	2.95	8.37
pentamer	2.48	2.70	8.07

6.3.4 Application

For the demonstration of the potential application of ProDOT-Me$_2$ oligomers as electrochromic dyes end-capped oligomers were synthesized. The synthesis as shown in **Scheme 2** begins with the transetherification of neopentyl glycol with dimethoxythiophene, and then is alkylated. The alkylation is achieved by deprotonation of the thiophene ring with LDA, and then a halogenated alkane is added to the reaction mixture. The oligomerization is accomplished by oxidative coupling with ferric chloride in chloroform, and the desired oligomer can be obtained by controlling the stoichiometric amounts of the reactants. The preferred alkyl end group was hexyl due to the increased solubility of the oligomer, and also the selectivity in the alkylation step allowing for a simpler purification.

Otley (2015)

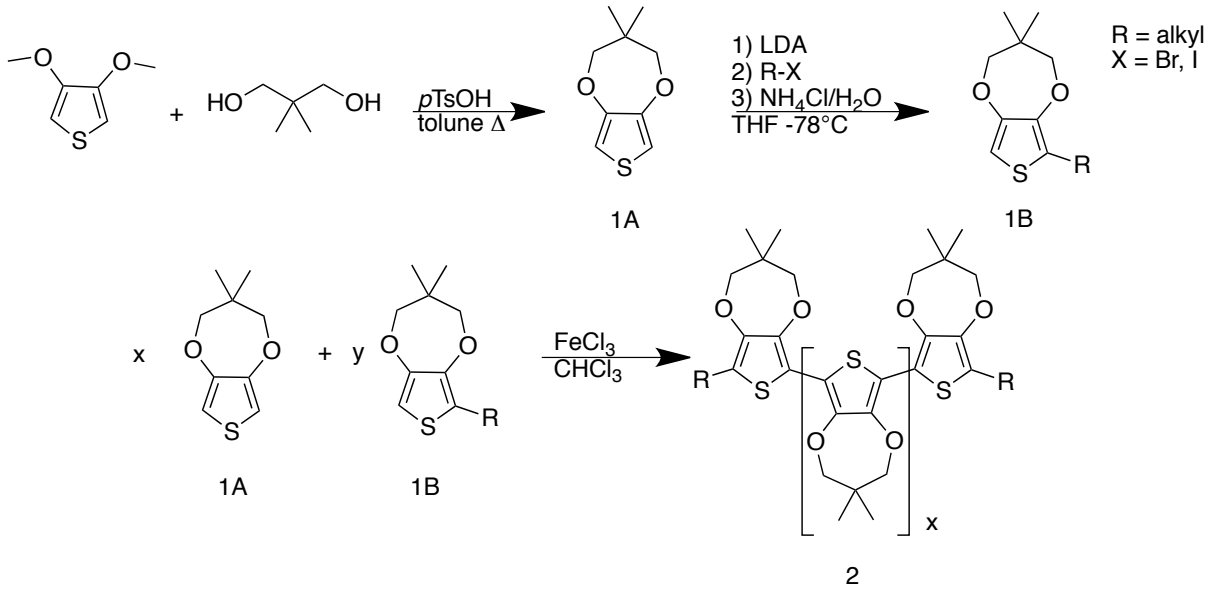

Scheme 6.2 Synthesis of electrochromic dyes.

Electrochromic dyes were synthesized controlling the stoichiometric amounts as 1 endcapped ProDOT-Me_2 and to 2 ProDOT-Me_2 monomers to hypothetically achieve a hexamer. As shown in **Figure 6** the λ_{max} of 470 nm is in the predicted range of the ProDOT-Me_2 hexamer, and the ^{1}H-NMR and ^{13}C–NMR data integrates to 6 ProDOT-Me_2 units.

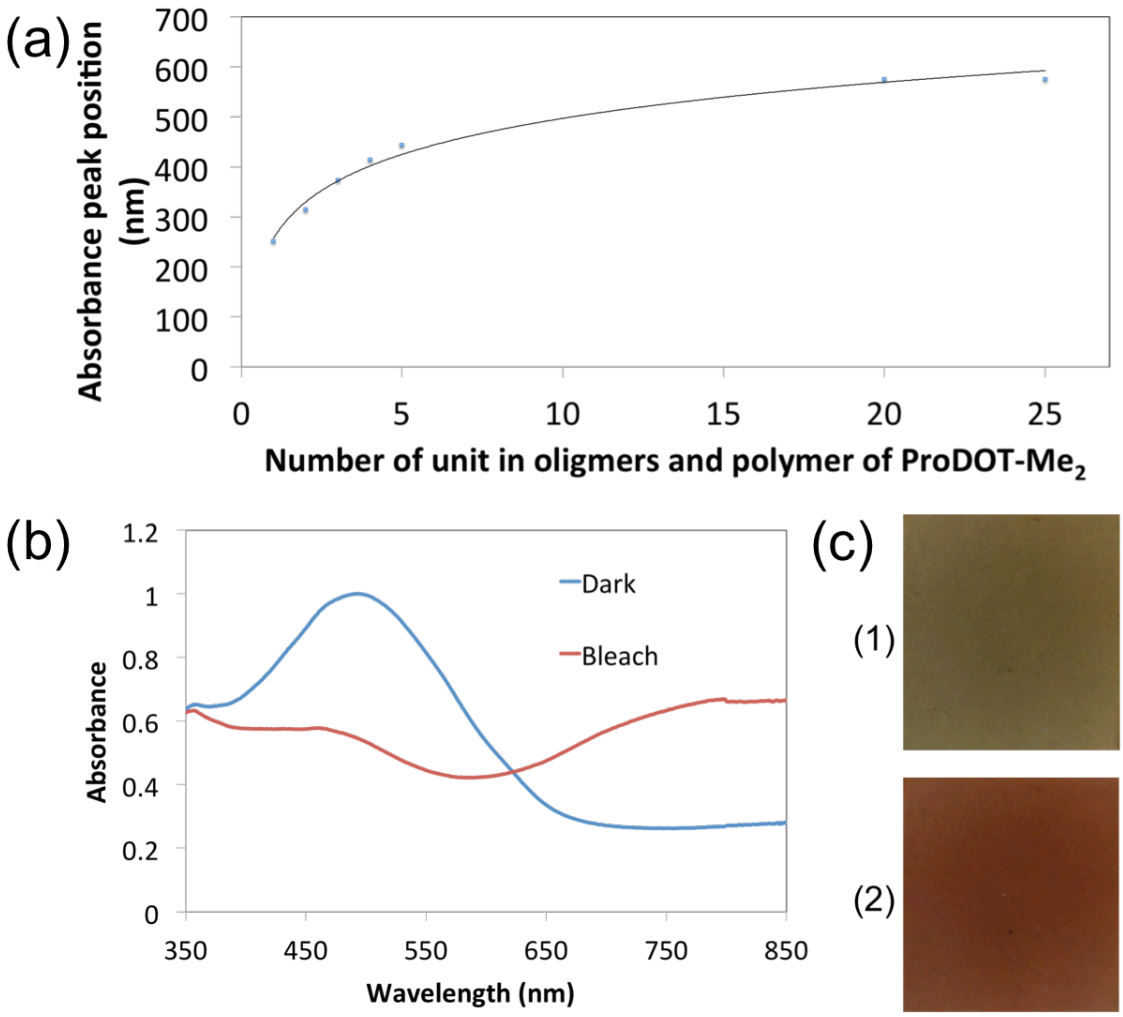

Figure 6.9 (a) Absorbance peak position vs. number of unit for all oligmers and polymer of ProDOT-Me_2. (b) Normalized UV-Vis absorption spectra of hexyl endcapped hexamer device (Dark state: -2V; Bleach state: +2V). (c) Images of hexyl endcapped hexamer device in (1) Bleach state; (2) Dark state.

6.4 Conclusion

We have demonstrated that π-conjugated oligomers based on the ProDOT motif can successfully generate electrochromic dyes of increasing wavelength as the conjugation chain increases. The theoretical calculations provided insight into the electronic properties of these molecules. These electrochromic dyes (if endcapped) could

be used with other electrochromic oligomers and/or polymers to compliment each other to achieve a desired color or neutrality for a specific application.

6.5 Experimental

6.5.1 Materials

Lithium trifluoromethanesulfonate (LITRIF), dimethoxyphenylacetophenone (DMPAP), propylene carbonate, poly (ethylene glycol) diacrylate (M_n = 700), and acetonitrile were purchased from Sigma-Aldrich and were used as received. Indium-doped tin oxide (ITO) glass was purchased from Delta Technologies and cleaned by sonication in acetone prior to use. The electroactive monomer, 2,2-dimethyl-3,4-propylenedioxythiophene (ProDOT-Me_2), was synthesized using a transetherification ring closure starting with commercially available 3,4-dimethoxythiophene and 2,2-dimethylpropane-1,3-diol (Sigma-Aldrich) according to the literature procedure.

6.5.2 Equipment

All electrochemistry was performed using CHI 400 or CHI 660A potentiostats. Spectroelectrochemical studies were carried out using a CARY 5000 UV-VIS-NIR spectrophotometer. Colorimetric measurements were obtained by a PR-670 SpectroScan Spectroradiometer (Photo Research, Inc.). Cyclic voltammetry for ProDOT-Me_2 and it's oligomers were performed using 0.1 M LITRIF/ACN electrolyte solutions containing 10 mM monomers/oligomers. A platinum button electrode (2 mm diameter) was chosen as working electrode. A platinum flag (0.5 cm^2) was used as counter electrode and a silver wire as the pseudo-reference electrode. Potential was scanned between -0.6 and +1.6 V for 4 cycles at a scan rate of 100 mV/s. Both ^1H and ^{13}C NMR was performed on a

Bruker DMX500 high resolution digital NMR spectrometer. Gas chromotography and mass spectrometry was carried out on a Hewlett Packard 6890 Series Gas Chromatography Mass Spectrometer. Infrared spectroscopy was performed on a Nicolet Magna 560 FTIR Spectrometer.

6.5.3 Synthesis

Dimer (and Tetramer follows the same procedure):

A solution consisting of 50 mL of dry THF and 5 g (27 mmol) of ProDOT-Me_2 (3,3-dimethyl-3,4-dihydro-2H-thieno[3,4-b][1,4]dioxepine) was cooled to -78 °C in an acetone/dry ice bath. Then 11.1 mL (27 mmol) of 2.45 M *n*-butyllithium was added dropwise to the solution. After 45 minutes the solution was warmed to 0 °C and 5.14 g (27 mmol) of copper iodide was added. The solution was allowed to warm to room temperature and stir for an additional 8 hours. The reaction mixture was then passed through a bed of celite, washed with brine, filtered, dried with $MgSO_4$, and the solvent was rotary evaporated. The solid was then passed through a column using a 30% ether/hexanes solvent system where any remaining monomer elutes first, and then the dimer fractions were collected, combined, and concentrated. The pure solid was then purified further by recrystallization with hexanes as a solvent producing a white solid.

Otley (2015)

Trimer (and Pentamer follows the same procedure):

A solution of dry THF and ProDOT-Me_2 (9.23 g, 0.065 mol) in THF (200 mL) under argon was cooled to -78 °C via a dry ice/acetone cooling bath. To the stirred precooled solution was added 34 mL (0.068 mol) of *n*-butyllithium via syringe. After 45 min, the reaction mixture was allowed to warm to 0 °C via ice bath, after which 16.8 g (0.065 mol) of $MgBr_2$,Et_2O was added in one portion. After 45 min, 3.14 g (0.032 mol) of trans- dichloroethylene and 0.50 g (0.92 mmol, 1.4 mol %) of catalyst, $NiCl_2$,dppp, was added. The reaction was allowed to warm slowly to room temperature. The reaction was allowed to continue for 48 h, after which, it was passed through a bed of celite. The solution was then washed with brine, the organic layer was dried with $MgSO_4$, filtered, and concentrated by rotary evaporation. The product was purified by column chromatography on silica gel using 60% CH_2Cl_2/Hexanes as the eluent to give 5.8 g (58%).

6.5.4 Theoretical Methods

All ground state geometries of the oligomers based on the 3,4-propylenedioxythiophene subunit were obtained using a Becke, three-parameter, Lee-Yang-Parr (B3LYP) hybrid functional[36] and a 6-31+G(d,p) basis set.[37,38] The solvent environment for each molecule was simulated by using the Polarizable Continuum Model (PCM).[39-42] The optimized molecules were used as the ground state geometries for subsequent excited state calculations. In order to determine the molecular orbital (MO) energies of the highest occupied molecular orbital (HOMO) and the lowest unoccupied molecular orbital (LUMO) for each molecule, the optimized molecules were minimized using the self-

consistent field theory through restricted Hartree-Fock (HF)[43] procedures and a 6-31+G(d,p) basis set. All calculations were performed using Gaussian 09.[42] The excited state properties of each molecule were calculated using multiple methods, including equation-of-motion coupled-cluster procedures with singles and doubles (EOM-CCSD),[19-21] symmetry-adapted-cluster configuration-interaction (SAC-CI),[27-31] and single-configuration interaction with full single CI (CISF).[44] Excited state calculations were performed using a Dunning/Huzinaga full double-ζ (D95) basis set,[45] and transition energies were calculated relative to the HF ground state. An active space of the eight highest energy filled orbitals and the eight lowest energy virtual orbitals (8 x 8) was used, with the exception of the CISF calculations, which included the default active space selected by Gaussian 09.

6.6 References

1. Y. Zhu, M. T. Otley, A. Kumar, M. Li, X. Zhang, C. Asemota, G. a Sotzing, *Chem. Commun.* **2014**, *50*, 8167.
2. R. J. Mortimer, *Am. Sci.* **2013**, *101*, 38.
3. P. M. S. Monk, *The Viologens: Physicochemical Properties, Synthesis and Applications of the Salts of 4,4'-Bipyridine*, J. Wiley & Sons, Chichester, **1998**; b) R. Cinnsealach, G. Boschloo, S. N. Rao, D. Fitzmaurice, *Sol. Energ. Mat. Sol. C.* **1998**, *55*, 215; c) X. W. Sun, J. X. Wang, *Nano Lett.* **2008**, *8*, 1884; d) D. G. Kurth, J. P. López, W. Dong, *Chem. Commun.* **2005**, *16*, 2119; e) C. G. Granqvist, *Handbook of Inorganic Electrochromic Materials*, Elsevier, **1995**, 663; f) Y. Ohsedo, I. Imae, Y. Shirota, *J. Poly. Sci. Part B: Polym. Phys.* **2003**, *41*, 2471; g) I. Imae, K. Nawa, Y. Ohsedo, N. Noma, Y. Shirota, *Macromolecules* **1997**, *30*, 380.
4. P. M. Beaujuge, J. R. Reynolds, *Chem. Rev.* **2010**, *110*, 268.
5. a) C. G. Granqvist, *Sol. Energ. Mater. Sol. C.* **2000**, *60*, 201; b) S. K. Deb, *Sol. Energ. Mat. Sol. C.* **2008**, *92*, 245; c) E. Avendaño, L. Berggren, G. A. Niklasson, C. G. Granqvist, A. Azens, *Thin Solid Films* **2006**, *496*, 30.
6. A. P. Weidner, U.S. Patent No. 7,450,294, **2008**.
7. a) Q. B. Pei, G. Zuccarello, M. Ahlskog, O. Inganas, *Polymer* **1994**, *35*, 1347; b) A. Elschner, S. Kirchmeyer, W. Lovenich, U. Merker, K. Reuter, *PEDOT: Principles and Applications of an Intrinsically Conductive Polymer*, CRC Press **2010**.

8. D. M. Welsh, A. Kumar, E. W. Meijer, J. R. Reynolds, *Adv. Mater.* **1999**, *11*, 16.

9. T. Dey, M. A. Invernale, Y. Ding, Z. Buyukmumcu, G. A. Sotzing, *Macromolecules* **2011**, *44*, 2415.

10. P. M. Beaujuge, S. Ellinger, J. R. Reynolds, *Nat. Mater.* **2008**, *7*, 795.

11. M. T. Otley, Y. Zhu, X. Zhang, M. Li, G. A. Sotzing, *Adv. Mater.* **2014**, *26*, 8004.

12. a) F. Alhashmi Alamer, M. T. Otley, Y. Ding, G. A. Sotzing, *Adv. Mater.* **2013**, *25*, 6256; b) M. T. Otley, F. Alhashmi Alamer, Y. Zhu, A. Singhaviranon, X. Zhang, M. Li, A. Kumar, G. A. Sotzing, *ACS Appl. Mater. Interfaces* **2014**, *6*, 1734; c) A. Kumar, M. T. Otley, F. A. Alamar, Y. Zhu, B. G. Arden, G. A. Sotzing, *J. Mater. Chem. C* **2014**, *2*, 2510; d) Y. Zhu, M. T. Otley, F. Alhashmi Alamer, A. Kumar, X. Zhang, D. M. D. Mamangun, M. Li, B. G. Arden, G. A. Sotzing, *Org. Electron.* **2014**, *15*, 1378. e) Y. Zhu, M. T. Otley, X. Zhang, M. Li, C. Asemota, G. Li, M. a. Invernale, G. a. Sotzing, *J. Mater. Chem. C* **2014**. f) F. A. Alamer, M. T. Otley, Y. Zhu, A. Kumar, G. a. Sotzing, *Sol. Energy Mater. Sol. Cells* **2015**, *132*, 131.

13. a) A. R. Murphy, J. M. J. Fréchet, *Chem. Rev.* **2007**, *107*, 1066. b) D. Fichou, ed. *Handbook of oligo-and polythiophenes*. John Wiley & Sons, Weinheim, 2008. c) R. E. Martin, F. Diederich, *Angew. Chemie Int. Ed.* **1999**, *38*, 1350.

14. a) G. Horowitz, F. Garnier, A. Yassar, R. Hajlaoui, F. Kouki, *Adv. Mater.* **1996**, *8*, 52. b) G. Horowitz, P. Delannoy, H. Bouchriha, F. Deloffre, J.-L.

Fave, F. Garnier, R. Hajlaoui, M. Heyman, F. Kouki, P. Valat, Vér. Wintgens, A. Yassar, *Adv. Mater.* **1994**, *6*, 752. c) N. Loussaïef, F. Kouki, P. Delannoy, F. Garnier, L. Hassine, H. Bouchriha, *Mater. Sci. Eng. C* **2002**, *21*, 255.

15. R. J. Mortimer, *Chem. Soc. Rev.* **1997**, *26*, 147.
16. C. B. Nielsen, A. Angerhofer, K. A. Abboud, J. R. Reynolds, *J. Am. Chem. Soc.* **2008**, *130*, 9734.
17. R. S. Loewe, P. C. Ewbank, J. Liu, L. Zhai, R. D. McCullough, *Macromolecules* **2001**, *34*, 4324.
18. R. L. Christensen, et al. *The Journal of Physical Chemistry A* **2013**, *117*, 1449-1465.
19. J. F. Stanton, R. J. Bartlett, *J. Chem. Phys.* **1993**, *98*, 7029-7039.
20. H. Koch, R. Kobayashi, A. Sánchez de Merás, P. Jørgensen, *J. Chem. Phys.* **1994**, *100*, 4393-4400.
21. M. Kállay, J. Gauss, *J. Chem. Phys.* **2004**, *121*, 9257-9269.
22. R. L. Christensen, et. al.; *The Journal of Physical Chemistry A* **2013**, *117*, 1449-1465.
23. N. L. Wagner, J. A. Greco, M. M. Enriquez, H. A. Frank, R. R. Birge, *Biophys. J.* **2013**, *104*, 1314-1325.
24. M. M. Enriquez, et al. *J. Phys. Chem. B* **2013**, *116*, 10748-10756.
25. N. M. Magdaong, et al. *Phys. Lett.* **2014**, *593*, 132-139.
26. J. A. Greco, A. Rossi, R. R. Birge, C. A. Brückner, *Photochem. Photobiol.* **2014**, *90*, 402-414.

27. H. Nakatsuji, K. Hirao, *J. Chem. Phys.* **1978**, *68*, 2053-2065.

28. H. Nakatsuji, *Chem. Phys. Lett.* **1979**, *67*, 334-342.

29. H. Nakatsuji, *Chem. Phys. Lett.* **1991**, *177*, 331-337.

30. M. Ishida, K. Toyota, M. Ehara, M. J. Frisch, H. Nakatsuji, *J. Chem. Phys.* **2004**, *120*, 2593-2605.

31. T. Nakajima, H. Nakatsuji, *Chem. Phys.* **1999**, *242*, 177-193.

32. J. N. Murrell, *The theory of the electronic spectra of organic molecules*; Chapman and Hall: London, **1963**.

33. H. Kuhn, *J. Chem. Phys.* **1949**, *17*, 1198-1212.

34. H. Kuhn, *J. Chem. Phys.* **1948**, *16*, 840-841.

35. J. R. Platt, *J. Chem. Phys.* **1956**, *25*, 80-105.

36. A. D. Becke, *J. Phys. Chem.* **1993**, *98*, 5648-5652.

37. T. Clark, J. Chandrasekhar, G. W. Spitznagel, P. V. R. Schleyer, *J. Comp. Chem.* **1983**, *4*, 294-301.

38. M. J. Frisch, J. A. Pople, J. S. Binkley, *J. Chem. Phys.* **1984**, *80*, 265-3269.

39. M. Caricato, B. Mennucci, G. Scalmani, G. W. Trucks, M. J. Frisch, *Journal of Chemical Physics* **2010**, *132*, 084102.

40. R. Fukuda, M. Ehara, H. Nakatsuji, R. Cammi, *Journal of Chemical Physics* **2011**, *134*, 104109.

41. A. V. Marenich, C. J. Cramer, D. G. Truhlar, C. A. Guido, B. Mennucci, G. Scalmani, M. J. Frisch, *Chem. Sci.* **2011**, *2*, 2143-2161.

42. Frisch, M. J.; Trucks, G. W.; Schlegel, H. B.; Scuseria, G. E.; Robb, M. A.; Cheeseman, J. R.; Scalmani, G.; Barone, V.; Mennucci, B.; Petersson, G. A.; Nakatsuji, H.; Caricato, M.; Li, X.; Hratchian, H. P.; Izmaylov, A. F.; Bloino, J.; Zheng, G.; Sonnenberg, J. L.; Hada, M.; Ehara, M.; Kitao, O.; Nakai, H.; Vreven, T.; Montgomery, J., J. A.; Peralta, J. E.; Ogliaro, F.; Bearpark, M.; Heyd, J. J.; Brothers, E.; Kudin, K. N.; Staroverov, V. N.; Kobayashi, R.; Normand, J.; Raghavachari, K.; Rendell, A.; Burant, J. C.; Iyengar, S. S.; Tomasi, J.; Cossi, M.; Rega, N.; Millam, J. M.; Klene, M.; Knox, J. E.; Cross, J. B.; Bakken, V.; Adamo, C.; Jaramillo, J.; Gomperts, R.; Stratmann, R. E.; Yazyev, O.; Austin, A. J.; Cammi, R.; Pomelli, C.; Ochterski, J. W.; Martin, R. L.; Morokuma, K.; Zakrzewski, V. G.; Voth, G. A.; Salvador, P.; Dannenberg, J. J.; Dapprich, S.; Daniels, A. D.; Farkas, O.; Foresman, J. B.; Ortiz, J. V.; Cioslowski, J.; Fox, D. J.; Gaussian, Inc.: Wallingford, CT, 2009.

43. C. C. J. Roothaan, *Rev. Mod. Phys.* **1960**, *32*, 179-185.

44. J. B. Foresman, M. Head-Gordon, J. A. Pople, M. J. Frisch, *Journal of Physical Chemistry* **1992**, *96*, 135-149.

45. T. H. Dunning Jr., P. J. Hay, In *Modern theoretical chemistry*; Schaefer, H. F., Ed.; Plenum, New York: New York, **1976**; Vol. 3, pp 1-28.

Otley (2015)

7. Chapter 7: High-Throughput Screening of Conjugated Polymers towards Neutral Colors

7.1 Overview

This chapter is a continuation of Chapter 5 that detailed a study of solid-state high-throughput screening of electroactive monomers that was used to generate a continuum of copolymers of various absorptions across the entire visible spectrum. In this chapter we took the knowledge gained from the previous study of being able to match a specific color anywhere within the visible spectrum, and then added a second copolymer to obtain a flat absorption across the entire visible spectrum resulting in a neutral or 'black' color. The significance of this study is the development of low-level computational modeling that allowed us to predict the absorption and contrast of a device before even building one by combining the absorbance of the two copolymers theoretically. In addition, this study contains the first example of an ultra-flexible (introduced in Chapter 3) neutral device to demonstrate the utility of this method.

7.2 Background

Flexible/conformal display devices that are easily manufactured in a method exhibiting low cost, low waste, and cover large areas have yet to be realized consisting of electrochromic polymers. Electrochromic devices (ECD)s have traditionally been fabricated by depositing the electrochromic polymer onto the electrode via electrodeposition that can be a costly and inefficient procedure for manufacturing. Color tuning for architectural windows, smart glass/privacy glass, automotive, aerospace, and

contrast-enhancement for see-through displays all require grey/black/neutral colors. Herein, a method to color-tune electrochromic devices using a single-lamination procedure, where the monomers are electrochemically polymerized *in situ,* is demonstrated to achieve neutrality using three monomers to form two distinct copolymers. The monomer ratios for the conjugated random copolymers were predetermined and optimized via theoretical calculations to provide the most desirable optical properties when combined within an electrochromic device. These devices exhibited photopic contrasts up to *ca*. 38%, 2% neutrality, color uniformity across a 75 cm^2 active area device, haze below 2%, and switch speeds of less than 1 second.

Electrochromic materials hold potential as becoming the next generation of flexible displays due to their ability to work on flexible substrates and low power consumption.[1] Recent high-profile commercialization of electrochromics includes the Boeing 787 Dreamliner windows manufactured by Gentex.[2] Electrochromic materials consist of inorganics,[3] small molecule organics,[4] and conjugated polymers.[5] Electrochromic materials made from π–conjugated polymers (CP)s have been gaining in popularity due to fast switch speeds, color variability, and high optical memory that results in low power consumption. CPs extended π-conjugation along the polymer backbone allow for its spectral absorption, and the energy gap between the HOMO and LUMO for CPs changes with an applied voltage due to the ability of the CP to change from an insulator to a semiconductor. The effect is a difference in absorption shifts resulting in visible color changes. A full visible spectral range of colors for CPs have been reported.[6] These optical properties make CPs of significant interest for applications

such as displays, windows, OLEDs or anywhere the optical variation of transmittance and/or reflectance is required.

The benchmark electrochromic polymer poly(3,4-ethylenedioxythiophene) (PEDOT) has been extensively studied since it was first reported in 1994.[7] Poly(3,4-propylenedioxythiophene) P(ProDOT) and its derivatives, demonstrate higher contrasts than PEDOT due to a more transmissive bleached state.[8] This is due, in part, to PEDOT's six-membered planar ring in comparison to PProDOT's non-planar seven-membered ring resulting in increased spacing along the polymer backbone, which minimizes the stacking of the polymers, and thus decreasing electron chain hopping. Therefore, the absorption in the near infrared (NIR) is reduced along with the tail into the visible region, making them more transmissive in their oxidized state. By modifying the R groups on P(ProDOT), the color transitions can be tuned across the visible spectrum. For example, poly(2,2-dimethyl-3,4-propylenedioxythiophene) P(ProDOT-Me_2) transitions between purple and sky blue while poly(1,3-di-*tert*-butyl-3,4-propylenedioxythiophene) P(1,3-PProDOT-tBu_2) transitions between yellow and sky blue.[9] ProDOT-Me_2 and ProDOT-tBu_2 were previously reported in a copolymerization study where high-throughput screening of the two ProDOT monomers exhibited a continuum of single-wavelength colors spanning the entire subtractive visible spectrum.[6] This study revealed the color variability of ProDOTs where two monomers, when copolymerized, can achieve the entire single-wavelength spectrum, but more importantly went to the same clear transparent color when oxidized. An earlier study demonstrated the electrochemical copolymerization of EDOT and thieno[3,4-*b*]thiophene (T34bT) that resulted in a red shift of the EDOT λ_{max}.[10]

A neutral color is a color not associated with any single hue, but is a color close to the white point for emittance and black point for absorbance. Recent efforts in fabricating ECDs that display neutral color transitions are of special interest in the current architectural window, smart glass/privacy glass, automotive, and aerospace industry. Currently, neutral color or near-black electrochromic polymers are highly researched in the academic and industrial community. Several published studies have utilized the donor-acceptor (DA) approach to broaden the absorbance spectra of these polymers to obtain neutrality including a notable study by Reynolds *et. al.* who published the first neutral or "black" electrochrome. Reynolds' method consists of soluble CPs that can be spray coated onto tin-doped indium oxide (ITO) coated substrates.[11] Our group published a random copolymerization method using two precursor polymers that was comprised of both DA and donor-only groups.[12] The precursor blends were electrochemically converted into a donor-acceptor electrochromic polymer that switched between black to sky blue in its neutral and oxidized states, respectively, with a photopic contrast of 30%. In a more recent study from our group, a method was demonstrated using all commercially available materials to achieve neutrality with EDOT and an organic solvent dye using the "subtractive color mixing" theory.[13] In addition, the recent literature includes studies comprising of copolymers on two separate electrodes, and multiple layers of several polymer electrochromes with complementary color absorption.[14]

Previously reported from our research group was a one-step procedure to simplify the fabrication and enhance the success rate of constructing ECDs.[15] The *in situ* method dissolves the monomers directly into a liquid electrolyte and this solution is sandwiched

between two ITO coated substrates. Next, the device is exposed to UV light, forming a solid electrolyte matrix, where conversion of the electroactive monomers to electrochromic polymers happens with the application of an appropriate potential. This method was developed as an alternative to electrodepositing the electroactive monomer onto the ITO coated substrate inside an electrolyte bath, thus eliminating a step. In the electrodeposition procedure an ITO coated substrate is placed into an electrolyte bath containing monomers. Then the electroactive monomers are converted to electrochromic polymers on the ITO coated substrate for an electrochromic polymer layer or film on the ITO. The bath has a limited lifespan for producing pristine films, normally one or two depositions, thus increasing solvent and waste consumption. Another method for fabricating ECDs is spray coating the electrochromic polymer or precursor polymer onto the ITO substrate. The advantages of the *in situ* method over spray coating is the electrochromic polymer does not have to be soluble since it is made *in situ*, and the polymer does not have to be synthesized because only monomers are needed, thereby shortening the synthesis by one step. Recently reported from our group using the one-step lamination procedure was high-throughput screening of electroactive monomers,[6] long-term stability of acrylated ProDOTs in high-contrasting ECDs,[16] and ProDOT-Me_2 was used in several optimization studies for ECDs.[17]

Initially, the copolymerization of three monomers 2,2-dimethyl-3,4-propylenedioxythiophene (ProDOT-Me_2), 1,3-di-*tert*-butyl-3,4-propylenedioxythiophene (ProDOT-tBu_2), and thieno[3,4-*b*]thiophene (T34bT) in two separate copolymerizations were studied. The monomers were chosen due to their visible absorbance where

ProDOT-tBu_2 has a λ_{max} at 392 nm at the extreme low end of the visible spectrum, ProDOT-Me_2 has a λ_{max} of 575 nm, and T34bT is in the near infrared (NIR) with a broad absorbing λ_{max} at 850 nm so that a combination of these could cover the entire visible spectrum. Then theoretical calculations were performed combining the different copolymer compositions of the two copolymer systems to determine the best combination to achieve neutrality without sacrificing contrast using the "subtractive color mixing" theory. The most promising were experimentally evaluated using the *in situ* approach, but with a slight modification to allow copolymerization of the two different copolymer systems to form a single electrochromic layer within the device. Once the procedure was optimized, a flexible device was fabricated on ITO coated polyethylene terephthalate (PET) to demonstrate the broad utility of this procedure.

7.3 Results and Discussion

To color tune for neutrality a series of copolymers were investigated. First a series of copolymers consisting of ProDOT-Me_2 and ProDOT-tBu_2 were studied in solid state devices using the previously described *in situ* procedure.[15] This copolymer system was chosen due to the results yielded in a previous study from our lab involving high-throughput screening that demonstrated the ability to color tune using diffusion in a solid state device that generated a series of copolymers of different feed ratios covering the entire visible spectrum.[6] The gel electrolyte composition for the copolymerization studies consisted of 1g of lithium triflate (LiTRIF), 3g of propylene carbonate (PC), 7g of poly(ethylene glycol) methacrylate (PEG-MA) and 17.5mg of dimethoxyphenylacetophenone (DMPAP) together and was sonicated until fully

dissolved. The feed ratios for the monomers that was added to the gel electrolyte composition were adjusted as seen in **Figure 7.1**A to produce 6 copolymers of absorptions between the two homopolymers of ProDOT-tBu_2 and ProDOT-Me_2 with a λ_{max} of 392 nm and 575 nm, respectively.

Otley (2015)

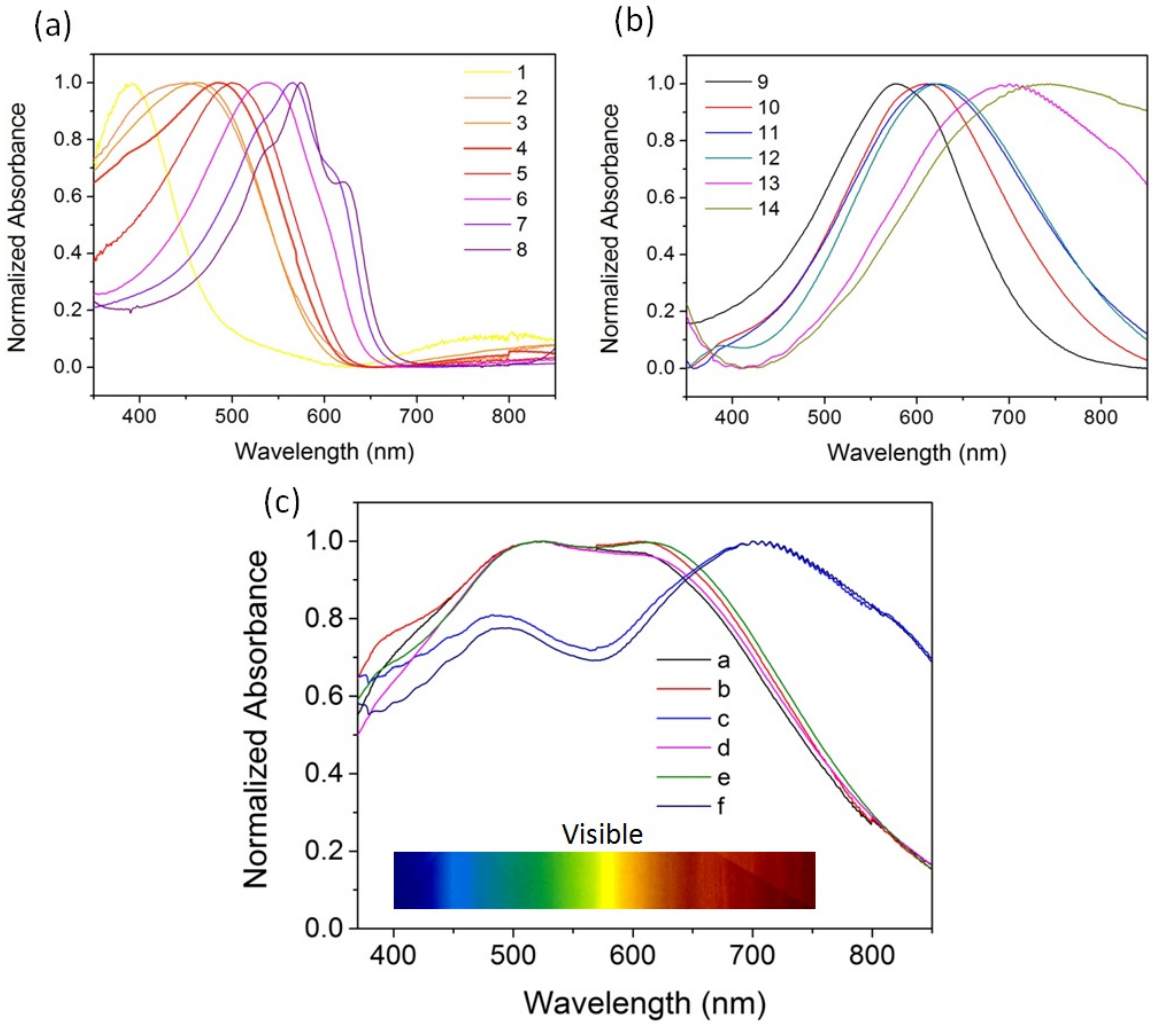

Figure 7.1. (a) Normalized Absorbance of Homopolymers or Copolymers by *in situ* polymerization of monomers at different feed ratios: 1) 100 wt% ProDOT-tBu_2; 2) 80 wt% ProDOT-tBu_2 : 20 wt% ProDOT-Me_2; 3) 75% wt% ProDOT-tBu_2: 25% ProDOT-Me_2; 4) 65% ProDOT-tBu_2 : 35% ProDOT-Me_2; 5) 60% ProDOT-tBu_2 : 40% ProDOT-Me_2; 6) 40% ProDOT-tBu_2: 60% ProDOT-Me_2, Abs max= 537 nm 7) 25% ProDOT-tBu_2: 75% ProDOT-Me_2; 8) 100% ProDOT-Me_2.
(b) Normalized Absorbance of Copolymers *in situ* polymerization of monomers at different feed ratio: 9) 99 wt% ProDOT-Me_2 : 1 wt% T34bT; 10) 98 wt% ProDOT-Me_2 : 2% T34bT; 11) 97.5% ProDOT-Me_2: 2.5 wt% T34bT; 12) 97 wt% ProDOT-Me_2 : 3 wt% T34bT; 13) 94 wt% ProDOT-Me_2 : 6 wt% T34bT; 14) 90 wt% ProDOT-Me_2 : 10 wt% T34bT.
(c) Theoretical modeled normalized absorbance spectrum with desired neutrality (<12%) by combing the absorbance spectra of a) Copolymer 2 + 11; b) Copolymer 2 + 12; c) Copolymer 2 + 13; d) Copolymer 3 + 11; d) Copolymer 3 + 12; e) Copolymer 3 + 13 to cover the entire visible region (400 -750 nm).

Otley (2015)

The goal was to find a copolymer combination that filled the lower wavelength visible spectrum, and also had a broad absorption. The most promising PProDOT-tBu_2-co-PProDOT-Me_2 systems were copolymers 2, 3, and 4 whose λ_{max} were 446 nm, 460 nm, and 485 nm, respectively, and all three systems exhibited broad absorptions. Subsequently, a series of copolymers were explored to cover the higher wavelengths of the visible absorption spectrum to achieve a dual copolymer system that complimentarily covers the entire visible spectrum thus achieving neutrality. ProDOT-Me_2 was again chosen for use in this system due to it's low cost for synthesizing and high contrast, and T34bT was chosen due to its λ_{max} at 850 nm and broad absorption. T34bT when copolymerized with ProDOT-Me_2 theoretically would red shift the λ_{max} of ProDOT-Me_2 and cover the higher wavelengths with a broad absorption. A series of copolymers consisting of ProDOT-Me_2-co-T34bT were studied as shown in Figure 7.1B and the most promising copolymer systems were 10, 11, and 12 whose λ_{max} absorptions were 608 nm, 618 nm, and 626 nm, respectively. The copolymerizations of the ProDOT-Me_2-co-T34bT systems were also performed using the *in situ* procedure similar to the PProDOT-tBu_2-co-PProDOT-Me_2 system, but one modification to the procedure was required, due to T34bT's sensitivity to UV irradiation, to electrochemically convert the electroactive monomers to copolymers in the *liquid state* before UV curing the liquid gel electrolyte to the solid state. Then all forty-eight combinations of homopolymers and copolymers were then combined to perform theoretical absorbance calculations as shown in Figure 7.1C, and the goal was to combine spectra of the two copolymer systems, PProDOT-tBu_2-co-

Otley (2015)

PProDOT-Me_2 with ProDOT-Me_2-co-T34bT, to determine which combination of the two had the best absorbance between 400 nm and 750 nm.

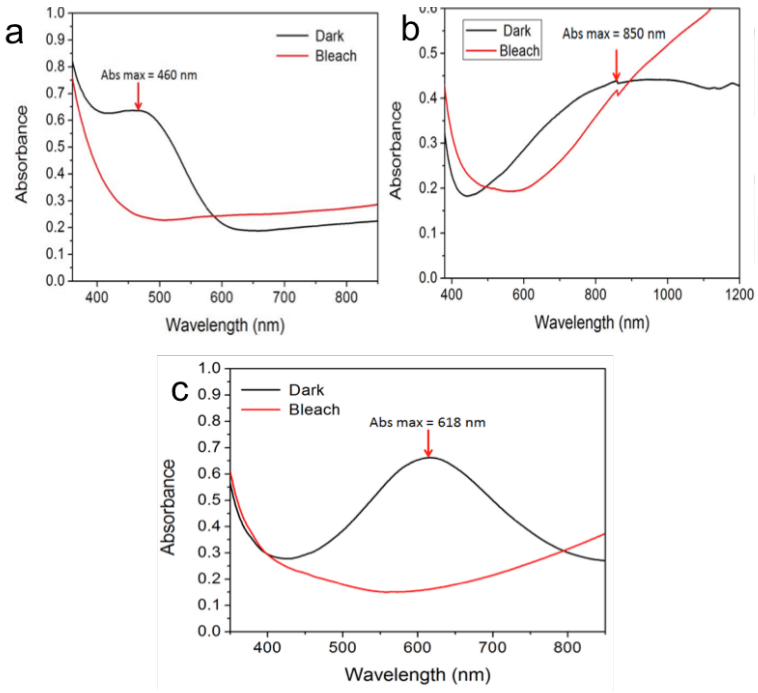

Figure 7.2. (a) Absorbance spectrum of dark and bleach states for the *in situ* ProDOT-Me_2/ProDOT-tBu_2 device (monomer feed ratio: 75 wt% ProDOT-Me_2 : 25 wt% ProDOT-tBu_2) (a). The absorbance max is at 460 nm in its dark state. The device has the same peak intensity at 460 nm as the control dual copolymer layer device in the main article. (b) Absorbance spectra of dark and bleached states for an *in situ* PT34bT device. The absorbance max is at 850 nm in its dark state. (c) Absorbance spectra of dark and bleached states for the *in situ* PProDOT-Me_2/PT34bT device (monomer feed ratio: 98.5 wt% ProDOT-Me_2 : 1.5 wt% T34bT). The absorbance max is at 618 nm in its dark state.

Based upon Lambert-Beer's law, the absorbance of the high energy copolymer and the absorbance of the low energy copolymer were adjusted by different factors and combined together to achieve the optimal neutrality value (below 12%) after final

absorbance normalization. A total of six systems meet the requirement out of the forty-eight 48 different combinations (8 × 6) that are modeled, and they are listed in **Table 7.1**. Upon inspection of the theoretical data in Table 7.1 system c and system f were not selected due to their higher dark state photopic transmittance compared with the other four systems, which will lead to a lower contrast. Photopic transmittance is a calculation weighted to the sensitivity of the human eye for the amount of light passing through the sample that gives a more accurate description of transmittance, and the photopic contrast is the weighted difference between the dark and bleached states.[17]

System d exhibits a similar photopic transmittance value to system a, but a superior neutrality, therefore, system d was selected and evaluated in a solid-state device. Also, system b and system e demonstrate the same transmittance and neutrality values but the color coordinates of system b are closer to the reference white point, therefore it was chosen and tested in a solid-state device. In total, two neutral systems are reported in this study consisting of copolymer 3 + 11, and copolymer 2 + 12 as neutral system 2. The data of the solid-state devices consisting of copolymers 3 + 11 and 2 + 12 detailed in this study are closely matched to the theoretical modeled data displayed in Table 1.

Otley (2015)

Table 1. Theoretical Results of the Copolymer Systems

System		Color coordinate		Photopic transmittance (%)	Neutrality (%)
		x	y		
a	copolymer 2 + 11	0.300	0.290	10.5	11
b	copolymer 2 + 12	0.294	0.290	10.5	8.5
c	copolymer 2 +13	0.300	0.327	17	11
d	copolymer 3 + 11	0.294	0.280	10.5	10
e	copolymer 3 + 12	0.288	0.279	10.5	8.5
f	copolymer 3 + 13	0.296	0.319	18.5	11.5

Otley (2015)

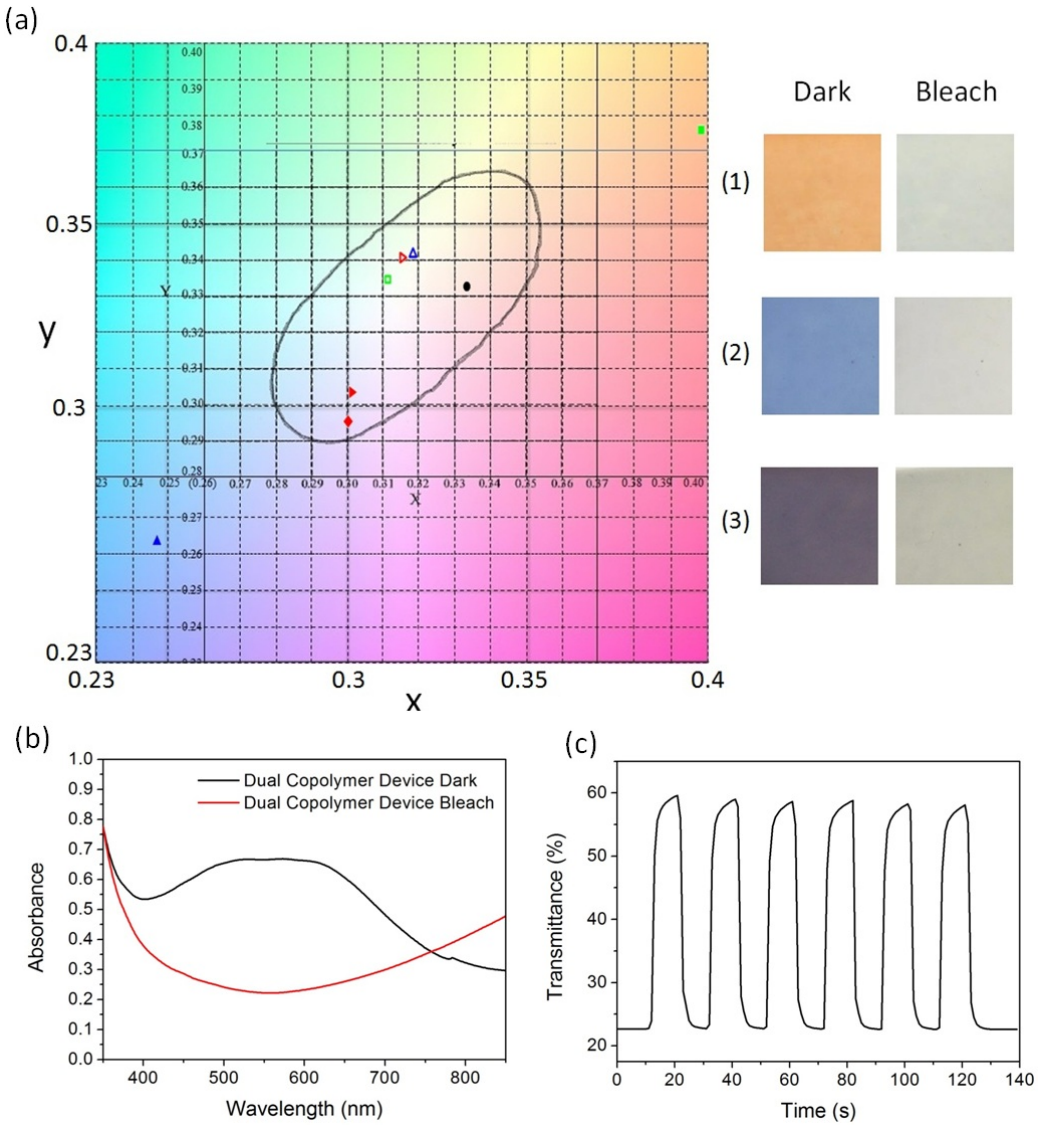

Figure 7.3. (a) Color coordinates and images of (1) ProDOT-Me_2/ ProDOT-tBu_2 copolymer device: dark state (solid green square on color space) and bleach state (open green square on color space); (2) ProDOT-Me_2/T34bT copolymer device: dark state (solid blue triangle on color space) and bleached state (open blue triangle on color space); (3) Dual layer Copolymer Device: dark state (solid red triangle on color space), theoretical modeled dark state (solid red diamond), and bleached state (open red triangle on color space), Reference white point (solid black circle on color space); Grey circle in color space represents the neutral color region.
(b) UV-Vis absorption spectra of the dual copolymer single electrochromic layer device.
(c) Percent transmittance change at 555 nm for dual copolymer layer device during constant potential stepping between -2 V to +2 V. © 2014 M. T. Otley, et al. Advanced Materials © 2014 John Wiley and Sons.

7.3.1 Neutral System 1: Copolymers 3 + 12

A series of dual copolymer devices were then investigated to achieve neutrality using the single-lamination procedure, and the variety of copolymers allowed for precise color tuning of the neutral system to achieve the most favorable characteristics for windows and displays. The main system reported in this study is shown in **Figure 7.3** consisting of PProDOT-tBu_2-co-PProDOT-Me_2 copolymer 3 and ProDOT-Me_2-co-T34bT copolymer 11. The color coordinates for each copolymer system and the actual dual copolymer solid state device is shown in Figure 7.3A. The copolymer system 3 exhibits an orange dark state (Figure 7.3B) with color coordinates of x = 0.398 and y = 0.376, while copolymer 11 shows a blue color in the dark state with color coordinates of x = 0.311 and y = 0.335. The dual copolymer solid state device has a dark state of x = 0.301 and y = 0.304 with a calculated neutrality of 6%. The photopic contrast of this system was 37%, and was the best compromise of neutrality and photopic contrast of all the systems studied.

Otley (2015)

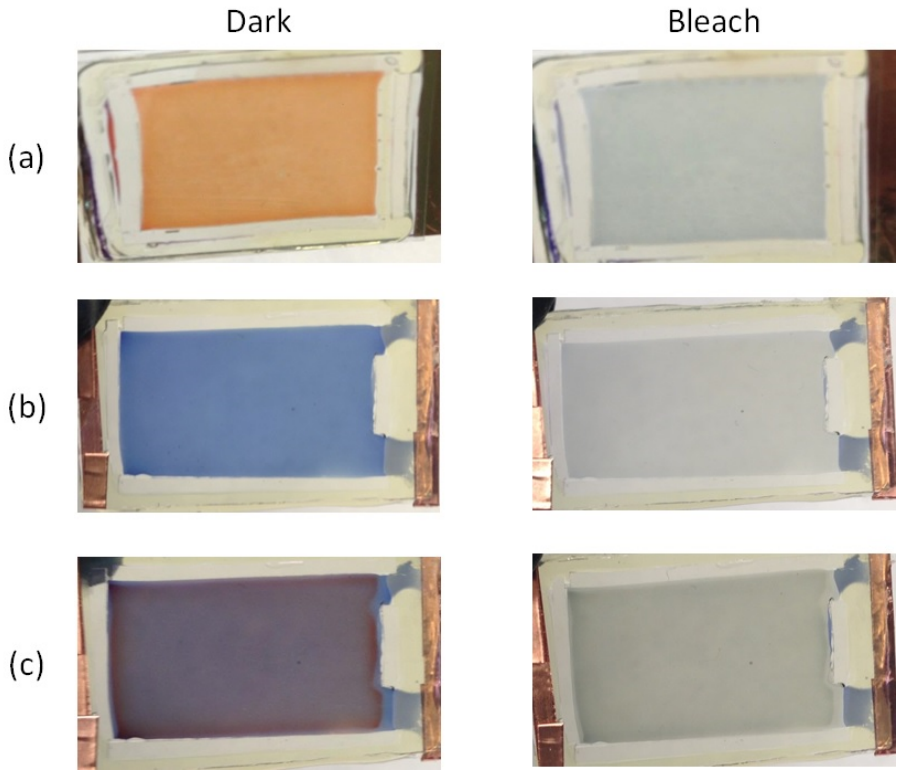

Figure 7.4. Images of Dark and Bleached states for the small area (2 × 4 cm^2) devices shown in Figure 7.3(a) : (a) ProDOT-Me_2/ProDOT-tBu_2 device (b) *in situ* PProDOT-Me_2/PT34bT device and (c) dual layer copolymer device (absorbance spectrum corresponds to Figure 7.3(b)). © 2014 M. T. Otley, et al. Advanced Materials © 2014 John Wiley and Sons.

Also, the dual copolymer devices all exhibited fast switch speeds of < 1 s, and stability was measured by switching the device for 2600 cycles which resulted in a 4.5% loss of photopic contrast from an initial 38.8% contrast to 34.3% after 2600 cycles (**Figure 7.5**). To further increase stability of the dual copolymer device, the ProDOT-Me_2 monomer can be substituted with an acrylated ProDOT monomer which has shown stability to over 10,000 cycles with only a 3% loss of photopic contrast if desired for a specific application.[16] The fabrication of the dual copolymer devices entailed one

additional step than the single copolymer devices described previously. The modification was to first drop cast and electrochemically convert ProDOT-Me_2 and T34bT in the liquid state in between two ITO coated substrates. Then the device was disassembled, the electrochromic layer was washed with PC, and then built normally using the previously described *in situ* method with ProDOT-tBu_2 and ProDOT-Me_2 added to the gel electrolyte to form the second copolymer layer.

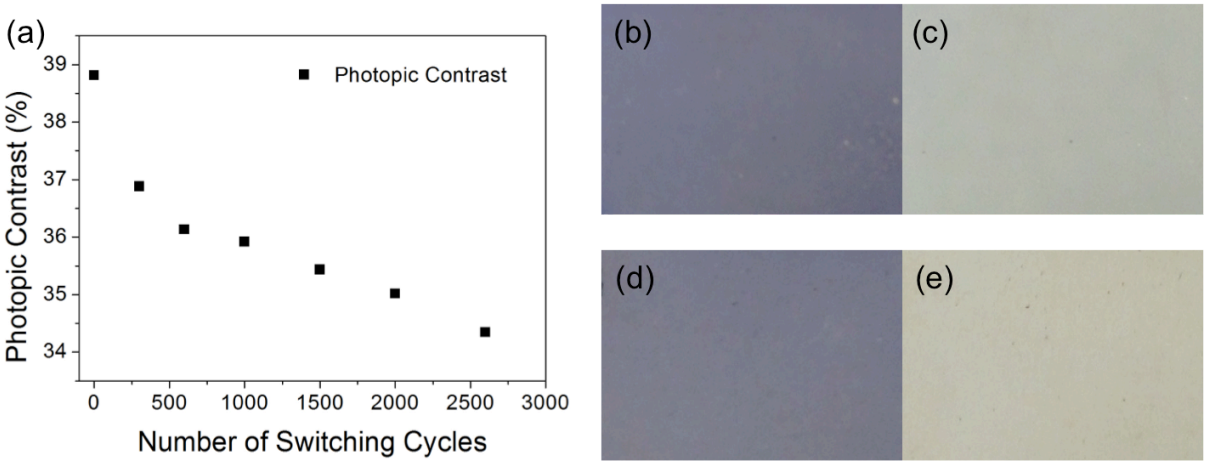

Figure 7.5. (a) Stability plot of an *in situ* neutral colored device. (b) and (c) are the dark and bleached states, respectively, at 0 cycles, (d) and (e) are the dark and bleached states after 2600 cycles. © 2014 M. T. Otley, et al. Advanced Materials © 2014 John Wiley and Sons.

7.3.2 Neutral System 2: Copolymers 2 +11

In a second study, another dual copolymer device was fabricated utilizing copolymer 2 and copolymer 12, of which the absorbance max were at 446 nm and 626 nm respectively. The reason to select this two copolymers is because one is more blue shifted and the other one is more red shifted, which, could lead to a wider expansion of the overall absorbance of the final dual copolymer layer device across the entire visible region to achieve better neutrality.

Otley (2015)

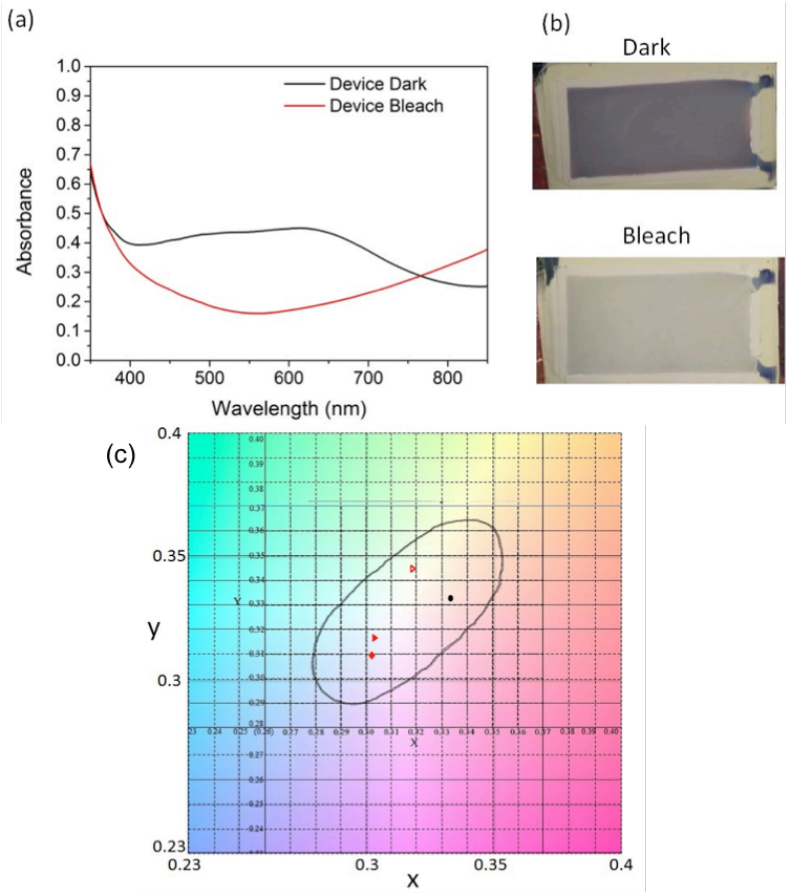

Figure 7.6 (a) Absorbance spectrum and (b). Images of dark and bleached states for the *in situ* neutral color device utilizing Copolymer 2 and Copolymer 12. (c) Color coordinates for the supporting neutral system (solid red triangle represents dark state and open red triangle represents bleach state); Theoretical modeled dark state (solid red diamond); Reference white point (solid black circle on color space); Grey circle in color space represents the neutral color region. © 2014 M. T. Otley, et al. Advanced Materials © 2014 John Wiley and Sons.

In this system, ProDOT-Me_2/T34bT (monomer feed ratio: 97 wt% ProDOT-Me_2 : 3 wt% T34bT) was converted in liquid state for 40 s, 20 s fewer than the control system in main article and following solid state conversion time of ProDOT-Me2/ProDOT-tBu2 (monomer feed ratio: 80 wt% ProDOT-Me_2 : 20 wt% ProDOT-tBu2) was 30 s, 20 s fewer than that in control system. As a result, two thinner polymer layers were generated,

giving less absorbance in both device dark and bleach states. The absorbance spectra and images of the device are shown in **Figure 7.6**. Color coordinates, photopic transmittance and neutrality for each state is summarized in **Table 7.2**.

Table 7.2. Color coordinates, photopic transmittance and neutrality for the *in situ* neutral color device utilizing Copolymer 2 and Copolymer 12.

	x	y	Neutrality (%)	Photopic transmittance (%)
Dark	0.303	0.317	2	36.5
Bleach	0.318	0.345	4	67.5
Theoretical modeled Dark	0.302	0.310	3.5	36

The color coordinates (x, y) for neutral system 2 are shown in **Figure 7.6**.

In comparison with the neutral systems mentioned earlier, a low of neutrality of 2% was achieved in the device dark state due to a better balanced absorbance intensity across the entire visible region, and as a result, color coordinates of the device dark state also got closer to the white reference point. However, the device photopic contrast decreased to 31% due to the shift of copolymer absorbance to the end of visible region and the low absorbance in both dark and bleach states.

Several other variables can be experimented in the future, for example, shorter polymer conversion time that results in a thinner electrochromic layer increasing the clear state's %T and thus increasing photopic contrast.

Otley (2015)

7.3.3 Ultra Flexible Neutral Colored Electrochromic Devices

The dual copolymer system (copolymer 3 + 11) exhibited in Figure 7.2C was then used as the electrochrome for neutral colored flexible devices. The flexible device seen in **Figure 7.7**A consists of two ITO coated PET substrates with a modified gel electrolyte differing from the gel electrolyte in the previously described devices with the addition of poly(ethylene glycol) dimethacrylate to the electrolyte composition. This allows the device to flex without cracking of the gel electrolyte that would shorten the lifetime of the device. The flexible PET device displayed similar properties to the rigid glass with a photopic contrast of 32% due to the lower transmissivity substrate. However, the neutrality remained the same at 5% for the dark state, and also exhibited sub second switch speeds.

Otley (2015)

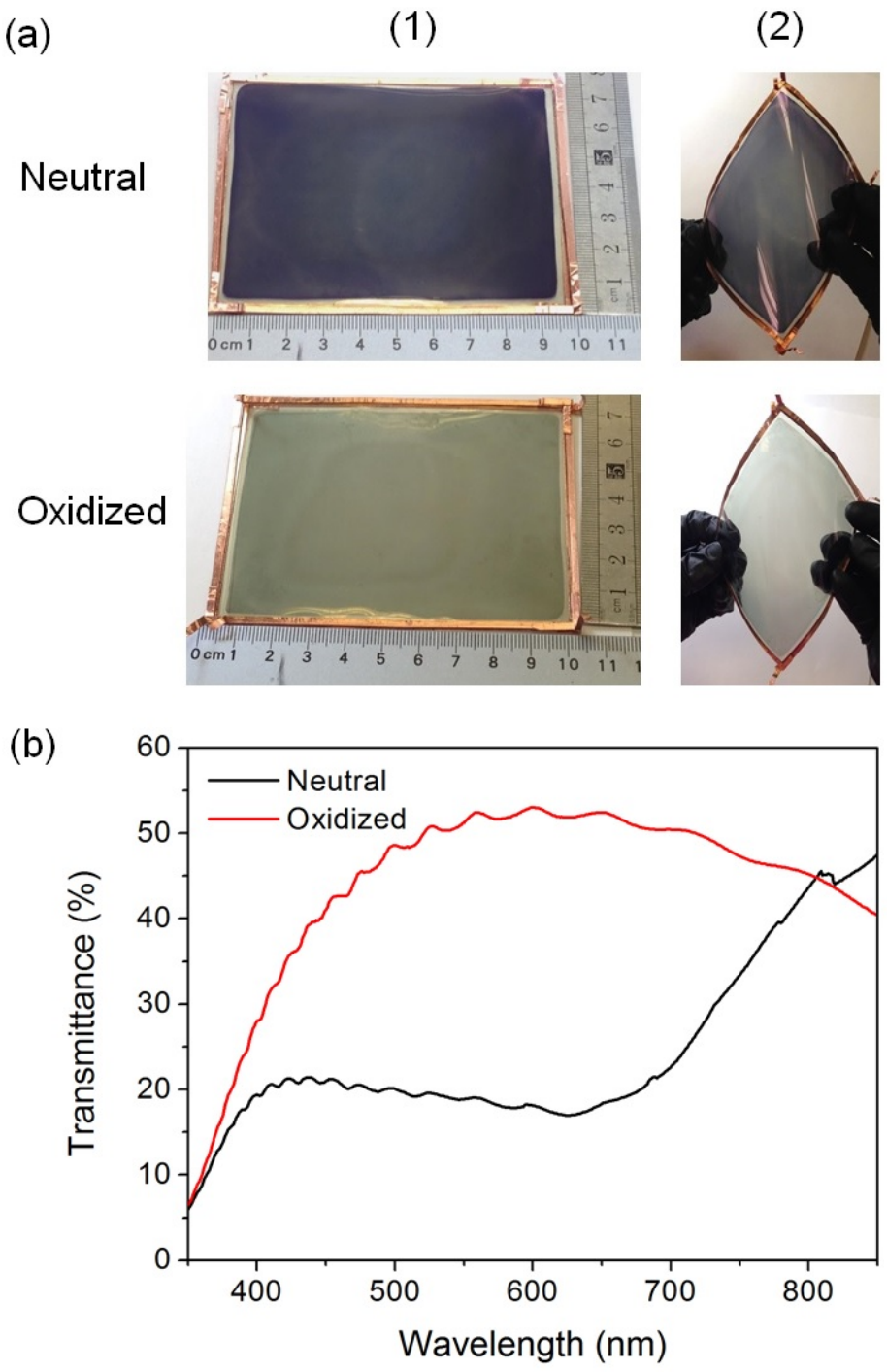

Figure 7.7 (a) Neutral and oxidized state images of a 75 cm^2 flexible dual copolymer layer device in its (1) non-bent and (2) bent states. (b) Percent Transmittance of the 75 cm^2 flexible dual copolymer layer device in its neutral and oxidized states. © 2014 M. T. Otley, et al. Advanced Materials © 2014 John Wiley and Sons.

Otley (2015)

7.4 Conclusion

In summary, the demonstration of color tuning based on determining feed ratios using two distinct complimentary copolymer systems consisting of only 3 monomers in a single electrochromic layer solid state device achieved excellent neutrality (2%). To date most neutral colored electrochromic devices in the literature report single-wavelength contrasts, and this is the highest reported photopic contrast of a neutral colored electrochromic device *ca*. 38%. Also of note, is the use of theoretical calculations to predict absorptions for electrochromic devices that can save time eliminating the fabrication of unwarranted devices. These devices also exhibited color uniformity, haze < 2%, and switch speeds of less than 1 second. In addition, this method was used to fabricate a large area flexible electrochromic device of 75 cm^2 exceeding the size of small displays demonstrating the ability for use in future electrochromic displays and even fabric.

7.5 Experimental Section

7.5.1 Materials

Lithium trifluoromethanesulfonate (LiTRIF), propylene carbonate (PC), poly (ethylene glycol) methyl ether acrylate (Mn = 480 g/mol) (PEG-MA), poly (ethylene glycol) dimethacrylate (Mn = 550 g/mol) (PEG-DMA) and dimethoxyphenylacetophenone (DMPAP) were purchased from Sigma-Aldrich and used as received. Indium Tin Oxide (ITO) coated glasses (sheet resistance 8-15 Ohms/sq, Part Number: CH-50IN) were purchased from Delta Technologies and cleaned by acetone, isopropanol and methanol prior to use. ITO coated polyethylene terephthalate (PET)

substrates (sheet resistance 60 Ohms/sq, Part Number: OC50/CP54/500) were purchased from CP Films Inc. and were cleaned by acetone prior to use. UV-sealant glue (UVS 91) was purchased from Norland Optics Inc. and conductive copper adhesive tape was purchased from Newark and used as received. Transparent silicone rubber gasket (0.508 mm thickness) was purchased from 3M Inc.

7.5.2 Monomer Synthesis

2,2-dimethyl-3,4-propylenedioxythiophene (ProDOT-Me_2, 1,3-di-*tert*-butyl-3,4-propylenedioxythiophene (ProDOT-tBu_2), and thieno[3,4-*b*]thiophene was synthesized according to the reported procedures.[9,18]

7.5.3 Gel Polymer Electrolyte

Standard Gel polymer electrolyte was prepared by adding 1g of LiTRIF, 3g of PC, 7g of PEG-MA and 17.5mg of DMPAP together and sonicated until fully dissolved. Gel polymer electrolyte used for flexible electrochromic device fabrication was composed of 1g of LiTRIF, 4g of PC, 0.12g of PEG-DMA, 5.88g of PEG-MA and 17.5mg of DMPAP and sonicated until fully dissolved.

7.5.4 Electrochromic Device Assembly

A liquid Monomer electrolyte was first prepared by loading an overall 2.5 wt% ratio of monomers into the abovementioned gel polymer electrolyte. Fabrication of ECD involves the following two steps:

*Step 1***.** Liquid State Copolymerization of ProDOT-Me_2 and T34bT:

ProDOT-Me_2/T34bT dissolved liquid monomer electrolyte was drop casted onto a piece of ITO coated glass (2 ×4 cm^2) of which the perimeter was covered with a silicon rubber

gasket (0.508 mm thickness) to give an active device area of ~5 cm^2 and to serve as the spacer. Another piece of ITO coated PET (2 × 4 cm^2) was then placed atop. A constant potential of +3 V was applied to the device for an appropriate conversion time (30 seconds to 60 seconds), converting the monomers in the liquid state to form the copolymer film onto ITO coated glass. The ITO coated PET was then removed and resulting copolymer film was rinsed with PC to wash off the leftover monomers and air-dried.

*Step 2***.** Solid State copolymerization of ProDOT-Me_2 and ProDOT-tB_2:

Liquid monomer electrolyte containing ProDOT-Me_2 and ProDOT-tB_2 was drop casted onto the active area of the DMP/TT copolymer deposited ITO coated glass obtained in Step 1. Another piece of ITO coated glass was covered atop. The device was then placed inside a UV crosslinker and exposed to UV light (365 nm, 5.8 mW/cm^2) for 20 mins and sealed with UV curable glue. Cured devices were subjected to the same polymerization process as stated above, converting the monomers in the solid state to form the copolymer film onto the previously formed copolymer layer.

Relatively Larger flexible devices (7.5 ×10 cm^2) were fabricated following the same procedure mentioned above except that the both substrates used were ITO coated PET. All assembled ECDs were cycled between their neutral and oxidized states between +2 V ~-2 V (pulse width = 3 s) five times before data was recorded.

7.5.5 Equipment

A UVP CL-1000 Crosslinker (365 nm) was used for UV curing. All electrochemistry was carried out using a CHI 720c potentiostat. Optical studies were

performed on a PerkinElmer Lambda 1050 UV/VIS/NIR spectrometer. Colorimetric data of assembled devices were calculated using corresponding color software based on a D65 standard illuminant and confirmed by a PR-670 SpectroScan spectroradiometer (Photo Research, Inc.). Haze measurements were performed on a BYK Gardner Haze Guard Plus.

7.6 References

1. R. J. Mortimer, *Am. Sci.* **2013**, *101*, 38.
2. A. P. Weidner, U.S. Patent No. 7,450,294, **2008**.
3. a) C. G. Granqvist, *Sol. Energ. Mater. Sol. C.* **2000***, 60*, 201; b) S. K. Deb, *Sol. Energ. Mat. Sol. C.* **2008**, *92*, 245; c) E. Avendaño, L. Berggren, G. A. Niklasson, C. G. Granqvist, A. Azens, *Thin Solid Films* **2006**, *496*, 30.
4. P. M. S. Monk, *The Viologens: Physicochemical Properties, Synthesis and Applications of the Salts of 4,4'-Bipyridine*, J. Wiley & Sons, Chichester, **1998**; b) R. Cinnsealach, G. Boschloo, S. N. Rao, D. Fitzmaurice, *Sol. Energ. Mat. Sol. C.* **1998**, *55*, 215; c) X. W. Sun, J. X. Wang, *Nano Lett.* **2008**, *8*, 1884; d) D. G. Kurth, J. P. López, W. Dong, *Chem. Commun.* **2005**, *16*, 2119; e) C. G. Granqvist, *Handbook of Inorganic Electrochromic Materials*, Elsevier, **1995**, 663; f) Y. Ohsedo, I. Imae, Y. Shirota, *J. Poly. Sci. Part B: Polym. Phys.* **2003**, *41*, 2471; g) I. Imae, K. Nawa, Y. Ohsedo, N. Noma, Y. Shirota, *Macromolecules* **1997**, *30*, 380.
5. P. M. Beaujuge, J. R. Reynolds, *Chem. Rev.* **2010**, *110*, 268.
6. a) F. Alhashmi Alamer, M. T. Otley, Y. Ding, G. A. Sotzing, *Adv. Mater.* **2013**, *25*, 6256; b) R. H. Bulloch, J. A. Kerszulis, A. L. Dyer, J. R. Reynolds, *ACS Appl. Mater. Interfaces* **2014**, *6*, 6623; c) G. Sonmez, C. K. F. Shen, Y. Rubin, F. Wudl, *Angew. Chem. Int. Ed.* **2004**, *116*, 1524; d) J. Jensen, M. V. Madsen, F. C. Krebs. *J. Mater. Chem. C* **2013**, *1*, 4826; e) S. A. Sapp, G. A. Sotzing, J. R. Reynolds, *Chem. Mat.* **1998**, *10*, 2101; f) M. E. Mulholland, D.

Navarathne, M. L. Petrus, T. J. Dingemans, W. G. Skene, *J. Mater. Chem. C* **2014,** DOI:10.1039/C4TC01003E; g) C. M. Amb, A. L. Dyer, J. R. Reynolds, *Chem. Mater.* **2010**, *23*, 397; f) G. E. Gunbas, A. Durmus, L. Toppare, *Adv. Mater.* **2008**, *20*, 691.

7. Q. B. Pei, G. Zuccarello, M. Ahlskog, O. Inganas, *Polymer* **1994**, *35*, 1347.
8. D. M. Welsh, A. Kumar, E. W. Meijer, J. R. Reynolds, *Adv. Mater.* **1999**, *11*, 16.
9. T. Dey, M. A. Invernale, Y. Ding, Z. Buyukmumcu, G. A. Sotzing, *Macromolecules* **2011**, *44*, 2415.
10. V. Seshadri, L. Wu, G. A. Sotzing, *Langmuir* **2003**, *19*, 9479.
11. a) P. M. Beaujuge, S. Ellinger, J. R. Reynolds, *Nat. Mater.* **2008**, *7*, 795; b) P. J. Shi, C. M. Amb, E. P. Knott, E. J. Thompson, D. Y. Liu, J. G. Mei, A. L. Dyer, J. R. Reynolds, *Adv. Mater.* **2010**, *22*, 4949; c) S. V. Vasilyeva, P. M. Beaujuge, S. Wang, J. E. Babiarz, V. W. Ballarotto, J. R. Reynolds, *ACS Appl. Mater. Interfaces*, **2011**, *3*, 1022; d) G. Oktem, A. Balan, D. Baran, L. Toppare, *Chem. Commun.* **2011**, *47*, 3933.
12. K. R. Lee, G. A. Sotzing, *Chem. Commun.* **2013**, *49*, 5192.
13. Y. Zhu, M. T. Otley, A. Kumar, M. Li, X. Zhang, C. Asemota, G. A. Sotzing. *Chem. Commun.* **2014**, *50*, 8167.
14. a) P. Chandrasekhar, B. J. Zay, C. Cai, Y. Chai, D. Lawrence, *J. Appl. Polym. Sci.* **2014**, *131*, 41043. b) M. Icli, M. Pamuk, F. Algi, A. M. Onal, A. Cihaner, *Org. Electron.* **2010**, *11*, 1255.

15. a) Y. Ding, M. A. Invernale, D. M. D. Mamangun, A. Kumar and G. A. Sotzing, *J. Mater. Chem.* **2011**, *21*, 11873; b) M. A. Invernale, Y. Ding, D. M. D. Mamangun, M. S. Yavuz, G. A. Sotzing, *Adv. Mater.* **2010**, *22*, 1379.

16. M. T. Otley, F. Alhashmi Alamer, Y. Zhu, A. Singhaviranon, X. Zhang, M. Li, A. Kumar, G. A. Sotzing, *ACS Appl. Mater. Interfaces* **2014**, *6*, 1734.

17. a) A. Kumar, M. T. Otley, F. A. Alamar, Y. Zhu, B. G. Arden, G. A. Sotzing, *J. Mater. Chem. C* **2014**, *2*, 2510; b) Y. Zhu, M. T. Otley, F. Alhashmi Alamer, A. Kumar, X. Zhang, D. M. D. Mamangun, M. Li, B. G. Arden, G. A. Sotzing, *Org. Electron.* **2014**, *15*, 1378.

18. N. Agarwal, S. P. Mishra, C. H. Hung, A. Kumar, M. Ravikanth, *Bull. Chem. Soc. Jpn.* **2004**, **77**, 6, 1173.

Otley (2015)

8. Chapter 8: Highly Conductive Polymers for Flexible and Stretchable Electronics

8.1 Introduction

This chapter encompasses four different projects which started when we were performing thermoelectric studies on nonwoven polyethylene terephthalate (PET) that was soaked with PEDOT:PSS and then annealed to form a conductive polymer film. We noticed that the samples with a higher weight percent of PEDOT:PSS were able to pass much more current than we expected. After a literature search, we did not find any studies pertaining to both the high conductivity of conducting polymers and also the high breakdown current seen in our system. This led to complete characterization of the nonwoven PET fabric, and revealed that the fabric was infused with silica nanoparticles. Then reverse engineering of the system using electrospun PET and hydrophilic silica nanoparticles showed similar trends to the nonwoven PET fabric. We expanded the study to spandex and saw the same trend of high conductivity, and the result is the first report of an organic stretchable 'metal'. We have also used a variety of techniques to print lines/antenna including inkjet printing, screen printing, stamping, sponge roller, and brush pen stenciling. The most recent study uses PEDOT:PSS with hydrophilic silica nanoparticles as a thin film for the potential use as an optically transparent electrode to replace ITO.

8.2 Overview of PET Fabric and Electrospun PET with PEDOT:PSS

Organic conductors on flexible substrates will play a critical role in the future of displays as well as the general field of electronics. Herein, we report poly(3,4-

ethylenedioxythiophene)-polystyrene sulfonate (PEDOT:PSS) with metallic behavior on polyethylene terephthalate fibers having conductivities as high as 27,600 S/cm, and current carrying capacities of up to 3.3 amperes/mm^2. These values exceed that of bulk titanium metal, 24,000 S/cm and 0.13 amperes/mm^2, respectively. Copper has a current carrying capacity (CCC) of 30 amps/mm^2 with ca. 9 times the density of PEDOT-PSS. To demonstrate wire replacement capability, PET synthetic leather coated with 5.7% by weight PEDOT-PSS carried power sufficient for lighting an 18W compact fluorescent light bulb at 0.92A, 19.7 V DC and a 50W incandescent bulb at 0.42 A, 120V AC. Here, high electrical conductivities of PEDOT:PSS are proposed to be attributed to interactions of exposed fumed silica nanoparticles on the fiber surface with the PEDOT:PSS causing a PSS phase segregation from PEDOT as evidenced by a *ca.* 40% increase in the PEDOT to PSS ratio at the surface of the PEDOT:PSS film as measured by x-ray photoelectron spectroscopy. The PEDOT:PSS coated fibers are air stable retaining electrical conductivity up to temperatures of *ca.* 150^{o}C for 10 minutes.

8.2.2 Introduction to PET Fabric with PEDOT:PSS

Flexible/conformal and wearable electronics and displays are the current trend in the consumer market today exhibited with the recent smart phones and patents by LG, Apple, and Samsung.[1-3] The ability to bend and shape electronics without diminishing the electronic characteristics of a device is imperative for long-term stability. Current technologies employ metals as conductive layers which have several shortcomings including rising cost, high density and rigidness limiting the amount of flex that a device can achieve before degradation of the conductive substrate.[4] In the 1970's Shirakawa,

MacDiarmid, Heeger, *et al.* were the first to report an organic polymer, polyacetylene, that exhibited conductivities comparable to metals.[5-7] These novel findings were the genesis of the field of synthetic metals, however polyacetylene was not air stable limiting commercialization. Since then conducting polymers have been extensively studied leading to organic polymers that are air stable and now commercially available such as aqueous dispersions of PEDOT:PSS.[8-18] Other conducting polymers that have shown high conductivities include polyaniline and regioregular poly(3-alkylthiophenes).[19-21] Further, conjugated polymers have been commercialized as chemical sensors.[22-23] In addition to conducting polymers, other flexible electronics recently published in the literature include flexible and stretchable silicon that can be used on a variety of substrates including rubber.[24-25] Stretchable electronics consisting of PEDOT:PSS have been previously reported on spandex where it produced an all-organic electrochromic fabric.[26-27] An advantage of organic polymers is the ability for use in fabrics that are either worn or touch the skin but metal particles on fabrics can result in an allergic toxicity.[28] Critical in the apparel industry is the 'feel' of the fabric. Therefore, limiting the amount of conductor in the fabric is imperative in order to maintain mechanical properties. The potential applications for high surface area, highly conductive all-organic fabrics include but are not limited to sensors, thermoelectrics, thermocouples, antennae, wearable electronics and displays such as organic light emitting diodes (OLEDs), radio frequency identification tags (RFIDs), electromagnetic shielding, high surface area electrodes for capacitors and/or batteries, and the applications described herein as carrying power for the replacement of wire in circuits as well as resistive heating.

Otley (2015)

Unfinished polyethyleneterephthalate (PET) synthetic leather, referred to here as a nonwoven, was procured as a 1.26 m wide roll and examined using transmission electron microscopy, as well as scanning electron microscopy with energy dispersive spectroscopy (EDS). Nonwovens with, and without fuming silica were studied for comparative purposes. Figure 1b and 1d are the photograph of a 2.5 cm x 2.5 cm x 0.075 cm, and the cross-sectional transmission electron microscopy (TEM) of a nonwoven, respectively. The synthetic leather has a bulk density of **0.49** g/cm^3 with an average individual fiber diameter of *ca.* 3,000 nm. As seen from the TEM, silica nanoparticles ranging from 50 to 150 nm in diameter are present both within the fiber, as well as on the fiber surface. According to ten images obtained by scanning electron microscopy (SEM), and in accordance to thermogravimetric analysis, the total silica content within the nonwoven was determined to be 2.4 wt% translating to 0.34 vol% for total volume of PET. From calculations using the SEM images, there are *ca.* 4 x 10^8 silica nanoparticles/cm^2 located on the fiber surface with an average particle spacing of 500 nm. Silica is commonly used in the industry as a delustering agent.[29] PEDOT-PSS coated synthetic leather samples were prepared by cutting uniform 2.5 cm x 2.5 cm unfinished silica/PET nonwovens. For the preparation of the PEDOT-PSS coatings, 5 wt% of dimethyl sulfoxide (DMSO) of total weight of solution was added to Clevios-PH1000. The nonwovens were placed on a glass drying dish and treated with Clevios-PH1000 containing DMSO by drop-casting to a desired weight of solution onto the nonwoven and this solution was allowed to absorb into the nonwoven for 30 minutes. The samples were then oven dried at 110 °C, ambient pressure for 30 minutes, flipped, and then dried for an

additional 30 minutes under the same conditions. Other temperatures and times were carried out, but the above conditions provided optimum electrical properties. The addition of PEDOT:PSS causes the nonwoven to change from grey to blue, with the blue color intensifying with higher weight percentages of PEDOT-PSS.

All fabric samples were weighed before and after treatment to calculate the weight percent of doped PEDOT:PSS on the nonwovens. As the amount of residual doped PEDOT:PSS increases, the sheet resistance decreases exponentially as shown in Figure 1A until 0.3 wt%, at which a plateau is reached. A percolation threshold at 0.3% is unusually low in comparison to other studies for PEDOT-PSS coated textile.[30] The best sheet resistance obtained was 3.2 ohms/□ for a nonwoven containing 5.7 wt% PEDOT:PSS. For lower wt% PEDOT:PSS coated nonwovens, dilutions of the DMSO containing Clevios-PH1000 solution were necessary in order to achieve homogeneity of the PEDOT:PSS throughout the nonwoven in a single step solution saturation of the nonwoven.[31]

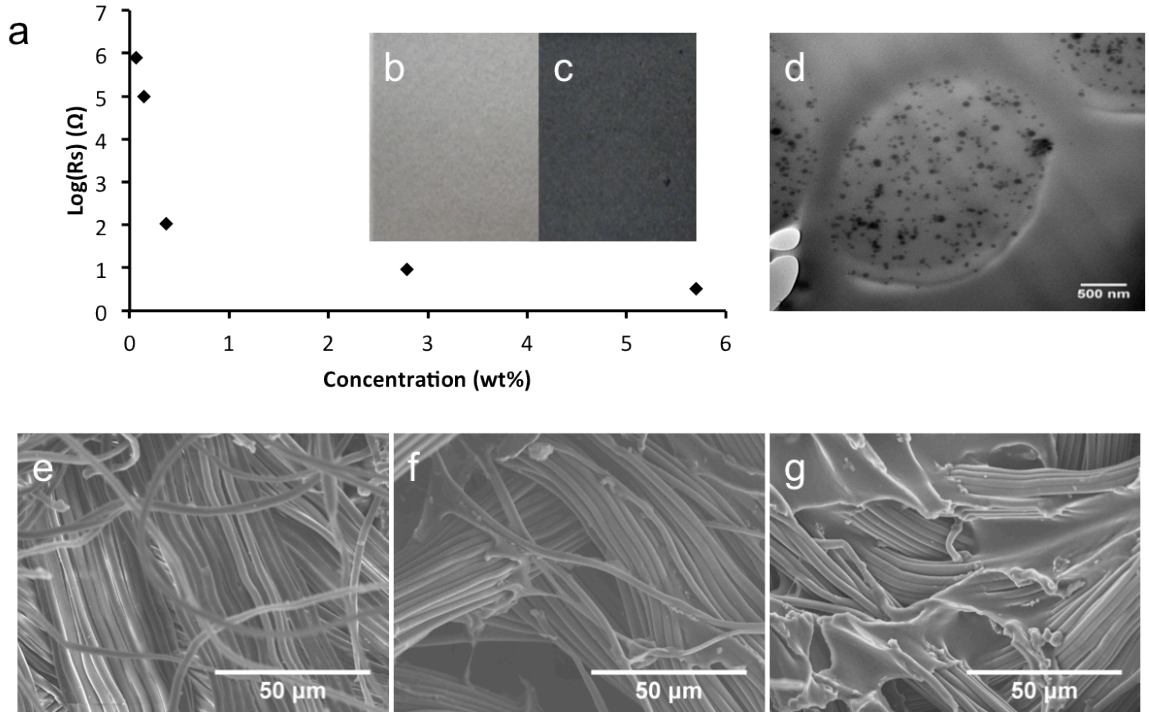

Figure 8.1 a, Log (Rs) of the PEDOT-PSS coated PET synthetic leather vs. wt% of the PEDOT-PSS coated on the PET synthetic leather. **b,** Unfinished PET sythetic leather, as received **c,** PET synthetic leather with 5.7 wt% PEDOT-PSS **d,** TEM image of untreated, as received PET synthetic leather with SiO_2 nanoparticles **e,** SEM surface image of untreated, as-received synthetic leather **f,** SEM surface image of sythetic leather having 1 wt% PEDOT-PSS coating **g,** SEM surface image of sythetic leather having 4 wt% PEDOT-PSS coating.

Nonwovens with 5.7 wt% PEDOT:PSS were capable of passing 3.2 A at 5.2 V of DC current through alligator clip point contacts for a 2.5 cm x 2.5 cm x 0.1 cm sample without breakdown. To demonstrate application, a power source was connected in series to light a 50W incandescent light bulb as seen in Figure 8.2a with 0.4 A of alternating current at 120 V. To further demonstrate applicability, the PEDOT-PSS coated synthetic leather was placed in series with an 18 W light bulb (Figure 2b) and a power source, and a current of 0.90 A at 24 V of direct current was passed through the fabric. Since the sheet resistance of the PEDOT:PSS can be tuned to be 3 ohms/□ or greater and the

PEDOT-PSS coatings on nonwovens are relatively homogenous, the amount of heat generated per the amount of power supplied can be optimized for resistive heating applications.[32-35] Figure 8.2c depicts a 2.5 cm x 5 cm a 2.5 wt% PEDOT-PSS coated nonwoven used for resistive heating by application of power between to copper wires threaded through the ends of the fabric and temperature recorded from a type J placed bottom-center of the sample. A plot of the ΔT as a function of power as shown in Figure 8.2d generates a linear correlation with a slope of 15.8°C/W. For a maximum of 8.6 W (8 V DC at 1.076 A), a maximum temperature of 151°C, ΔT=130°C, is achieved. PEDOT:PSS electrical conductivity stability was proven by holding 8.6 W for a period of ten minutes which did not result in any fluctuation in the resistive heating temperature indicating that the PEDOT:PSS electrical conductivity remained unperturbed. The resistance of the 2.5 wt% PEDOT-PSS coated nonwoven increased during the experiment, as measured through the two copper leads, from 6.0 ohms/□ at room temperature to 7.5 ohms/□ at 150 °C.

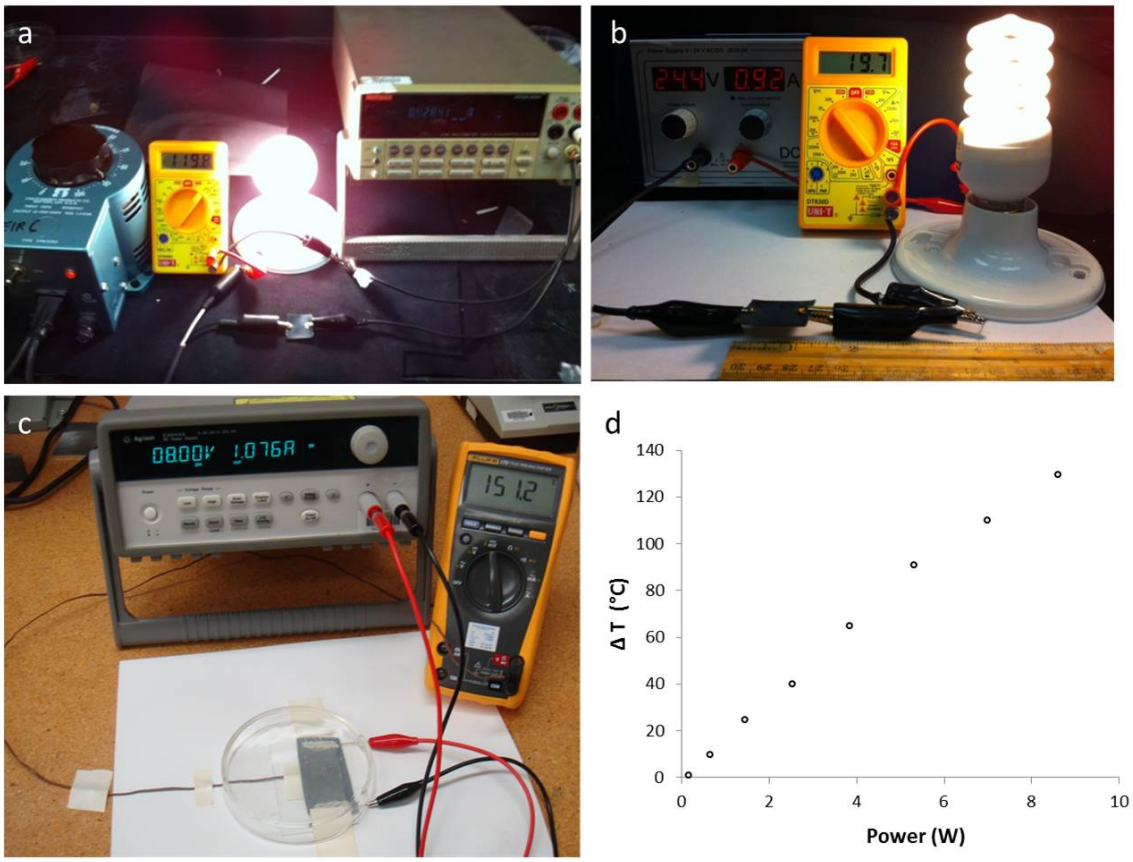

Figure 8.2 Applications of PEDOT-PSS fabric a, 5.7 wt% PEDOT-PSS coated nonwoven in series carrying power to light a 50W incandescent bulb at 0.42 A, 120V AC. **b**, carrying power to light an 18W compact fluorescent light bulb at 0.92A, 19.7V DC. **c**, A 2.5 wt% PEDOT-PSS coated nonwoven was attached to a power supply and 8 V at 1.076 A was applied, heating the sample to 151.2 °C. **d**, DT versus power plot for a 2.5 wt% PEDOT-PSS coated nonwoven with room temperature being 20°C.

The electrical conductivities of 5.7 wt% PEDOT:PSS coated nonwovens were determined to be *ca.* 24,000 S/cm in accordance to both four point probe Hall Effect measurements as well as four probe collinear array measurements. This value competes with the highest previously reported electrical conductivity of 22,000 S/cm at 300K and 10 Kbar for the Naarman iodine doped polyacetylene that was obtained upon a fourfold stretch.[36] For context, regioregular poly(3-alkylthiophenes) have been reported to reach conductivities of *ca.* 1000 S/cm upon iodine doping, and polyaniline has been reported

with conductivities of *ca.* 300 S/cm.[19-21] The current highest PEDOT:PSS electrical conductivity reported is 4380 S/cm for PEDOT:PSS that was post treated with sulfuric acid leading to removal of the PSS template to form nanofibrils of PEDOT that could later be spin coated.[37]

The charge-carrier mobility as measured by Hall Effect for 5.7 wt% PEDOT:PSS coated nonwoven was determined to be 8.26 cm^2 V^{-1} s^{-1} with a charge carrier concentration of 1.48 x 10^{22} /cm^3. A key to calculating these values is obtaining a reasonably accurate value for film thickness. In accordance to the SEM, it is clear that films of PEDOT:PSS are forming on the fiber surface; however, film thicknesses by SEM are in error due to both angle of view, and a glow that is produced as a result of discharge during the experiment. Alternative to SEM, mercury porosimetry was used to calculate surface area, by knowing the weight of PEDOT:PSS on the nonwoven and the density of the PEDOT-PSS, the film thickness was more accurately determined to be 129 nm (±30). To test the difference in interactions of Hg with the fiber surface and that of water with the fiber, the saturated Hg volume was compared to the saturated water volume and both values came within 20% of each other. In comparing mobilities to other reported conjugated and conductive polymers, thieno[3,2-*b*]thiophene polymers demonstrated a charge-carrier mobility of 0.2-0.6 cm^2 V^{-1} s^{-1}.[38] The PEDOT-PSS films reported by Lee et al. were reported to have charge carrier mobilities of 4 cm^2 V^{-1} s^{-1} and a charge carrier concentration of 6 x 10^{21} cm^{-3}.[37] Films of PEDOT-PSS on the nonwoven had approximately twice the charge carrier mobilities and twice the charge carrier concentration.

The maximum current, I_{max}, was measured using the four line probe method for increasing concentrations of PEDOT:PSS (Figure 3a), and the reported maximum current is the highest current achieved for each PEDOT-PSS coated nonwoven sample was able to pass before breakdown as evidenced by charring of the sample. As the concentration of PEDOT:PSS in the material increases, the maximum current to breakdown increases in a linearly as shown in Figure 3a. At a concentration of 0.3 wt% the maximum current was 1 μA, but increased to a value of 3.22 A at a concentration of 5.7 wt%. The maximum current to breakdown per wt% of conductor for the PEDOT-PSS coated nonwoven was compared to that for four different commercially available metal particle infused fabrics. As shown in Figure 3b, the PEDOT-PSS coated nonwoven exhibits greater than twice the breakdown current per wt% of conductor to the best of the four metal infused fabrics, silver coated nylon. Apart from the manufacturer specifications, the amount of metal in each sample was calculated using thermogravimetric analysis.

Resistance for the 2.2 wt% and 5.7 wt% PEDOT-PSS coated nonwovens of dimension 5 x 10 mm^2 were probed as a function of increasing temperature, using a Physical Property Measurement System,[39] in order to evaluate whether the PEDOT-PSS demonstrates semi-conductor-like or metal-like behavior. As shown in Figure 3C for 2.2 wt% PEDOT:PSS on nonwoven, the resistance generally decreases as the temperature increases with the most substantial changes in resistance occurring below 100 K. At a temperature of 263 K, the resistance holds constant until 360 K, where, as shown in the inset of Figure 3C, the resistance of the sample increases indicating metal-like behavior.[40]

The same characteristic behavior is observed for the nonwoven with 5.7 wt% PEDOT:PSS. The temperature dependent conductivity of a semiconductor such as PEDOT-PSS and other doped organic materials is generally described by the variable range hopping (VRH) mechanism:

(1) $$\sigma = \sigma_0 exp\left[-\left(\frac{T_0}{T}\right)^{\alpha}\right]$$

where σ_0 is the conductivity at infinite temperature, T_0 is the characteristic temperature, and α is equal to 1/(1+D) where D is the dimension of the system.[40-44] This linear relationship is used in the VRH mechanism to determine T_0, the energy barrier between localized states due to disorder. There is linear relationship of ln R plotted as a function of $T^{-1/2}$ within the temperature range of 139 to 235 K as shown in Figure 3c for 2.2 wt% PEDOT-PSS coated nonwoven. From this, the T_o was calculated to be 25.8 K. This is approximately the same value for T_o obtained for PEDOT:PSS semiconductor reported by Ouyang *et al.* in the sulfuric acid treatment of PEDOT-PSS.[45]

Otley (2015)

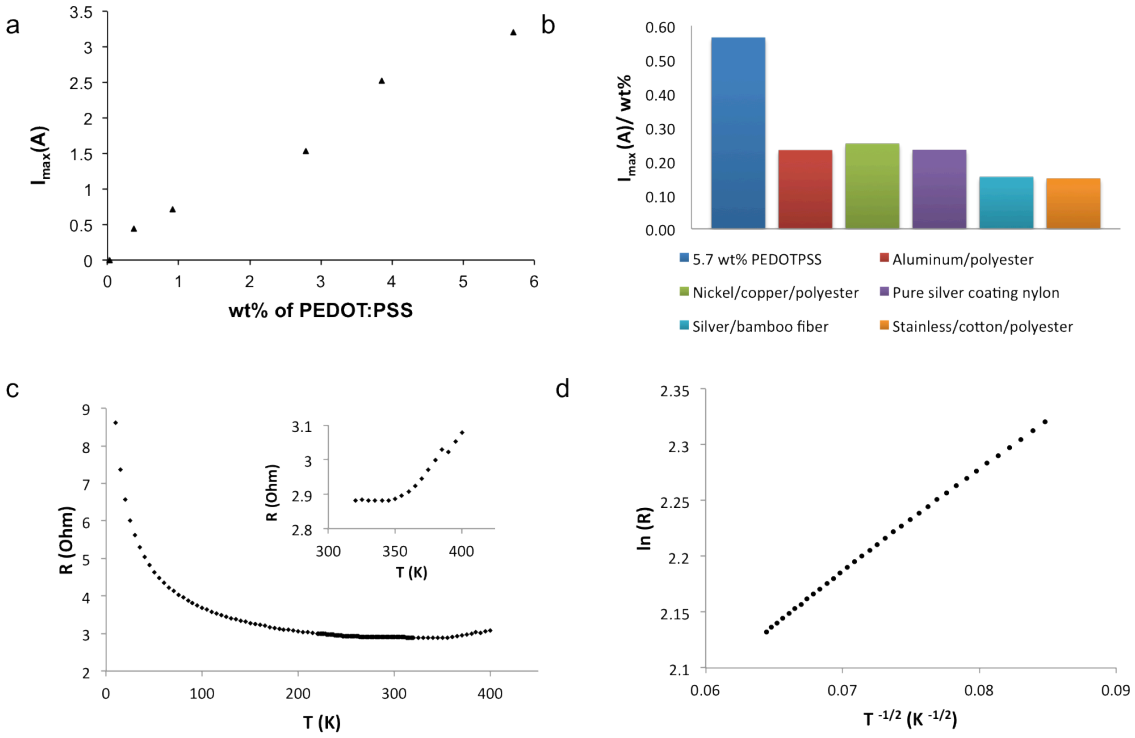

Figure 8.3 a, Maximum current to breakdown as a function of PEDOT-PSS wt% in nonwoven **b,** Maximum current to breakdown per wt% conductor for PEDOT-PSS coated nonwoven compared to commercially available metal particle infused fabrics **c,** Resistance as a function of temperature for 2.2 wt% PEDOT-PSS coated on nonwoven with inset showing an increase in resistance as a function of temperature at *ca.* 350 K. **d,** ln R as a function of T-1/2 for 2.2 wt% PEDOT-PSS coated on nonwoven.

The conductivities obtained from the PEDOT:PSS coated PET synthetic leather were further verified by the electrospinning of a PET fiber nonwoven mat with silica nanoparticles and then coated with PEDOT:PSS. Electrospinning parameters were optimized to achieve comparable fiber diameter, silica loading, and nonwoven mat thickness as that for the PET synthetic leather nonwoven containing silica nanoparticles. The PET fiber diameter was, on average, 3 μm in diameter with 3 wt% loading of hydrophilic silica evenly dispersed within the fibers. Reproducing a non-woven by electrospinning provides insight into determining whether fiber bundles in the Nike

synthetic leather created during the melt process contributes to low sheet resistance. FESEM charge contrast imaging shows PEDOT:PSS film formation (dark contrast) on the PET fiber (white contrast) with some delamination although satisfactory adhesion and dispersion throughout the fiber mat is seen in Figure 8.4 in comparison to the PEDOT:PSS coated PET synthetic leather. Thickness measurements were taken in several areas and averaged to account for any poor dispersion with an average film thickness of 154 ± 56 nm for 2.3 wt% PEDOT:PSS on PET-Silica. Sheet resistance was measured at 2.35 Ω/□, therefore, resulting in our initial electrical conductivity of 27,600 S/cm using the equation $1/ (R_s*t)$. We have not performed mercury porosimetry to get film thicknesses but suspect that the SEM has over-estimated the film thickness values as it might have for the PEDOT-PSS films on synthetic leather. The sheet resistance for the electrospun samples surpass the sheet resistance of the synthetic leather with only a third of the material indicating fiber bundles possibly contribute to diminishing the electrical conductivity. Furthermore, Hall effect measurements verified the same electrical properties with charge carrier concentration of $5*10^{20}$ cm^{-3} and charge mobility of 350 cm^2 V^{-1} s^{-1} resulting in an electrical conductivity of 27,600 S/cm using 154 nm as the average thickness.

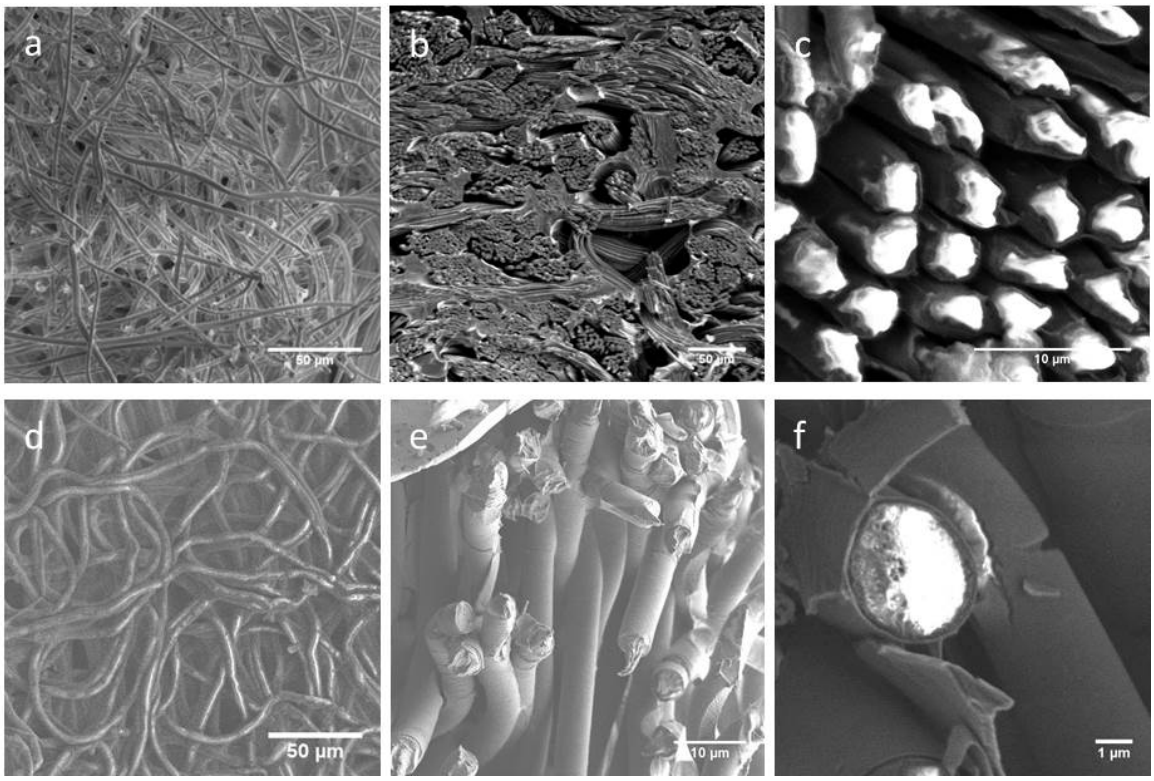

Figure 8.4 Comparison of nonwoven PET and electrospun PET a,b,c are SEM pictures of PEDOT:PSS coated PET fabric a increasing magnification, and **c,d,e** are PEDOT:PSS coated electrospun PET nanofibers at increasing magnification.

Important to this study, is the phenomenon of PEDOT and PSS phase segregation as observed on the outer surface of the PEDOT-PSS films as analyzed by x-ray photoelectron spectroscopy (XPS). As shown in Figure 5, the two bands between 162 and 166 eV are the spin-split doublet S(2p), S($2p_{1/2}$) and S($2p_{3/2}$), bands from the sulfur in PEDOT.[46,47] The energy splitting is ~1.2 eV, the respective intensities have a ratio of 1:2 and the components typically have the same full width at half maximum and shape. In the case of the sulfur S2p from PSS, the binding energy bands are found at higher energy between 166 and 172 eV. The broad peak is composed of the spin-split doublet peaks. This broadening effect is due to the sulfonate group existing in both the

neutral and anionic state. Therefore, there is a broad distribution of different energies in this high molecular weight polymer. The same applies to PEDOT although the number of charged and neutral species are not as large in number. The PEDOT:PSS ratio was calculated by measuring the integral area ratio of peaks assigned to PEDOT and PSS. The ratio of PEDOT to PSS increased from 1 to 1.95 for the control consisting of PET fibers without silica having a coating of PEDOT-PSS to a ratio of 1 to 1.2 for PET fibers containing silica nanoparticles translating to an 80% reduction of PSS at the surface. The PEDOT to PSS ratio of 1 to 1.95 of the control sample consisting of PEDOT-PSS film coated on PET fibers without silica agrees well with the manufacture specifications for the Clevios PH1000 indicating there is no phase segregation in the absence of silica.

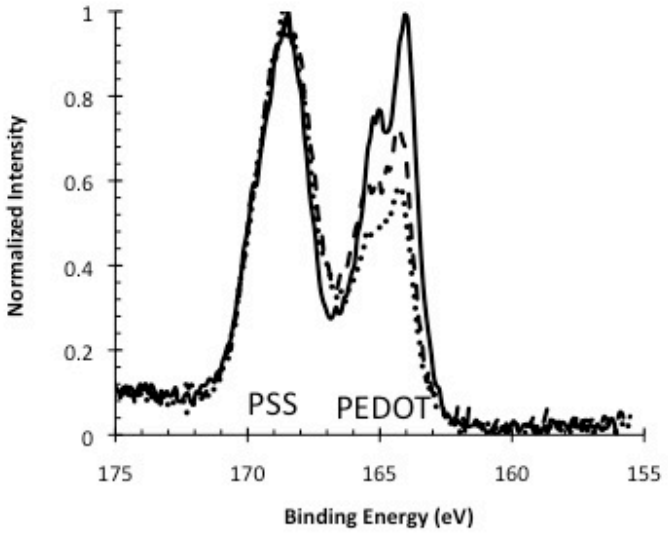

Figure 8.5 XPS for PEDOT-PSS films on (dotted line) a control sample of electrospun PET fibers of 3 μm diameter with 150 nm thick PEDOT-PSS film (dashed line) PET electrospun mat of same fiber diameter having silica nanoparticles with 150 nm thick film of PEDOT-PSS and (solid line) PEDOT-PSS film of 130 nm thickness on synthetic leather fibers having silica nanoparticles.

These results indicate PEDOT:PSS has undergone phase segregation forming a PEDOT rich surface to the PEDOT-PSS film likely due to hydrogen bonding between the sulfonate anions on PSS and the hydroxyl rich surface of silica.[50] The phase segregation was not significant enough to induce high level ordering or crystal growth as the microstructure mostly remained amorphous based on glancing angle X-ray measurements. This could likely be due to PSS as previous reports did not observe PEDOT crystalline formation until it was removed.[37,50,51] Since inter and intra-charge hopping is believed to be the dominant conduction mechanism in conducting polymers[52] hydrogen bonding interactions leading to phase segregation between PEDOT and PSS enables more interchain interaction between the conducting PEDOT domains. Hence, the energy barrier for charge hopping is lowered leading to better charge transfer among the PEDOT chains.[49]

The mechanism for the phase segregation can be described by not only ionic interactions but also covalent interactions with PSS and the silica nanoparticles. The Clevious PH-1000 formulation of PEDOT:PSS has a pH of 3.5, therefore the sulfonate will have a negative charge and the silica's hydroxyl groups will be protonated. The conditions are acidic during the annealing which occurs at 110°C driving off water, and as a result the pH will decrease as the solution on the fabric becomes more concentrated as water is evaporated. Thus, the hydroxyl groups on the silica can be protonated forming a good leaving group, and then the sulfonate can attack the silica.[54,55]

Otley (2015)

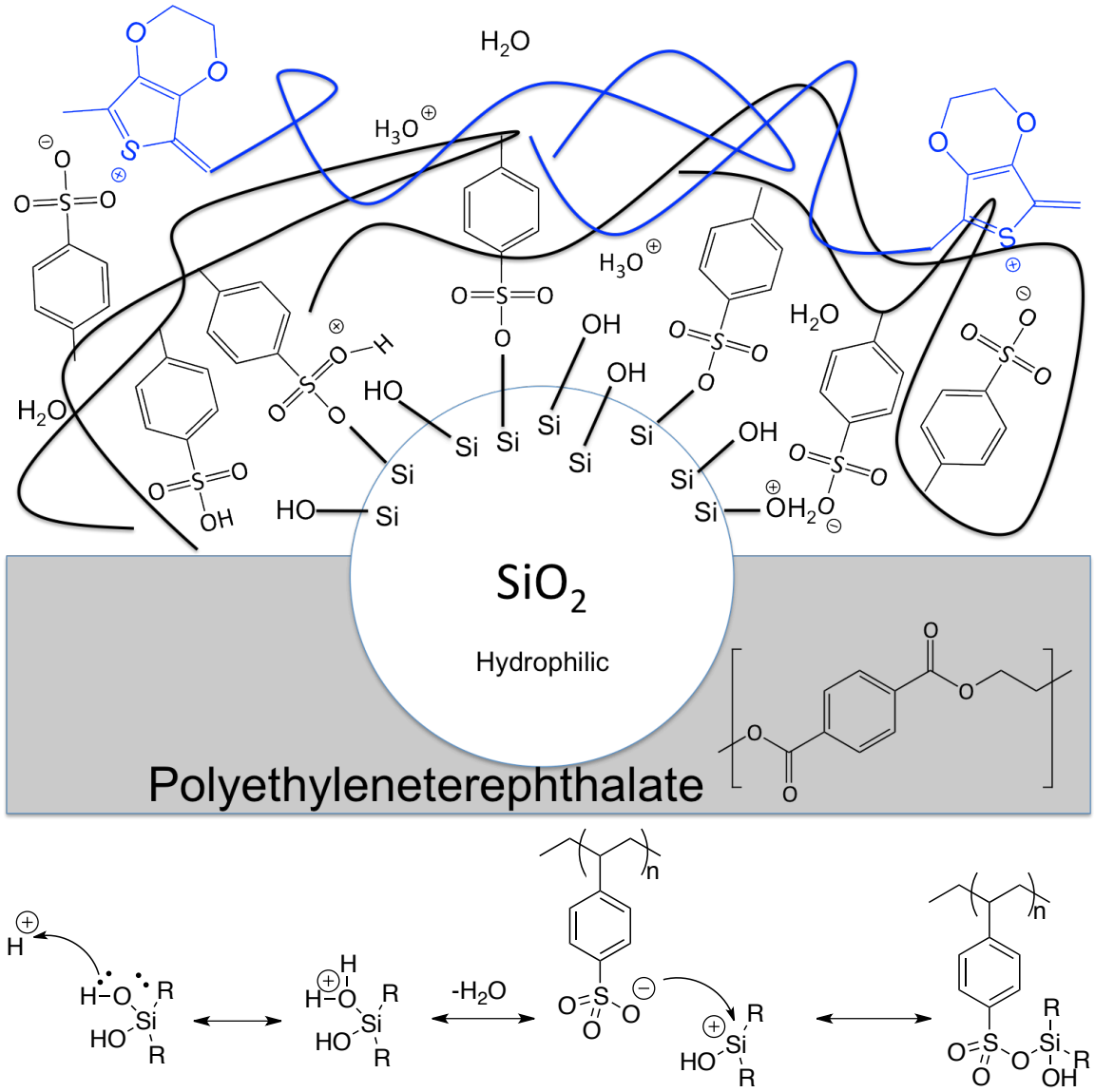

Figure 8.6. The proposed reaction of phase segregation. (top) The schematic of possible interactions at the surface of the fabric, (bottom) and the proposed mechanism of the PSS and silica nanoparticles to form a covalent bond.

8.2.3 Conclusions of PET Fabric and Electrospun PET with PEDOT:PSS

Clevious PH-1000 consisting of PEDOT-PSS nanoparticles as a dispersion in water, when coated onto nonwovens containing silica from solution processing resulted

in films that had undergone phase segregation resulting in a higher PEDOT:PSS ratio at the surface. This phase segregation is induced through strong interactions of polystyrenesulfonate with silica exposed at the surface of the PET fibers. The resulting coatings of PEDOT-PSS have electrical conductivities greater than 20,000 S/cm, while exhibiting air and temperature stability up to 150°C for ten minutes. The highest electrical conductivities obtained were 27,600 S/cm for coatings on electrospun PET nonwovens and 24,000 S/cm for coatings on melt processed PET nonwovens (aka synthetic leather) indicating that having coatings isolated on random individual fibers are advantageous over having coatings on and within fiber bundles. According to the resistance vs. temperature behavior and the ohmic behavior of the current vs. voltage, the PEDOT-PSS reported here can be considered an organic metal at room temperature. Using the PEDOT-PSS coated PET nonwoven in series with a 50W incandescent bulb, and its ability to carry the 50W of power through point contacts made to the nonwoven is a demonstration of the high electrical conductivity of the PEDOT-PSS coating. The current carrying capacity (CCC) for PEDOT-PSS was calculated from the limit of the current to breakdown measurement and the cross-sectional area of the PEDOT-PSS coating on the nonwoven to be 3 A/mm^2 which is a tenth of that for bulk copper metal, yet the PEDOT-PSS has approximately a tenth the density of copper. These PEDOT-PSS coatings could find utility in metal replacement applications as well as in the field of textile and wearable electronics.

Otley (2015)

8.3 Stretchable Organic 'Metal' PEDOT:PSS on Spandex

This study focuses on PEDOT:PSS coated spandex which we hypothesized if contained silica nanoparticles could show similar results to the nonwoven PET fabric. More importantly, the spandex is not only flexible but stretchable allowing for the possibility of creating stretchable electronics, and if conductive enough it would be the first report of an organic stretchable 'metal'. The spandex was procured from a local fabric shop and two fabrics were chosen: one was orange and consisted of 85% nylon/15% spandex while the other fabric was white that consisted of 90% polyester/10% spandex. The studies followed the same soaking and annealing procedure that was used for the nonwoven fabrics using 95% Clevios PH1000 PEDOT:PSS with 5% DMSO.

8.3.1 Characterization of PEDOT:PSS soaked Spandex

The characterization of the spandex samples began with optical microscopy to gain a better understanding of the material. As shown in Figure 8.7 the nylon/spandex has a denser weave and thus has more fibers per area then the polyester/spandex. The soaking of the two fabrics in PEDOT:PSS revealed that the amount of PEDOT:PSS the fabrics would hold after 1 soak and 2 soaks was also different. The nylon/spandex would hold an average of 4 wt% of PEDOT:PSS compared to the polyester/spandex which only held 2.3 wt% on average after one soak. After two soaks of PEDOT:PSS the nylon/spandex would hold an average of 5.5 wt% while the polyester/spandex held an average of 4 wt% of PEDOT:PSS. The lower surface area of the woven fabrics (spandex) compared to the large surface area of the nonwoven PET showed lowered weight percent's per soak that can be attributed to both the surface area and also the wetting characteristics.

Otley (2015)

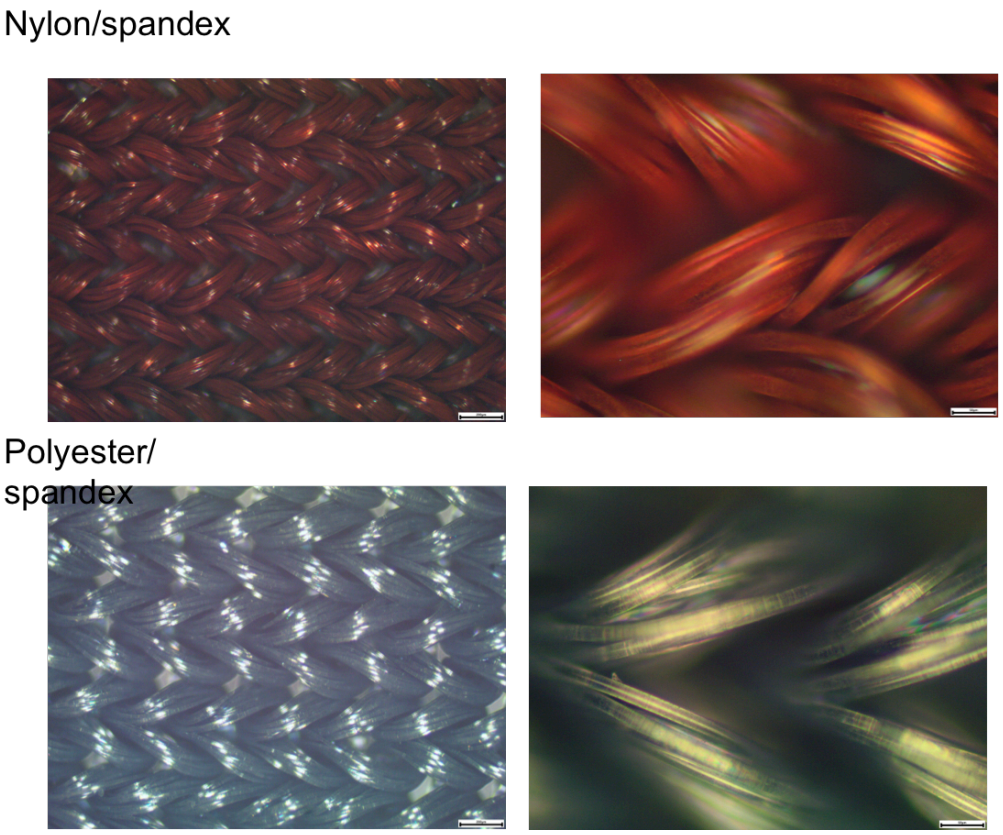

Figure 8.7 Optical microscopy of nylon/spandex (top) and polyester/spandex (bottom) both show a weaved design.

X-Ray photoelectron spectroscopy (XPS) was run on both the nylon/spandex and polyester/spandex, and as seen in Figure 8.8 both fabrics contain silica (Figure 8.8 shows the nylon/spandex spectrum). Due to the spandex having silica nanoparticles on the surface, the spandex fabrics showed similar conductivity trends as the nonwoven PET. We again contribute this to phase segregation, however, the spandex samples were not stable in the XPS long enough to run enough scans to resolve the sulfur 2p peak to ascertain the ratio between the PEDOT sulfur and the PSS sulfur.

Otley (2015)

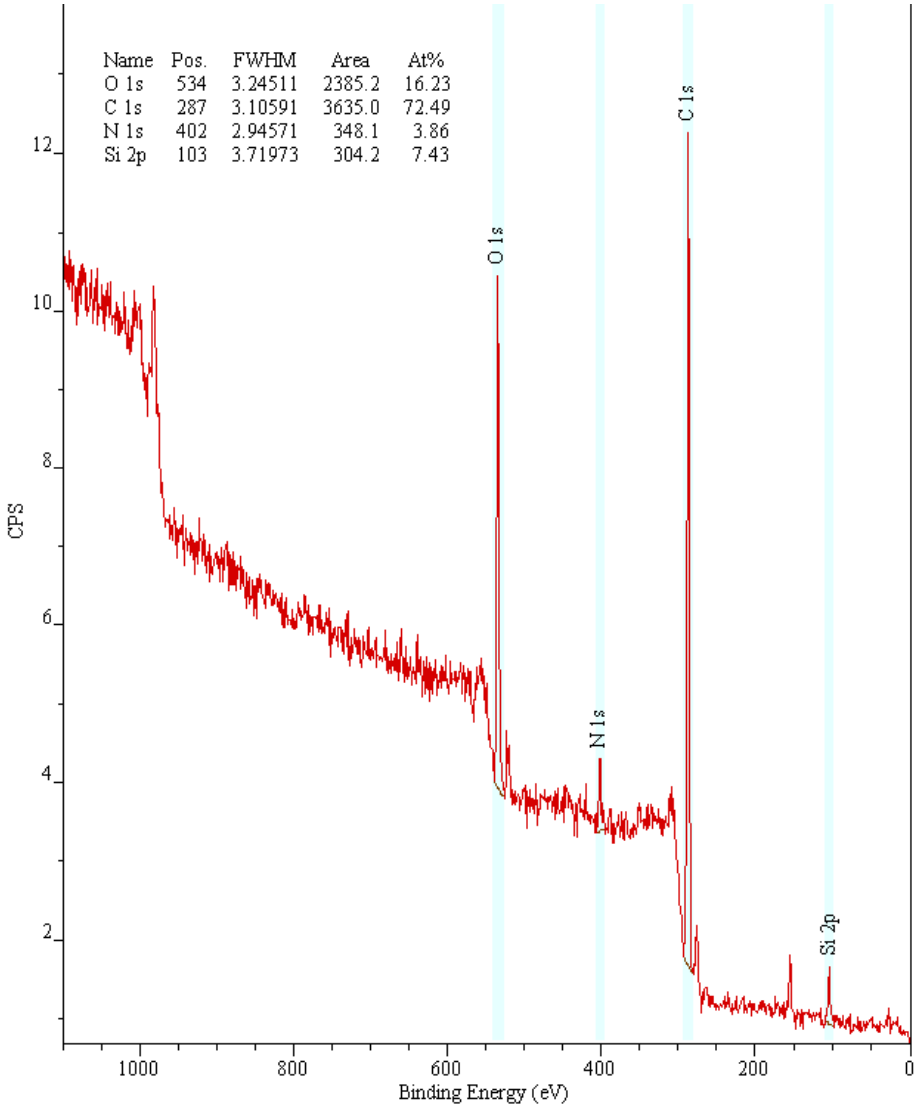

Figure 8.8 XPS survey spectrum of nylon/spandex coated with PEDOT:PSS containing silica nanoparticles on the surface.

The ability for the spandex to stretch repeatedly without a large increase in resistance and/or breakdown can be attributed to the film formation of PEDOT:PSS on the individual fibers. As seen in Figure 8.9 are ripples or 'waves' along the PEDOT:PSS film. These ripples allow for the PEDOT:PSS film to stretch and unstretch without

breaking or cracking. These SEM pictures are the basis for what we call an organic stretchable ‘metal’ along with the resistance versus temperature study shown in Figure 8.10.

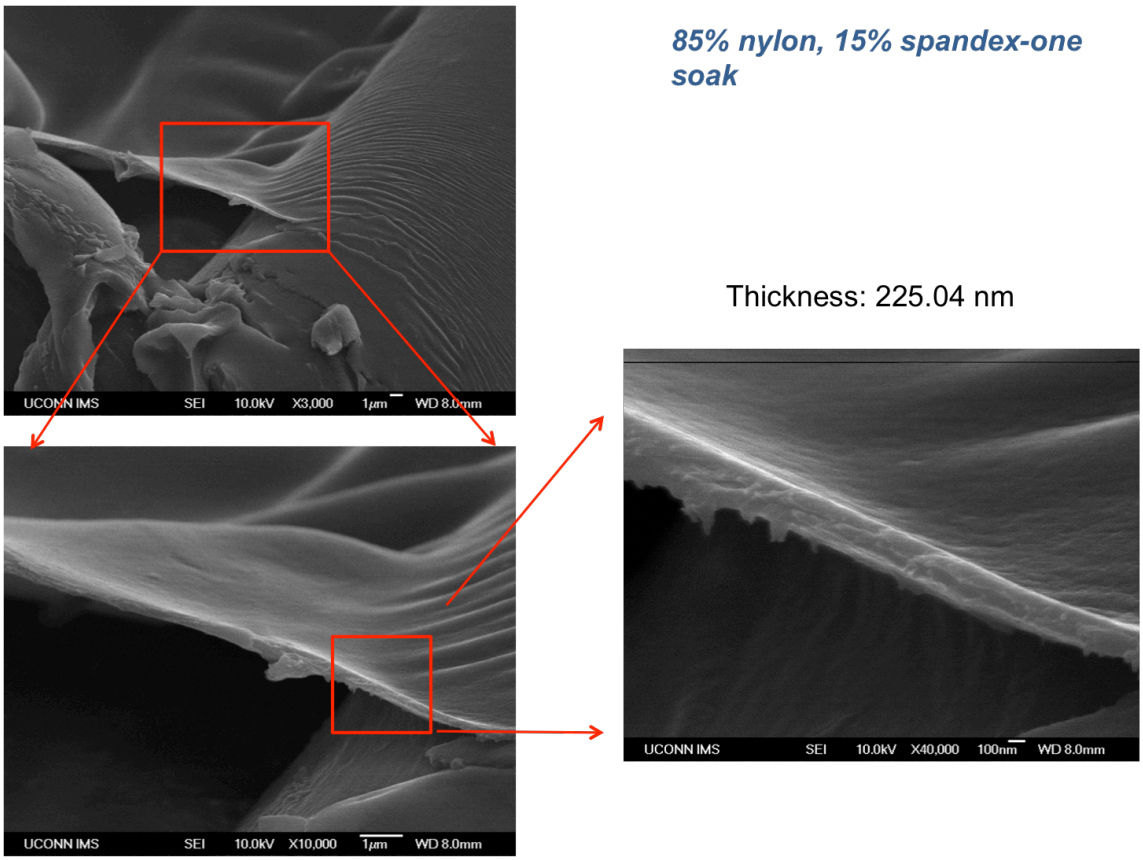

Figure 8.9 SEM images of PEDOT:PSS coated nylon/spandex. The images show ripples of the PEDOT:PSS film along the fiber thus allowing it to stretch without breaking.

Otley (2015)

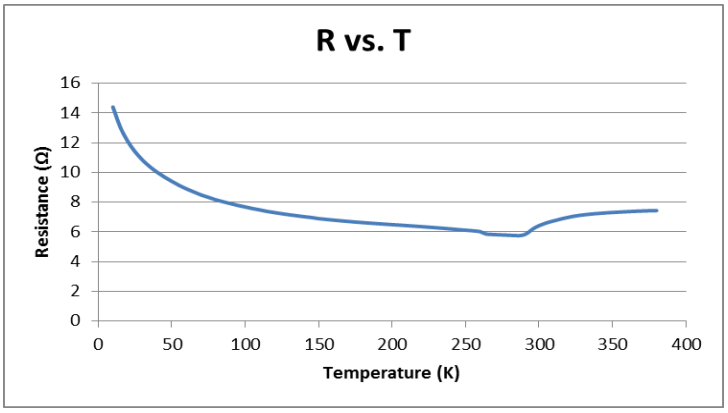

Figure 8.10 Resistance versus temperature plot of PEDOT:PSS soaked nylon/spandex sample exhibiting metallic behavior with an increase in resistance above room temperature.

Resistance versus temperature studies were performed on both types of spandex. Shown in Figure 8.10 is the resistance versus temperature plot of the nylon/spandex which showed an increase in resistance from room temperature to 100 °C. This increase in resistance with an increase in temperature is known as metallic behavior, thus another reason we report the PEDOT:PSS coated spandex as a stretchable 'metal'. The polyester spandex displayed a nearly identical resistance versus temperature, so both spandex had a much more conclusive R vs. T plot than the PEDOT:PSS on PET nonwoven fabric since the metallic phase transition had to be zoomed in to see on the PET fabric R vs. T plot.

Figure 8.11 The images of the percolation study of PEDOT:PSS on spandex where the top is the highest weight percent to the bottom which is the lowest weight percent of PEDOT:PSS.

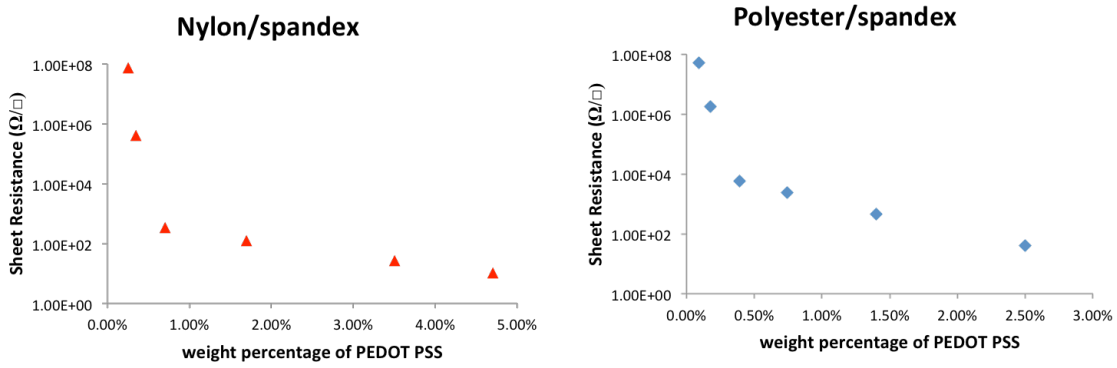

Figure 8.12 The plots of the percolation study of both nylon/spandex and polyester/spandex. PEDOT:PSS (95%) + DMSO (5%) was diluted to different concentrations, fabric was soaked and annealed, and sheet resistance was measured using four line method.

A percolation study was performed in order to find the point at which the PEDOT:PSS soaked spandex was no longer metallic/highly conductive. As seen in Figure 8.11 the PEDOT:PSS solution used to soak the spandex was diluted and both spandex fabrics were soaked in each dilution for one soak and anneal cycle. The top samples in Figure 8.11 are 100 % PEDOT:PSS, the samples below are 50 % PEDOT:PSS, then 25%, then 12.5%, then 6.25% and so on. As shown in Figure 8.12 the sheet resistance of both spandexes increase exponentially around 0.5 wt% of PEDOT:PSS, so at 0.5 wt% is the limit at which a continuous film (full coverage) of PEDOT:PSS can form.

8.3.2 Application

To verify the low sheet resistances and metallic behavior various demonstrations of power were envisioned. First to demonstrate the stretchable ‘metal’ aspect of the

Otley (2015)

PEDOT:PSS soaked spandex, a sample of twice soaked nylon/spandex was attached in series to a power source and 5 watt light. The 5-watt light bulb was chosen due to safety.

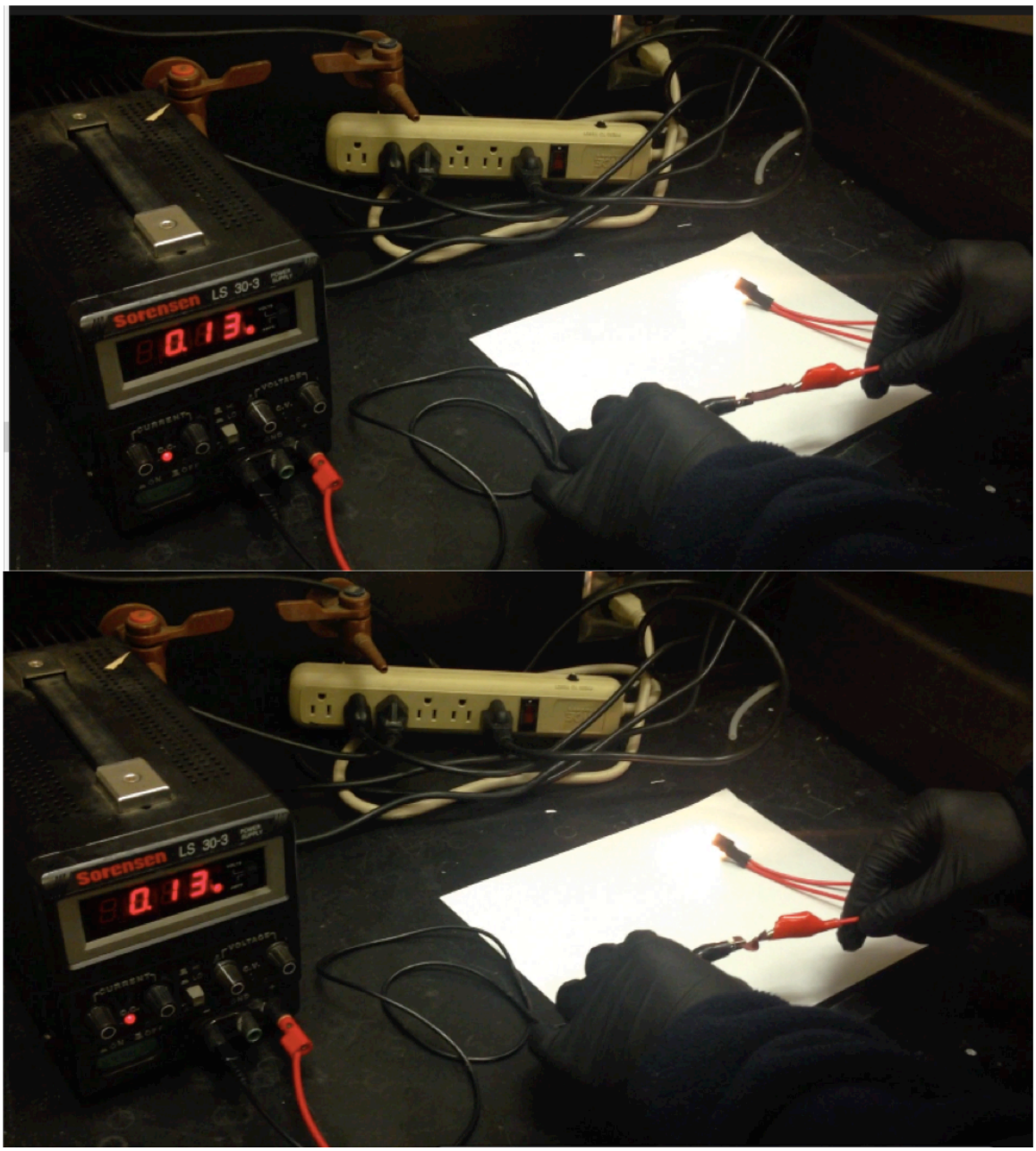

Figure 8.13 Demonstration of PEDOT:PSS coated nylon/spandex in the stretched (top) state and unstretched (bottom) state lighting a 5W incandescent bulb at 0.13 amperes (the low wattage bulb was chosen for safety purposes).

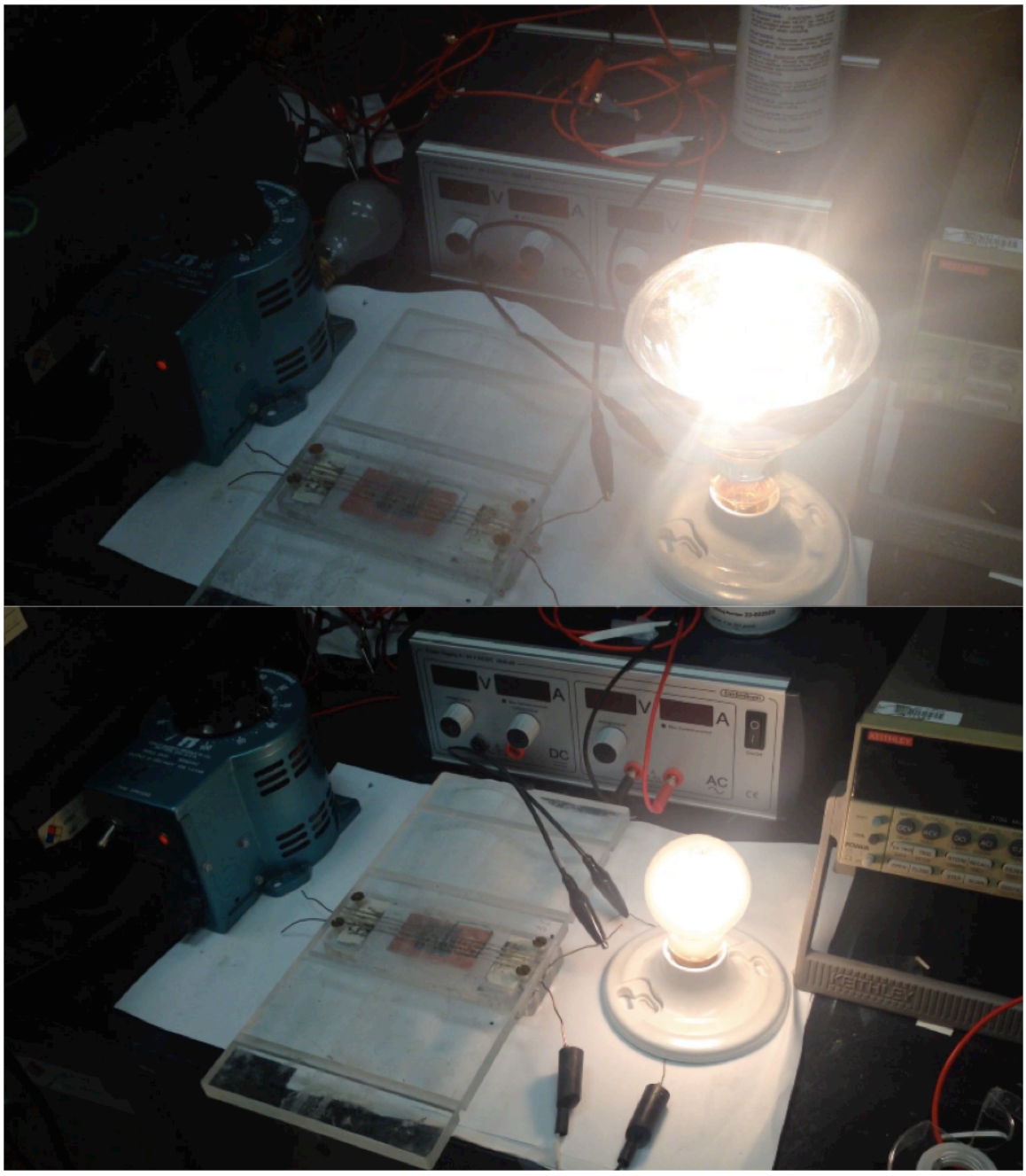

Figure 8.14 Demonstration of PEDOT:PSS and graphene coated spandex using AC current through a variac to power a 250W heat lamp (top) and a 60W incandescent light bulb (bottom).

As seen in Figure 8.13 the PEDOT:PSS soaked spandex was stretched and relaxed. As the spandex was stretched the light bulb dims demonstrating an increase of resistance, and as the spandex is relaxed the resistance drops and the brightness of the light bulb increases at a constant potential of 0.2 amps DC at 24 V. This simple demonstration proved that the PEDOT:PSS soaked spandex could be used in various types of sensors because when stretched there is a change in resistance. In Figure 8.14 is a demonstration of high conductivity by lighting a 60 W incandescent lamp and also lighting a 250 W heat lamp. This was achieved by coating the fabric with graphene from graphite in water and heptane using the interfacial method, and then coating with PEDOT:PSS to form a graphene/conductive polymer hybrid. The results from the addition of graphene include sheet resistances of less than 1 ohm/square, and the ability to pass high current.

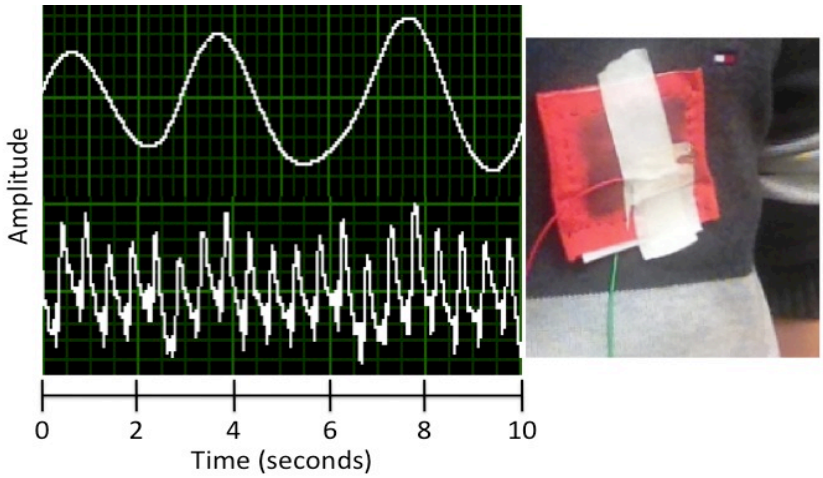

Figure 8.15 A demonstration of a cardiorespiratory sensor with PEDOT:PSS coated spandex.

Otley (2015)

A cardiorespiratory sensor was constructed from two (spray coated) PEDOT:PSS coated spandex samples sandwiched with a dielectric layer in between consisting of polyvinylidene fluoride (PVDF) as shown in Figure 8.15. Then electrodes were attached and the heart rate of a student was taken after running. As seen in Figure 8.15 the resolution of the heartbeat at 130 beats per minute is extraordinary, and with this level of resolution heart irregularities such as arrhythmias and impending heart attacks can be revealed. Further studies will include joint sensors, chemical sensing, and other types of pressure sensors with the PEDOT:PSS coated spandex.

8.4 Methods

8.4.1 Coating of PEDOT:PSS onto Synthetic Leather and Spandex

A high-conductivity formulation of PEDOT:PSS (Clevios PH1000) (Heraeus) was used with 5 wt% of the secondary dopant dimethyl sulfoxide (Sigma-Aldrich) for coating onto synthetic leather poly(ethyleneterephthalate) fabric provided as a free sample by Nike.

The coating was applied by soaking via drop casting on a 2.5 cm x 2.5 cm fabric until the fabric was visibly soaked. This was followed by drying in air at room temperature for 30 minutes then annealing for 60 minutes at 110℃. This temperature and time were found to be the optimal drying conditions for the PET fabric based on several iterations of temperature and time until sheet resistance was at its lowest. All fabric samples were weighed before and after treatment to calculate weight percent.

Otley (2015)

8.4.2 Electrical Characterization

All resistances were calculated from an I-V curve at room temperature, with a minimum of 10 data points. Electrical data was obtained using a four line probe fabricated in house according to literature design with grooves carved for the leads ensuring a uniform length and spacing was obtained.[53] Current was passed through the outer two electrodes, while the inner two measured voltage. Sheet resistance was calculated based on the relationship $R_s = R(w/l)$ where w is the width of the sample (2.5 cm), and l is the distance between the leads (0.35 cm).[53] Two current sources were used, a Keithley 224 Programmable for small current (I_{max} = 101.1 x 10^{-3} A), Power Supply 3630 for high current I_{max}= 10 A, and a 196 system DMA was used to measure the voltage.

Resistance vs temperature was performed using (from 10 K–400 K) using a standard four-probe technique in a Physical Property Measurement System (Quantum Design).

Hall effect experiments were conducted using a Hewlett Packard 41458 Semiconductor Parameter Analyzer with a four-probe mount containing brass contacts inside a 0.7 tesla magnetic field.

8.4.3 Resistive Heating

Resistive heating was performed using 2.5 wt% PEDOT:PSS in synthetic leather (PET). 5 volts was applied with a power supply (Power Supply 3630), heating the sample to 200°C within 2 minutes. The supplied voltage was sustained for 10 minutes and then removed, allowing the sample to cool back to room temperature.

Otley (2015)

8.4.4 Microscopy Characterization and Sample Preparation

Transmission Electron Microscopy (TEM) samples were prepared by mounting 2 mm X 6 mm sections of the fabric into an epoxy resin (SPI-Chem Araldite 6005 kit), and cured at 80˚C for at least 12 hrs., followed by cutting ultrathin sections using 45˚ Diatome diamond blade on Reichert – Jung ultra cut E microtome. 20 μm slices, dispersed on DI water, were collected on 400 mesh copper grids.

Bright field TEM images were taken using a FEI Tecnai-T12 at 80 kV. EDS was used to identify the SiO_2 within the microtomed fiber cross-sections. EDS measurements were performed on an EDAX silicon crystal detector (30 mm^2) operated by FEI TIA software and acquired for at least 120 s.

Field Emission Scanning Electron Microscopy (SEM) sample preparation was performed by cross-sectioning free standing fiber mesh while submersed in liquid nitrogen with a razor blade. Imaging was obtained on a Jeol JSM-6335F at 2.5 kV, probe currant: 14 μA to induce charging on the surface of a cross-sectioned sample. Charging allowed differentiation between the conducting and non-conducting regions via charge contrast imaging.

8.4.5 Electrospinning to Re-construct PET Fabric

Trifluoracetic Acid (TFA) (Fisher), Dichloromethane (DCM) (Fisher), and Polyethyleneterephthalate (PET) (M_v: 30,000, Scientific Polymer) and hydrophilic fumed silica (200 m^2/g, avg. particle size: 12 nm, Aerosil) for the solution needed to electrospin was used. Prior to electrospinning, 20 wt% PET-3 wt/wt% silica was dissolved in a 50:50 TFA:DCM solution. Once fully solubilized, silica was introduced and dispersed with a

Otley (2015)

Turrax T25 high shear mixer for 15 minutes. Electrospinning apparatus used consisted of a tunable high voltage supply with low-current power. A positive voltage was applied, 15 kV, between an 18G syringe tip and a grounded sheet of aluminum 15 cm away. The solution was pumped through a syringe pump at 3ml/hr. through a 5ml syringe for 8 hrs. Fiber mat was washed with sonication in water for 15 min. then dried in vacuum oven at 75 °C for 30 minutes. Prior to introducing PEDOT:PSS, the fiber mat was plasma treated for 5 sec. in 25:75 Oxygen:Argon using a Fishchione Instruments 1020 plasma cleaner.

Otley (2015)

8.5 References

1. S. Kwon, S. H. Kwak, S. Youn, Flexible organic light emitting display device and method for manufacturing the same. U.S. Patent Application 14/179,211, filed February 12, **2014**.
2. L. Huang, S. J. Hong, J. Z. Zhong, Curved touch sensor. U.S. Patent No. 8,603,574. 10 Dec. **2013**.
3. H-K. Jung, M-S. Cheon, J-H Min, I-L Kim, Method and apparatus for encoding video in consideration of scanning order of coding units having hierarchical structure, and method and apparatus for decoding video in consideration of scanning order of coding units having hierarchical structure. U.S. Patent 20,140,334,535, issued November 13, **2014**.
4. K. Alzoubi, M. M. Hamasha, S. Lu, B. Sammakia, *Disp. Technol. J.* **2011,** *7*, 593–600.
5. C. K. Chiang, A. J. Heeger, A. G. Macdiarmid, *Berichte der Bunsengesellschaft für Phys. Chemie* **1979,** 83, 407–417.
6. C. K. Chiang, *et al. J. Am. Chem. Soc.* **1978,** *100*, 1013–1015.
7. C. K. Chiang, *et al. Phys. Rev. Lett.* **1977,** 39, 1098–1101.
8. O. Bubnova, *et al. Nat. Mater.* **2014,** *13*, 190–194.
9. Ando, K., Watanabe, S., Mooser, S., Saitoh, E. & Sirringhaus, H. *Nat Mater* **2013,** *12*, 622–627.
10. X. Crispin, *et al. Chem. Mater.* **2006,** *18*, 4354–4360.

11. M. Granstrom, *et al. Nature* **1998,** *395*, 257–260.

12. M. Hamedi, R. Forchheimer, O. Inganas, *Nat Mater* **2007,** *6*, 357–362.

13. J. Janata, M. Josowicz, *Nat Mater* **2003,** *2*, 19–24.

14. J. Isaksson, *et al. Nat. Mater.* **2007,** *6,* 673–679.

15. S. Moller, C. Perlov, W. Jackson, C. Taussig, S. R. Forrest, *Nature* **2003,** *426*, 166–169.

16. S. Steudel, *et al. Nat Mater* **2005,** *4,* 597–600.

17. J. Z. Wang, Z. H. Zheng, H. W. Li, W. T. S. Huck, H. Sirringhaus, *Nat. Mater.* **2004,** *3*, 171–176.

18. B. L. Groenendaal, F. Jonas, D. Freitag, H. Pielartzik, J. R. Reynolds, *Adv. Mater.* **2000,** *12*, 481–494.

19. W. Li, M. Wan, *Synth. Met.* **1998,** *92,* 121–126.

20. R. D. McCullough, *Adv. Mater.* **1998,** *10*, 93–116.

21. R. D. McCullough, S. Tristram-Nagle, S. P. Williams, R. D. Lowe, M. Jayaraman, *J. Am. Chem. Soc.* **1993,** *115*, 4910–4911.

22. T. M. Swager, *Acc. Chem. Res.* **1998,** *31*, 201–207.

23. D. T. McQuade, A. E. Pullen, T. M. Swager, *Chem. Rev.* **2000,** *100*, 2537–2574.

24. D.-Y. Khang, H. Jiang, Y. Huang, J. A. Rogers, *Science* **2006,** *311*, 208–212.

25. D.-H Kim, *et al. Science* **2008,** *320*, 507–511.

26. Y. Ding, M. A. Invernale, G. A. & Sotzing, *ACS Appl. Mater. Interfaces* **2010,** *2*, 1588–1593.

27. M. A. Invernale, Y. Ding, G. A. Sotzing, *ACS Appl. Mater. Interfaces* **2010,** *2*, 296–300.

28. J. J. Hostýnek, R. S. Hinz, C. R. Lorence, M. Price, R. H. Guy, *Crit. Rev. Toxicol.* **1993,** *23*, 171–235.

29. H. Deiner, Process for improving the slipping resistance and the delustering of textiles. U.S. Patent 3,730,762, issued May 1, **1973**.

30. J. D. Mendez, C. Weder, *Polym. Chem.* **2010,** *1*, 1237–1244.

31. A. M. Nardes, *et al. Adv. Mater.* **2007,** *19*, 1196–1200.

32. R. Yue, J. Xu, *Synth. Met.* **2012,** *162*, 912–917.

33. M. Chabinyc, *Nat Mater* **2014,** *13*, 119–121.

34. O. Bubnova, *et al. Nat Mater* **2011,** *10*, 429–433.

35. G.-H. Kim, L. Shao, K. Zhang, K. P. Pipe, *Nat Mater* **2013,** *12*, 719–723.

36. N. Basescu, *et al. Nature* **1987,** *327*, 403–405.

37. N. Kim, *et al. Adv. Mater.* **2014,** *26*, 2268–2272.

38. I. McCulloch, *et al. Nat. Mater.* **2006,** *5,* 328–333.

39. Y. Xia, J. Ouyang, *J. Mater. Chem.* **2011,** *21*, 4927–4936.

40. A. M. Nardes, R. A. J. Janssen, M. Kemerink, *Adv. Funct. Mater.* **2008,** *18*, 865–871.

41. J. Ouyang, *Polymer* **2004,** *45*, 8443–8450.

42. A. M. Nardes, M. Kemerink, R. A. J. Janssen, *Phys. Rev. B* **2007,** *76*, 85208.

43. Y. Xia, J. Ouyang, *ACS Appl. Mater. Interfaces* **2010,** *2*, 474–483.

44. Y. Xia, H. Zhang, J. Ouyang, *J. Mater. Chem.* **2010,** *20,* 9740–9747.

45. Y. Xia, K. Sun, J. Ouyang, *Adv. Mater.* **2012,** *24*, 2436–2440.

46. U. Voigt, W. Jaeger, G. H. Findenegg, R. V. Klitzing, *J. Phys. Chem. B* **2003,** *107*, 5273–5280.

47. X. Crispin, *et al. J. Polym. Sci. Part B Polym. Phys.* **2003,** *41*, 2561–2583.

48. Coating Guide Clevios ™ P Formulations. 1–12 (2012). at http://www.heraeus-clevios.com/media/webmedia_local/media/datenblaetter/Clevios_P_coating_guide_08-03-18jb2.pdf

49. D. A. Mengistie, M. A., Ibrahem, P.-C. Wang, C.-W. Chu, *ACS Appl. Mater. Interfaces* **2014,** *6*, 2292–2299.

50. S.-J. Wang, Y.-J. Choi, S. C. Gong, Y.-H. Kim, H.-H. Park, *Mol. Cryst. Liq. Cryst.* **2012,** *568*, 179–185.

51. D, Alemu, H.-Y. Wei, K.-C. Ho, C.-W. Chu, *Energy Environ. Sci.* **2012,** *5*, 9662–9671.

52. A. Aleshin, R. Kiebooms, R. Menon, A. J. Heeger, *Synth. Met.* **1997,** *90*, 61–68.

53. R. K. Hiremath, M. K. Rabinal, B. G. Mulimani, *Rev. Sci. Instrum.* **2006,** *77*, 126106.

54. D. M. Knotter, *J. Am. Chem. Soc.* **2000,** *122*, 4345–4351.

55. O. Allemann, S. Duttwyler, P. Romanato, K. K. Baldridge, J. S. Siegel, *Sci.* **2011,** *332,* 574–577.